Modelling floodplain biogeomorphology

Cover photograph: panoramic view of a meander bend in the Allier river, France. Photo by Martin Baptist.

Modelling floodplain biogeomorphology

Proefschrift

ter verkrijging van de graad van doctor
aan de Technische Universiteit Delft,
op gezag van de Rector Magnificus prof.dr.ir. J.T. Fokkema,
voorzitter van het College voor Promoties,
in het openbaar te verdedigen

op maandag 18 april 2005 om 15:30 uur

door

Martin Josephus BAPTIST

landbouwkundig ingenieur
geboren te Voorburg.

Dit proefschrift is goedgekeurd door de promotor:
  Prof. dr. ir. H.J. de Vriend

Samenstelling promotiecommissie:

Rector Magnificus	voorzitter
Prof. dr. ir. H.J. de Vriend	Technische Universiteit Delft, promotor
Prof. dr. ir. H.H.G. Savenije	Technische Universiteit Delft
Prof. dr. ir. G.S. Stelling	Technische Universiteit Delft
Prof. dr. A.J.M. Smits	Radboud Universiteit Nijmegen
Prof. dr. P. Meire	Universiteit Antwerpen
Prof. Dr.-Ing. A. Dittrich	Technische Universität Braunschweig
Dr. ir. E. Mosselman	WL	Delft Hydraulics

Printed in the Netherlands

De steen

Ik heb een steen verlegd in een rivier op aarde.
Het water gaat er anders dan voorheen.
De stroom van een rivier hou je niet tegen.
Het water vindt er altijd een weg omheen.

Misschien eens, gevuld door sneeuw en regen,
neemt de rivier mijn kiezel met zich mee,
om hem dan glad en rond gesleten
te laten rusten in de luwte van de zee.

Ik heb een steen verlegd in een rivier op aarde.
Nu weet ik dat ik nooit zal zijn vergeten.
Ik leverde bewijs van mijn bestaan.
Omdat door het verleggen van die ene steen
de stroom nooit meer dezelfde weg zal gaan.

Bram Vermeulen

Abstract

There is an increasing awareness that rivers need more room in order to safeguard flood safety under climate change conditions. Contemporary river management is creating room in the floodplains and allowing, within certain bounds, natural processes of sedimentation and erosion. One of the aims is to restore dynamic conditions, so as to get a sustainable and more diverse river ecosystem that can cope with floods. This new approach requires understanding of the interaction between the biotic and abiotic components of river systems. More specifically, it requires a better understanding of the interaction between flora and fauna and geomorphological factors. This is the object of investigation of the interdiscipline of *biogeomorphology*. Modelling biogeomorphological processes in river floodplains is the topic of this thesis.

To reduce flood risks in the Netherlands, measures to increase the flood conveyance capacity of the Rhine River will be implemented. However, it is expected that floodplain sedimentation and softwood forest development in rehabilitated floodplains will gradually reduce the conveyance capacity and the biodiversity. Moreover, in regulated rivers, such as the Rhine River, erosion and sedimentation processes caused by channel migration, which periodically interrupt vegetation succession, cannot be allowed. Therefore, a floodplain management strategy was proposed that would meet both flood protection and nature rehabilitation objectives. This strategy, "Cyclic Floodplain Rejuvenation (CFR)", aims at mimicking the effects of channel migration by removal of softwood forests, by lowering floodplains or by (re)constructing secondary channels. In chapter 2, the effects of CFR measures on reducing flood levels and enhancing biodiversity along the Waal River were assessed. A one-dimensional hydraulic modelling system, SOBEK, was applied together with rule-based models for floodplain vegetation succession and floodplain sedimentation. The model simulations demonstrated that the flood management strategy of Cyclic Floodplain Rejuvenation is able to sustain safe flood levels in the Waal River. Rejuvenation is then needed every 25 to 35 years on average, each time in an area of about 15% of the total floodplain area. The rejuvenation strategy led to a diverse floodplain vegetation distribution that largely complies to the historical reference for the Waal River. Cyclic Floodplain Rejuvenation may be the appropriate answer to find symbiosis between flood protection and nature rehabilitation in highly regulated rivers.

A next step would be to apply a two-dimensional numerical model to test the strategy more thoroughly. A two-dimensional model can link spatial information on vegetation development and floodplain topography to simulations of the hydrodynamic and morphodynamic developments in floodplains. In chapter 3, a first effort is made to model the biogeomorphological interactions of three secondary channels located in a floodplain section of the River Waal, near the town of Gameren. A two-dimensional depth-averaged application of the numerical model Delft3D-MOR was applied in combination with a rule-based vegetation succession model that describes the development of floodplain vegetation. A key aspect of this study was that a coupling has been made between the changing hydraulic roughness of vegetation over time and its effects on the hydrodynamics and morphodynamics. The model describes the morphological developments of the secondary channels over a simulation period of 30 years. Two different cases have been distinguished. In one case the hydraulic roughness of the floodplain vegetation remains constant over time, determined by the initial vegetation composition and distribution of the year 2000. In the other case, a rule-based floodplain vegetation model computes the expected growth and succession of vegetation, affected by the inundation duration, substrate, grazing intensity by large herbivores and sedimentation rate. The results showed that the simulated morphological trends caused by the *remote effects* of vegetation largely comply with observations and measurements. However, *local* morphological effects in vegetated sections of the floodplain seem to be erroneous. In the model, the increased hydraulic roughness of the vegetation leads to an overestimation of the bed shear stress and hence the sediment transport capacity.

A following important step, therefore, was to find analytical approaches for the bed shear stress on a vegetated bed, applicable in two-dimensional morphodynamic models. In chapter 4, two different analytical expressions for the bed shear stress have been derived. One approach yields a relatively simple expression, valid for submerged vegetation, giving a reduction factor for the total fluid shear stress. For non-submerged vegetation it is even simpler, the common formula for open channel flow can be applied, given the simplifying assumptions. The other approach yields a relatively complex expression, based on an analytical solution of the momentum balance for vegetated flow, and is valid for submerged as well as non-submerged conditions. For both approaches, vegetation is schematised as rigid cylinders. A comparison of the bed shear stress calculated with both analytical expressions and with a numerical 1-DV model shows that for submerged conditions the complex formulations of the analytical approach give better estimates for the bed shear stress as compared to the reduction factor approach, especially for a smooth bed. For non-submerged conditions, the analytical approach gives an improved estimate, as well. The analytical approach accounts for the dependence on water depth for non-submerged conditions, which is not included in the reduction factor approach.

Subsequently, chapter 5 describes the results of a flume experiment that has been carried out to determine the bed shear stress and the sediment transport rate for a sand bed with submerged vegetation. It was found that the effects of submerged vegetation on sediment transport are twofold:

1.   A reduction of the time-averaged bed shear stress, due to reduced time-averaged near-bed velocities and fluid stresses;

2.   An increase of the sediment pick-up rate, due to an increased near-bed turbulence intensity.

The primary effect is that of reduction of the bed shear stress. Only near the threshold of motion, and for relatively short vegetation, the increased pick-up rate becomes an important additional transport mechanism. From this flume experiment it was concluded that the reduced bed shear stress on a vegetated bed can be described reasonably well with a numerical 1-DV model or with the analytical expressions, given an accurate description of the vegetation geometry. Subsequently, the sediment transport rate for a vegetated bed can be described reliably by a common sediment transport formula, as long as the bed shear stress reduction is accounted for.

Finally, in chapter 6, the analytical expressions for the bed shear stress on a vegetated bed were applied in a real-world case study of the Allier, France. A comparison has been made between the results of a three-dimensional (3-D) model for vegetated flow and the results of two-dimensional depth-averaged (2-DH) models with analytical expressions for the bed shear stress. Taking the 3-D model as a reference, results show that the bed shear stress distribution of a river with flooded vegetated areas can be described well in a 2-DH numerical model with the application of analytical expressions for the bed shear stress reduction.

<div style="text-align: right">

M.J. Baptist

April 2005

</div>

Samenvatting

Er is een toenemend besef dat rivieren meer ruimte nodig hebben ten behoeve van de hoogwaterveiligheid, zeker bezien in het licht van klimaatverandering. Het huidige rivierbeheer is gericht op het creëren van ruimte, onder andere in de uiterwaarden. Hierin worden tevens, binnen zekere grenzen, erosie en -sedimentatieprocessen toegestaan. Eén van de doelstellingen is om de dynamiek van rivieren te herstellen, waarmee een duurzaam en meer divers rivierecosysteem wordt verkregen dat beter bestand is tegen hoge afvoeren.

Deze nieuwe aanpak vraagt een gedegen kennis van de samenhang tussen de biotische en de abiotische onderdelen van riviersystemen. Meer specifiek gezegd, het vereist een beter begrip van de interactie tussen flora en fauna en geomorfologische factoren. Dit is het onderwerp van de *biogeomorfologie*. Dit proefschrift gaat over het modelleren van biogeomorfologische processen in rivieruiterwaarden.

Om de veiligheid tegen overstromen te verbeteren worden de komende jaren grootschalige rivierprojecten uitgevoerd in Nederland die onder andere zijn gericht op het vergroten van de afvoercapaciteit. Echter, er bestaat de vrees dat de natuurlijke ophoging van uiterwaarden en de ontwikkeling van grootschalige ooibossen zal leiden tot een afname van de afvoercapaciteit. Daarom is een strategie bedacht die zowel de afvoercapaciteit garandeert alsmede de biodiversiteit vergroot. Dit is de strategie van *cyclische verjonging van uiterwaarden*. Cyclische verjonging van uiterwaarden is een hoogwater- en natuurbeheerstrategie gebaseerd op het simuleren van erosie- en sedimentatieprocessen van natuurlijke riviersystemen. In gereguleerde systemen ontbreken deze processen grotendeels en dreigen de uiterwaarden letterlijk dicht te groeien met ooibossen. Daarbij neemt zowel de landschapsdiversiteit als de afvoercapaciteit af. In Hoofdstuk 2 van dit proefschrift is een modelstudie uitgevoerd naar de toepassing van cyclische verjonging langs de Waal. Het doel van deze modelstudie is om te bepalen hoe frequent en met welke omvang de vegetatieontwikkeling moet worden verjongd om zowel de hoogwaterveiligheid als de landschapsdiversiteit te vergroten. Deze studie is uitgevoerd met behulp van een één-dimensionaal waterbewegingsmodel, SOBEK, gekoppeld aan kennismodellen voor uiterwaardvegetatie en uiterwaardsedimentatie. In een één-dimensionaal horizontaal (1-DH) model wordt een rivier met uiterwaarden geschematiseerd door een lijn, bestaande uit meerdere stukjes. De modelsimulaties lieten zien dat de strategie van cyclische verjonging van uiterwaarden

in staat is de hoogwaterveiligheid te waarborgen. Verjonging is dan noodzakelijk iedere
25 tot 35 jaar in een gebied ter grootte van 15% van de totale oppervlakte aan uiterwaar-
den. Cyclische verjonging kan hiermee de oplossing zijn voor het spanningsveld tussen
hoogwaterveiligheid en natuurontwikkeling in gereguleerde rivieren.

Een volgende stap die de nauwkeurigheid van de voorspellingen kan verbeteren, is het toe-
passen van een twee-dimensionaal model. In een twee-dimensionaal model wordt een rivier
met uiterwaarden geschematiseerd door vakjes. In een dergelijk ruimtelijk model kan een
betere koppeling worden gemaakt tussen de vegetatie-ontwikkeling, de hoogteverschillen
in een uiterwaard en de waterbeweging. In Hoofdstuk 3 van dit proefschrift zijn de biogeo-
morfologische ontwikkelingen van drie nevengeulen in de Waal bij Gameren gemodelleerd.
Een twee-dimensionale, diepte-gemiddelde (2-DH) toepassing van Delft3D-MOR is gekop-
peld aan een kennismodel voor vegetatiegroei en -successie. De veranderende hydraulische
weerstanden als gevolg van de veranderingen in vegetatiegroei beïnvloeden de waterbewe-
ging en de morfologie van de nevengeulen en de hieruit volgende veranderingen in over-
stromingsduur beïnvloeden de vegetatiegroei. Het model simuleert de morfodynamische
veranderingen van de geulen over een periode van 30 jaar voor twee verschillende situaties.
In het ene geval blijft de vegetatiebedekking onveranderd, in het andere geval maakt de
vegetatie een ontwikkeling door afhankelijk van de overstromingsduur, het substraat, de
begrazingsdruk door grote grazers en de sedimentatiesnelheid. De resultaten laten zien
dat de vegetatiegroei een significante invloed heeft op morfologische veranderingen. De
gesimuleerde morfologische veranderingen van de geulen komen grotendeels overeen met
observaties en metingen, echter, lokale veranderingen op de begroeide uiterwaarden lijken
verkeerd voorspeld. In het model leidt de toegenomen hydraulische weerstand van de ve-
getatie tot een overschatting van de bodemschuifspanning, dat is de kracht van het water
aan de bodem, en hiermee tot een overschatting van het sedimenttransport.

Een volgende belangrijke stap is daarom om een betere formule te vinden voor de bodem-
schuifspanning op een begroeide bodem. In Hoofdstuk 4 van dit proefschrift worden twee
verschillende formules afgeleid. De eerste formule is relatief eenvoudig en geeft een reduc-
tiefactor voor de totale schuifspanning. In het geval van doorstroomde vegetatie reduceert
deze tot de bekende formule voor de bodemschuifspanning in open waterlopen. De tweede
formule is complex en is gebaseerd op een analytische oplossing van de impulsbalans voor
stroming met vegetatie. Voor beide formules geldt dat de vegetatie is geschematiseerd
door starre cilinders. De resultaten van de formules zijn vergeleken met, en deels geca-
libreerd aan, de resultaten van een numeriek één-dimensionaal verticaal (1-DV) model.
In dit model worden verticale profielen over de waterhoogte berekend op één plaats. De
complexe formule geeft betere resultaten.

Vervolgens wordt in Hoofdstuk 5 een gootexperiment beschreven waarin de bodemschuif-
spanning op een begroeide zandbodem is bepaald en is gekeken naar de erosie van zand

tussen kunstmatige vegetatie. Er is gevonden dat het effect van overstroomde vegetatie op sedimenttransport tweeledig is:

1. Een reductie van de tijdsgemiddelde bodemschuifspanning, als gevolg van de afgenomen tijdsgemiddelde stroomsnelheid nabij de bodem;

2. Een toename van de capaciteit om zandkorrels op te wervelen, als gevolg van een toegenomen turbulentie nabij de bodem.

Het belangrijkste effect is de reductie van de bodemschuifspanning. Alleen bij een lage bodemschuifspanning, nabij het begin van bewegen van zandkorrels, en voor relatief korte vegetatie, wordt de toegenomen 'opwervelcapaciteit' een belangrijk extra transportmechanisme. De resultaten van deze experimentele studie wijzen uit dat de gereduceerde bodemschuifspanning redelijk goed beschreven kan worden met het numerieke 1-DV model, alsmede met de analytische formules, gegeven een accurate beschrijving van de geometrie van de vegetatie. Dientengevolge kan het sedimenttransport op een begroeide bodem goed beschreven worden door een bestaande sedimenttransportformule, zolang de reductie in bodemschuifspanning wordt meegenomen.

In Hoofdstuk 6, tot slot, zijn de analytische formules voor de bodemschuifspanning toegepast in een model voor een echte rivier, de Allier in Frankrijk. Er is een vergelijking gemaakt tussen de resultaten van een drie-dimensionaal (3-D) model voor stroming door vegetatie en de resultaten van twee-dimensionale, dieptegemiddelde (2-DH) modellen met de analytische formules. In een drie-dimensionaal model wordt een rivier met uiterwaarden geschematiseerd door blokjes onderverdeeld in laagjes. Een dergelijk 3-D model kan de bodemschuifspanning correct berekenen, maar dat gaat ten koste van de rekentijd. Het is daarom vooralsnog niet geschikt voor morfodynamische berekeningen. De resultaten laten zien dat de ruimtelijke verdeling van de bodemschuifspanning goed kan worden beschreven door 2-DH modellen met analytische formules. Dit is een belangrijke voorwaarde voor de toepassing in morfodynamische modellen.

<div align="right">

M.J. Baptist

April 2005

</div>

Contents

Chapter 1

Introduction

1.1 Modelling floodplain biogeomorphology

Worldwide, there is an increasing awareness that rivers need more room in order to safe-guard flood safety under climate change conditions. Contemporary river management is creating room in the floodplains and allowing, within certain bounds, natural processes of sedimentation and erosion. One of the aims is to restore dynamic conditions, so as to get a sustainable and more diverse river ecosystem that can cope with floods. The challenge of river restoration is to redesign the floodplains in such a way that they will synergistically strengthen the functions of navigability and safe discharge of water, sediment and ice and the natural diversity of river ecosystems. One of the main problems, however, is that the hydraulic resistance of vegetation, in combination with sedimentation in floodplains, de-creases the required conveyance capacity. Therefore, a new management approach called 'Cyclic Floodplain Rejuvenation' (Smits *et al.*, 2000) was proposed in which rejuvenation of landscape elements will clear the way for discharge of water and simultaneously main-tain the system's diversity. This new approach requires understanding of the interaction between the biotic and abiotic components of river systems. More specifically it requires a better understanding of the interaction between flora and fauna and geomorphological factors. This is the object of investigation of the interdiscipline of *biogeomorphology*.

To identify biogeomorphological developments associated with global climate change and the effects of human intervention schemes, such as 'Room for the River' (Van Stokkom & Smits, 2002), or 'Cyclic Floodplain Rejuvenation', predictive models are needed. Clearly, such models need to include the effects of floodplain vegetation. Vegetation not only determines the river's flood conveyance capacity, it also affects the transport of sediment and geomorphological dynamics. Mean flow, turbulence, sediment motion, erosion and deposition of sediment over and between vegetation are key elements in the prediction of the long-term response of lowland rivers. Modelling these biogeomorphological processes in river floodplains is the topic of this thesis.

1.2   Biogeomorphology, state of the art and essential concepts

1.2.1 Definition

The term biogeomorphology was first used in the 1980s (Viles, 1988), although earlier studies have been conducted that focused on biogeomorphology without using this term. Biogeomorphology[1] is a discipline that combines ecology and geomorphology. Geomorphology is the study of landforms and their formation. Ecology is the study of the relationships between biota and their environment. The environment is defined as factors that affect biota. These factors can be abiotic (physical, chemical), biotic (other organisms), or anthropogenic (humans). Abiotic geomorphological processes may affect biota and biota may in turn affect geomorphological processes. The interaction between the two defines the interdiscipline of biogeomorphology. *Biogeomorphology is the study of the interaction between geomorphological factors and biota.*

1.2.2 Essential concepts

Biogeomorphology is studied in terrestrial as well as in aquatic systems. Relevant geomorphological factors in aquatic systems are bed topography, bed composition (rock, gravel, sand, silt, clay), and the transport of sediment. It also includes factors that drive morphological processes, such as water flow and waves. The biota involved in biogeomorphology include plants and animals, ranging from small species, such as algae (Widdows *et al.*, 2000) to large species, such as cows (Trimble & Mendel, 1995). The geomorphological influence on biota is in its most direct form the influence on habitats (living environments) of flora and fauna. The morphology and geomorphological processes define the gradients between high and low, between wet and dry, between fast flowing and stagnant water and between sedimentation and erosion. These gradients and the processes that cause them are determinative for gradients in grain size of the sediment, nutrient levels, organic matter levels and moisture. Plants and animals are tuned to specific conditions and will therefore be abundant at specific locations. The biological influence on geomorphological processes is the influence of biota to create, maintain or transform their own geomorphological surroundings. This is demonstrated by the influence of vegetation on the hydraulic resistance, erodibility and sedimentation, or by the influence of fauna on sediment characteristics through bioturbation and biostabilization. In some cases morphological processes are dominant over biological processes and therefore the biota have to adjust to their environment. In other cases biological processes are dominant. The most interesting are those cases where there is a mutual interaction that leads to feedback coupling of processes. When looking for these cases, it is important to examine the temporal and spatial scales of the mutually interacting processes.

---

1.   From: Schwartz, in press. Encyclopedia of Coastal Science. Dordrecht: Kluwer Academic Publishers, p.91, **Biogeomorphology**, definition by Martin J. Baptist.
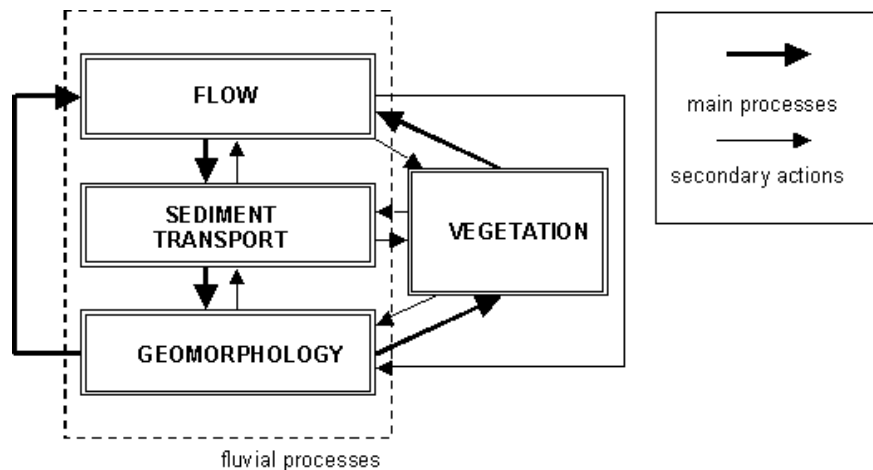
Figure 1.1: The influence of vegetation on fluvial processes, modified after Tsujimoto, 1999.

This thesis deals with modelling floodplain biogeomorphology. In fluvial systems biogeomorphological interactions are clearly demonstrated in the shallow, productive waters, riparian zones and various sedimentary environments. In floodplains, vegetation has the most pronounced biogeomorphological interactions. On the one hand, the growth and succession of floodplain vegetation is highly dependent on the local abiotic conditions. The most important factors are the inundation period and the substrate composition (Dister, 1980; Gurnell, 1997; Peters, 2002). On the other hand, floodplain vegetation significantly affects the abiotic environment. First of all, floodplain vegetation affects the hydrodynamics through effects on the hydraulic resistance. Secondly, floodplain vegetation affects sediment transport and morphodynamics through effects on the bed shear stress, the sediment erodibility and sediment trapping. Together, this leads to several feedback cycles that affect the overall natural development of floodplains. Figure 1.1 presents a schematic overview of the influence of vegetation on the fluvial system. Examples of biogeomorphological interrelationships include floodplain sedimentation (Middelkoop, 1997; Asselman & Van Wijngaarden, 2002; Steiger *et al.*, 2003), resistance of vegetation against bank erosion (Thorne, 1990; Abernethy & Rutherford, 1998; Abernethy & Rutherford, 2000; Abernethy & Rutherford, 2001; Murray & Paola, 2003), stream diversion by large woody debris (Shields & Gippel, 1995; Manga & Kirchner, 2000) and the evolution of channel planform, secondary channels, and point and scroll bars affected by vegetation (Gurnell, 1995; Gurnell & Gregory, 1995; Marston *et al.*, 1995; McKenney *et al.*, 1995; Hupp & Osterkamp, 1996; Brown, 1997; Rodrigues, 2000; Gran & Paola, 2001; Brooks & Brierley, 2002; Richards *et al.*, 2002; Specht, 2002; Dijkstra, 2003; Hession *et al.*, 2003).

1.2.3 Literature review on river biogeomorphology

Geomorphological processes occur on time scales ranging from microseconds, relevant to turbulence, up to hundreds of millions of years for geological processes. The spatial
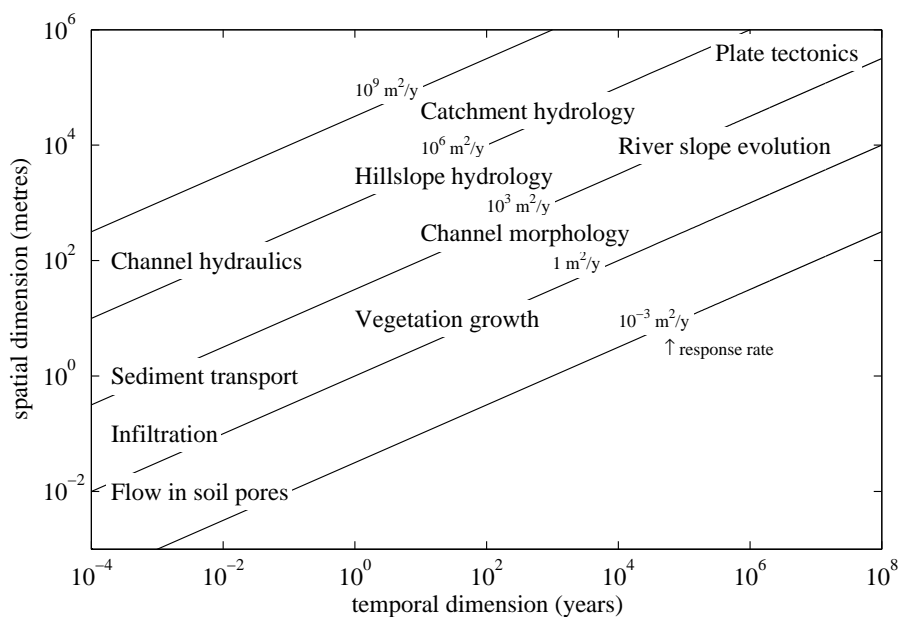
Figure 1.2: Temporal and spatial scales for geomorphological processes. The response rate indicates the evolution rate of the processes. Modified after Kirkby (1990).

scale range is similarly wide, from micrometres for capillary flows in sediments up to the continental and global scales. Kirkby (1990) presents an example for the wide variety in scales for river systems, see Figure 1.2. He presents a measure for the response rate of systems, defined as a diffusive transport rate, i.e. the ratio of the squared spatial dimension (m^2) over the temporal dimension (y). The response rates for morphological processes such as sediment transport, channel morphology and river slope evolution are of the same size (about 10^3 m^2/y), irrespective of the scale order. Hydraulic and hydrologic processes also share a response rate, which is larger than for morphological processes (about 10^6 m^2/y). Vegetation growth has a relatively small response rate (about 1 m^2/y), meaning that changes in vegetation patterns are a less dynamic landscape element than changes in morphology. As a general concept, this comparison of response rates may hold true for natural river systems. Consequently, this leads to the observation that for floodplain biogeomorphology, morphodynamics is leading over vegetation dynamics and not the other way around. On the other hand, the reverse may be true in small, vegetation dominated streams.

This literature review reveals that biogeomorphological processes in rivers are present on a wide variety of scales. A common method to cope with scale problems of landscapes is a hierarchical classification for linked processes at multiple scales (Klijn, 1997). However, it must be noted that the scale hierarchy concept may hold for a single river basin, but probably not between basins. In other words: one cannot transfer a hierarchy from one basin to another without adjusting the overall scale. To classify and discuss the influence of biogeomorphological processes at different spatio-temporal scales the classification scheme of

Table 1.1: Overview of literature references on floodplain biogeomorphology.

Process	Scale
Reference	
Reduced vegetation cover leads to valley floor aggradation	Basin
(Thorne *et al.*, 1997)	
Human deforestation affected river channel evolution	Basin
(Gregory & Gurnell, 1988)	
Climatic effects on vegetation cover changes channel pattern	Segment
(Starkel, 1990)	
Vegetation plays key role in anabranching	Segment
(Tooth & Nanson, 1999)	
Large woody debris diverts streams and changes channel planform	Segment
(Shields & Gippel, 1995; Manga & Kirchner, 2000)	
Floodplain vegetation induces sedimentation	Reach
(Middelkoop, 1997; Asselman & Van Wijngaarden, 2002; Steiger *et al.*, 2003)	
Increased bank resistance due to vegetation cover frustrates meandering	Reach
(Gregory & Gurnell, 1988)	
Vegetation affects erosion and bank retreat	Reach
(Thorne, 1990; Abernethy & Rutherford, 1998; Abernethy & Rutherford, 2000;	
Abernethy & Rutherford, 2001; Murray & Paola, 2003)	
Cow grazing reduces vegetation cover and decreases erosional resistance	Reach
(Trimble & Mendel, 1995)	
Vegetation affects secondary channel development	Ecotope
(Rodrigues, 2000)	
Log and debris dams create new physiotopes	Ecotope
(Gregory, 1992; Brown, 1997)	
Riparian zones affect land-water interaction	Ecotope
(Goodwin *et al.*, 1997; Gregory *et al.*, 1991)	
Floodplain forests affect geomorphology through overbank flow	Ecotope
(Piégay, 1997)	
Grass enhances deposition and retains sediment	Ecotope
(Abt *et al.*, 1994)	
Submerged vegetation affects turbulence and sediment transport	Ecotope
(Li & Shen, 1973; Nakagawa *et al.*, 1992; Tsujimoto, 1999)	

Frissell *et al.* (1986) is applied in a revised form. Frissell *et al.* (1986) distinguish between the stream system, segment system, reach system, pool/riffle system and the microhabitat system. Their original classification is oriented toward relatively small mountain streams in forested environments, whereas this study focuses on large lowland river systems such as the Rhine and the Meuse. A revised classification scheme based on Klijn (1997) and Rademakers and Wolfert (1994) is therefore drawn up. The classes of Frissell *et al.* (1986) have been changed into a more generic framework of hierarchical ecosystem classification. The hierarchical scales used in this study are the river basin scale, segment scale, reach scale, and ecotope scale. Literature references on floodplain biogeomorphology have

Table 1.2: Biogeomorphological influence on different scale levels.

Scale level	Spatial scale (m)	Temporal scale (y)	Biogeomorphology
River basin	10^5 - 10^7	10^3 - 10^6	$--$
Segment	10^4 - 10^6	10^2 - 10^4	$-$
Reach	10^3 - 10^5	10 - 10^3	$+$
Ecotope	10 - 10^3	1 - 10^2	$++$

subsequently been hierarchically classified and summarised in Table 1.1. For background reading reference is made to Baptist (2001b).

The biogeomorphological process interactions found in literature were categorised according to a hierarchical classification. By lack of better and more quantitative methods, this is probably the best method available, but it proves difficult to put a single scale-label onto a process. Since biogeomorphological interactions can have effects on different scale levels, the scale cascade of De Vriend (2001), where scale levels interact, is applicable in biogeomorphology as well. Table 1.2 gives a rough rating of the biogeomorphological influence on different scale levels. The magnitude of influence is not quantified thoroughly, but is based on the importance for mutual interactions as indicated by the authors. In this table, the space scale indicates the longitudinal size of the system and the time scale is defined as the persistence of geomorphic features.

This review provides an overview of biogeomorphological interactions in river systems for different scales. Although the discipline of biogeomorphology has been invented only recently, a lot of literature deals with the combination of geomorphology and ecology. A characteristic of the literature, however, is the qualitative nature of most papers. Process-interactions are often defined, but seldom quantified. This lack of quantification is typical of the field of biogeomorphology. We understand that there is a complex interaction between geomorphology and biota, but are hardly able to put these into parameters and values, let alone apply numerical modelling tools to simulate the intricate interactions. An exception is the advanced scientific work with respect to the hydraulic resistance of vegetation. However, research has been focusing mainly on the effects of vegetation on flow and turbulence. The effects on sediment transport and morphology are a rather new topic. This topic is further elaborated in this thesis.

1.3   Motivation, problem identification, objectives and outline

The outline of this thesis is presented in Fig. 1.3. This thesis consists of a combination of model application and theory development and validation. The study started with the

floodplain strategy of 'Cyclic Floodplain Rejuvenation'. This strategy was proposed by Smits *et al.* (2000) as a theoretical concept that reintroduces geomorphological and vegetation diversity and serves flood safety. This formed a **motive** to quantify and analyse the concept of CFR. In this thesis, the application of this concept is elaborated quantitatively for the Waal River with the use of an integrated one-dimensional model (Chapter 2). The conclusion of this study is that Cyclic Floodplain Rejuvenation is necessary to sustain safe flood levels and at the same time increase the diversity of floodplain vegetation. Subsequently, this study formed a stimulus for the application of two-dimensional models, since patterns and processes in river biogeomorphology, i.e. vegetation distribution and morphodynamics, have two-dimensional properties. The biogeomorphological processes of secondary channels were, therefore, investigated with a two-dimensional model (Chapter 3). This study has shown that the lifetime of river improvement measures, such as the construction of secondary channels, is determined to a large extent by the interaction between vegetation and sediment. The present state of knowledge, however, is insufficiently advanced to be able to formulate reliable quantitative models. It was concluded that for future model applications of the morphological evolution of floodplains it is necessary to find better formulations for the quantification of the bed shear stress on a vegetated bed. This forms the **problem identification** of further study in this thesis.

The **objectives** of this thesis are formulated as follows:

- to develop a methodology to assess the required frequency and extent of Cyclic Floodplain Rejuvenation measures necessary with respect to the flood levels and landscape diversity, with the Waal River as an example;
- to assess the morphodynamic behaviour of secondary channels under different conditions of vegetation development;
- to improve two-dimensional numerical model instruments for modelling floodplain biogeomorphology with regard to the quantification of the bed shear stress on a vegetated bed.

A first step towards improved modelling of floodplain biogeomorphology is to schematise vegetation as rigid cylinders and to model the effects of these cylinders on mean flow, turbulence, sediment transport, erosion and deposition. Turbulence modelling has advanced so far by now that models have been developed to simulate flow between and over cylindrical obstacles (Uittenbogaard, 2003). A notable disadvantage, however, is that the effects of vegetation on flow are three-dimensional, so it requires high resolution 3-D models with a high computational effort. Especially for long-term morphodynamic simulations, two-dimensional depth-averaged (2-DH) models are more commonly applied. Therefore, analytical expressions for the bed shear stress on a vegetated bed, meant to be used in 2-DH models, are derived in this thesis (Chapter 4).

To improve the understanding of sediment transport on a vegetated bed, and to test the
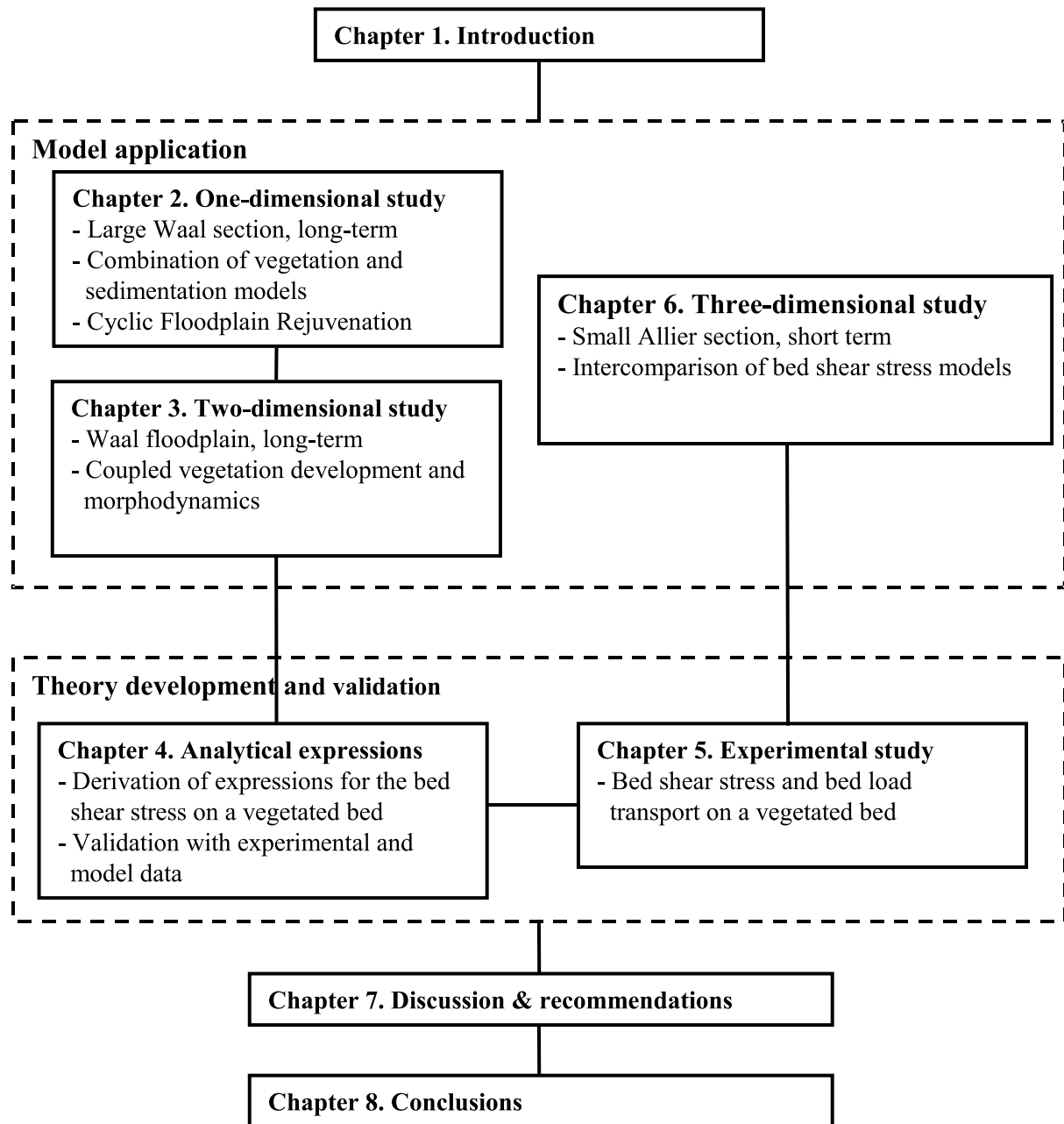
Figure 1.3: Outline of this thesis.

analytical expressions for the bed shear stress derived in Chapter 4, a flume experiment on sediment transport over a vegetated bed has been carried out (Chapter 5). The results of this experiment show that the bed shear stress is reduced significantly with a vegetated bed and that the transport of sediment can be described reasonably well as long as this reduction in bed shear stress is accounted for. On the other hand, further analysis shows that vegetation effects on turbulence and sediment transport capacity are by no means trivial. Especially when the mean bed shear stress is near the initiation of motion of sand particles, additional turbulence generated by the vegetation complicates the process descriptions.

Subsequently, the newly developed knowledge is applied in a case study of a highly dynamic river with important vegetation interactions, the Allier River, France (Chapter 6). The new formulations for the bed shear stress on a vegetated bed are applied and compared using various modelling techniques in 3-D and 2-DH. The results of this case study show that for large scale river model applications, a 2-DH model that includes the analytical expressions for the bed shear stress derived in this thesis gives comparable results for the bed shear stress distribution as a 3-D model for flow and turbulence through and over vegetation. This is an important prerequisite for the numerical 2-DH modelling of morphodynamics affected by vegetation.

Finally, Chapter 7 describes the general discussion and recommendations and Chapter 8 gives the conclusions.

Chapter 2

Modelling floodplain biogeomorphology, a 1-D case study

2.1 Introduction

Along the Rhine River distributaries in the Netherlands, the main embankments provide protection against flooding. The embankments are designed in such a way that the so called 'design discharge' will not lead to flooding of the adjacent land. The design discharge is determined as the flood event with a probability of $1/1250^{th}$ per year. The design discharge was defined at 15,000 m^3/s, but as a result of recent floods in 1993 and 1995, and expected increase of extreme discharges due to climate change, the flood event with a $1/1250^{th}$ year probability has recently been redefined. The design discharge of the Rhine River has now been determined at 16,000 m^3/s (Van Stokkom & Smits, 2002). Without additional flood reduction measures, a flood event of 16,000 m^3/s will result in exceedance of the safe 'design levels'. For the main branch of the Rhine River an increase of the water levels with approximately 20 - 30 cm is expected (Silva *et al.*, 2001). In the past this problem would have been addressed by raising the dikes. Nowadays, new measures are introduced that should result in a more sustainable approach of flood protection. The current flood protection strategy in the Netherlands is based on creating more room for the river by measures such as (i), lowering floodplains, (ii), adapting groynes, (iii), removing hydraulic obstacles in the floodplains, (iv), widening floodplains by dike relocation and (v), excavating secondary channels (Silva *et al.*, 2001; Van Stokkom & Smits, 2002).

The floodplains of the Rhine River are part of the National Ecological Network of the Netherlands (LNV, 2000) and many efforts are made to rehabilitate floodplain nature

(NW4, 1999). Currently, in most floodplains land-use practice prevents natural vegetation succession. However, the proposed flood protection measures provide opportunities for ecological rehabilitation of the floodplains. Following land-use change, the floodplains will develop into a mosaic landscape of different vegetation types, consisting of grassland, herbaceous vegetation and softwood floodplain forest, mainly of willow species (*Salix spp.*) and Black poplar (*Populus nigra*) (Jongman, 1992; Duel & Kwakernaak, 1992; Van Splunder, 1998; Peters, 2002). The mosaic vegetation pattern results from differences in hydromorphology and from the grazing activities of large herbivores that create and maintain open spots between the softwood forest (Cornelissen & Vulink, 2001). In an undisturbed situation a climax stage of forest succession may be reached after more than 100 years and is characterised by a hardwood forest of Oak (*Quercus spp.*), Ash (*Fraxinus excelsior*) and Elm (*Ulmus minor*) (Vera, 2000; Peters, 2002).

Recent river rehabilitation projects in the Netherlands show a successful increase of fluvial biodiversity (Simons *et al.*, 2001; Raat, 2001; Buijse *et al.*, 2002). However, there is an increasing concern over the biodiversity and flood conveyance capacity on the long-term. River rehabilitation projects show a rapid development of willow forests that are increasing the hydraulic roughness of the floodplains. Lowered floodplain sections show a rapid sedimentation and furthermore, trees and bushes trap sediment. Together, these effects reduce the flood conveyance capacity.

Under natural conditions, erosion and sedimentation processes caused by channel migration periodically interrupt vegetation succession and create suitable sites for regeneration of early successional species (Hughes, 1997). These cyclic rejuvenation events are an important mechanism to sustain habitat diversity in natural river systems (Ward *et al.*, 1999; Tockner *et al.*, 2000; Hughes *et al.*, 2001), and is observed in lowland rivers (Salo *et al.*, 1986; Hupp, 1992; Shields *et al.*, 2000), piedmont rivers (Pautou *et al.*, 1997; Piégay, 1997), and mountainous streams (Nakamura *et al.*, 2000). In regulated rivers, such as the Rhine River, uncontrollable erosion and sedimentation processes cannot be allowed. However, without these rejuvenation processes, dense softwood floodplain forests may dominate the floodplain vegetation. As a consequence, both the conveyance capacity and the biodiversity of the floodplains will reduce over time. Therefore, a floodplain management strategy is proposed in which anthropogenic rejuvenation safeguards both flood protection as well as nature rehabilitation objectives (Smits *et al.*, 2000; Duel *et al.*, 2002). This strategy, 'Cyclic Floodplain Rejuvenation (CFR)', aims at mimicking the effects of channel migration by removal of softwood forests, by lowering floodplains and by (re)constructing secondary channels. These measures are applied recursively in case the flood conveyance capacity of floodplains is limiting the flood safety. The measures have to reduce the hydraulic roughness and increase the cross-sectional area of the floodplains. Furthermore, the senescence of softwood forests is prevented by rejuvenating the vegeta-
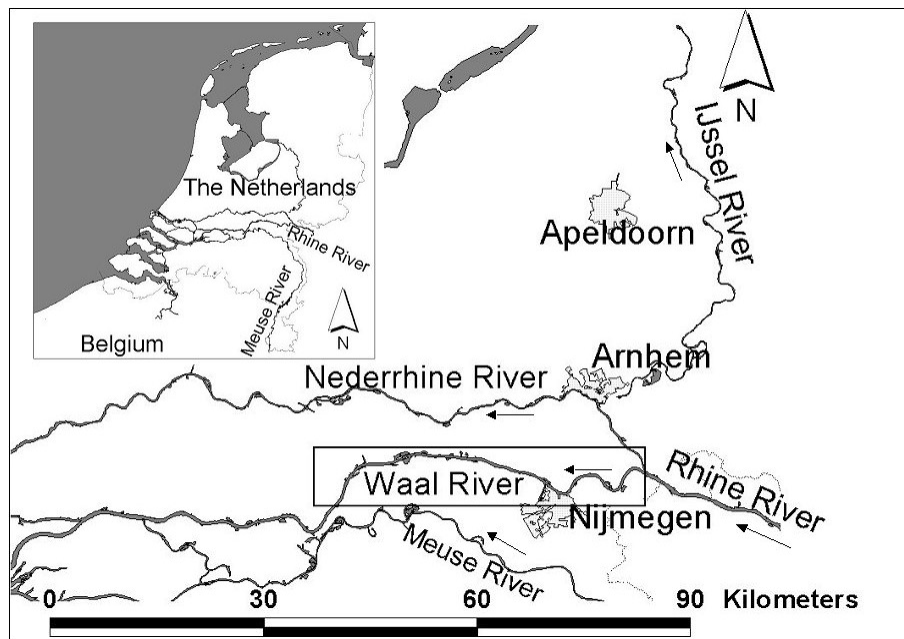
Figure 2.1: The Rhine River branches in the Netherlands. The boxed area denotes the study area in the Waal River branch, the flow direction is from east to west.

tion and introducing bare substrate. This is advantageous for the seedling recruitment of many wet meadow species, for example the Meadow Clary (*Salvia pratensis*) (Hegland *et al.*, 2001), and increases the overall diversity of floodplain habitats. The strategy of Cyclic Floodplain Rejuvenation thus aims to conserve biodiversity in terms of structural diversity (landscape dynamics), functional diversity (ecological succession) and species diversity (Ward & Tockner, 2001). In this study the concept of CFR is applied to the main branch of the Rhine River, the Waal River, using simulation models. The main objective of this study is to assess the frequency and extent of CFR measures with respect to the flood levels and landscape diversity of the Waal River.

2.2 Methods

2.2.1 Study area

The study area comprises 50 km of the Waal River, the largest branch of the Rhine River in the Netherlands, carrying about 2/3 of the total discharge of the Rhine River that enters the Netherlands at Lobith. The study area starts at the bifurcation at Pannerdensche Kop and ends near Vuren, see Fig. 2.1. The focal areas of this study are the 0.5 to 1 km wide embanked floodplains, where a net sedimentation takes place (Asselman & Middelkoop, 1998). Most floodplain sections are in use as pasture land for intensive cattle grazing, with local tree stands and a few fields of arable land. The total floodplain area along the Waal River is 9,500 ha.

2.2.2 Integrated modelling approach

In this study, hydrological, morphological and ecological processes were modelled in an integrated way to predict the development of flood levels over time. Three types of models were used: a hydraulic model, a floodplain sedimentation model and a vegetation development model. The water levels in the Waal River were modelled with the Decision Support System (DSS) - Large Rivers that comprises the one-dimensional hydraulic model system SOBEK (Schielen *et al.*, 2001). This DSS is developed to compute the effects of various river measures on flood levels. Vegetation succession and changes in floodplain sedimentation were simulated in two separate sedimentation and vegetation models. These are rule-based models that were developed in a GIS environment on a two-dimensional rectangular grid of 50 m by 50 m, allowing automation of the knowledge rules. The models were applied with time steps of five years for a simulation period of 50 years (Van der Lee *et al.*, 2001a).

2.2.3 Design and planning of CFR measures

The dimensions of the main embankments along the River Rhine are based on a flood discharge of 15,000 m^3/s, the 'design flood'. The corresponding water levels are the 'design water levels' and are considered as the threshold levels for safety in this study. To accommodate a future flood discharge of 16,000 m^3/s without exceeding these levels, measures to reduce the flood levels are necessary. The model simulations therefore start with the implementation of a suite of water level reduction measures as part of a large-scale flood protection and river restoration scheme, derived from the study of Silva *et al.* (2001). Following a change in land-use from agriculture into nature areas and an additional lowering of the floodplains, these plans aim at a maximisation of natural habitats. Figure 2.2 depicts the different stages for the floodplain developments and Cyclic Floodplain Rejuvenation measures. In Stage I, directly following flood protection measures, the difference between the computed flood levels for a discharge of 16,000 m^3/s and the design water levels is relatively large. This difference will subsequently decline due to morphological and vegetation developments in the floodplains that decrease the conveyance capacity, see Stage II. In case the computed flood levels exceed the design water levels in certain floodplain sections, Cyclic Floodplain Rejuvenation measures are implemented in Stage III. The type of CFR measures that were applied in the model simulations are:

(i) removal of softwood floodplain forest;
(ii) removal of sediment by (re)constructing secondary channels.
(iii) removal of sediment and softwood forest by lowering floodplains;

Following CFR measures, the simulation continues in time steps of five years, until the computed water levels exceed the design levels in parts of the study area again. The exact

side channel

main
river bed

stage I

initial stage:
bare substrate and pioneer vegetation,
no flood risk

stage II

sedimentation and vegetation growth

flood risk

measure I   measure 2   measure 3   **stage III**

1 - removal of vegetation
2 - secondary channel improvement
3 - removal of vegetation and
    sediment in floodplain

no flood risk

the concept of cyclic floodplain rejuvenation

new cycle

E030925h

Figure 2.2: Natural developments and Cyclic Floodplain Rejuvenation in a schematic cross-section. In Stage I, the floodplains have been lowered, new secondary channels have been constructed and pioneer vegetation prevails. Stage I evolves to Stage II, where the conveyance capacity is reduced due to softwood forest growth, filled up secondary channels and floodplain sedimentation. In Stage III Cyclic Floodplain Rejuvenation measures are applied, (1) removal of softwood forest, (2) reconstructing secondary channels and (3) floodplain lowering, including removal of vegetation. CFR measures are repeated when Stage II has been reached again.

type, location and extent of CFR measures were worked out in a GIS containing detailed maps of the study area. An iterative procedure was followed in which the water level reduction effects of a proposed set of measures were assessed with the DSS. Adjustments to the measures were made until the desired water level reduction was attained. Decisions on CFR measures were based on a number of criteria:

1. *The hydraulic effectiveness.* The hydraulic effectiveness of a proposed measure is the most important criterion. The effectiveness differs per measure, based on the type, size and location within the floodplain. For example, when measures are implemented in the conveying part of a floodplain, the hydraulic effectiveness is larger than in the storage part of a floodplain.

2. *The value of landscape elements.* Valuable ecological elements (e.g. hardwood forests), geomorphological elements (e.g. natural levees) or historical elements (e.g. remnants of old settlements) can be preserved although their removal may be hydraulically effective.

3. *The natural mechanisms for rejuvenation.* Rejuvenation by natural processes, such as by channel migration or ice scouring, occurs in specific locations. The anthropogenic rejuvenation can therefore best be located with regard to its natural analogy.

4. *Landscape composition and structure.* The landscape composition and structure of floodplains on a large scale (at least several thousands of hectares) should be maintained and reinforced. Important landscape elements such as sandy banks, softwood forests, hardwood forests, natural levees, marshland and grassland should be proportionally present to increase the naturalness of the floodplains.

2.2.4 The hydraulic model

The hydraulic model system SOBEK was applied in this study. SOBEK is a one-dimensional open-channel dynamic numerical modelling system for unsteady water flow, salt intrusion, sediment transport, morphology and water quality (Verwey, 2001; SOBEK, 2002). The hydraulic model solves the 1-D cross-sectionally integrated shallow water equations of Saint-Venant, distinguishing between the main channel, the flow-conveying floodplain and the storage areas. For each of these areas, properties such as the hydraulic roughness can be defined. In this study, the one-dimensional schematisation of the Rhine River branches in the Netherlands has been used. This schematisation has been developed and calibrated especially for flood forecasting of the Rhine River (Schielen *et al.*, 2001). The model was applied to determine the water levels along the Waal River for a design discharge of 16,000 m^3/s.

Table 2.1: Sedimentation rates for morphological floodplain units of the River Waal (after Asselman, 2001; Mosselman, 2001).

Morphological unit	Deposit composition	Sedimentation rate (mm/day inun.)	(m/year)
Inflow area	sand	1.0	–
Point bar extension	sand	1.0	–
Natural levee	sand	–	0.15
Entrance of slowly aggrading sec. channel	sand	0.2	–
Entrance of moderately aggr. sec. channel	sand	1.0	–
Entrance of fast aggr. sec. channel	sand	2.0	–
Other sections of secondary channel	silt, clay	0.13	–
Rest of floodplain	silt, clay	0.13	–

2.2.5 The sedimentation model

The rule-based sedimentation model distinguishes eight different morphological units defined for the floodplains along the Waal River. A net sedimentation rate was assigned to each unit based on the morphological behaviour of the unit, expressed in millimetres per day of inundation, except for the natural levees. This method implies that the rates of sedimentation decrease as bed elevation increases. The knowledge rules incorporated in the model stem from studies by Asselman (2001), Mosselman (2001) and Asselman and Van Wijngaarden (2002). Low sedimentation rates were defined to be about 2 to 7 cm per 5 years in concordance with field measurements (Asselman & Middelkoop, 1998; Middelkoop & Asselman, 1998). Areas with such low sedimentation rates represent the floodplains receiving fine textured sediments. High sedimentation rates were defined from less than 1 m per 5 years in lowered floodplain sections to nearly 2 m per 5 years in channel entrance sections. The morphological units and their sedimentation rates are presented in Table 2.1. Inundation times were calculated from the water levels computed for a range of river discharges using the digital terrain model of floodplain elevation in the GIS. The frequency of occurrence for each discharge interval was estimated from measured discharges in the periode 1901 - 1995. Estimated inundation times were combined with the mapped morphological units to compute changes in floodplain elevation. After each time step of five years, the floodplain elevation map was updated. The two-dimensional results for floodplain height were aggregated to one-dimensional river cross-sections as input in the hydraulic model.

2.2.6 The vegetation model

In the rule-based vegetation model the development and succession of floodplain vegetation is controlled by four input variables: (i) the inundation duration, (ii) the former

Table 2.2: Succession of vegetation types in rehabilitated floodplains for three classes of inundation and three types of former land-use. Vegetation types distinguish between a homogeneous natural grassland cover, a homogeneous herbaceous vegetation cover and several heterogeneous mosaic patterns of floodplain forest, 10% herbaceous vegetation and remaining cover of grassland (after Van der Lee *et al.*, 2001b).

Time (a) Start	Pasture	Arable land	Bare sand
Inundation <50 d/a			
5	grassland	mosaic I	grassland
10	mosaic I	mosaic I	grassland
25	mosaic I	mosaic II	mosaic I
50	mosaic II	mosaic III	mosaic I
Inundation 50-100 d/a			
5	herbaceous	mosaic I	mosaic I
10	mosaic I	mosaic II	mosaic II
25	mosaic I	mosaic III	mosaic II
50	mosaic II	mosaic IV	mosaic III
Inundation 100-180 d/a			
5	herbaceous	mosaic I	mosaic III
10	mosaic I	mosaic II	mosaic IV
25	mosaic I	mosaic III	mosaic IV
50	mosaic II	mosaic IV	mosaic IV

Legend: mosaic I, mosaic with 0-10% forest; mosaic II, mosaic with 10-25% forest; mosaic III, mosaic with 25-50% forest; mosaic IV, mosaic with 50-100% forest.

land-use (iii) the grazing intensity and (iv) the sedimentation rate (Van der Lee *et al.*, 2001b). Table 2.2 presents the succession series for three classes of inundation duration and three classes of initial conditions for a selection of vegetation types.

In particular the *inundation duration* of a floodplain is a strong discriminating factor with respect to vegetation types (Dister, 1980; Jongman, 1992; Duel & Kwakernaak, 1992; Van Splunder, 1998). In the model, vegetation types are divided into homogeneous vegetation structures and mosaic floodplain forest patterns. Homogeneous structures include pioneer vegetation, grassland, herbaceous vegetation and marsh vegetation. Four classes of mosaic floodplain forest patterns are distinguished. These classes are defined as: 0-10%, 10-25%, 25-50% or 50-100% tree cover. All classes include 10% herbaceous vegetation and the remaining percentage consists of grassland. The *former land-use* of a floodplain is crucial for the direction and rate of natural vegetation succession (Peters, 2002). In the model, a difference is made between a former grassland pasture, a former arable land or a sandy,

Table 2.3: Nikuradse roughness height of vegetation types (after Van der Lee *et al.*, 2001b).

Vegetation type	Nikuradse roughness height (m)
Homogeneous vegetation types	
Bare substrate / pioneer vegetation	0.2
Structure-rich floodplain grassland	0.8
Herbaceous vegetation	2.0
Marsh vegetation	5.0
Vegetation mosaics	
0-10% floodplain forest	1.84
10-25% floodplain forest	3.22
25-50% floodplain forest	5.52
50-100% floodplain forest	10.00

bare substrate. The shortest time to reach the climax stage with a closed canopy is when the succession starts from a sandy, bare substrate combined with a relatively high inundation duration of 100 - 180 days per year (d/a). When the floodplain is inundated for more than 180 d/a only pioneer or herbaceous vegetation can persist. *Grazing* by large herbivores such as cows and horses creates mosaic patterns consisting of forest, grassland and herbaceous vegetation (Cornelissen & Vulink, 2001). In the model, a low grazing pressure of one animal per 3 hectare is assumed, which leads to a natural mosaic pattern. High *sedimentation* rates can reset vegetation succession (Peters, 2002). Sedimentation is incorporated in the model by using the output from the sedimentation model. When the sedimentation rates were higher than 0.2 m/a, a transfer of grassland and/or herbaceous vegetation to bare substrate takes place, while leaving floodplain forest unaffected (Van der Lee *et al.*, 2001b). The vegetation patterns that result from the vegetation model were subsequently converted to a hydraulic roughness for each floodplain section. The hydraulic roughness of vegetation is defined in terms of a Nikuradse equivalent roughness height in metres (Nikuradse, 1930). The hydraulic roughness of each one-dimensional cross-section was calculated by the weighted average of the hydraulic roughness for each vegetation pattern, weighted by the surface area from the two-dimensional vegetation model. For each time step of five years, a new vegetation pattern results in a new hydraulic roughness value that was compared to the roughness value at the start of the simulation. Subsequently, the relative change in roughness value is multiplied with the initial calibrated roughness value. The new roughness values thus obtained for each floodplain section were used as input for a new computation of flood levels. Table 2.3 presents the hydraulic roughness data for the vegetation types used in the model.
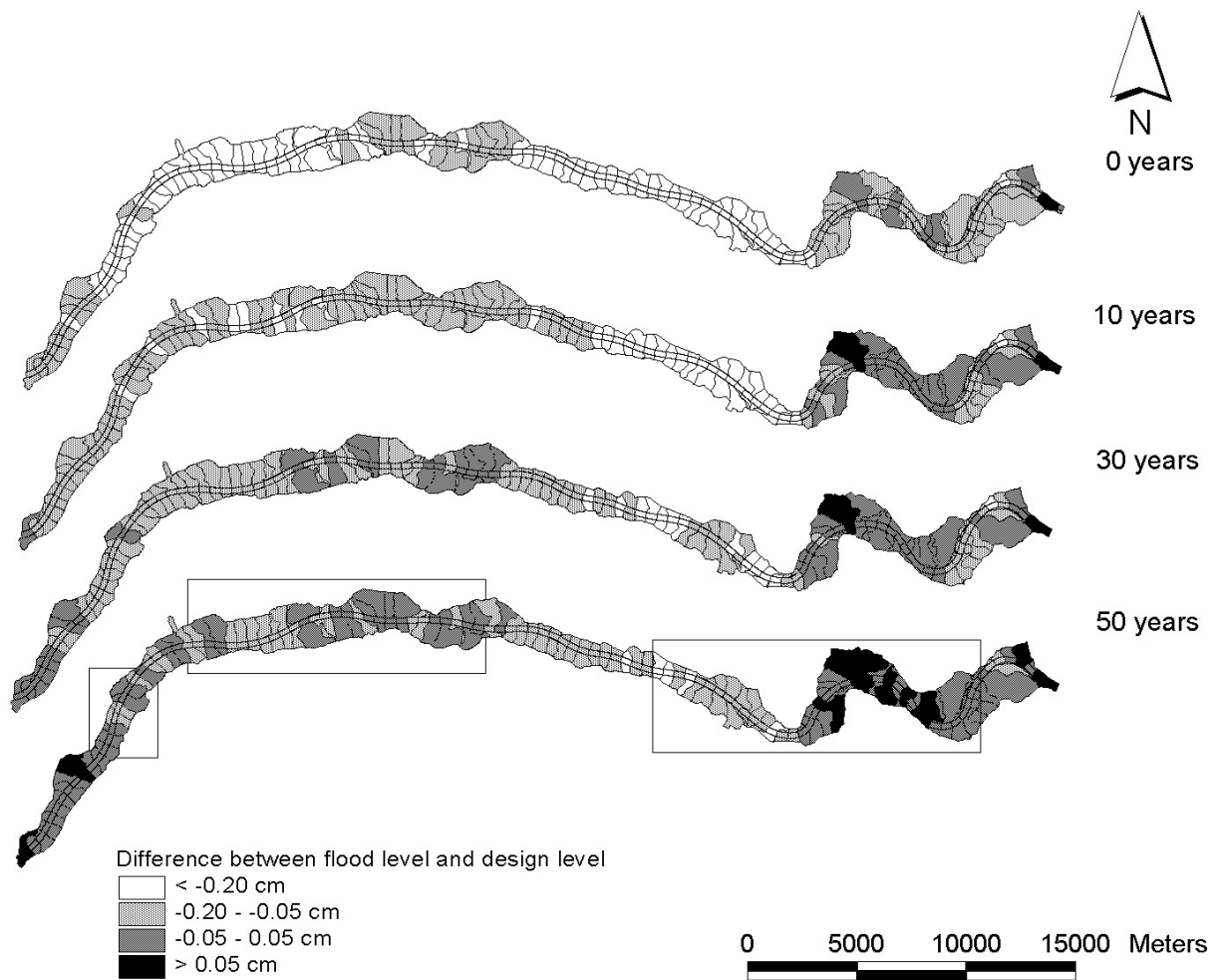
Figure 2.3: Difference between the computed flood level at 16,000 m³.s⁻¹ and the design level for floodplain sections of the Waal River, 0, 10, 30 and 50 years after initial flood protection measures. The boxed areas indicate parts where cyclic floodplain rejuvenation was applied.

2.3   Results

2.3.1 Computed flood levels and CFR measures

Figure 2.3 presents the difference between the computed flood levels and the design levels per floodplain section at 0, 10, 30 and 50 years after the initial flood protection measures, and includes the water level reduction by CFR measures. CFR measures were applied at 10, 25 and 35 years in the floodplain areas that lie within the boxes shown for $t = 50$ years. The difference between the excess design levels above the computed flood levels is defined as the 'allowable rise' in water level that will decline due to sedimentation and vegetation development. Figure 2.3 shows that the allowable rise in water level varies considerably along the river stretch of 50 km at $t = 0$. In a few floodplain sections it reaches only 5 cm, whereas in most sections it is more than 20 cm. The most upstream floodplain sections (the meander bends to the east) show the smallest allowable rise because these are lo-

Table 2.4: Removed sediment volume, removed softwood forest and total areas affected by the CFR measures in the Waal River. The area of removed softwood forest is converted to hectares of 100% forest cover (from Duel *et al.*, 2001).

Implementation (years after restoration)	Removed sediment volume (10^6 m^3)	Removed forest (ha of 100% forest cover)	Total area affected by CFR measures (ha)
10	5	100	530
25	5	30	230
35	12	230	1230

cated upstream of the hydraulic bottleneck of the city of Nijmegen. The increase in water levels in the first ten years after the initial flood protection measures is relatively large, because softwood floodplain forests with a relatively high hydraulic roughness develop rapidly. In addition, the sedimentation rates on the floodplains are also relatively high in response to the floodplain lowering. During the simulated 50 years it appeared to be necessary to implement CFR measures in various floodplain parts at 10, 25 and 35 years after the initial flood protection measures. At $t = 10$ years the measures concentrated on the most upstream meander bends. An additional secondary channel was constructed, parts of the floodplain were lowered to create shallow floodplain lakes and in other parts the floodplain was lowered and the softwood forest was rejuvenated to herbaceous vegetation. These measures realised a water level reduction of 3.0 cm. At t = 25 years, existing secondary channels were deepened in the upstream section, an additional secondary channel was created in the downstream section and parts of the downstream floodplains were rejuvenated to wet grassland. These measures realised a water level reduction of average 3.0 cm to maximum 5.5 cm. At t = 35 years, existing secondary channels were deepened in the upstream section. Furthermore, a large-scale floodplain lowering by 1 metre, including softwood forest removal, was applied in the downstream section. These measures realised a water level reduction of average 7.5 cm to maximum 14.0 cm. Table 2.4 presents key figures for the CFR measures that were applied in the model calculations.

2.3.2 Sedimentation in the floodplains

The total cumulative volume of sediment added to the floodplains averaged 4·10^6 m^3 per 5 years. This corresponds to an average increase of floodplain height of 0.8 cm/a. During the first decade the accumulation of sediment was highest. Sedimentation rates were generally low in alleviated floodplain parts and high in the lowered floodplain parts and excavated secondary channels. Ten percent of the floodplain area of the Waal River was responsible
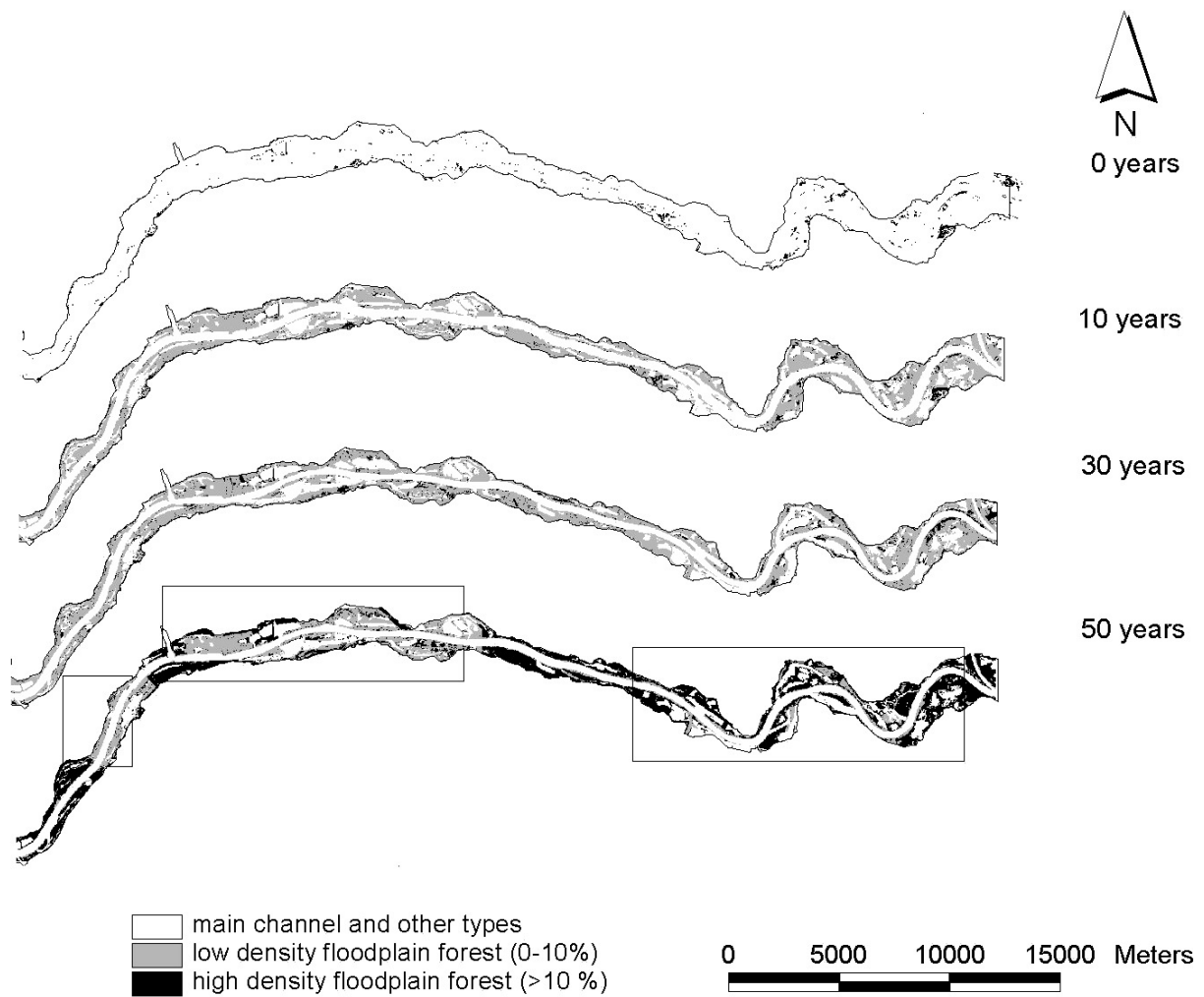
Figure 2.4: Floodplain forest cover in the Waal River, respectively 0, 10, 30 and 50 years after initial flood protection measures. Boxed areas indicate parts where cyclic floodplain rejuvenation was applied.

for as much as 30 - 50% of the total accumulated sediment volume during the simulation period.

2.3.3 Floodplain vegetation development

The model simulations show how the initial pioneer vegetation develops into different types of floodplain vegetation and softwood forest mosaics. Figure 2.4 presents the floodplain forest development at respectively 0, 10, 30 and 50 years after the initial flood protection measures and includes the effects by CFR measures. CFR measures were applied at 10, 25 and 35 years in the floodplain areas that lie within the boxes shown for t = 50 years. In the first decades the forest cover is generally less than 10%, the floodplain landscape consists mainly of herbaceous vegetation and grasses with sparse patches of trees. From 30 years onwards the forest cover increases to 10 - 25%. Areas that have a

Table 2.5: Vegetation development in steps of 10 years for the Waal River (after Duel *et al.*, 2001), compared to the historical reference (after Postma *et al.*, 1995; Pedroli *et al.*, 1996).

Vegetation type	Historical reference (ha)	10-years' ecological development following river resoration (ha)				
		10a	20a	30a	40a	50a
Floodplain forest	>1250	1000	1000	1100	1600	1800
Floodplain marshland	> 300	<100	<100	<100	<100	<100
Dry grasslands	> 100	3100	3900	3600	3100	3200
Wet grasslands	>1000	1400	1300	1200	1200	1100
Dry herbaceous vegetation	> 150	400	400	500	400	500
Wet herbaceous vegetation	> 500	300	200	300	200	200

forest cover of more than 25% are scarce and develop locally along the river and on the banks of secondary channels. They are not presented in Fig. 2.4. Each time when softwood forest was removed, the vegetative succession was set back and floodplain forest mosaics regenerated from pioneer vegetation, with an intermediate stage of herbaceous vegetation. The effect of softwood forest removal is visible in the forest cover at t = 50 years, where the cover in the rejuvenated parts is significantly different from the cover in the other parts. Over the 50 years simulation period, the total area of floodplain forest increased significantly, despite the CFR measures in which forest was removed in relatively large areas. Table 2.5 presents the model outcome for the development of major vegetation types compared to the historical reference for the Waal River. The historical reference denotes the distribution of vegetation types in the historical, non-regulated Waal River (Postma *et al.*, 1995; Pedroli *et al.*, 1996). Our model outcomes show that the strategy of Cyclic Floodplain Rejuvenation results in a diverse floodplain vegetation that largely complies with the historical reference, although vegetation types such as marshland and wet herbaceous vegetation are insufficiently present.

2.4 Discussion

2.4.1 Frequency and extent of rejuvenation

This study indicates that considerable floodplain areas are needed to meet both flood protection and nature restoration goals using the Cyclic Floodplain Rejuvenation strategy. The model simulations have shown that CFR is optimally applicable in river stretches where a relatively large allowable rise of more than 20 cm in water level is available before the critical flood level is reached. A large allowable rise is favourable because then the rejuvenation frequency can be limited to once per several decades and undisturbed

vegetation succession to softwood forests with a closed canopy can be allowed in the floodplains. An appealing aspect of the CFR strategy is that it allows river managers to choose in which location what types of measures can be implemented. One can for example decide to leave an existing forest on the one river bank unaffected by choosing to deepen a filled up secondary channel on the other river bank. On the other hand, certain locations will be more effective in reducing water levels than others, for example in places where sedimentation is large or where floodplain forest grows in flood-conveying parts. With the exception of the section upstream of the hydraulic bottleneck of Nijmegen, floodplain rejuvenation was applied in 1400 hectares, or 15% of the total floodplain area, at 25 and 35 years after the initial flood protection measures. After 50 years of simulation, the computed flood levels were beneath the design levels for the majority of the floodplain sections, although the water levels were still rising. Sedimentation in the floodplains continued, especially in those parts where floodplain lowering as CFR measure was applied, and the softwood forest cover also increases. The rate of increase of the water levels however was reduced compared to the initial situation directly following the large-scale flood protection measures. Cyclic Floodplain Rejuvenation with a return period of 25 to 35 years in an area of 15% of the total floodplain area seems to control the flood levels on the longer term. The exception is formed by the river sections upstream of the hydraulic bottleneck where the intervention frequency needed to be increased to 10 to 15 years. In these bottleneck areas CFR is not an appropriate strategy and it might be better to look for alternative methods, such as widening the river by setting back the main embankments or constructing a river by-pass (Van Alphen, 2002). An anthropogenic rejuvenation of 15% of the floodplain area in 25 to 35 years time corresponds to historical data on natural rejuvenation of the Waal River. In the period between 1780 and 1830, the non-regulated free-flowing floodplains were characterised by a mean rejuvenation rate of 0.4% per year (Wolfert, 2001). This equals 10% in 25 years, or 14% in 35 years time. The extent of the cyclic floodplain rejuvenation measures therefore fit to the historical reference for the Waal River.

2.4.2 Knowledge shortcomings

The results of the hydraulic model computations rely on the model calibration for flood conditions. Various sensitivity and uncertainty tests have therefore been carried out with the model system (Silva *et al.*, 2001). Though state-of-the-art, the results of this study have to be interpreted with care, since the modelling is based on simplifications of complex, natural processes. Rule-based models for both vegetation succession and floodplain sedimentation are based on best-available knowledge, but there remains a large uncertainty in their outcomes, because there is little experience yet with floodplain lowering. The best example is a floodplain near the town of Ewijk that was lowered in 1988. After floods in 1993 and 1995, each time a volume of $0.22 \cdot 10^6$ m^3 of sand has been deposited with an average thickness of 10 to 20 cm (Sorber, 1997). Locally more than 50 cm of deposited

sand was found (Schoor, 1999). These figures are in accordance with our simulation results. The floodplain of Ewijk further showed a fast regeneration of softwood forests on bare substrate, to the extent that after 12 years a dense willow forest has developed (De Heij, 2001), which is also in accordance with our model results. The conveyance capacity of this floodplain has become too low now and a new cycle of rejuvenation is planned. Nevertheless, additional studies focusing on the hydraulic roughness of vegetation, vegetation succession and interaction between vegetation and sedimentation are needed to improve the predictive value of the simulation models.

2.4.3 Application to other rivers

The management strategy of Cyclic Floodplain Rejuvenation has been designed to find symbiosis between flood protection and nature rehabilitation in highly regulated rivers where navigation and safety prohibit fully natural rejuvenation processes. Cyclic Floodplain Rejuvenation may be a feasible strategy in rivers where geomorphic dynamics has diminished and flood safety is a concern, in the USA (USACE, 2000; Bolton & Shellberg, 2001), as well as in Europe (Buijse et al., 2002). In highly regulated rivers it is impossible to return the ecosystem to its pristine state (Amoros et al., 1987). Moreover, it may even prove difficult to reintroduce geomorphological dynamics that are strong enough to restore habitat heterogeneity. This approach of process-oriented river restoration is tried in several river systems. The 'Danube Restoration Project' aims to bring back geomorphic dynamics to enhance natural rejuvenation at Regelsbrunn, Austria (Schiemer et al., 1999). In the Rhône River, France, just downstream of the confluence with the Saône River, geomorphological dynamics in two side-arms were restored in order to bring back flood scouring (Amoros, 2001). In the Brenno River, Switzerland, the geomorphological impact of flooding is severely reduced, and managing the discharge regime may induce natural rejuvenation (Brunke, 2002). We feel that in such cases the strategy of Cyclic Floodplain Rejuvenation might help in restoring natural dynamics.

2.5 Conclusions

In the coming decade(s), large-scale flood protection and river restoration projects will be carried out along the entire Dutch Rhine River with the objective to increase the flood conveyance capacity and to rehabilitate floodplain habitats. Without further measures implemented in the adjacent land (i.e. flood relief channels, detention areas), it is necessary to regularly reset vegetation succession and to remove deposited sediment in order to sustain safe flood levels and increase landscape diversity. It was demonstrated that the flood management strategy of Cyclic Floodplain Rejuvenation is able to sustain safe flood levels in the Waal River when about 15% of the total floodplain area is rejuvenated with a

return period of 25 to 35 years. Furthermore, applying the management strategy of Cyclic Floodplain Rejuvenation leads to a diverse floodplain vegetation distribution that largely complies with the historical reference for the Waal River. Cyclic Floodplain Rejuvenation may be the appropriate answer to find symbiosis between flood protection and nature rehabilitation in highly regulated rivers.

Chapter 3

Modelling secondary channel biogeomorphology, a 2-D case study

3.1 Introduction

The previous chapter has demonstrated that, based on a one-dimensional modelling study, the Cyclic Floodplain Rejuvenation strategy might be able to serve two seemingly conflicting goals, i.e. increasing flood safety and biodiversity. A next step would be to apply a two-dimensional numerical model to test the strategy more thoroughly. A two-dimensional model can link spatial information on vegetation development and floodplain topography to simulations of the hydrodynamic and morphodynamic developments in floodplains. In this chapter, a first effort is made to model the biogeomorphological interactions of three secondary channels located in a floodplain section of the River Waal, near the town of Gameren.

Secondary channels are constructed to increase the conveyance capacity and simultaneously restore floodplain nature (Silva *et al.*, 2001; Wolfert, 2001). Man-made secondary channels have been constructed in the Rhine River since the nineties. Monitoring shows that these channels provide suitable habitat for rheophilic macroinvertebrates and fish (Grift, 2001; Simons *et al.*, 2001). However, the combination of constructing secondary channels to increase the conveyance capacity and to develop nature in floodplains is potentially conflicting, since the growth of vegetation increases hydraulic resistance and might enhance sedimentation. It is expected that the entrance of secondary channels will silt up and that the desired increase in the conveyance capacity will gradually diminish. Another potential problem is that uncontrollable erosion of the secondary channels can undermine the river embankment or cause piping, which leads to an increased safety hazard. River managers therefore need to know at what rate these natural developments take place in order to plan measures to undo the detrimental effects on flood safety. Furthermore, they want to know how the biodiversity is affected by these developments.

The morphological developments of secondary channels in general, and the relationship with floodplain vegetation in particular, are not completely understood. Historic refer-
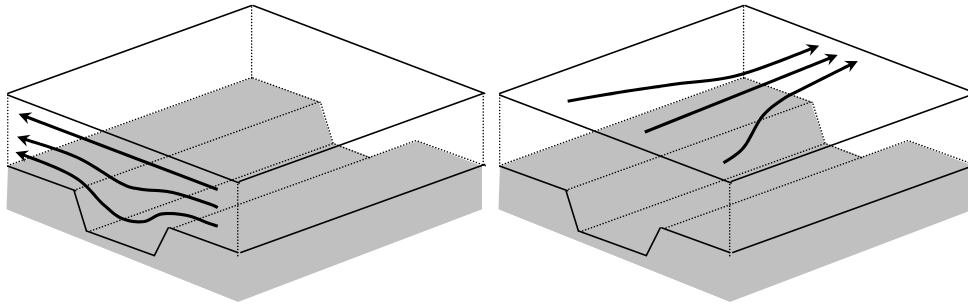
Figure 3.1: Distribution of flow fields in secondary channels. Left panel: conservation of mass gives stronger flow in shallower areas. Right panel: conservation of momentum gives stronger flow in deeper areas.

ences are not representative, present conditions have been changed with regard to the construction of sills at the entrances of channels, the present floodplain height is elevated and groynes are now present in the main channel. To predict the natural developments of the man-made secondary channels, mathematical models need to be developed. This case study explores and models the developments of geomorphology in relation to vegetation development in secondary channels in the Waal River. The study approach is to model the long-term morphological trends in the secondary channels in the Gameren floodplain in combination with the modelling of the growth and succession of floodplain vegetation.

3.1.1 Floodplain vegetation and morphodynamics of secondary channels

The morphological development of secondary channels under in-bank flow conditions, when the flow is limited to the channel itself, differs from the development under overbank flow conditions. For in-bank flow conditions, two parameters are important: the ratio between the lengths of the two branches and the bifurcation angle between the branch and the upstream flow direction (Bulle, 1926). The influence of the latter is related to the spiral water motion generated in curved flows. For overbank flow conditions, the effects of the channel on the flow field depends on the orientation of the secondary channel, Fig. 3.1. Conservation of mass is the dominating principle that governs flows that cross a secondary channel under a large angle. This causes a local deceleration of the flow. As a consequence, the channel works as a sediment trap. When the flow makes only a small angle with the secondary channel, conservation of momentum is the dominating principle that governs the flow field. The secondary channel then works as a zone of lower hydraulic resistance, accelerating the flow. As a consequence, the secondary channel attracts flow and may grow through erosion (Mosselman, 2001).

The presence of floodplain vegetation may affect the flow field of secondary channels in various ways. Floodplain vegetation may enhance the flow velocity in channels when the hydraulic resistance of the secondary channel is much lower than that of the vegetated banks. However, Kitamura *et al.* (1998) have shown that when the proportion of vegetation
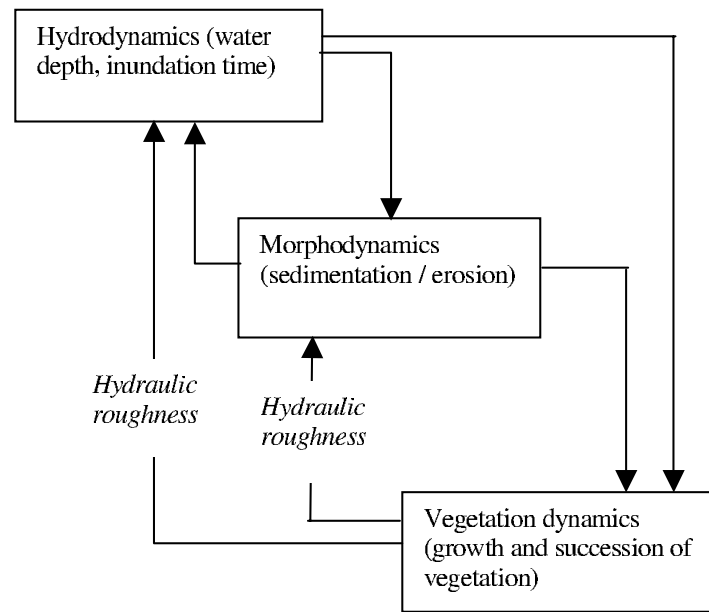
Figure 3.2: Conceptual framework of the relationships between hydrodynamics, morphodynamics and vegetation dynamics in this study.

in the cross-section increases, the total flow resistance increases, thus leading to higher water depths and reduced flow velocities. To study the effects of these interactions on the morphodynamics of secondary channels, numerical modelling can be applied.

The morphological development of secondary channels can be computed with one-, two- or three-dimensional morphodynamic models. The simpler approach of using a one-dimensional model requires an empirical 'nodal point relation'. This relation expresses the ratio of the sediment transport rates into the main channel and the secondary channel as a function of other parameters. Usually its details are poorly known. That is a serious problem, because the time scale and end state of the morphological development depend critically on this relation. As a consequence, one-dimensional computations of the morphological development of secondary channels are inherently inaccurate. For two- and three-dimensional models, data requirements and computational effort are very demanding. Moreover, there is a lack of good submodels for some of the key processes, because application of two- and three-dimensional models to floodplain morphodynamics is only a recent development. Applications in the past were traditionally limited to river engineering problems in the main channel. Considering the shortcomings of three-, two- and one-dimensional modelling, this case study aims at a two-dimensional numerical modelling approach to quantify the morphodynamic developments in secondary channels influenced by vegetation development.
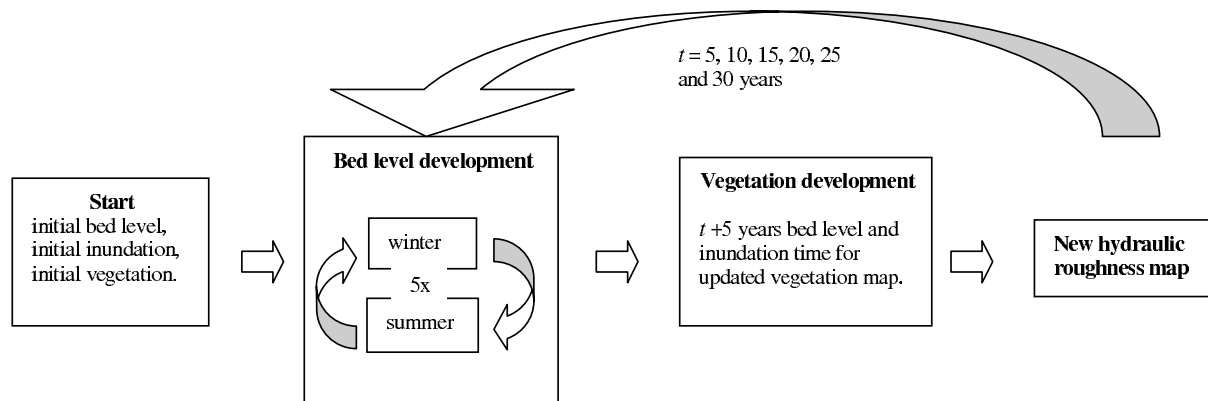
Figure 3.3: Flow diagram of the computational procedure.

3.1.2 Study approach and objective

In this case study, a two-dimensional application of the numerical model Delft3D-MOR is applied in combination with the vegetation succession model that is described in Section 2.2.6 of this thesis. The model equations of Delft3D-MOR for river morphodynamics are described in Struiksma *et al.* (1985) and Jagers (2003). In addition, a key aspect of this study is that a coupling is made between the changing hydraulic roughness of vegetation over time and its effects on the hydro- and morphodynamics, as depicted in Fig. 3.2. The flow diagram of the computational procedure is depicted in Fig. 3.3. A coupling has been realised in which after each period of five years, the output from Delft3D delivers the abiotic conditions for the vegetation model. This results in a new map of hydraulic roughness for the floodplain that is fed back into a new Delft3D computation. The morphodynamics of the secondary channels have been evaluated for two different cases:

1.   Without vegetation development, i.e., the initial vegetation composition and distribution remains unchanged;

2.   With vegetation development, i.e., growth and succession of vegetation changes the vegetation composition and distribution and therefore the hydraulic roughness.

The objective of this case study is to assess the morphodynamic behaviour of secondary channels under either condition of vegetation development over a thirty-year period, to increase insight into the physical processes and into the shortcomings in our knowledge. For background reading, reference is made to Baptist and Mosselman (2002), Baptist (2001a), Duel *et al.* (2001), Van der Lee *et al.* (2001b) and Kerle *et al.* (2001).

3.1.3 Study area

The study area is the Gameren floodplain at the left bank of the river Waal just west of Zaltbommel, the Netherlands. After a high flood in 1995, a dike improvement project near
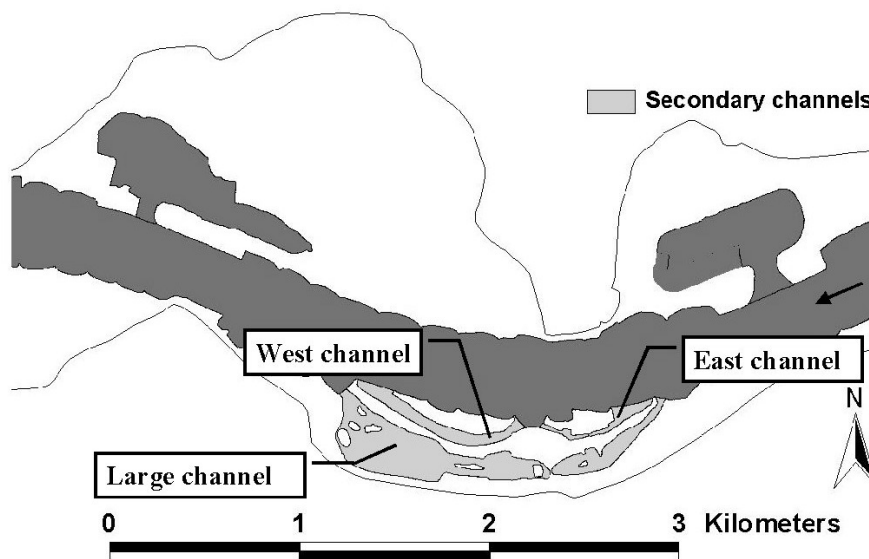
Figure 3.4: Secondary channels in the Gameren floodplain.

Table 3.1: Secondary channel characteristics.

	East	West	Large
Length (km)	0.5	1.0	2.0
Entrance level (m NAP)	2.04	0.95	–
Design inundation time (d.a^{-1})	100	265	365
Min. discharge for flow (m^3.s^{-1})	1511	821	–
Year of completion	1996	1996	1999

the town of Gameren was carried out. Large amounts of clay and sand were excavated from the Gameren floodplain to create three secondary channels. The aim of this project was to create the right conditions for characteristic river-bound flora and fauna, as part of a nature development scheme, and to increase the conveyance capacity of this part of the river. The Gameren floodplain is now a nature reserve of 144 hectares. Here, river dynamics are given full play, as long as this does not lead to an increased safety hazard. Grazing by herbivores in low densities (less than 1 head of cattle per 3-5 ha) is applied as nature management (Jans *et al.*, 2001). Figure 3.4 presents the location of the three secondary channels within the Gameren floodplain. The three channels have different characteristics, see Table 3.1. The West and East Channel have sills at their entrance that determines the frequency of flow through these channels. The Large Channel does not have a weir and is permanently flowing. The Large Channel includes a deep former sand-mining pit close to the downstream end.
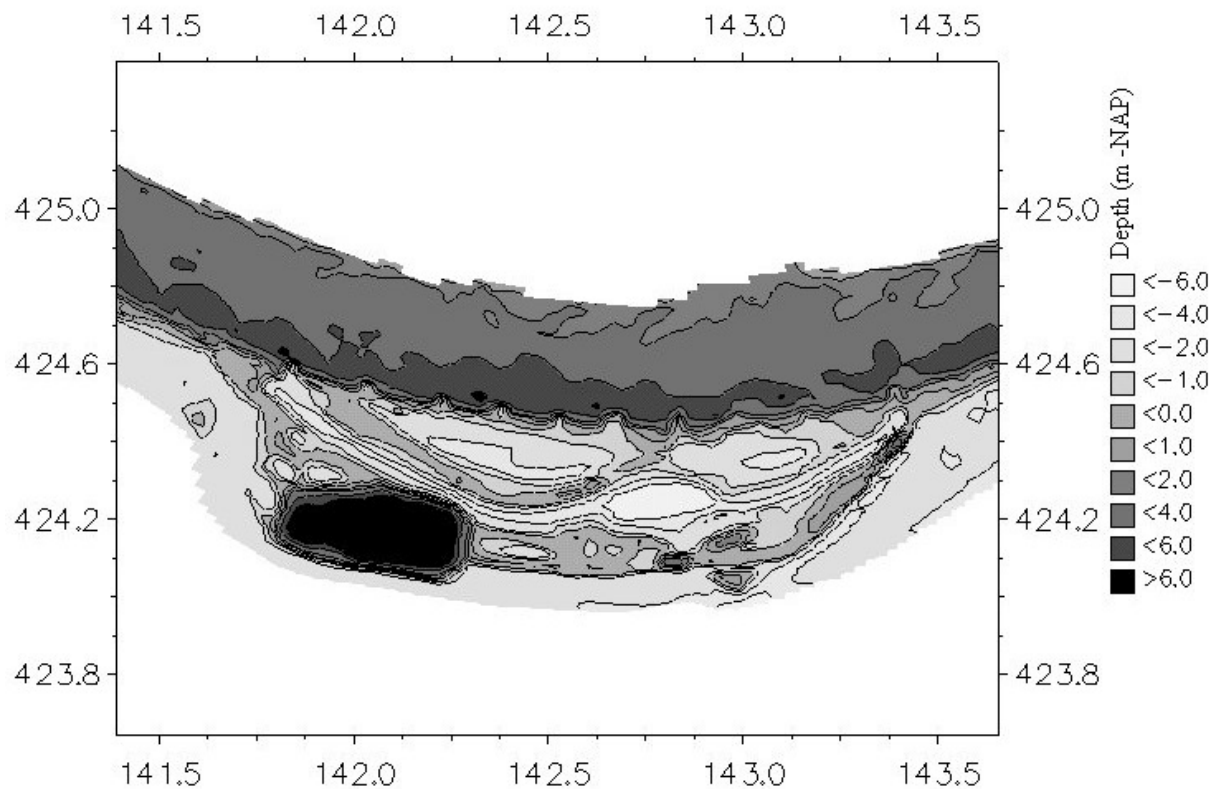
Figure 3.5: Initial bed topography

3.2   Model description

Model grid and topography

A two-dimensional horizontal curvilinear grid has been defined for the study area. The grid covers an area of approximately 5.5 km by 1.0 km and includes the main channel and the floodplains south of the main channel. The total number of grid cells used for the computations is 13,872. The grid cells within the Gameren floodplain are roughly 30 m long and 10 m wide. For the definition of the bed topography in the grid cells, monitoring data from the Institute for Inland Water Management and Wastewater Treatment (RIZA) were used. These Digital Elevation Model (DEM) data totaled 65,535 data points for both the main channel and the floodplains within the model grid area. The DEM point data were transposed to the computational grid to obtain the bed topography. The first year in which all three channels were operational is 1999, but because of an error in the bed topography measurements of 1999, it was decided to use the measurements of 2000 for the initial bed topography. Figure 3.5 presents this initial bed topography, in which a positive depth indicates metres below the Dutch datum NAP.

Table 3.2: Nikuradse roughness (k_N) for ecotopes.

Ecotope	k_N (m)
Forest and shrub (softwood/hardwood)	10.0
Structure-rich herbaceous vegetation and reed	5.0
Open herbaceous vegetation	2.0
Structure-rich floodplain grassland	0.8
Floodplain grassland	0.5
Poor floodplain grassland	0.4
Bare substrate and production grassland	0.2

Boundary conditions

At the upstream model boundary the discharge distribution is prescribed, at the downstream model boundary the water level. The discharge at the upstream boundary is distributed over each grid cell of the boundary in function of Chézy roughness, grid cell width, water level slope and water depth. The upstream inputs of sediment have been taken equal to the local sediment transport capacities, such that the bed level remains at its original value. For the downstream water level boundary a stage-discharge relationship is interpolated between measurement stations up- and downstream of the study area. Furthermore, the downstream boundary is defined as weakly reflecting, so that free surface waves are absorbed.

Initial hydraulic roughness

The hydraulic roughness of the model area is defined in the traditional way, by applying a Nikuradse equivalent roughness height (Nikuradse, 1930). The hydraulic roughness of the floodplain is obtained by combining an existing map of floodplain ecotopes with their corresponding roughness values, which are derived from Verheij (2000). The roughness height is subsequently used in the White-Colebrook formula to derive a Chézy roughness. Table 3.2 presents a summary table for different ecotope types and their Nikuradse equivalent roughness heights. The hydraulic roughness of the main and secondary channel beds was set to 0.2 m.

Sediment transport

The sediment transport formula of Engelund and Hansen (Engelund & Hansen, 1967) was applied in this study. This formula is based on the balance between the work required to elevate the sediment load and the work to move the particles over the bed form length. The Engelund and Hansen formula is a total load transport formula, describing the combined

transport rate of bed load and suspended load. It is particularly suitable for rivers with substantial suspended load (Jansen *et al.*, 1979). For the modelling of sediment transport in secondary channels of the Waal this formula is considered the most suitable total transport formula. The Engelund and Hansen formula can be written as:

$$s = mu^5 \tag{3.1}$$

in which:

$$m = \frac{0.05\alpha}{\sqrt{g}C^3\Delta^2 D_{50}} \tag{3.2}$$

where s is the total sediment transport capacity per unit width, expressed in volume of transported sand (m^2/s), u is the flow velocity (m/s), g is the acceleration due to gravity ($m\cdot s^{-2}$), C is the Chézy coefficient ($m^{1/2}\cdot s^{-1}$), Δ is the relative density of sediment under water (1.65), D_{50} is the median grain size (m) and α is a calibration parameter (-). A uniform median grain size is applied. However, a distinction is made between the sediments in the main channel and in the secondary channels, on the basis of measurements. The median grain size is defined as 300 μm for the secondary channels and 1000 μm for the main channel. The Engelund and Hansen formula does not take into account any influence of vegetation on sediment transport, but neither does any other existing sediment transport formula.

The morphodynamic computations start with a hydrodynamic computation to obtain equilibrium flow conditions for a given steady discharge and a given initial bed topography. The sediment transport computation and the corresponding bed level update run in a loop and additionally new hydrodynamic computations are made after every 10 loops. The bed level changes are computed using a sediment balance equation, which essentially states that deposition or erosion of sediment in a computational grid cell is proportional to the divergence of the transport vector field. The bed level changes affect the flow velocities, which in their turn affect the sediment transport capacity in a feedback cycle.

The simulation of the morphodynamic behaviour is carried out with two alternating steady discharges that represent an average summer discharge and an average winter flood respectively. The model aims at forecasting long-term average conditions. The summer discharge is defined at 1500 m^3/s and the winter discharge at 5000 m^3/s. The annual sediment transport of the Waal river equals 300,000 m^3 to 400,000 m^3, expressed as bulk volume, so including pore space (Visser, 2000). The calibration factor, α, in Eq. (3.2) was defined such that the total transport over one week of a steady flood discharge yields the total transport for a winter flood, approximately 250,000 m^3/a. Applying the same value for α, four summer weeks yield the total transport for an entire summer, approximately 60,000 m^3/a. In this way one year is represented by two stationary seasons and the computational effort is strongly reduced. The value for α was determined at 0.7. In total thirty years of morphodynamic developments were simulated.

Non-erodible layer

In some parts of the model schematisation a so-called non-erodible layer is defined. This layer is applied in regions where erosion is not possible (for example for groynes and paved terrain) or not realistic. The presence of a non-erodible layer reduces the magnitude of the sediment transport over this layer (Struiksma, 1999). In this application, grid cells that represent groynes were made non-erodible, as well as the floodplains that are not located in the Gameren system itself and those parts in the Gameren floodplain that are higher than NAP +3m. In this way, erosion of these areas is prevented.

3.3 Results

3.3.1 Vegetation

According to the model, the growth and succession of vegetation results in a gradual increase of softwood forest cover in the mosaic vegetation types. A primary trend is that softwood trees in increasing density will gradually replace the previous floodplain cover of grassland and ruderal vegetation types. Secondarily, softwood forest may quickly develop on bare substrate. The results show that after thirty years the inflow opening of the West Channel is filled up to such a level that floodplain vegetation can develop. The point-bar that develops in the inner bend will also be covered by grassland and softwood trees. The main part of the smallest East Channel is covered with floodplain grassland, ruderal vegetation and softwood forest after thirty years of simulation.

3.3.2 Channel morphology

The influence of riparian vegetation on river morphology can be subdivided in a *remote* effect and a *local* effect. The *remote* effect is an effect on river morphology caused by the redirection of flow patterns due to the presence of riparian vegetation. An example is the presence of vegetation on a point bar. Due to the increased hydraulic roughness of the point bar vegetation, the flow is forced towards the outer bend, leading to enhanced transport in the main channel and possibly an enhanced erosion of the outer bend. The *local* effect concerns the morphology in between the vegetation. An example is the enhanced settling of sediment on a point bar due to the presence of vegetation.

Figure 3.6 presents the bed topography for the three channels after thirty years of model simulation including vegetation development. Figure 3.7 presents the morphology after thirty years of model simulation without further vegetation development. These maps indicate significant effects on the channel morphology in parts of the channels. Modelled trends and differences in channel morphology were analysed for sections of the Gameren
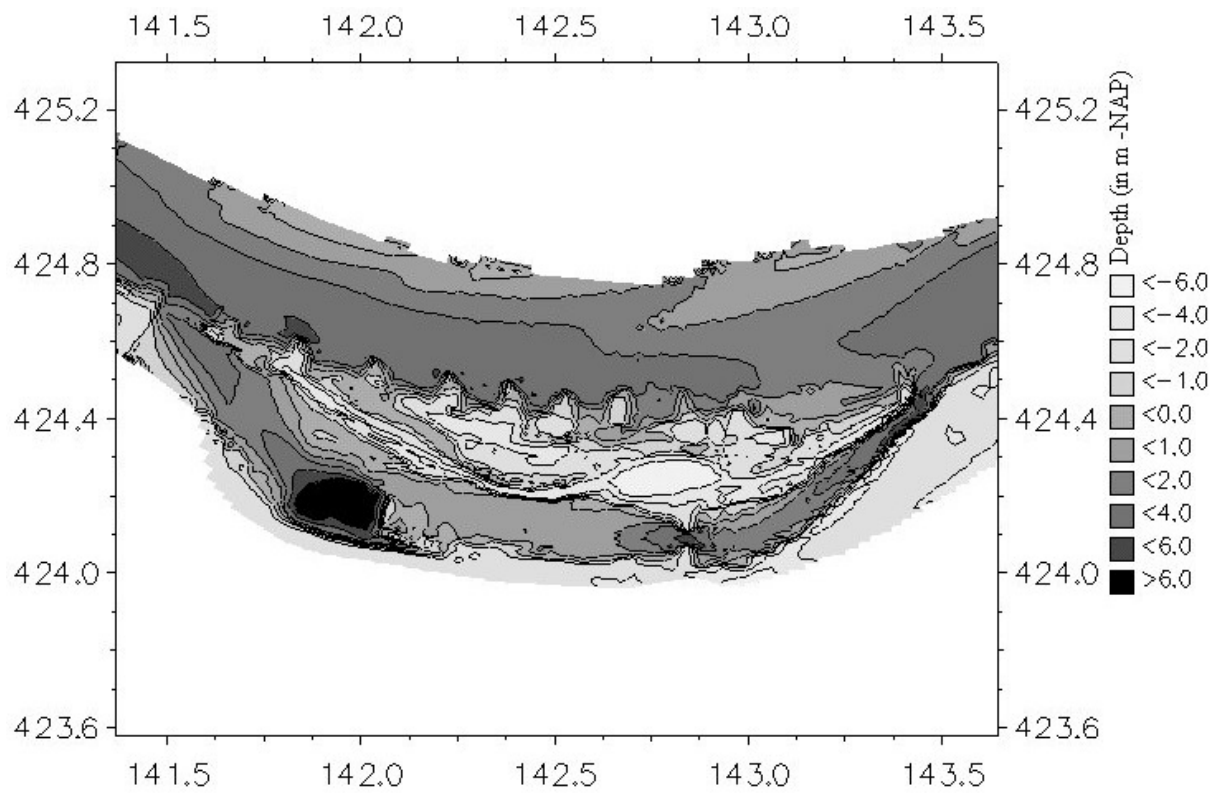
Figure 3.6: Bed topography after thirty years of simulation with vegetation development.
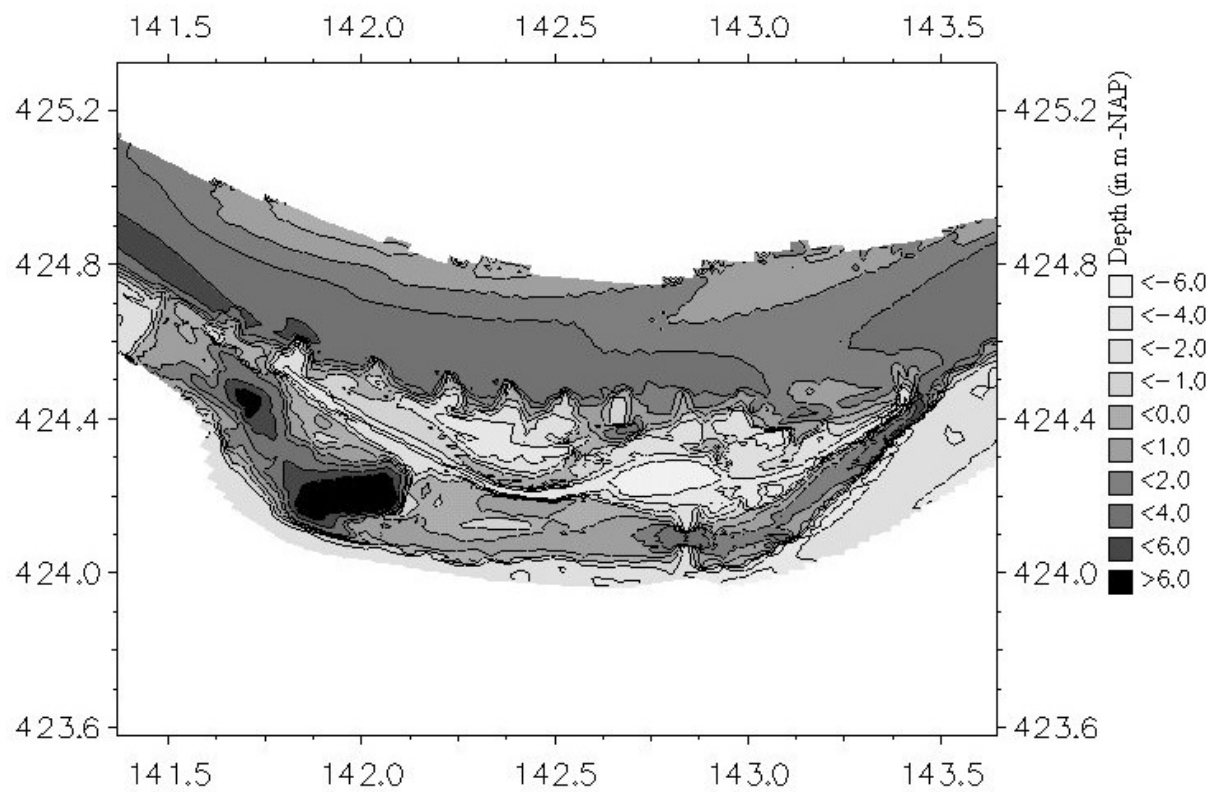
Figure 3.7: Bed topography after thirty years of simulation without vegetation development.

Table 3.3: Measured and simulated net sedimentation (+) or erosion (−) rates in sections of the Gameren floodplain, for four time periods, with (w) or without (w/o) vegetation growth and succession, in cm.a^{-1}.

Section	Measured	yr 0 - 5	Vegetation	yr 5 - 10	yr 10 - 20	yr 20 - 30
East Channel	+8 (7 yr)	+14	w	+1	−2	0
			w/o	+3	−2	−1
West Channel	+2 (6 yr)	+3	w	+3	+2	0
			w/o	+2	+1	0
Large Channel						
Entrance	+6 (2 yr)	+20	w	−6	−8	−6
			w/o	+3	−2	0
Sand pit	+14 (2 yr)	+6	w	+3	+8	+10
			w/o	+4	+9	+8
Islands	−7 (2 yr)	−7	w	−4	−2	−2
			w/o	−4	−4	−2
Downstream end	0 (2 yr)	−8	w	−9	−7	−3
			w/o	−7	−9	−5

floodplain and presented in Table 3.3 for different time periods of the model simulations; yr. 0-5, yr. 5-10, yr. 10-20 and yr. 20-30. In the model simulations, the first update of the vegetation distribution map takes place after five years. From that moment on, differences in morphologic development due to vegetation growth and succession can be assessed. For model verification, bed topography measurements carried out by the Institute for Inland Water Management and Wastewater Treatment (RIZA) are used to compare with the model simulations over the first five years. The bed topography measurements of the East and West Channel commenced in 1996 and cover a longer time period than those for the Large Channel, which is in use since 1999 (see Table 3.1). The model simulations start with the bed topography measured in 2000, therefore, in reality the morphodynamic changes of the channels have already started. This poses a methodological problem in comparing the simulations with the measurements. Another methodological problem is that the model simulates long-term average conditions; it was not intended to mimic the actual floods and morphodynamics over recent years. The comparison with the measurement data is therefore only indicative.

The model predicts a net sedimentation of the East Channel over the first 10 years, followed by stabilisation, or even a small net erosion of the channel bed. The measured net sedimentation rate of the East Channel between December 1996 and October 2003

is 8 cm/a (Jans, 2004). Furthermore, the model predicts a rapid erosion of the eastern point of the island north of the East Channel in the first five years. The erosion of this bank is clearly observed in the field. The modelled effects of vegetation development on sedimentation rates are negligible for the East Channel.

The West Channel shows a net deposition for the first 20 years in the model simulations. The measured sedimentation rate for the West Channel between December 1996 and October 2002 is 8 cm/, excluding the 2002 measurement (Jans, 2004). Including the 2002 measurement the net sedimentation rate is 2 cm/a. The simulated channel bed morphology shows the development of a point bar in the inner bend, which can be already observed in the field. Comparison of Figures 3.6 and 3.7 shows significant changes in channel planform for this channel. The net sedimentation rate is increased by the vegetation growth.

The entrance of the Large Channel shows a net sedimentation in the first five years of the model prediction, followed by net erosion in later years. Measurements between October 2000 and October 2002 show a net erosion rate of 6 cm/a. The first five years of the model simulations do not agree with these observations. The cause of this is that the morphodynamic computation shows an initial flattening of the relatively deep channel bed, which may be caused by an erroneous (too high) erodibility of the banks. The modelled effects of vegetation development on the entrance of the Large Channel are significant: the net erosion rates (in later years) are enhanced, because the increased hydraulic roughness of the banks pushes the flow toward the channel axis, leading to a larger sediment transport capacity.

The model predicts a scour hole in the constriction of the Large Channel, at the location of the bridge. Because the modelled constriction is not quite as narrow as in reality, the local scour and deposition further downstream are not as large as measured in the field.

Further downstream in the Large Channel, the model predicts filling up of the former sand mining pit, starting upstream in the sand pit and moving progressively downstream. The modelled net sedimentation rate in the first five years is 6 cm/a, which is less than the measured value of 14 cm/a (Jans, 2004). After a simulation period of 30 years, the sand pit is about halfway filling up.

The simulated morphological trends caused by the *remote* effects of vegetation on the bare channel bed largely comply with observations and measurements. However, *local* morphological effects on vegetated sections of the floodplain seem to be erroneous. During the model calculations it was observed that in some vegetated places, excessively high sediment transport rates occurred. Furthermore, the modelled morphological changes of vegetated islands are questionable. The group of small islands that is present in the initial bed topography just downstream of the sand mining pit is completely washed away in the morphodynamic simulations. Although this section is supposed to show net erosion,

since the transport of sediment is stopped upstream by the deep sand mining pit that acts as a sand trap, the erosion should not be so severe. Field measurements show a net erosion rate between October 2000 and October 2002 of 7 cm/a, in compliance with model simulations, however, a notable difference is that the measured erosion takes place in between the islands, not at the islands themselves. We hypothesize that the *local* effect of erosion of the vegetated islands is most probably a model shortcoming. In the model, the increased hydraulic roughness of the vegetation on the islands enhances the transport of sediment, whereas in reality, vegetation stabilizes islands (Thorne, 1990; Gregory & Gurnell, 1988; Tsujimoto, 1999; Helal Ahmed, 2003; Murray & Paola, 2003).

Furthermore, the model simulations show a large eroding area at the downstream end of the Large Channel. The net erosion rate is about 8 cm/a. Field observations do not show any signs of erosion here. Again, we hypothesize that the presence of vegetation unrealistically enhances the local transport capacity in the simulations, which leads to erroneous erosion rates.

3.4 Discussion

This study aimed at increasing insight into the biogeomorphological developments of secondary channels, i.e. into the interaction of vegetation with sediment transport and morphodynamics. It did not aim to predict the exact evolution of the Gameren floodplain. There are not enough data available for proper calibration, let alone validation, of the morphodynamic model. The secondary channels have been in use for only a short period, so there is not a long enough time series of morphodynamic measurements for these channels. The model is therefore based on a calibration of the yearly sand transport in the main channel and in combination with a calibrated hydrodynamics of the secondary channels it is assumed that this gives a best estimate for the morphodynamic developments. Additional effects of navigation, yielding effects of ship waves and of filling and emptying of the channels on their morphology, were not taken into account. Given these shortcomings, a quantitative and qualitative comparison of the model simulations with the actual morphological developments in the channels shows similar patterns of erosion and sedimentation. However, the results of the morphological simulations in the vegetated areas seem to be erroneous.

The results of this study therefore reveal an important knowledge gap with regard to the quantification of sediment transport in vegetated regions. Traditionally, the influence of riparian vegetation on the hydrodynamics is modelled as a form of bed roughness. This can be achieved in various ways, for example by an increased Manning coefficient, a decreased Chézy value, or an increased Nikuradse equivalent sand roughness. The higher the expected resistance of the vegetation, the larger the local bed roughness in the model.

Submerged weeds, for example, are modelled as a relatively high bed roughness, as in this case study. Although the traditional methodology has its shortcomings with respect to the description of flow, the *remote* effects of vegetation on morphology can be modelled relatively well, since the flow patterns and water depths respond to the increased bed roughness. However, when it comes to the *local* effects, the predictions can be wrong. This is because an enhanced bed roughness leads to an increased bed shear stress, which subsequently leads to an increased sediment transport (Jagers, 2003). Subsequently, the computed morphological changes are modelled unreliably, especially inside vegetated parts, and indirectly also for the non-vegetated parts. An improved formulation for the effects of vegetation on the bed shear stress, and subsequent sediment transport capacity, must be sought in order to reliably apply 2-DH morphodynamic models in river floodplains.

3.5   Conclusions

The lifetime of river improvement measures, such as the construction of secondary channels, is determined by a number of factors, and to some extent by the interaction between vegetation and sediment. The integrated modelling of morphodynamics and vegetation development provides a valuable insight into the possible natural developments in man-made secondary channels in the Waal River. Secondary channels are important both from a safety point of view as well as from a nature restoration point of view. Dynamic processes of erosion and sedimentation create a diverse vegetation in the relatively shallow secondary channels. The model simulations show that riparian vegetation increases the hydraulic resistance of the banks and therefore concentrates the flow in the channel, which leads to an increased sediment transport capacity. In aggrading channels, the inflow opening fills up and consequently vegetation can develop within the channels. The restoration of secondary channels and the subsequent natural development result in an increase of biodiversity, but simultaneously a conflict may arise with flood safety.

More importantly, this study has shown that a major knowledge gap exists with regard to the simulation of bed shear stress on a vegetated bed in 2-DH models. The common approach of modelling vegetation resistance as increased bed roughness leads to erroneous results for the bed shear stress. As a consequence, we are at present unable to accurately predict the long-term evolution of river and floodplain morphology, or the longevity of river improvement measures. It is concluded that for future 2-DH model applications of the morphological evolution of floodplains it is necessary to find better formulations for the quantification of the bed shear stress on a vegetated bed.

Chapter 4

Analytical expressions for the bed shear stress on a vegetated bed

4.1 Introduction

The previous chapter has shown that applying an increased bed roughness coefficient to account for the hydraulic resistance of vegetation leads to erroneous values of the bed shear stress. In a 2-DH morphodynamic model this subsequently leads to an erroneous computation of bed level changes in vegetated regions. A possible solution is to model the hydraulic resistance of vegetation in a different way. In contrast to determining the hydraulic resistance by a bed roughness coefficient, it can also be determined by schematising vegetation as cylinders that exert a drag force to the flow. The vegetation drag force in addition to the bed roughness, which represents a bed drag force, then determine the hydraulic resistance. Subsequently, it is possible to set up a force balance over the vertical to determine the bed shear stress. The bed shear stress is then dependent on a more realistic bed roughness coefficient in combination with flow characteristics near the bed that are affected by the vegetation properties. This method is elaborated in this chapter, yielding analytical expressions for the bed shear stress on a vegetated bed, for non-submerged and submerged vegetation.

Two different methods are applied to derive analytical expressions for the bed shear stress. The first method is named *Reduction factor approach*. In the *Reduction factor approach* the bed shear stress is calculated from the total fluid shear stress, which follows from the total resistance of the flow, multiplied with a vegetation reduction factor. The second method is named *Analytical approach*. In the *Analytical approach* the bed shear stress is calculated directly by an analytical expression based on the momentum balance for flow through and over vegetation. It is named *Analytical approach* since it gives an analytical solution to the differential equation for the momentum balance, although strictly speaking both methods provide analytical expressions. Both methods also need the hydraulic resistance of the flow. Therefore, this chapter will also address various analytical expressions for the hydraulic resistance of flow with vegetation.

In the next sections, first the state-of-the-art in modelling flow through and over vegetation and modelling the bed shear stress on a vegetated bed are presented. This is followed by the theoretical background of flow through and over vegetation used for the derivation of the two formulae for the bed shear stress. After the formulae for the bed shear stress are derived, formulae for the hydraulic resistance will be defined. Subsequently, attention is given to the unknown parameters in these derivations. Finally, the results of these formulae will be compared with flume data found in literature and with the results of a numerical one-dimensional vertical (1-DV) flow model.

This 1-DV model for flow through and over an open porous medium defined by cylinders, such as vegetation, was developed by Dr. R. Uittenbogaard of WL | Delft Hydraulics for a study by Tanczos and De Vries (1999). The momentum balance in this model contains the additional drag force of cylinders in the flow. Furthermore, additional generation and dissipation of turbulence affected by flow through cylinders is implemented. Model parameters for vegetation are a drag coefficient, $C_D(z)$, a typical diameter of branches or stems, $D(z)$, and the number of cross sections of stems or branches per m^2 horizontal plane, $m(z)$. The model allows for multiple bifurcation of vegetation, by adjusting the number of stems, the diameter of the stems and the drag coefficient per depth-layer. An additional model parameter is the coefficient c_l that relates the typical length scale of eddies to the mesh size of a grid, i.e. a bundle of vegetation stems. For a grid of rigid cylinders, $c_l = 1$. The model is described in more detail in Appendix B. The performance of this model has been tested by comparing the model outcome with the results of flume experiments from Meijer and Van Velzen (1999), Nepf and Vivoni (2000) and López and García (2001) in studies executed by Oberez (2001), Karanxha (2002) and Uittenbogaard (2003).

4.2   State of the art in modelling flow and bed shear stress for flow with vegetation

The effect of vegetation on flow is generally expressed as an effect on the hydraulic roughness. In early measurements (18th century) on flow velocities in channels it was found that the depth-averaged velocity, $\bar{u}$ (m/s), was a function of the water level slope, i (-), and the hydraulic radius, R (m). In 1776 Antoine de Chézy published a simple equation that includes a factor C, the Chézy value, which was at first thought to be a constant (Vernon-Harcourt, 1896). The well-known Chézy formula is:

$$\bar{u} = C\sqrt{Ri} \qquad (4.1)$$

In this equation C (m$^{1/2}$·s^{-1}) is a parameter that expresses the hydraulic roughness of the bed and banks of a channel.
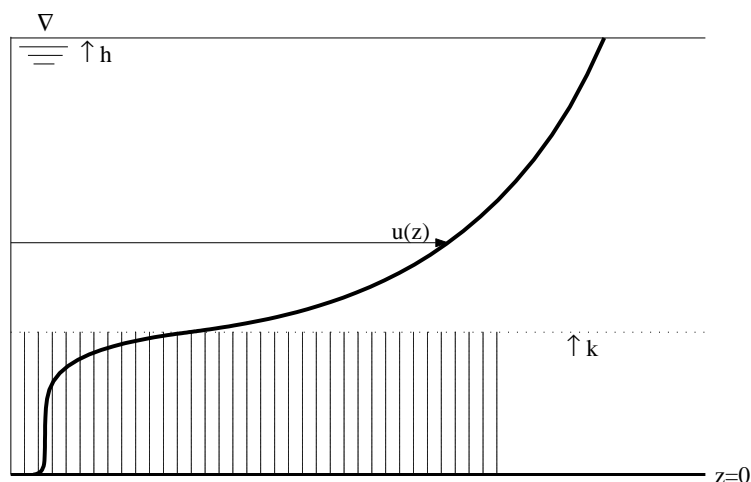
Figure 4.1: Vertical profile of horizontal flow velocity for submerged vegetation, h is water depth, k is vegetation height.

Further investigations, by Nikuradse (1930), revealed that the roughness of the bed affects the roughness length, z_0 (m), in the logarithmic velocity profile above a fully rough bed, which was derived by, among others, Prandtl and Von Kármán:

$$u(z) = \frac{u_*}{\kappa} \ln \frac{z}{z_0} \tag{4.2}$$

where u_* is the shear velocity (m/s). Nikuradse (1930) showed that for hydraulically rough walls, the roughness length of the logarithmic velocity profile can be expressed as $k_N/30$, where k_N is the Nikuradse equivalent roughness (m). Calculating the depth-averaged velocity from Eq. (4.2), and applying the Chézy formula and the Nikuradse roughness height yields the White-Colebrook formula for the Chézy value:

$$C = 18 \log \frac{12R}{k_N} \tag{4.3}$$

With an increasing roughness height the value for C decreases. Various alternative expressions for flow resistance exist, for example those of Strickler or Manning. In hydraulic engineering in the Netherlands it is quite common to apply the White-Colebrook formulation, also to determine the Chézy factor for vegetation, like in the previous chapters. Essentially, vegetation is thus treated as large bed structures with a logarithmic flow profile above them. In reality, however, there is flow over and through submerged vegetation, and the vertical flow profile deviates from the logarithmic one. This has been established by many authors in the past decades, but even recent researchers attempt to fit a logarithmic profile and conclude that this does not work (Shi & Hughes, 2002). A typical velocity profile for submerged vegetation is shown in Fig. 4.1. The White-Colebrook formula fails here and another type of resistance formula should be sought for.

A considerable amount of research has been carried out on the effects of vegetation on the hydraulic resistance, extending the basic ideas of Nikuradse (1930). Early work includes

Einstein and Banks (1950), Kouwen *et al.* (1969), Kouwen and Unny (1973), Klaassen and Van der Zwaard (1974) and Petryck and Bosmajian III (1975). In a study by Dawson and Charlton (1988), a literature search has been carried out on the hydraulic resistance of vegetation, resulting in over 360 publications. Since then, many more publications have followed. A limited overview of recent research includes studies on the improvement of flow resistance formulae (Darby, 1999; Hasegawa *et al.*, 1999; Meijer & Van Velzen, 1999; Stephan & Gutknecht, 2002; Järvelä, 2002; Fisher & Knight, 2002; Mason *et al.*, 2003; James *et al.*, 2004; Järvelä, 2004), on analytical approaches for the vertical profile of horizontal velocity (Klopstra *et al.*, 1997; Carollo *et al.*, 2002; Katul *et al.*, 2002), on biomechanics and streamlining of vegetation (Fathi-Maghadam & Kouwen, 1997) and on turbulence characterisation for submerged rods and vegetation (Shimizu & Tsujimoto, 1994; Ikeda & Kanazawa, 1996; Nezu & Naot, 1999; Nepf & Vivoni, 1999; Nepf & Vivoni, 2000; Ikeda *et al.*, 2001; Fischer-Antze *et al.*, 2001; López & García, 2001; Ghisalberti & Nepf, 2002; Righetti & Armanini, 2002; Wilson *et al.*, 2003; Ghisalberti & Nepf, 2004).

Investigations on the effect of vegetation on the bed shear stress, however, are scarce. Li and Shen (1973) analysed theoretically the mean drag coefficient for *non-submerged* multiple cylinders distributed in a given pattern. In addition they used the Shield's sediment transport equation to theoretically calculate the sediment transport rate for parallel and staggered patterns. The bed shear stress (average boundary shear stress) was calculated from the grain roughness. From a horizontal balance of fluid forces they concluded: "The average boundary shear stress increases with increasing discharge, plot bottom slope, and sediment size, but decreases with increasing diameter of vegetation (therefore, the expectation is that vegetation will have much more effect on sediment yield as trees grow larger)."

Tollner *et al.* (1982) theoretically analysed the shear on a *non-submerged* vegetated channel bed. They propose that an analogy can be made between the flow of depth, h (m), through a porous medium (i.e. cylinders) with a spacing of b (m) and the flow through a deep, narrow rectangular channel with the same flow depth, h, and a width equal to b. The resulting shear on the channel would then be expressed as:

$$\tau_b = \rho\, g\, R_s\, i \tag{4.4}$$

in which τ_b is the shear on the bed (N·m^{-2}), ρ is the mass density of water (kg·m^{-3}), g is the acceleration of gravity (m·s^{-2}), i is the surface slope (-), and R_s is the "spacing hydraulic radius"(m) given by:

$$R_s = \frac{b\,h}{b + 2h} \tag{4.5}$$

They successfully applied this relationship in an experimental study on sediment transport on a bed with non-submerged metal rods.

Nakagawa *et al.* (1992) studied suspended sediment transport in a channel with *submerged* vegetation on the bed. A numerical 1D k-ϵ turbulence model, based on Wilson and Shaw (1977), was applied that has additional formulations for the drag force of cylinders. The modelled results for velocity, Reynolds stress and turbulence intensity were compared to measurements in a flume experiment. They observed that the vertical fluid shear stress profile above the vegetation resembles the common linear Reynolds stress distribution for open channel flow. Inside the vegetation, however, the Reynolds stress reduces strongly. Nakagawa *et al.* (1992) approximate the vertical profile for the Reynolds stress (τ_R) inside the submerged vegetation layer by an exponential growth function. In their paper, the exponent is $\alpha\,z$, but this cannot be correct. A corrected version is:

$$\tau_R(z) = \rho\,u_{*k}^2\,\mathrm{e}^{\alpha\,(z-k)} \tag{4.6}$$

in which α is the reciprocal of the length scale where an active momentum exchange with the surface flow is recognised (m^{-1}). If k is the vegetation height (m), u_{*k} is the shear velocity (m/s) at height $z = k$, given by:

$$u_{*k} = \sqrt{\tau_k/\rho} \equiv \sqrt{g(h-k)i} \tag{4.7}$$

where τ_k is the shear stress at $z = k$. The parameter α is determined by the penetration depth of turbulence from above the vegetation into the vegetation. Tsujimoto *et al.* (1991) proposed an empirical equation as:

$$\alpha\sqrt{bk} = -0.32 - 0.85\log\left(\frac{(h-k)i}{k}\right) \tag{4.8}$$

in which b is the spacing between cylinders (m), and k is the cylinder height (m). For the bed shear stress, Nakagawa *et al.* (1992) suggest that the ratio of the total Reynolds stress (τ_R at $z = 0$) over τ_b can be approximated by:

$$\frac{\tau_R}{\tau_b} = \exp\left[\gamma(-k/h)\right] \tag{4.9}$$

in which γ is a coefficient that, according to the measurements, increases with an increasing dimensionless vegetation density Dk/b^2 (-), where D is cylinder diameter (m). A formula for γ, however, is not given. In conclusion, Nakagawa *et al.* (1992) suggest extrapolating the total fluid shear stress profile to the bed and subsequently propose an exponential decrease of the ratio of the total fluid shear stress over the bed shear stress as a function of vegetation density and submerged depth.
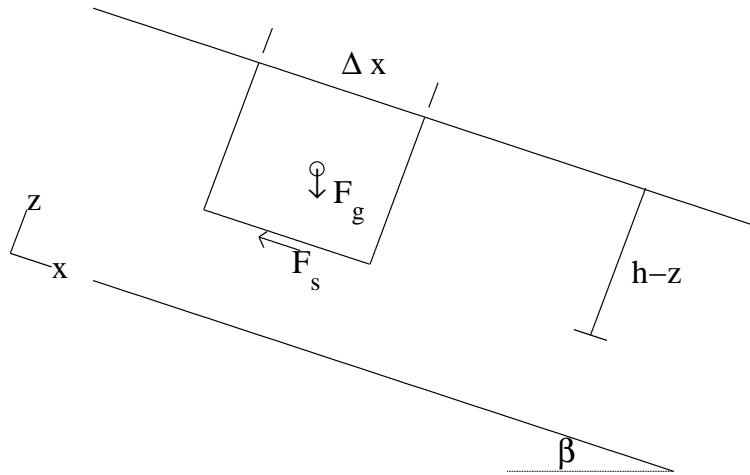
Figure 4.2: Fluid forces on a control volume, for uniform, steady flow in a wide rectangular channel without vegetation.

4.3 Theoretical background of flow through and over vegetation

4.3.1 Open channel flow

For uniform, steady flow in a wide rectangular channel without vegetation, the forces on a fluid element Δx are given in Fig. 4.2. The gravity component in x-direction is:

$$F_g = \rho \, g \, \Delta x \, B \, (h - z) \, \sin \beta \tag{4.10}$$

where ρ is the density of water (kg·m^{-3}), g is the gravitational acceleration (m·s^{-2}), x is the streamwise co-ordinate (m), B is the width (perpendicular to the figure), h is the water depth (m), z is the coordinate perpendicular to x (m) and β is the angle of the bed with the horizontal plane. The friction component in x-direction is:

$$F_s = -\tau_{xz} \, \Delta x \, B \tag{4.11}$$

Where τ_{xz} is the fluid shear stress in streamwise direction (N·m^{-2}). The force balance gives:

$$\rho \, g \, \Delta x \, B \, (h - z) \, \sin \beta - \tau_{xz} \, \Delta x \, B = 0 \tag{4.12}$$

Therefore, for open channel flow without vegetation:

$$\tau_{xz}(z) = \rho \, g \, (h - z) \, \sin \beta \tag{4.13}$$

Since $\sin \beta$ is small and therefore approximately equal to the bottom slope, i_b, which equals the energy gradient i (-) for steady uniform flow, it follows that:

$$\tau_{xz}(z) = \rho \, g \, (h - z) \, i \tag{4.14}$$
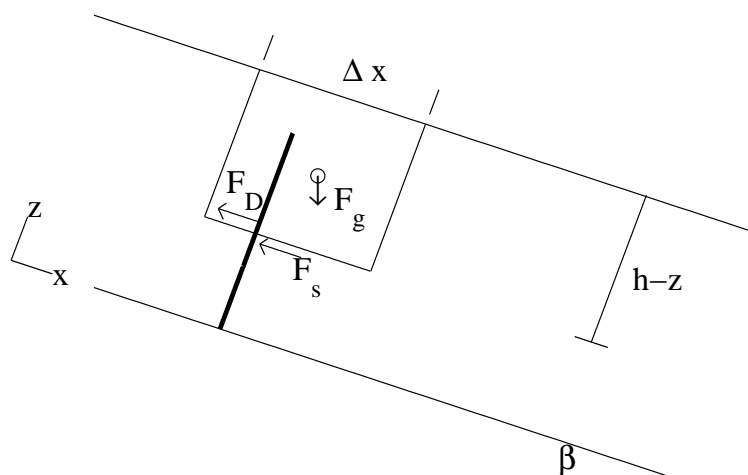
Figure 4.3: Fluid forces on a control volume, for uniform, steady flow in a wide rectangular channel with vegetation.

Therefore, at the bed, $z = 0$:

$$\rho\,g\,h\,i = \tau_b \qquad (4.15)$$

where τ_b is the bed shear stress (N·m^{-2}). For open channel flow, the total fluid shear stress, $\rho\,g\,h\,i$, equals the bed shear stress.

4.3.2 Flow through and over vegetation

For uniform, steady flow in a wide rectangular channel with vegetation, fundamental differences are firstly, part of the fluid forces are carried to the plants as a kind of body resistance force, and secondly, the energy gradient increases considerably due to the additional resistance of the vegetation. The forces on a fluid element Δx in flow through and over vegetation are given in Fig. 4.3. The force balance for flow with vegetation contains an additional plant resistance force per unit area, F_D (N·m^{-2}). It is common to model vegetation as a group of parallel, staggered or randomly arranged rigid vertical cylinders with homogeneous properties. The resistance force is defined as:

$$F_D(z) = \tfrac{1}{2}\rho \int_z^k C_D(z)m(z)D(z)\,|u(z)|\,u(z)\mathrm{d}z \qquad (4.16)$$

where k is the cylinder height (m), C_D is the drag coefficient (-), m is the cylinder density per unit area (m^{-2}), D is the cylinder diameter (m), and u is the time-averaged horizontal flow velocity (m/s). From now on a positive flow direction is assumed, so that F_D is a function of u^2. At the bed, $z = 0$, the force balance for flow through and over vegetation thus becomes:

$$\rho\,g\,h\,i = \tau_b + \tfrac{1}{2}\rho \int_0^k C_D(z)m(z)D(z)u^2(z)\mathrm{d}z \qquad (4.17)$$

For flow through and over vegetation, the total fluid shear stress, $\rho\,g\,h\,i$, equals the bed shear stress plus the additional vegetation resistance.

4.3.3 Correction for plant volume

Modelling flow through a porous medium, such as vegetation, in principle involves a correction for the presence of vegetation within the volume of water. A common way to deal with this is to introduce the dimensionless parameter λ, the solidity, which is defined as the fraction of horizontal area taken by the cylinders (Li & Shen, 1973; Taylor *et al.*, 1985; Wu *et al.*, 1999; Stone & Shen, 2002; Uittenbogaard, 2003; Hoffmann, 2004):

$$\lambda = \frac{\pi}{4}D^2 m \tag{4.18}$$

This gives the definition of the vegetation porosity:

$$\epsilon = 1 - \lambda \tag{4.19}$$

The porosity can be introduced to calculate the pore, or microscopic, velocity in between the vegetation, which determines the resistance force of the vegetation. In addition, the porosity can be used to correct for the available volume, or available horizontal area in the calculation of the fluid shear stress or the bed shear stress respectively. However, various authors in the literature apply various theoretical approaches to determine the pore velocity, the drag coefficient associated with this pore velocity, or the correction for available volume or area. None of the approaches are underpinned in a satisfactory manner with experimental evidence. More importantly, experimental evidence has shown that this correction term can be neglected to calculate vegetation resistance with no significant loss of accuracy (James *et al.*, 2004). We conclude that the solidity can be disregarded in simple analytical expressions for flow through and over vegetation, especially in the light of the uncertainties introduced by describing vegetation properties in terms of stem density, height and diameter.

4.4   Method 1: Reduction factor approach

In this section, a simplified approach will be presented to calculate the bed shear stress for non-submerged and submerged vegetation. This approach yields a reduction factor on the total shear stress and is thus called the *Reduction factor approach*. In this approach it is assumed that the flow velocity through the vegetation is uniform, similar to that for non-submerged vegetation. Note that this condition only holds under the assumption of a relatively high vegetation density and height.

4.4.1 Submerged vegetation

The reduction factor approach gives an estimate for the bed shear stress on a vegetated bed with submerged vegetation. It is assumed that the bed shear stress is determined by the uniform velocity through the vegetation, u_c:

$$\tau_b = \frac{\rho g}{C_b^2} u_c^2 \tag{4.20}$$

where C_b is the Chézy bed roughness ($\text{m}^{1/2}.\text{s}^{-1}$). The uniform velocity in the vegetated layer follows from the momentum balance for flow through and over vegetation, Eq. (4.17). For a uniform flow profile over the vegetation height, k (m), the stem drag force becomes:

$$\tau_v = \tfrac{1}{2} \rho C_D m D k u_c^2 \tag{4.21}$$

Now we can rewrite the force balance, Eq. (4.17), as:

$$g h i = u_c^2 \left(\frac{g}{C_b^2} + \tfrac{1}{2} C_D m D k \right) \tag{4.22}$$

Therefore the flow velocity in the uniform part of the profile is:

$$u_c = \sqrt{\frac{h i}{C_b^{-2} + \frac{C_D m D k}{2g}}} \tag{4.23}$$

Combination of equations 4.20 and 4.23 yields an expression for the vegetated bed shear stress, τ_{bv}, written as a reduction factor times the well-known equation for the total shear stress, τ_t, for open channel flow without vegetation:

$$\tau_{bv} = \frac{1}{1 + \frac{C_D m D k C_b^2}{2g}} \rho g h i \tag{4.24}$$

The reduction factor, f, for vegetated bed resistance is thus given by:

$$f = \frac{1}{1 + \frac{C_D m D k C_b^2}{2g}} \tag{4.25}$$

By defining:

$$\overline{u} = C_r \sqrt{h i} \tag{4.26}$$

where C_r is the representative Chézy value for vegetation, Eq. (4.24) can also be written as:

$$\tau_{bv} = f \frac{\rho g}{C_r^2} \overline{u}^2 \tag{4.27}$$

where $\overline{u}$ is the depth-averaged flow velocity (m/s).

Using dimensional analysis and two physical hypotheses, Raupach (1992) derived a similar type expression for the drag partition of wind stress:

$$\frac{\tau_{bv}}{\tau_t} = \frac{1}{1 + \beta \lambda} \tag{4.28}$$

where β is the ratio of vegetation to surface drag coefficients:

$$\beta = \frac{C_D}{C_p} \tag{4.29}$$

and λ is the roughness density or frontal area per unit ground area:

$$\lambda = \frac{Nbk}{S} \tag{4.30}$$

in which N is the number of roughness elements, with width b (m), and height k (m), per unit ground area S (m^2). For cylinders, λ equals mDk. The surface drag coefficient, C_p, equals g/C_b^2, yielding:

$$\frac{\tau_{bv}}{\tau_t} = \frac{1}{1 + \frac{C_D mDk C_b^2}{g}} \tag{4.31}$$

which is similar to Eq. (4.25) with the exception of the factor $\frac{1}{2}$. Raupach (1992) defined the vegetation drag coefficient without the factor $\frac{1}{2}$ in accordance with meteorological rather than aerodynamic convention.

4.4.2 Non-submerged vegetation

For non-submerged vegetation the reduction factor approach can be applied in a similar way. The uniform flow velocity through non-submerged vegetation follows from the force balance, Eq. (4.17). Since the water depth, h, is now smaller than the vegetation height, k, it holds:

$$ghi = u_c^2 \left(\frac{g}{C_b^2} + \tfrac{1}{2} C_D mDh \right) \tag{4.32}$$

The uniform flow velocity for non-submerged vegetation thus is:

$$u_{cb} = \sqrt{\frac{hi}{C_b^{-2} + \frac{C_D\, m\, D\, h}{2g}}} \tag{4.33}$$

Often, the bed resistance is neglected, giving the simpler expression:

$$u_{s0} = \sqrt{\frac{2\, g\, i}{C_D\, m\, D}} \tag{4.34}$$

The combination of Eq. (4.20) for the bed shear stress and Eq. (4.33) for the uniform flow velocity through the vegetation leads to the following expression:

$$\tau_{bv,nonsub} = \frac{1}{1 + \frac{C_D mDh C_b^2}{2g}} \rho ghi \tag{4.35}$$

in which the reduction factor is:

$$f_{nonsub} = \frac{1}{1 + \frac{C_D mDh C_b^2}{2g}} \tag{4.36}$$

This expression has been derived before by Karanxha (2002). The only difference with the expression for submerged vegetation is that the reduction factor, f_{nonsub}, for non-submerged vegetation contains the water depth, h, instead of the vegetation height, k. In other words, for both submerged and non-submerged conditions, the bed shear stress is dependent on the submerged height of the vegetation. However, it must be realised that for non-submerged conditions, the uniform flow velocity equals the mean velocity, $u_c = \overline{u}$. Therefore:

$$\tau_{bv,nonsub} = \frac{\rho g}{C_b^2} u_c^2 = \frac{\rho g}{C_b^2} \overline{u}^2 \tag{4.37}$$

In other words, following the method of effective water depth and its underlying assumptions, the bed shear stress for non-submerged vegetation is simply given by the common formula for bed shear stress, given the bed roughness.

4.5 Method 2: Analytical approach

4.5.1 Theoretical background

In the second approach, the bed shear stress is derived from an analytical solution of the momentum balance for the flow in the vegetation layer. This leads to a better description for the flow velocity profile in the vegetated layer than the previoulsy assumed uniform profile. This approach is derived in a similar way as Klopstra et $al.$ (1996) and Klopstra et $al.$ (1997) did. Klopstra et $al.$ (1997) derive an analytical expression for hydraulic resistance in which the bed shear stress is neglected. However, the underlying report of Klopstra et $al.$ (1996) describes an alternative approach in which the bed shear stress is included in the form of the right-hand side of Eq. (4.37). Here, we follow a different approach in which the bed shear stress near the bed is made dependent of the turbulence intensity near the bed, which is in its turn affected by the water depth, vegetation properties and bed roughness. In this approach, an increasing turbulence intensity leads to an increase of the bed shear stress. The underlying idea is that the shear stress profile near the bed is not so much affected by the drag forces of the sediment particles, or possibly bedforms, alone, but by a combination of the drag forces of sediment and vegetation.

First we write the momentum balance for uniform flow through and over vegetation:

$$\frac{\partial \tau_{xz}}{\partial z} - \rho g i - \frac{1}{2} \rho C_D m D u^2(z) = 0 \tag{4.38}$$

We assume that the vegetation properties for C_D, m and D are uniform over the plant height. For the Reynolds shear stress, τ_{xz}, we assume a Boussinesq approach for the eddy viscosity:

$$\tau_{xz} = \rho \nu_T \frac{\partial u}{\partial z} \tag{4.39}$$
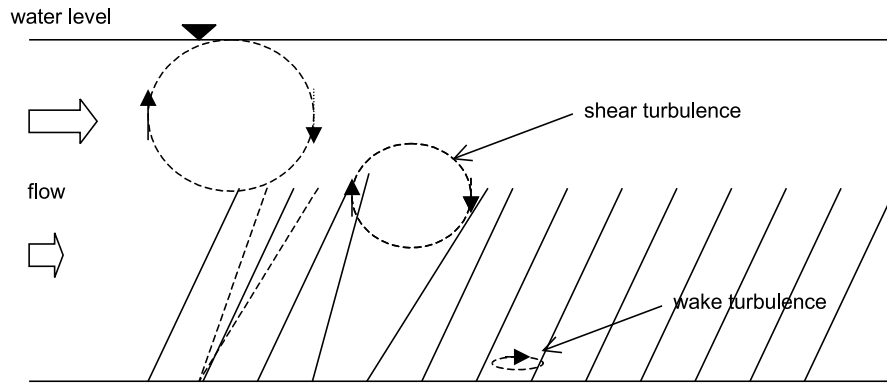
Figure 4.4: Schematic view of the penetration of shear turbulence into the top layer of the vegetation and the wake turbulence inside the vegetation.

where ν_T is the eddy viscosity (m^2/s). For the eddy viscosity we apply the mixing-length approach:

$$\nu_T = \ell \sqrt{k_T} \tag{4.40}$$

where ℓ is the mixing length (m) and k_T is the turbulent kinetic energy per unit mass (m^2·s^{-2}). Inside the vegetation layer we assume that turbulence is governed by the wake turbulence, thus neglecting shear turbulence generated above the vegetation which may penetrate into the top layer of the vegetation, see Fig. 4.4. This assumption might not be valid for low vegetation or for vegetation with a low density, for the region near the top of the vegetation, and for the near-bed region. Due to the large differences in flow velocity between the vegetated region and the overlying region, shear turbulence is generated in the overlying region with a maximum eddy length scale determined by the classical boundary layer length scale: $\kappa(h - k)$. These eddies penetrate into the vegetated region where they will break up into smaller eddies, thus resulting in a smaller length scale determined by the stem distance or the distance between leaves. In the lowest region, wake turbulence is the dominant factor. We assume that the mixing length is determined by the characteristic stem distance ℓ, in other words, the size of the eddies in between the cylinders is determined by the space between the cylinders, in line with theory on flow through porous media (Breugem, 2004), although Poggi *et al.* (2004) provide support for the use of $D/0.21$ for the characteristic length scale, where 0.21 is the Strouhal number, typical for a Von Kármán street behind a cylinder.

The characteristic stem distance is given by:

$$\ell = c_l \left(\frac{1 - \lambda}{m} \right)^{\frac{1}{2}} \tag{4.41}$$

where λ is the dimensionless solidity of the vegetation, Eq. (4.18), and c_l is a coefficient that determines the characteristic length scale of eddies relative to the stem distance. For rigid cylinders, c_l is 1, but for vegetation with many leaves c_l might be smaller,

representing smaller eddy generation. We assume that the turbulent kinetic energy, k_T, is determined by the local time-averaged flow velocity. It then follows from Eq. (4.40) that the eddy viscosity becomes:

$$\nu_T = c_p \, \ell \, u \, (z) \tag{4.42}$$

where the coefficient c_p is the turbulence intensity, height-averaged over the vegetation height:

$$c_p = \frac{\frac{1}{k} \int_0^k \sqrt{k_T}(z)\mathrm{d}z}{\frac{1}{k} \int_0^k u(z)\mathrm{d}z} \tag{4.43}$$

The significance of this assumption for the determination of the bed shear stress will be discussed later. Substitution of Eq. (4.42) and Eq. (4.39) into Eq. (4.38) yields the ordinary differential equation:

$$\tfrac{1}{2}\rho \, c_p \, \ell \frac{\mathrm{d}^2 u^2}{\mathrm{d}z^2} - \tfrac{1}{2}\rho C_D \, mDu^2 = \rho g i \tag{4.44}$$

Now we introduce a length scale L (m):

$$L = \sqrt{\frac{c_p \, \ell}{C_D \, m \, D}} \tag{4.45}$$

Furthermore we define the flow velocity u_{s0}, equal to Eq. (4.34):

$$u_{s0} = \sqrt{\frac{2 \, g \, i}{C_D \, m \, D}} \tag{4.46}$$

Solving the differential Eq. (4.44) then yields:

$$u(z) = \sqrt{u_{s0}^2 + a \exp\left(\frac{z}{L}\right) + b \exp\left(-\frac{z}{L}\right)} \tag{4.47}$$

where a and b are integration coefficients, which will be discussed later. Equation (4.47) describes a double exponential profile inside the vegetation. More commonly, a single exponential decrease is applied that describes the profile near the top of the vegetation (Nikora *et al.*, 2004). Figure 4.5 presents a typical vertical profile for the horizontal velocity. It consists of two exponential parts, one near the top, described by $a \exp(z/L)$ and one near the bed, described by $b \exp(-z/L)$. The length scale L determines the rate of the curvature. Furthermore there is a part in between the curves with a uniform flow velocity u_{s0}. A larger L gives a smoother curve, thus decreasing the height of the uniform flow part. This is typical of vegetation with a low density. Dense vegetation yields a small L, a sharp curvature and therefore a larger part with a uniform flow velocity. Clearly, the values for the integration constants a and b determine the shape of the profile, as well.

The shear stress follows from Eq. (4.39) and Eq. (4.42):

$$\tau_{xz} = \rho c_p \, \ell \, u \, (z) \frac{\partial u(z)}{\partial z} \tag{4.48}$$
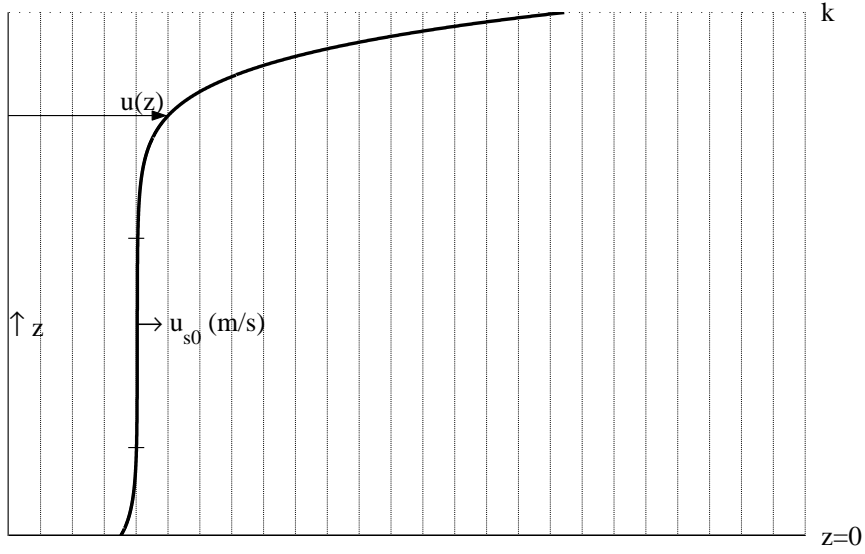
Figure 4.5: Vertical profile for the horizontal velocity inside submerged vegetation, $u(z)$. Note the uniform flow part, u_{s0}.

The bed shear stress is therefore:

$$\tau_b = \rho c_p \, \ell \, u(0) \frac{\partial u(0)}{\partial z} \tag{4.49}$$

The derivative of the vertical profile of horizontal velocity through the vegetation, Eq. (4.47), yields:

$$\frac{\partial u(z)}{\partial z} = \frac{a \exp\left(\frac{z}{L}\right) - b \exp\left(-\frac{z}{L}\right)}{2L\sqrt{u_{s0}^2 + a \exp\left(\frac{z}{L}\right) + b \exp\left(-\frac{z}{L}\right)}} \tag{4.50}$$

The bed shear stress then becomes:

$$\tau_b = \rho c_p \, \ell \, \frac{a - b}{2L} \tag{4.51}$$

Upon determining the coefficients a and b, the bed shear stress is known. The coefficients a and b follow from boundary conditions at the top of the vegetation and at the bed, see hereafter.

4.5.2 Boundary conditions

Boundary condition at the top of the vegetation

The boundary condition at the top of the vegetation follows from the momentum balance at $z = k$. The momentum balance for the flow in the layer above the vegetation is not affected by the drag forces of the vegetation and simplifies to:

$$\frac{\partial \tau_{xz}}{\partial z} - \rho g i = 0 \tag{4.52}$$

From which the shear stress at the top of the vegetation, at height $z = k$ follows:

$$\tau(k) = \rho g (h - k) i \tag{4.53}$$

In the vegetated section, at the top of the vegetation, the shear stress follows from the momentum balance with vegetation drag force, Eq. (4.48), and is given by:

$$\tau(k) = \rho c_p \, \ell \, u(k) \left. \frac{\partial u(z)}{\partial z} \right|_{z=k} \tag{4.54}$$

The boundary condition is given by equating Eq. (4.53) and Eq. (4.54):

$$\rho c_p \, \ell \, u(k) \frac{\partial u(k)}{\partial z} = \rho g \, (h - k) \, i \tag{4.55}$$

This then yields a first expression with the unknowns a and b:

$$\frac{a \exp\left(\frac{k}{L}\right) - b \exp\left(-\frac{k}{L}\right)}{2L} = \frac{g \, (h - k) \, i}{c_p \, \ell} \tag{4.56}$$

Boundary conditions at the bed

At the bed, a logarithmic boundary layer is assumed according to Uittenbogaard *et al.* (2000), which based on Hinze (1975) and Jackson (1981):

$$u(z) = \frac{u_{*b}}{\kappa} \ln \left(\frac{z + 9z_0}{z_0} \right) \tag{4.57}$$

This definition is valid only for fully-rough flow, i.e. $Re = u_{*b} k_s / \nu > 55$, (Hinze, 1975). In almost all circumstances the flow near the bed is turbulent, although this turbulence may have been generated by the plant stems instead of the bed roughness. In this definition the zero-plane of the logarithmic profile is defined at the top level of the roughness forming elements (i.e. sand grains or bedforms of height k_s), and the zero-plane displacement is at a level $0.3k_s$ underneath the zero-plane. Using the common relation $z_0 = 30k_s$, this yields the above logarithmic profile. The bed boundary condition for the flow velocity is given by:

$$u(0) = \sqrt{u_{s0}^2 + a + b} = \frac{u_*}{\kappa} \ln (9) \tag{4.58}$$

thus conveniently eliminating the roughness height z_0. We determine that the bed shear stress equals:

$$\tau_b = \rho c_p \, \ell \, \frac{a - b}{2L} = \rho u_*^2 \tag{4.59}$$

Combination of Eq. (4.58) and Eq. (4.59) determines the shear velocity at the bed:

$$u_* = \sqrt{c_p \, \ell \, \frac{a - b}{2L}} \tag{4.60}$$

The shear velocity is not directly dependent on the bed roughness, but is dependent on the vegetation properties and turbulence intensity near the bed. The latter may be dependent on the bed roughness and other vegetation properties, thus relating the bed shear stress to the forces of both the bed and the vegetation. This then yields a second expression with the unknowns a and b:

$$\frac{\sqrt{c_p \, \ell \, \frac{a-b}{2L}}}{\kappa} \ln(9) = \sqrt{u_{s0}^2 + a + b} \tag{4.61}$$

4.5.3 The bed shear stress from the analytical approach

To determine the analytical expression for the bed shear stress from the analytical approach, we have to determine the coefficients a and b from the boundary conditions. Firstly, we define two parameters to simplify the equations:

$$A = \frac{2L \, \kappa^2}{\ln^2(9) \, c_p \, \ell} \tag{4.62}$$

and:

$$B = \frac{2L \, g \, (h - k) \, i}{c_p \, \ell} \tag{4.63}$$

Secondly, the two expressions found with the unknowns a and b can then be written as:

$$\begin{cases} a(1 - A) - b(1 + A) = u_{s0}^2 \, A \\ a \exp\left(\frac{k}{L}\right) - b \exp\left(-\frac{k}{L}\right) = B \end{cases} \tag{4.64}$$

Now the values for a and b (m·s⁻2) follow:

$$a = \frac{B - u_{s0}^2 \frac{A}{1-A} \exp\left(-\frac{k}{L}\right)}{\exp\left(\frac{k}{L}\right) - \frac{1-A}{1+A} \exp\left(-\frac{k}{L}\right)} \tag{4.65}$$

$$b = \frac{B - u_{s0}^2 \frac{A}{1-A} \exp\left(\frac{k}{L}\right)}{\frac{1+A}{1-A} \exp\left(\frac{k}{L}\right) - \exp\left(-\frac{k}{L}\right)} \tag{4.66}$$

Together with Eq. (4.51) this gives the final expression for the bed shear stress on a vegetated bed with cylindrical resistance:

$$\tau_b = \frac{\rho \, c_p \, \ell}{2L} \left[\frac{B - u_{s0}^2 \frac{A}{1-A} \exp\left(-\frac{k}{L}\right)}{\exp\left(\frac{k}{L}\right) - \frac{1-A}{1+A} \exp\left(-\frac{k}{L}\right)} - \frac{B - u_{s0}^2 \frac{A}{1-A} \exp\left(\frac{k}{L}\right)}{\frac{1+A}{1-A} \exp\left(\frac{k}{L}\right) - \exp\left(-\frac{k}{L}\right)} \right] \tag{4.67}$$

where A and B are given by equations 4.62 and 4.63, respectively, ℓ is given by Eq. (4.41), and L is given by Eq. (4.45). Since the equation for B contains the energy gradient, i, as an unknown parameter, the representative Chézy value of the vegetation must be calculated first. This expression gives the bed shear stress for submerged as well as non-submerged conditions. In the latter case, the coefficient a becomes insignificantly small with respect to b.

4.6   Expressions for the hydraulic resistance of vegetation

Both the *Reduction factor approach* as the *Analytical approach* need the hydraulic resistance of vegetation as an input parameter to determine the bed shear stress. In this section we explore different methods to derive analytical expressions for the hydraulic resistance of vegetation.

4.6.1 Representative roughness of non-submerged vegetation

The representative roughness of non-submerged vegetation follows from the momentum balance for flow through vegetation, given by Eq. (4.32). The discharge per unit width through the vegetation is given by:

$$q = hu_{cb} \tag{4.68}$$

where u_{cb} is given by Eq. (4.33). From the discharge through the vegetation the representative Chézy value for non-submerged vegetation is calculated by:

$$C_{r,nonsub} = \frac{q}{h\sqrt{hi}} \tag{4.69}$$

Therefore, the representative Chézy value for non-submerged vegetation becomes:

$$C_{r,nonsub} = \sqrt{\frac{1}{C_b^{-2} + \frac{1}{2g}C_D m D h}} \quad \text{for } h \leq k \tag{4.70}$$

4.6.2 Representative roughness of submerged vegetation following from the method of effective water depth

To determine the representative roughness for submerged vegetation, we first elaborate on a relatively simple method known as the 'method of effective water depth', which is applied in earlier studies by, for example, Hong (1995), Campana (1999), Klaassen *et al.* (1999) and Stone and Shen (2002). In this method the vertical flow profile for submerged vegetation (Fig. 4.1) is schematised as two non-interacting flow layers. The lower layer describes the vertical flow profile through the vegetation, hereby it is assumed that the flow is uniform. For the upper layer, a logarithmic vertical flow profile is assumed above, or partly in, the vegetation. The discharge per unit width through and over the vegetation is weighted over the respective heights of the two profiles and from the total discharge relationship the resistance follows.

We assume two different variants for the distribution of flow through and over the vegetation. In variant 1, the vertical profile is schematised as in the left panel of Fig. 4.6. A logarithmic velocity profile with velocity $u_u(z)$ is assumed entirely above the vegetation. At the top of the vegetation, at height $z = k$, the logarithmic profile matches the uniform
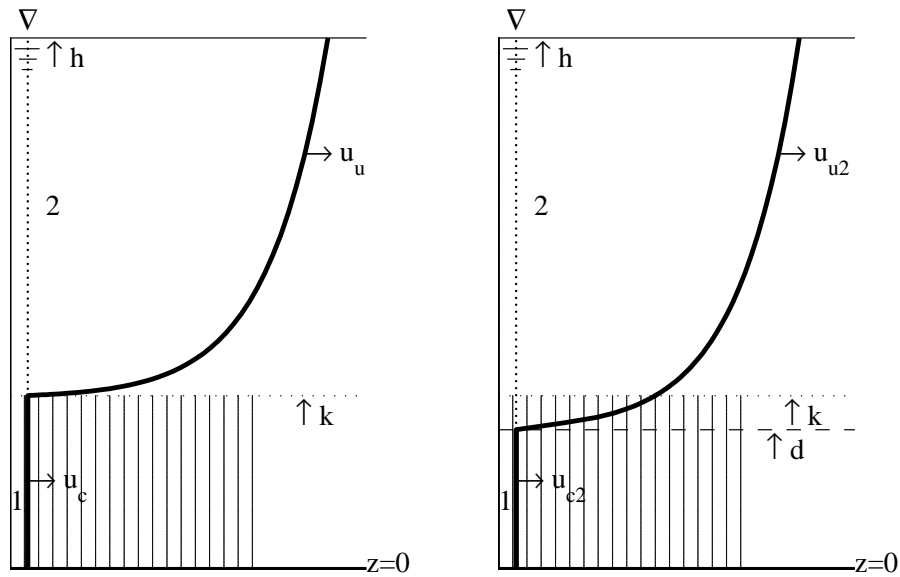
Figure 4.6: Schematised vertical flow division, without penetration of logarithmic velocity profile (left panel) and with penetration of logarithmic velocity profile (right panel). Part 1 is the uniform flow part and part 2 is the logarithmic flow part.

velocity, u_c, inside the vegetation. The discharge is distributed over two flow parts; part 1 describes the uniform flow part and part 2 describes the logarithmic flow part.

Variant 2 takes the penetration of turbulence into the top part of the vegetation into consideration. Now the vertical profile is schematised as in the right panel of Fig. 4.6. A logarithmic velocity profile with velocity $u_{u2}(z)$ is assumed above and partly in the vegetation, until the height $z = d$. At this height, the logarithmic profile matches the uniform velocity, u_{c2} which extends inside the vegetation down to the bed. The discharge is distributed over two flow parts; part 1 describes the uniform flow part and part 2 describes the logarithmic flow part.

Both variants are strong simplifications of reality. In the next section we will elaborate on a more complicated approach in which the vertical profile for velocity inside the vegetation is shown to be an exponential function.

Variant 1: no penetration of the logarithmic profile into the vegetated zone

The flow velocity in the logarithmic part of the profile is given by:

$$u_u(z) = \frac{u_*}{\kappa} \ln \left(\frac{z - k}{z_0} \right) + u_c \tag{4.71}$$

where u_c is the slip velocity of the logarithmic velocity profile. At the level $z = k$, the velocity above the vegetation matches the velocity inside the vegetation. κ is the Von

Kármán constant (0.4), k is the vegetation height (m), z_0 is a roughness length scale (m) and u_* is the shear velocity (m/s):

$$u_* = \sqrt{g(h-k)i} \tag{4.72}$$

The depth-averaged velocity above the vegetation then becomes:

$$\bar{u}_u = \frac{1}{h-k} \int_k^h u_u(z)\,\mathrm{d}z = \frac{u_*}{\kappa} \ln\left(\frac{h-k}{z_0} - 1\right) + u_c = \frac{u_*}{\kappa} \ln\left(\frac{h-k}{\mathrm{e}z_0}\right) + u_c \tag{4.73}$$

where e is the base of the natural logarithm (approximately 2.718).

The flow velocity in the vegetated section follows from the momentum balance for flow through vegetation, Eq. (4.22). The flow velocity in the uniform part of the profile is, therefore, given by the flow through fully submerged vegetation, Eq. (4.23). The discharge per unit width through and over the vegetation is distributed by the respective water depths of the two flow parts depicted in Fig. 4.6, left panel:

$$q = ku_c + (h-k)\bar{u}_u = h\sqrt{\frac{hi}{C_b^{-2} + \frac{C_D mDk}{2g}}} + (h-k)\frac{\sqrt{g(h-k)i}}{\kappa} \ln\left(\frac{h-k}{\mathrm{e}z_0}\right) \tag{4.74}$$

Note that for the calculation of discharge, part 1 in Fig. 4.6 is taken over the entire water column. From the discharge relationship the representative Chézy value for submerged vegetation is calculated as:

$$C_r = \frac{q}{h\sqrt{hi}} \tag{4.75}$$

This yields:

$$C_r = \sqrt{\frac{1}{C_b^{-2} + \frac{C_D mDk}{2g}} + \frac{(h-k)^{3/2}\frac{\sqrt{g}}{\kappa}\ln\left(\frac{h-k}{\mathrm{e}z_0}\right)}{h^{3/2}}} \tag{4.76}$$

Note that the first term on the right-hand side equals the representative roughness for non-submerged vegetation for $h = k$. Note further that part of second term on the right-hand side can be approximated by the White-Colebrook formula:

$$\frac{\sqrt{g}}{\kappa} \ln\left(\frac{h-k}{\mathrm{e}z_0}\right) \equiv 18 \log\left(\frac{12(h-k)}{k_v}\right) \tag{4.77}$$

where k_v, the equivalent Nikuradse roughness height of the (top of the) vegetation layer (m), is taken equal to $30z_0$ (Nikuradse, 1930).

Variant 2: With penetration of the logarithmic profile

The derivation of the representative roughness for the second approach, with penetration of turbulence into the top part of the vegetation, is slightly more complicated since the

flow through the vegetation now consists of two parts, which we divide into a uniform part over the entire vegetation height, $u1$ plus a logarithmic part $u2$:

$$\int_0^k u(z)\mathrm{d}z = \int_0^k u1(z)\mathrm{d}z + \int_d^k u2(z)\mathrm{d}z \tag{4.78}$$

where from the bed $z = 0$ to the level $z = k$ we assume a uniform velocity, so:

$$\int_0^k u1(z)\mathrm{d}z = ku_{c2} \tag{4.79}$$

From height d to the vegetation height k we assume the logarithmic velocity profile, $u2$ without the uniform velocity, u_c, since this is already included in $u1$:

$$u2(z) = \frac{u_*}{\kappa}\ln\left(\frac{z-d}{z_0}\right) \tag{4.80}$$

To calculate the force balance for the flow through the vegetation, we need to integrate the squared logarithmic velocity profile between the limits d and k:

$$\int_d^k u_{u2}^2(z)\mathrm{d}z = \left(\frac{u_*}{\kappa}\right)^2 \int_d^k \left\{\ln\left(\frac{z-d}{z_0}\right)\right\}^2 \mathrm{d}z \tag{4.81}$$

This yields:

$$\int_d^k u_{u2}^2(z)\mathrm{d}z = \left(\frac{u_*}{\kappa}\right)^2 \left[(k-d)\left\{\ln\left(\frac{k-d}{z_0}\right)\right\}^2 - 2(k-d)\ln\left(\frac{k-d}{z_0}\right) + 2(k-d)\right] \tag{4.82}$$

The shear velocity, u_* (m/s), is defined as:

$$u_* = \sqrt{g(h-k)i} \tag{4.83}$$

Note that we strictly follow the definition for a logarithmic velocity profile in a hydraulically rough turbulent boundary layer. In this definition, the level of the shear velocity is determined at that height above which the flow is not affected directly by individual roughness elements (Jackson, 1981). This equals the level $z = k$, the average height of the roughness forming elements. The logarithmic velocity profile has a zero-plane displacement, h_d, underneath the level k. Since we define the z-origin, $z = 0$, at the bed, the level of zero intercept of the logarithmic profile becomes $z = k - h_d = d$ (Figure 4.6; also see paragraph 4.6.4). Consequently, $u_* \neq \sqrt{g(h-d)i}$ (compare with Eq. (4.83)), as other authors have assumed.

For readability we introduce:

$$\mathrm{A} = \frac{(h-k)i}{\kappa^2}(k-d)\left[\left\{\ln\left(\frac{z-d}{z_0}\right)\right\}^2 - 2\ln\left(\frac{z-d}{z_0}\right) + 2\right] \tag{4.84}$$

We can now rewrite the momentum balance as:

$$ghi = u_{c2}^2 \left[\frac{g}{C_b^2} + \tfrac{1}{2}C_D m D k \right] + \tfrac{1}{2}C_D m D g \mathrm{A} \tag{4.85}$$

The uniform flow velocity in the zone from $z = 0$ to k thus becomes:

$$u_{c2} = \sqrt{\frac{hi - \tfrac{1}{2}C_D m D \mathrm{A}}{C_b^{-2} + \frac{C_D m D k}{2g}}} \tag{4.86}$$

The flow velocity profile in the logarithmic part above the vegetation is now including the slip velocity:

$$u_{u2}(z) = \frac{u_*}{\kappa} \ln \left(\frac{z - d}{z_0} \right) + u_{c2} \tag{4.87}$$

The depth-averaged flow velocity above the vegetation therefore is:

$$\bar{u}_{u2} = \frac{1}{h - d} \int_d^h u_{u2}(z)\,\mathrm{d}z = \frac{u_*}{\kappa} \ln \left(\frac{h - d}{\mathrm{e}z_0} \right) + u_{c2} \tag{4.88}$$

Applying the vertical flow division of Fig. 4.6, right panel:

$$q = d u_{c2} + (h - d)\bar{u}_{u2} = h \sqrt{\frac{hi - \tfrac{1}{2}C_D m D \mathrm{A}}{C_b^{-2} + \frac{C_D m D k}{2g}}} + (h - d)\frac{\sqrt{g(h - k)i}}{\kappa} \ln \left(\frac{h - d}{\mathrm{e}z_0} \right) \tag{4.89}$$

yields the representative Chézy value:

$$C_r = \frac{h \sqrt{\dfrac{h - \tfrac{1}{2}C_D m D \frac{(h-k)}{\kappa^2}(k-d)\left[\left\{ \ln\left(\frac{k-d}{z_0}\right) \right\}^2 - 2\ln\left(\frac{k-d}{z_0}\right) + 2 \right]}{C_b^{-2} + \frac{1}{2g}C_D m D k}} + (h - d)\frac{\sqrt{g(h-k)}}{\kappa} \ln\left(\frac{h-d}{\mathrm{e}z_0}\right)}{h^{3/2}} \tag{4.90}$$

Note that for $k = d$, Eq. (4.90) reduces to Eq. (4.76).

4.6.3 Representative roughness for submerged vegetation following from the analytical approach

The analytical solution to the momentum balance described in section 4.5 can be used to determine the representative roughness for submerged vegetation. In a similar fashion as before, we need to describe the vertical flow velocity profile through and above the vegetation.

The velocity profile through vegetation is given by Eq. (4.47). However, to determine the depth-averaged velocity through the vegetation, we have to integrate this expression and there is no analytical solution to this integral. Therefore, we now assume a simplified velocity profile inside the vegetation layer, in which the integration constant b is considered negligible for the depth-averaged velocity. This profile shows a decrease of the velocity from
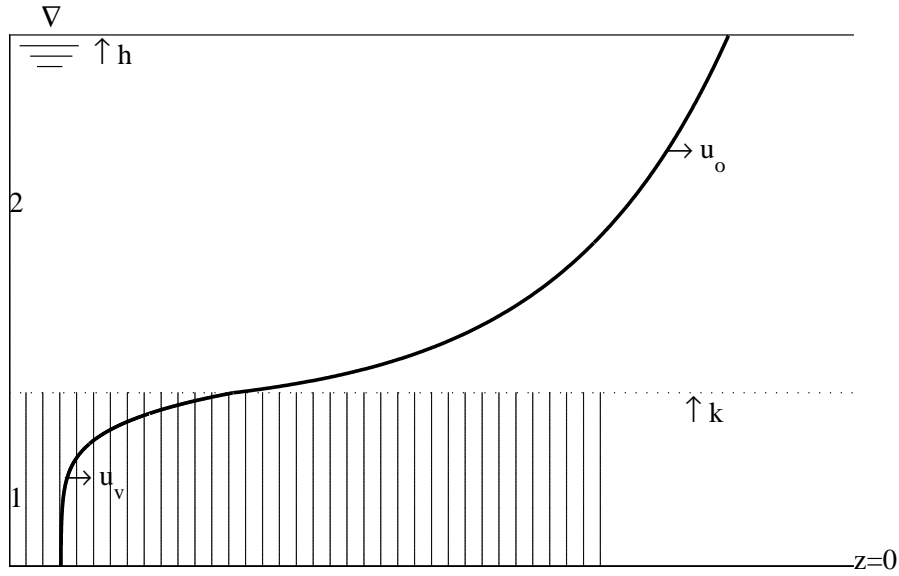
Figure 4.7: Vertical flow profile in the analytical approach.

the top of the vegetation downwards, until, for sufficiently high vegetation, the uniform flow velocity u_{s0} is reached that holds down to the bed level. This approach, therefore, cannot be correct near $z = 0$ where u must vanish, but we are now interested in the upper part of the profile. This velocity profile is defined by:

$$u_v(z) = \sqrt{u_{s0}^2 + a \exp\left(\frac{z}{L}\right)} \tag{4.91}$$

Figure 4.7 presents a schematic view of the velocity profile. The profile is subdivided in two parts, one above the vegetation, u_o (part 2) and one inside, u_v (part 1). Inside the vegetation, the velocity profile is given by Eq. (4.91), compare the shape with Fig (4.5). For the velocity profile above the vegetation we assume a logarithmic profile that includes the zero-plane displacement, d, given by:

$$u_o(z) = \frac{u_*}{\kappa} \ln\left(\frac{z - d}{z_0}\right) \tag{4.92}$$

Note that we don't add a constant to this velocity profile in order to match it with the velocity inside the vegetation.

Elaborating Eq. (4.91), we need an expression for a, which follows from the boundary condition that at the top of the vegetation the shear stress of the overlying flow must equal the shear stress of the flow in the vegetation layer, similar to the approach described in section 4.5.2. First we define the derivative to z:

$$\frac{\partial u_v(z)}{\partial z} = \frac{a \exp\left(\frac{z}{L}\right)}{2L\sqrt{u_{s0}^2 + a \exp\left(\frac{z}{L}\right)}} \tag{4.93}$$

Therefore:

$$u_v(z)\frac{\partial u_v(z)}{\partial z} = \frac{a\exp\left(\frac{z}{L}\right)}{2L} \tag{4.94}$$

The boundary condition for the shear stress at the top of the vegetation then reads:

$$\rho c_p \ell \frac{a\exp\left(\frac{k}{L}\right)}{2L} = \rho\,g\,(h-k)\,i \tag{4.95}$$

Thus a becomes:

$$a = \frac{2L\,g\,(h-k)i}{c_p\,\ell\exp\left(\frac{k}{L}\right)} \tag{4.96}$$

Once the velocity profiles inside and above the vegetation are known, the representative Chézy value for the vegetation can be determined. First, we isolate i from the equations for the vertical profile of horizontal velocity through and above the vegetation. The profile through the vegetation is written as:

$$u_v(z) = \sqrt{u_{v0}^2 + a_v\exp\left(\frac{z}{L}\right)}\sqrt{i} = u_{vi}(z)\sqrt{i} \tag{4.97}$$

in which:

$$u_{v0} = \sqrt{\frac{2g}{C_D\,m\,D}} \tag{4.98}$$

and:

$$a_v = \frac{2L\,g\,(h-k)}{c_p\,\ell\exp\left(\frac{k}{L}\right)} \tag{4.99}$$

The logarithmic flow velocity profile above the vegetation is written as:

$$u_o(z) = \left(\frac{\sqrt{g\,(h-k)}}{\kappa}\ln\left(\frac{z-d}{z_0}\right)\right)\sqrt{i} = u_{oi}(z)\sqrt{i} \tag{4.100}$$

The representative roughness follows from the discharge through and above the vegetation:

$$C_r = \frac{k\,\overline{u}_v + (h-k)\overline{u}_o}{h\sqrt{hi}} \tag{4.101}$$

Eliminating i yields:

$$C_r = \frac{k\,\overline{u}_{vi} + (h-k)\overline{u}_{oi}}{h\sqrt{h}} \tag{4.102}$$

where $\overline{u}_{vi}$ and $\overline{u}_{oi}$ are:

$$\overline{u}_{vi} = \frac{1}{k}\int_0^k u_{vi}(z)\mathrm{d}z \tag{4.103}$$

and:

$$\overline{u}_{oi} = \frac{1}{h-k}\int_k^h u_{oi}(z)\mathrm{d}z \tag{4.104}$$

respectively. Elaboration yields:

$$\overline{u}_{vi} = \frac{L}{k} \left[2 \left(u_v(k) - \sqrt{a_v + u_{v0}^2} \right) + u_{v0} \ln \left(\frac{(u_v(k) - u_{v0}) \left(\sqrt{a_v + u_{v0}^2} + u_{v0} \right)}{(u_v(k) + u_{v0}) \left(\sqrt{a_v + u_{v0}^2} - u_{v0} \right)} \right) \right] \quad (4.105)$$

and:

$$\overline{u}_{oi} = \frac{\sqrt{g(h-k)}}{\kappa(h-k)} \left((h-d) \left(\ln \frac{h-d}{z_0} \right) - (k-d) \left(\ln \frac{k-d}{z_0} \right) - (h-k) \right) \quad (4.106)$$

respectively. The expression for the representative roughness then becomes:

$$C_r = \frac{1}{h^{3/2}} \left\{ \begin{array}{l} L \left[2 \left(u_v(k) - \sqrt{a_v + u_{v0}^2} \right) + u_{v0} \ln \left(\frac{(u_v(k) - u_{v0}) \left(\sqrt{a_v + u_{v0}^2} + u_{v0} \right)}{(u_v(k) + u_{v0}) \left(\sqrt{a_v + u_{v0}^2} - u_{v0} \right)} \right) \right] \\ + \frac{\sqrt{g(h-k)}}{\kappa} \left((h-d) \left(\ln \frac{h-d}{z_0} \right) - (k-d) \left(\ln \frac{k-d}{z_0} \right) - (h-k) \right) \end{array} \right\} \quad (4.107)$$

This expression is similar to the one derived by Klopstra *et al.* (1997), although there are some differences. Firstly, there is a difference in the definition of the level of shear velocity in the logarithmic velocity profile. Secondly, the expression for α that is used by Klopstra *et al.* (1997) is replaced in the above derivations by $c_p \ell$. The stem distance ℓ is given by Eq. (4.41) and c_p is defined as the height-averaged turbulence intensity in between the cylinders. Assuming that coefficient c_l in Eq. (4.41) equals 1, which is the case for cylinders, the complete expression for the representative roughness contains one remaining closure coefficient, c_p.

4.6.4 Elaboration on the roughness height and zero-plane displacement

The equations derived for the representative Chézy value for submerged vegetation contain two unknown parameters. The first is the roughness height of the logarithmic velocity profile, z_0. The second is the displacement of the level of zero intercept, d. It must be noted first that in many studies the roughness height is expressed as a Nikuradse equivalent roughness height, k_v, where $k_v = 30 z_0$.

The zero-plane displacement, d, and roughness height, z_0, have been studied both in aquatic and atmospheric boundary layers. In atmospheric studies, the wind profile above vegetation is described by Prandtl's log law. Frequently, d and z_0 are estimated as simple ratios of vegetation height, $d = (2/3)k$ and $z_0 = 0.1k$ (Garratt, 1992). These estimates are substantiated by measurements on sand roughness, rods and vegetation. An application of these estimates for d and z_0 to aquatic flows in order to determine a formula for the Darcy-Weisbach friction factor is given by Jacobs and Wang (2003). More complicated expressions for z_0 and d, as function of vegetation characteristics were derived for atmospheric flows by for example Raupach (1992), Raupach (1994), Massman (1997), and

Table 4.1: Formulae for roughness height z_0 and zero-plane displacement d in aquatic as well as atmospheric studies.

Author(s)	$z_0 =$	$d =$
aquatic:		
Klaassen *et al.* (1999)	$\left(-0.37k^2 + 1.13k\right)/30$	
Stolker and Verheij (2000)	$0.6k^{0.45}/30$	
Van Velzen *et al.* (2003a)	$1.6k^{0.7}/30$	
Stephan and Gutknecht (2002)	$k/30$	k
Jackson (1981)	$\frac{k(1-\exp(-2\alpha))}{2\alpha\exp(1/\alpha)}$	$k\left(1 - \frac{1-\exp(-2\alpha)}{2\alpha}\right)$
atmospheric:		
Garratt (1992)	$0.1k$	$\frac{2}{3}k$
Raupach (1992)	$k(1-\frac{d}{k})\exp\left(\Psi_k - \kappa\frac{U_k}{u_*}\right)$	$k\left[\left(\frac{\beta\lambda}{1+\beta\lambda}\right)\left(1 - C_D\sqrt{\frac{b}{k\lambda}}\frac{u_*}{U_k}\right)\right]$
Raupach (1994)		$k\left(1 - \frac{1-\exp\left(-\sqrt{C_{d1}\Lambda}\right)}{\sqrt{C_{d1}\Lambda}}\right)$
Massman (1997)		$k\left(1 - \int\limits_0^1 \exp\left(-2n(1-\frac{\zeta(z)}{\zeta(k)})\right)d\xi\right)$
Takagi *et al.* (2003)		$k\left(0.10LAI + 0.51\right)$
Thom (1971)	$b(k-d)$	$\int\limits_0^k \frac{d\tau(z)}{dz}z\,dz \left(\int\limits_0^k \frac{d\tau(z)}{dz}dz\right)^{-1}$

k is vegetation height, α is an attenuation coefficient, U_k is the mean velocity at height k, u_* is the shear velocity, Ψ_k is a roughness-sublayer influence function, β is the ratio of vegetation to surface drag coefficients, λ is the roughness density or frontal area per unit ground area, C_{d1} is an empirical parameter (7.5), Λ is the canopy area index for stems and leaves, n is the within-canopy wind speed profile extinction coefficient $\zeta(k)/(2u_*^2/u(k)^2)$, $\zeta(z)$ is the nondimensional drag area density of foliage elements in the canopy, $\zeta(k)$ is the drag area index, $\xi = z/k$, LAI is the Leaf Area Index, b is an empirical parameter (0.29).

Takagi *et al.* (2003). A drawback of the use of these expressions is that they mostly rely on a description of leaf foliage, and that they often contain empirical values derived for atmospheric conditions, which differ from aquatic conditions with regard to the shallowness of the flow.

For aquatic flows, several approaches to determine the roughness height and the zero-plane displacement of the overlying logarithmic velocity distribution can be found in literature. In several Dutch studies data from flume experiments was used to find an expression for z_0, see Table 4.1, the first three references. Stephan and Gutknecht (2002) conclude on the basis of their flume experiments on three natural vegetation types that d as well as z_0 are equal to the deflected plant height. It must be noted here that generalisation of these findings to other conditions is questionable. Furthermore, their graphs of d and z_0 versus the deflected plant height, k', show a clear deviation of k', which is explained by the authors by the questionable argument of the oscillation amplitude of the leaves.
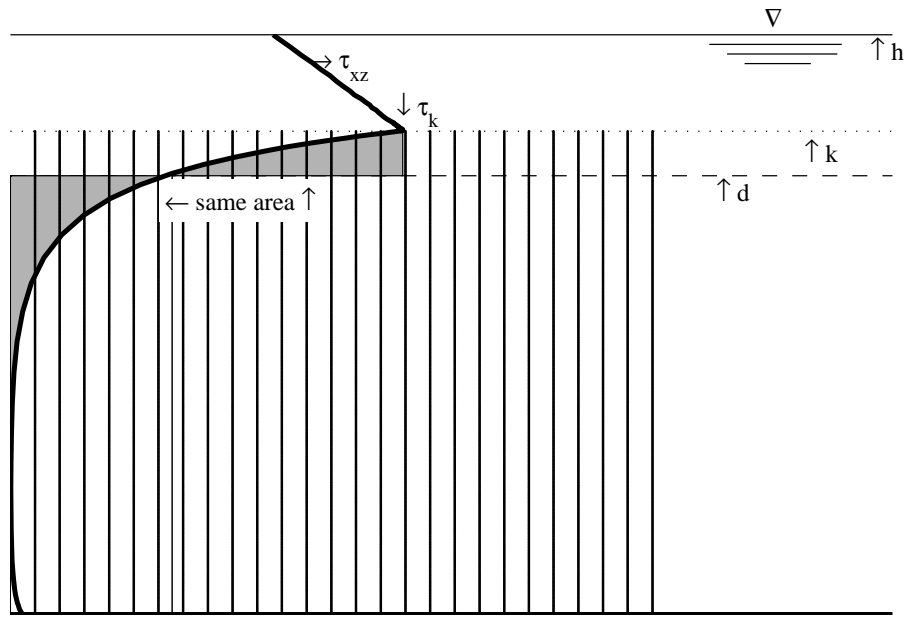
Figure 4.8: Vertical profile for the shear stress, τ_{xz} and definition of zero-plane displacement d. k is vegetation height, h is water depth, τ_k is maximum shear stress at the top of vegetation.

Thom (1971) found empirically that d corresponds to the vertical position of the centroid of momentum absorption:

$$d = \frac{\int\limits_0^k \frac{d\tau(z)}{dz} z \, dz}{\int\limits_0^k \frac{d\tau(z)}{dz} dz} \tag{4.108}$$

This definition is also applied in some aquatic studies, for example by Nepf and Vivoni (2000). Table 4.1 presents an overview of formulae for z_0 and d found in literature.

The mechanical basis for Eq. (4.108) can be determined by the balance of forces in the shear region inside the vegetation. Here we follow an approach which is based on the analysis of Jackson (1981) for bed roughness. He determines the zero-plane displacement by the balance of horizontal forces in the vegetation layer. The zero-plane displacement adjusts the reference level of the logarithmic velocity profile to the height at which the mean surface shear appears to act. The value for d thus follows from the definition that the level of action for the moment M of the resulting average horizontal force in the flow is at a distance M/τ_k above the z-origin:

$$d = \frac{M}{\tau_k} \tag{4.109}$$

where τ_k is the shear stress at the top of the vegetation, at height k. The shear velocity in the logarithmic velocity profile is defined by:

$$u_* = \sqrt{\frac{\tau_0}{\rho}} \tag{4.110}$$

The moment M per unit volume is defined by the integration over the vegetation height k of the resulting average horizontal force in the vegetation layer, $f(z)$, multiplied by the distance z:

$$M = \int_0^k z f(z) \mathrm{d}z \qquad (4.111)$$

where $f(z)$ follows from the momentum balance for flow through and over vegetation:

$$f(z) = \rho g \frac{\partial h}{\partial x} - F_{drag} = \frac{\partial \tau_{xz}}{\partial z} \qquad (4.112)$$

Applying the chain rule yields:

$$M = z\,\tau_{xz}\big|_0^k - \int_0^k \tau_{xz}(z)\mathrm{d}z = \tau_k k - \int_0^k \tau_{xz}(z)\mathrm{d}z \qquad (4.113)$$

Substitution in Eq. (4.109) yields the following definition for the zero-plane displacement, d:

$$d = k - \int_0^k \frac{\tau_{xz}(z)}{\tau_k}\,\mathrm{d}z = k\left(1 - \frac{\overline{\tau}_{xz}}{\tau_k}\right) \qquad (4.114)$$

Note that this definition precludes the zero-plane displacement to become negative. Figure 4.8 shows a typical vertical profile for the shear stress. The zero-plane displacement, d, is defined such that both gray shaded zones have the same area. Equation (4.114) therefore yields the same results as Eq. (4.108). Assuming a parabolic profile for the decrease of the shear stress to zero at the zero bed level yields $d = (2/3)k$, which is in line with earlier findings (Garratt, 1992). However, for tall and sufficiently dense vegetation, the shear stress rapidly falls of to zero at a certain level above the bed, defined as k_d. This will shift the zero-plane displacement upwards to $d = (2/3)k + (1/3)k_d$. The problem of course is estimating k_d. On the other hand, for short and sufficiently thin vegetation, the shear stress profile may extend towards the bed leading to a finite bed shear stress, τ_b, and therefore a relatively large average shear stress, $\overline{\tau}_{xz}$, thus shifting the zero-plane displacement downwards. In the next section we will derive analytical expressions for the zero-plane displacement and roughness height for cylindrical resistance.

4.6.5 Expressions for the zero-plane displacement and roughness height

We now determine analytical formulae for the zero-plane displacement, d, the roughness height, z_0, and the representative Chézy value, C_r, for submerged vegetation. We apply the simplified vertical profile for flow through vegetation, Eq. (4.91), which shows an exponential decrease in velocity, going from the top downwards near the bed.

An expression for the zero-plane displacement

The zero-plane displacement is determined by the momentum absorption of the vegetation, and adjusts the reference level of the logarithmic velocity profile to the height at which the mean surface shear appears to act. A formula for d was derived in which d is determined by the shear stress profile inside the vegetation layer and the shear stress at the top of the vegetation, see Eq. (4.114):

$$d = k - \int_0^k \frac{\tau_{xz}(z)}{\tau_k} \, \mathrm{d}z \tag{4.115}$$

The vertical shear stress profile is defined by Eq. (4.39) and Eq. (4.42):

$$\tau_{xz} = \rho c_p \ell u_v(z) \frac{\partial u_v(z)}{\partial z} \tag{4.116}$$

therefore:

$$\frac{\tau_{xz}}{\tau_k} = \frac{\rho c_p \, \ell \, u_v(z) \frac{\partial u_v(z)}{\partial z}}{\rho c_p \, \ell \, u_v(k) \frac{\partial u_v(k)}{\partial z}} \tag{4.117}$$

Substituting Eq. (4.94) gives an expression for d:

$$d = k - \int_0^k \frac{\exp\left(\frac{z}{L}\right)}{\exp\left(\frac{k}{L}\right)} \, \mathrm{d}z \tag{4.118}$$

which yields:

$$d = k - L\left(1 - \exp\left(-\frac{k}{L}\right)\right) \tag{4.119}$$

An expression for the roughness height

A next unknown parameter is the roughness height of the top of the vegetation, z_0. This follows from the boundary condition that at the top of the vegetation the flow velocity of the vegetation profile, $u_v(k)$, equals the flow velocity of the overlying logarithmic profile, $u_o(k)$:

$$\sqrt{u_{s0}^2 + a \exp\left(\frac{k}{L}\right)} = \frac{\sqrt{g\,(h-k)i}}{\kappa} \ln\left(\frac{k-d}{z_0}\right) \tag{4.120}$$

Note that we define the shear velocity at the level $z = k$, see section 4.6.4, as well. Thus z_0 becomes:

$$z_0 = (k-d)\exp\left(-\frac{\kappa\sqrt{u_{s0}^2 + a \exp\left(\frac{k}{L}\right)}}{\sqrt{g\,(h-k)i}}\right) \tag{4.121}$$

Substituting Eq. (4.46) for u_{s0} and Eq. (4.96) for a in Eq. (4.121) and rewriting using Eq. (4.45) for L, yields:

$$z_0 = (k-d)\exp\left(-\kappa\sqrt{\frac{2L}{c_p\ell}\left(1 + \frac{L}{h-k}\right)}\right) \tag{4.122}$$

4.6.6 On the coefficient c_p

Van Velzen *et al.* (2003b) compared experimental flume data on submerged reed with the results of the analytical equation of Klopstra *et al.* (1997) and found two adequate expressions for the characteristic length scale of turbulent eddies inside the vegetation, α (which equals $c_p \ell$). The turbulence intensity c_p is either given by:

$$c_p = \frac{0.015\sqrt{hk}}{\ell} \tag{4.123}$$

or:

$$c_p = \frac{0.0227k^{0.70}}{\ell} \tag{4.124}$$

Van Velzen *et al.* (2003b) prefer to use Eq. (4.124). They ground their choice on the basis of a better representation for the roughness of low types of vegetation (e.g. grasses) and their expectation of a limited validity for larger water depths, although Eq. (4.124) is not dimensionally correct.

Rodríguez Uthurburu (2004) applied Genetic Programming to derive an expression for c_p. Genetic Programming is a global optimisation technique that can be used to find interdependencies in a set of input-output data and provides explicit symbolic formulations of this input-output relationship. Genetic Programming applies evolutionary algorithms to optimize the symbolic model structure and its coefficients simultaneously. Furthermore, the resulting population of algebraic expressions can be made dimensionally correct (Babovic & Keijzer, 2000). Genetic Programming has been applied before on hydraulic problems (Babovic & Abbott, 1997), or on vegetation resistance (Babovic & Keijzer, 1999; Babovic & Keijzer, 2000; Harris *et al.*, 2003). Rodríguez Uthurburu (2004) found that many expressions consisted of a term for the submerged water depth, $h-k$, and the characteristic stem distance, ℓ, such as in:

$$c_p = \frac{1}{50}\frac{h-k}{\ell} \tag{4.125}$$

However, further analysis for this thesis revealed that this expression is not valid for relatively large water depths of several metres. Moreover, it must be noted here that further efforts with Genetic Programming to obtain a formula for c_p that fits better than Eq. (4.123) and (4.124) for large water depths have failed so far.

The above formulae state that c_p is mainly dependent on the (submerged) water depth or the vegetation height, divided by the stem distance. According to the assumptions made in the one-dimensional model for flow through and over vegetation developed by Uittenbogaard (2003), the turbulence intensity indeed increases with a decreasing stem distance, be it by $\ell^{-\frac{1}{3}}$, instead of ℓ^{-1}. In the analytical approach, the assumption was made that c_p is a height-averaged turbulence intensity. In reality, however, the turbulence intensity is a function of z, which is affected by the penetration of the overlying turbulent eddies and the wake turbulence of the stems (see Fig. 4.4). The turbulence intensity of
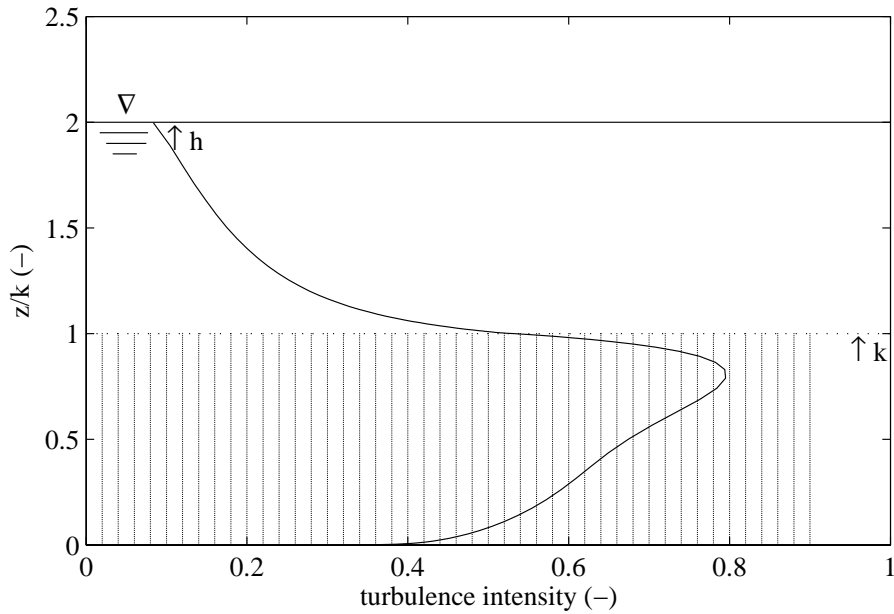
Figure 4.9: Example of a vertical profile of the turbulence intensity, I, for tall vegetation.

the horizontal velocity, I, is a measure for the deviation of the instantaneous velocity, u_i, from its mean, relative to the time-averaged mean velocity, u. It is commonly expressed as a non-dimensional parameter by the ratio of the standard deviation of the instantaneous velocity, σ_u, over the time-averaged flow velocity:

$$u' = u_i - u \tag{4.126}$$

$$\sigma_u(z) = \sqrt{\overline{u'^2}}(z) \tag{4.127}$$

$$I(z) = \frac{\sigma_u(z)}{u(z)} \tag{4.128}$$

where u' is the turbulent part of the velocity, or eddy velocity (m/s), u_i is the instantaneous velocity (m/s) and u is the time-averaged velocity (m/s).

A related parameter is the turbulent kinetic energy per unit mass, k_T (m^2·s^{-2}), which is defined:

$$k_T = \frac{1}{2}\left(\overline{u'^2}\right) \tag{4.129}$$

The 1-DV model computes the turbulent energy budget with the use of a k-ϵ turbulence closure model. The turbulence intensity then follows from (see Eq. (4.43), as well):

$$I(z) = \frac{\sqrt{k_T}(z)}{u(z)} \tag{4.130}$$

Figure 4.9 presents a typical vertical profile of the turbulence intensity for relatively tall vegetation calculated by the 1-DV model for flow through and over vegetation. The model results demonstrate that the turbulence intensity is not uniform over the height. A
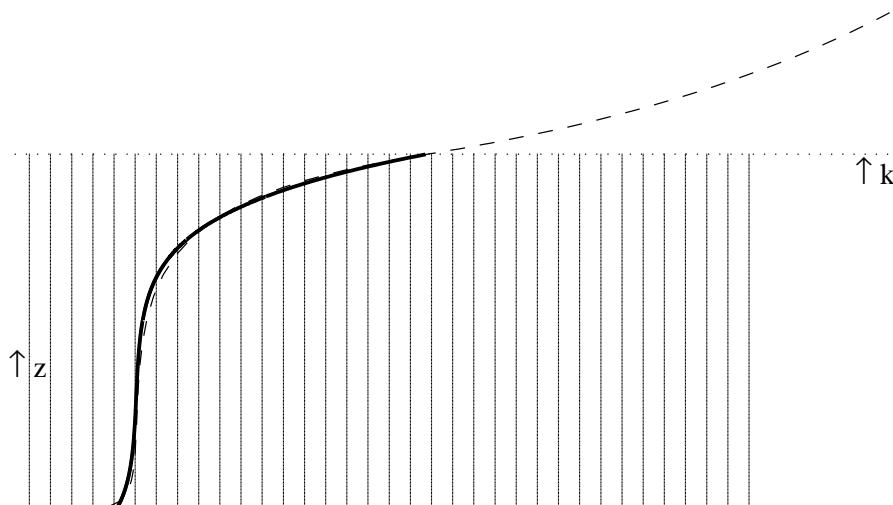
Figure 4.10: Vertical profile of horizontal velocity for reed, with properties taken from Van Velzen *et al.* (2003a), D=0.046 m, m=80 m^{-2}, C_D=1.8, k=2.5 m, h=5 m, computed with the 1-DV model (dashed line) and compared with the analytical solution (solid line) for a c_p-value of 0.40.
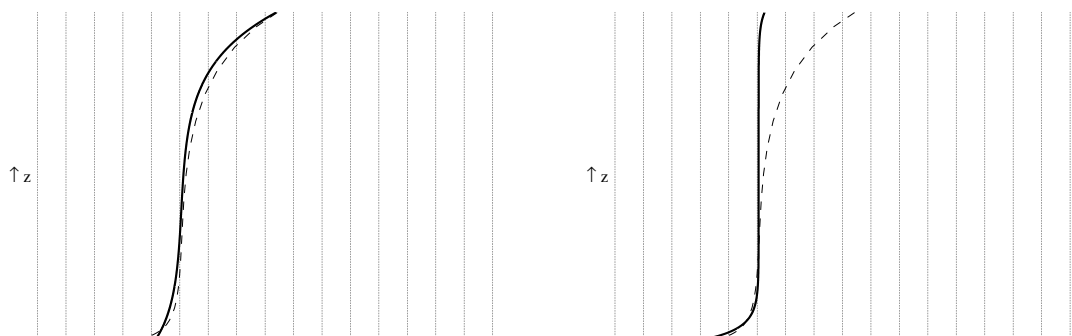
Figure 4.11: Vertical profile of horizontal velocity for reed, D=0.046 m, m=80 m^{-2}, C_D=1.8, k=2.5 m, h=5 m, computed with the 1-DV model (dashed line) in the near-bed region and compared with the analytical solution (solid line). Left panel: c_p=0.40. Right panel: c_p=0.04.

maximum intensity is found beneath the top of the vegetation in the region where a high turbulent kinetic energy coincides with a rapidly declining velocity. This was also found in measurements by Nepf and Vivoni (2000).

In the top layer of submerged vegetation, a high turbulence intensity is found, caused by the penetration of shear-induced turbulence from the overlying water column. For increasing water depths, the production of shear-induced turbulence increases and so does the penetration of this turbulence into the vegetation layer. In the lower layer of submerged vegetation, a lower turbulence intensity is found, governed by wake turbulence from the stems and by the bed roughness. In case of relatively short vegetation, the penetration of
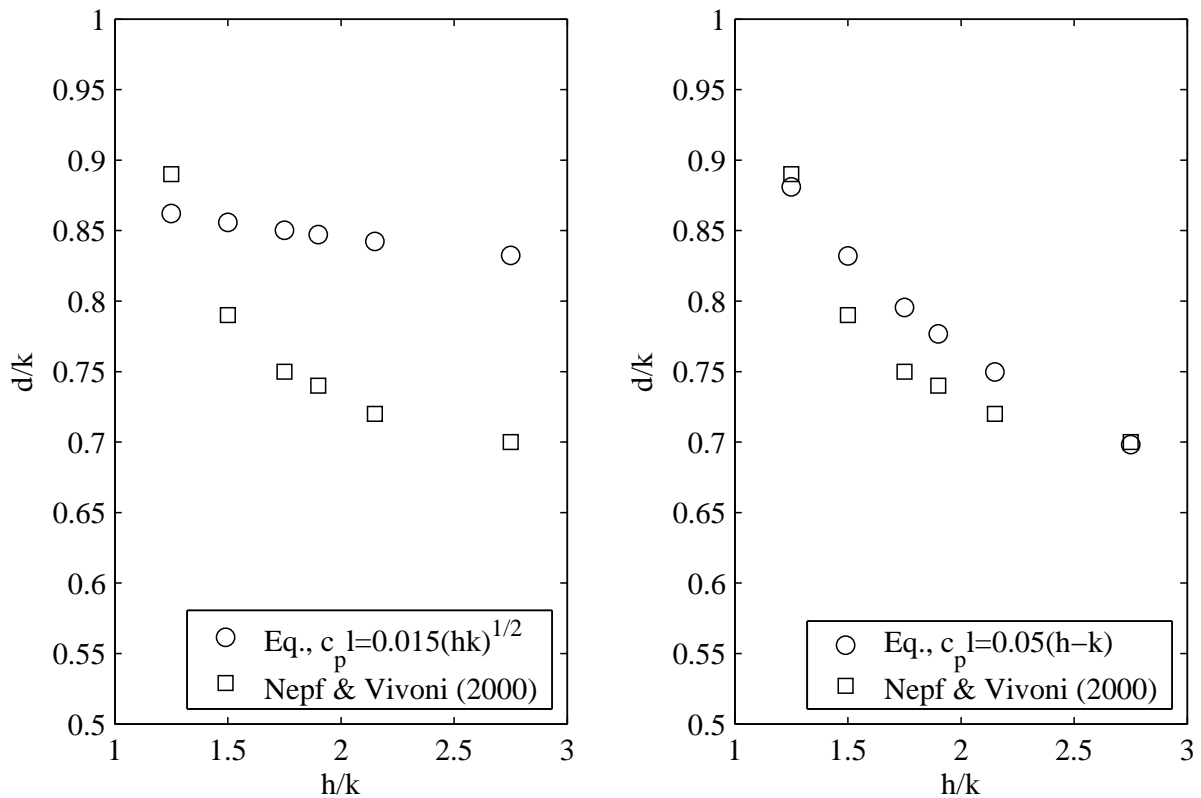
Figure 4.12: Comparison between measured and modelled dimensionless zero-plane displacement, d/k. Left panel: applying Eq. (4.119) with Eq. (4.123). Right panel: applying Eq. (4.119) with Eq. (4.131).

shear turbulence can reach the bed and, hence, the height-averaged turbulence intensity is high. This implies, however, that the turbulence intensity is inversely related to k.

The vertical profile for the turbulence intensity is thus represented in the height-averaged c_p as a function of k and h. All in all, the formulae found lack a physical basis. One can also argue that the applied assumption of a height-averaged turbulence intensity is not valid, but the analytical approach would become very complex if c_p were made z-dependent.

Figure 4.10 compares a vertical profile of horizontal velocity for submerged reed, computed with a 1-DV model (see section 4.7), with the profile from the analytical solution. A reasonable fit was found with a c_p-value of 0.4. However, for the near-bed region, a c_p-value of 0.04 much better represents the near-bed velocity profile, Fig. 4.11. This leads to the conclusion that to accurately describe the near-bed velocity profile, which is needed to determine the bed shear stress, the c_p-value needs to be fitted differently than for describing the representative roughness.
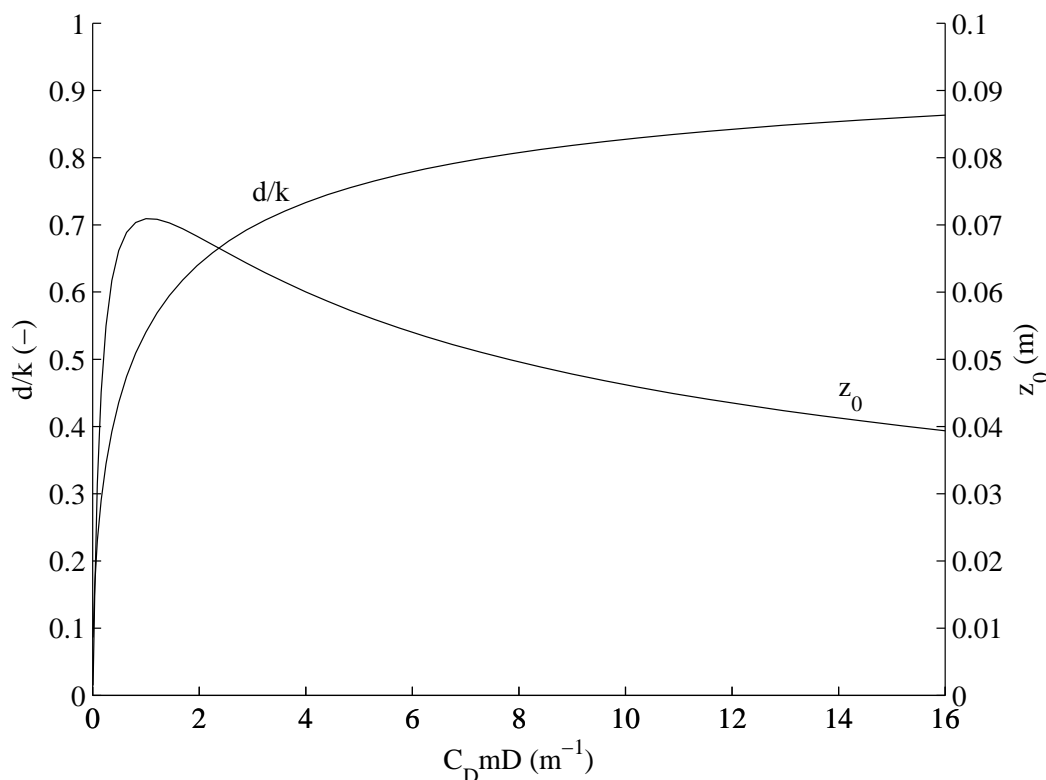
Figure 4.13: The dimensionless zero-plane displacement, d/k and the roughness height for the top of the vegetation, z_0 as function of $C_D m D$. h is 2 m, k is 0.5 m, C_D is 1.

4.6.7 On the zero-plane displacement

Equations (4.119) and (4.122) give fairly simple expressions for the zero-plane displacement and roughness height of flow over submerged vegetation, as a function of the vegetation characteristics and the coefficient of turbulence intensity, c_p. The latter is included in the expression for L. To test the validity of Eq. (4.119), a comparison is made with flume data from Nepf and Vivoni (2000). In their experiment with flexible plastic plants they carefully measured the vertical profiles of Reynolds stress and calculated the zero-plane displacement by applying Eq. (4.108). The plant characteristics are: D=0.0167 m, m=330 m^{-2} (yielding $mD = 5.5$ m^{-1}), C_D=1.0 and k=0.16 m. For increasing depth ratios of h/k, Nepf and Vivoni (2000) found decreasing ratios for d/k. Figure 4.12 presents the comparison of the measurements with the results of the analytical equation. The left panel shows that by applying Eq. (4.119) in combination with the dimensionally correct Eq. (4.123) for the c_p-value, the fit is not very good. The right panel shows a better correspondence with the measurements when the following formula for c_p is applied:

$$c_p = \frac{1}{20}\frac{h-k}{\ell} \qquad (4.131)$$

This comparison with data demonstrates that Eq. (4.119) seems a valid approximation for the zero-plane displacement, but to simulate the zero-plane displacement, and therefore,

the physical processes, more accurately, the closure coefficient for the turbulence intensity, c_p, needs to be fitted. The c_p coefficient is dependent on the submerged water depth, and may be different for flexible vegetation than for rigid vegetation.

In Fig. 4.13, Eqs. (4.119) and (4.122) are depicted graphically as a function of the product of density and cylinder diameter, mD, for a water depth of 2 m, a vegetation height of 0.5 m and a drag coefficient, C_D of 1. The c_p-coefficient is given by Eq. (4.131). Typical ranges for mD for natural vegetation are 0.1 to 1.0 m^{-1} for open herbaceous and marsh types of vegetation, and 10 to 15 m^{-1} for natural grasslands. Figure 4.13 shows that the simple estimate for $d = (2/3)k$ (see Table 4.1) is within the valid range, but the exact value for d is dependent on the vegetation type. For thin vegetation in low densities, the zero-plane displacement decreases, thus the penetration of turbulence inside the vegetation layer increases. For dense vegetation, the opposite goes, the zero-plane displacement increases, thus the penetration of turbulence inside the vegetation layer decreases.

The roughness height, z_0, is around 0.04 to 0.07 m for this combination of parameters, which is near the simple assumption of $z_0 = 0.1k$ (see Table 4.1), although Fig. 4.13 shows that the value for z_0 is highly dependent on mD. Furthermore, z_0 is dependent on c_p and the submerged water depth $(h - k)$, see Eq. (4.122).

4.6.8 An alternative formula for the representative roughness

Rodríguez Uthurburu (2004) also applied Genetic Programming to obtain directly a relationship for the representative roughness from numerical modelling results of the 1-DV model. After some rearranging of the results, he found:

$$C_r = \sqrt{\frac{2g}{C_D mDk}} + 2\sqrt{g}\ln\frac{h}{k} \qquad (4.132)$$

This expression can be related to the work of Kouwen *et al.* (1969) who assumed the following relation to hold for the logarithmic velocity profile above the vegetation:

$$\frac{u(z)}{u_*} = \frac{u_k}{u_*} + \frac{1}{\kappa}\ln\frac{z}{k} \qquad (4.133)$$

where u_k (m/s) is the slip velocity at the top of the vegetation. By further assuming that u_k is proportional to u_* they found:

$$\frac{\overline{u}}{u_*} = C + \frac{1}{\kappa}\ln\frac{h}{\chi} \qquad (4.134)$$

in which:

$$C = \frac{1}{u_* h}\int_0^k u\,\mathrm{d}z \qquad (4.135)$$

and:

$$\chi = k \exp\left(1 - \kappa \frac{u_k}{u_*}\right)\left(1 - \frac{k}{h}\right) \tag{4.136}$$

Based on their flume experimental data they concluded that the χ roughness parameter is roughly 12% larger than the deflected vegetation height k and, therefore, they rewrote Eq. (4.134) to:

$$\frac{\overline{u}}{u_*} = C_1 + \frac{1}{\kappa} \ln \frac{h}{k} \tag{4.137}$$

in which:

$$C_1 = C - \frac{1}{\kappa}\left(1 - \kappa \frac{u_k}{u_*}\right)\left(1 - \frac{k}{h}\right) \tag{4.138}$$

The representative roughness can then be obtained applying:

$$\frac{C_r}{\sqrt{g}} = \frac{\overline{u}}{u_*} \tag{4.139}$$

under the assumption that $u_* = \sqrt{ghi}$.

Rodríguez Uthurburu (2004) further analysed the formula found be Genetic Programming, Eq. (4.132), and found the following similarity:

$$C_r = C_2 + \frac{\sqrt{g}}{\kappa} \ln \frac{h}{k} \tag{4.140}$$

where:

$$C_2 = \sqrt{\frac{2g}{C_D m D k}} \tag{4.141}$$

Note that C_2 equals the vegetation resistance for maximally flooded non-submerged vegetation, which can be replaced by the improved form of Eq. (4.70) for $h = k$:

$$C_{r,nonsub} = \sqrt{\frac{1}{\frac{1}{C_b^2} + \frac{1}{2g}C_D m D k}} \tag{4.142}$$

Also note that $2\sqrt{g}$, found in the Genetic Programming solution can be replaced by the theoretically more sound $\sqrt{g}/\kappa \approx 2.5\sqrt{g}$, which yields:

$$C_r = \sqrt{\frac{1}{C_b^{-2} + \frac{1}{2g}C_D m D k}} + \frac{\sqrt{g}}{\kappa} \ln \frac{h}{k} \tag{4.143}$$

Rough wall turbulent flow relationship

Comparing Eq. (4.76) with Eq. (4.143) it can be easily seen that the GP-formula follows for $(h - k) = h$ and assuming that the roughness height of the vegetation, z_0, equals the vegetation height, k, divided by e. Although the improved formula found with Genetic Programming bears resemblance with the formula of Kouwen *et al.* (1969) it is not quite

clear why this formula is of this form. The following elaboration does not prove the physical correctness of Eq. (4.143), but merely gives a possible explanation.

We first assume that the roughness of vegetation is equivalent to the flow along a fully rough bed. Hinze (1975, p. 636) defines the condition of a fully-rough bed by:

$$\frac{u_* \, k_s}{\upsilon} \geq 55 \tag{4.144}$$

where k_s is the Nikuradse length scale, which is of the order of the geometrical height of the roughness forming elements that create the fluid-bed interface. Here, it is assumed that k_s equals k, the height of the vegetation.

An important definition is that of the reference level normal to the bed, the z-direction, and z is positive away from the bed. Hinze (1975, Eq. 7-76) defines the plane $z = 0$ as the average of the top levels of the roughness forming elements. In the case of (schematised) vegetation this is located at the top of the vegetation layer. Subsequently, Perry et $al.$ (1969) and Hinze (1975) define the logarithmic profile above a rough bed by:

$$\frac{U\left(z\right)}{u_*} = \frac{1}{\kappa} \ln \left(\frac{u_* \left(z + k_e\right)}{\upsilon} \right) + B - \frac{\Delta U\left(z\right)}{u_*} \tag{4.145}$$

where $U(z)$ is the flow velocity, $\Delta U(z)$ is the velocity defect between smooth and rough flow conditions (Hinze, 1975 p. 635) and B is a constant. For $\Delta U = 0$, Eq. (4.145) is equivalent to the turbulent layer flow along a hydraulically smooth wall, but with the origin k_e below the mean top levels of the fluid-bed interface. For a rough bed, there occurs a velocity shift ΔU (Perry et $al.$, 1969; Hinze, 1975):

$$\frac{\Delta U\left(z\right)}{u_*} = \frac{1}{\kappa} \ln \left(\frac{u_* \, k_e}{\upsilon} \right) + C \tag{4.146}$$

where C is a constant.

The apparent origin of the logarithmic velocity profile is $z = -k_e$. Based on various observations (Hinze, 1975, Fig. 7-16), Hinze estimates $k_e = 0.25 k_s$. Perry et $al.$ (1969) empirically found that for flow over a 'k' type rough wall, k_e is proportional to the scale (k) of the roughness and found $k_e = 0.25 k_s$ as an average, as well. Jackson (1981) shows on the basis of a literature study that for various roughness elements (sediment grains as well as vegetation) k_e ranges between 0.16 - $0.46 k_s$, with $k_e = 0.3 k_s$ as a good approximation. Dittrich and Koll (1997) found $k_e = 0.57 k_s$ for grains. In addition, Garratt (1992) shows that $k_e = 0.33 k_s$ is often applied as a zero-plane displacement in atmospheric flow over canopies. Finally, Stanhill (1969) shows that for atmospheric flow over vegetation types ranging from grass (0.02 m) to forest (20 m), $k_e = 0.36 k_s$ is a good approximation.

Here we postulate:

$$k_e = \frac{1}{e} k_s = 0.37 k_s \tag{4.147}$$

where e is the base of the natural logarithm (2.718). We have shown previously that the zero-plane displacement is a function of the length scale L and the vegetation height k, see Eq.(4.119) and Fig. 4.13. Note that in Fig. 4.13, d/k is expressed relative to a zero-level at the base of the vegetation, instead of the top of the vegetation. From Fig. 4.13 it can be derived that $d/k = (1 - 0.37) = 0.63$ seems a plausible average value over a wide range of vegetation properties.

Combining Eqs. (4.145), (4.146) and (4.147) yields:

$$\frac{U(z)}{u_*} = \frac{1}{\kappa} \ln \left(\frac{e\,z}{k_s} \right) + D \tag{4.148}$$

where D is a constant, depending on the characteristics of the roughness.

We now postulate that D is given by the uniform flow velocity through the vegetation:

$$D = \frac{u_{s0}}{u_*} \tag{4.149}$$

It then follows that:

$$U(z) = \frac{u_*}{\kappa} \ln \left(\frac{ez}{k_s} \right) + u_{s0} \tag{4.150}$$

The depth-averaged flow velocity equals:

$$\bar{u} = \frac{1}{h} \int_0^h U(z)dz = \frac{u_*}{\kappa} \ln \left(\frac{h}{k_s} \right) + u_{s0} \tag{4.151}$$

Applying the relation:

$$\frac{\bar{u}}{u_*} = \frac{C_r}{\sqrt{g}} \tag{4.152}$$

and assuming $k_s = k$ yields:

$$C_r = \frac{\sqrt{g}}{\kappa} \ln \left(\frac{h}{k} \right) + \frac{u_{s0}}{u_*} \sqrt{g} \tag{4.153}$$

If we now consider the uniform flow velocity inside the vegetation, it follows that:

$$\frac{u_c}{u_*} \sqrt{g} = \frac{\overline{u}_c}{u_*} \sqrt{g} = C_{r,nonsub} \tag{4.154}$$

Applying Eq. (4.139) for $C_{r,nonsub}$ yields finally:

$$C_r = \frac{\sqrt{g}}{\kappa} \ln \left(\frac{h}{k} \right) + \sqrt{\frac{1}{C_b^{-2} + \frac{1}{2g}C_D mDk}} \tag{4.155}$$

which is equal to Eq. (4.143) and will be called *GP-formula*. This expression is very simple in its form. The right-hand side of Eq. (4.155) consists of two parts, one equals the representative roughness of non-submerged vegetation, applied as a kind of bed boundary condition to the resistance of flow and the other is the representative roughness of the water column, affected by the roughness tops of the vegetation, which equals a form of bed roughness, as well. The performance of this equation is described in section 4.7.
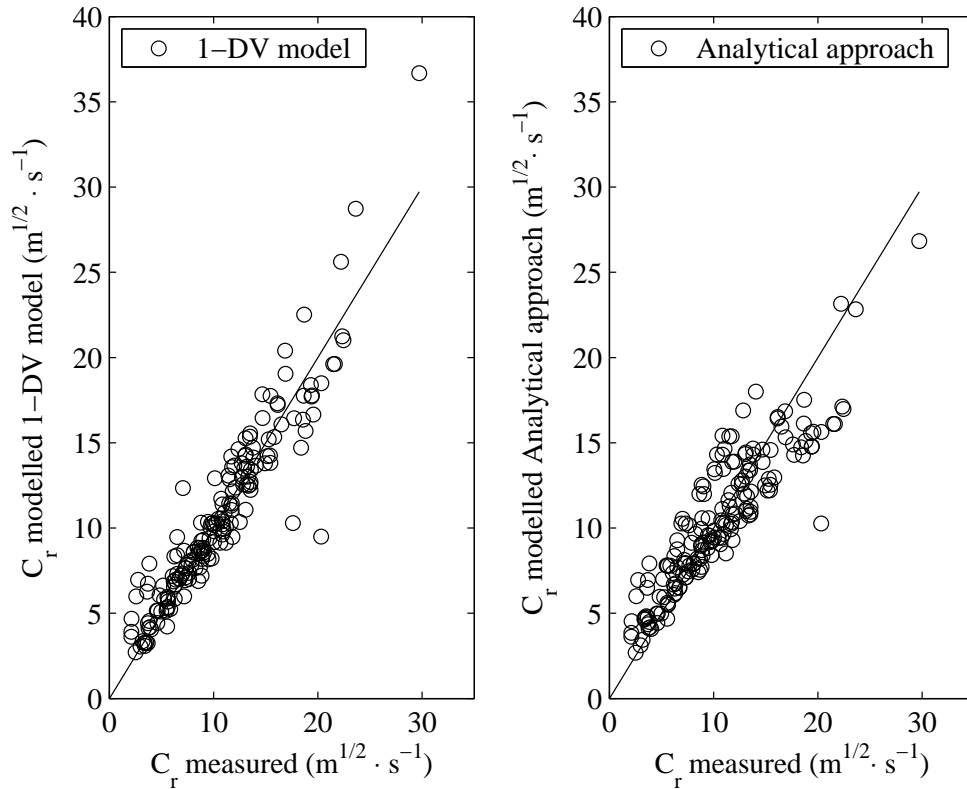
Figure 4.14: Comparison of modelled with measured values for the representative roughness. Left panel: applying the 1-DV numerical model. Right panel: applying the *Analytical approach*, equations 4.107 and 4.131.

4.7   Comparison of the representative roughness expressions with data

4.7.1 Comparison with representative roughness data from flume experiments

To test the derived analytical formulae for hydraulic resistance, a data set of flume data of submerged vegetation has been collected from literature. In total 177 experimental runs, from 10 different studies, were collected. Table A.1 presents the data, which consists of the diameter, density, (deflected) height, drag coefficient, water depth, depth-averaged velocity and representative roughness. The Chézy coefficient for the bed is assumed to be $60 \text{ m}^{1/2} \cdot \text{s}^{-1}$, thus representing relatively smooth flume walls in comparison with the vegetation resistance. These data were first compared with the results of the 1-DV numerical model, to test the performance of this model in simulating the representative roughness of submerged, rigid and flexible vegetation. Figure 4.14, left panel, presents the comparison of the model outcome with the measured representative roughness values. The fit between

the measured and the modelled data is expressed as a root mean square error (RMSE):

$$RMSE = \sqrt{\frac{1}{N} \sum_{i=1}^{N} (x_{Oi} - x_{Mi})^2} \tag{4.156}$$

where N is the number of observations, and x_{Oi} and x_{Mi} are the observed and modelled values, respectively.

The RMSE between the observed and modelled representative roughness values in Fig. 4.14, left panel, equals 1.86 $\mathrm{m}^{1/2}{\cdot}\mathrm{s}^{-1}$. It is concluded that the 1-DV numerical model is capable of simulating the representative roughness of vegetation sufficiently well, under the restriction of conditions in flume experiments.

Next, these data were compared with the *Analytical approach* for the representative roughness, Eq. (4.107) and its underlying equations given in section 4.6.5. Equation (4.131) for the c_p-value is applied, which was found by analysing the data for the zero-plane displacement of Nepf and Vivoni (2000). Figure 4.14, right panel, presents the comparison of modelled representative roughness values with the measured values from the experimental flume data. Compared with the results of the 1-DV model, the data show more scatter. The RMSE between the observed and modelled representative roughness values in Fig. 4.14, right panel, is 2.28 $\mathrm{m}^{1/2}{\cdot}\mathrm{s}^{-1}$.

Next, the experimental flume data were compared with the results of the *Method of effective water depth.* Here two different schematisations for the vertical profile of horizontal velocity have been defined, see Fig. 4.6. In the first, the zero-plane displacement is assumed zero, in the second the zero-plane displacement is taken into account for the overlying logarithmic velocity profile. Figure 4.15 presents the comparison of measured against modelled data for the method of effective water depth. The left panel shows the application of the formulae *without* penetration of the logarithmic profile (application of equations 4.76 and 4.122, applied in the strict sense under the condition of $d = 0$). The right panel shows the application of the formulae *with* penetration of the logarithmic profile (application of equations 4.90, 4.119 and 4.122). This figure shows that the approach without inclusion of d systematically underestimates the measured Chézy values. Including d in the schematisation of the vertical profile of horizontal velocity and subsequent calculation of the roughness height of the top of the vegetation improves the fit, but it tends to overestimate the measured Chézy values. The RMSE for the left panel is 4.28 $\mathrm{m}^{1/2}{\cdot}\mathrm{s}^{-1}$ and for the right panel 3.53 $\mathrm{m}^{1/2}{\cdot}\mathrm{s}^{-1}$.

Having found this, there might also be a *third variant* of the method of effective water depth in which the schematisation of the vertical flow profile above the vegetation is similar to variant 1 (without zero-plane displacement, d), but the roughness height of the vegetation includes d as a parameter. The simpler Eq. (4.76) is then applied in combination with the expression for z_0 given by Eq. (4.122), so including Eq. (4.119) for d. This yields
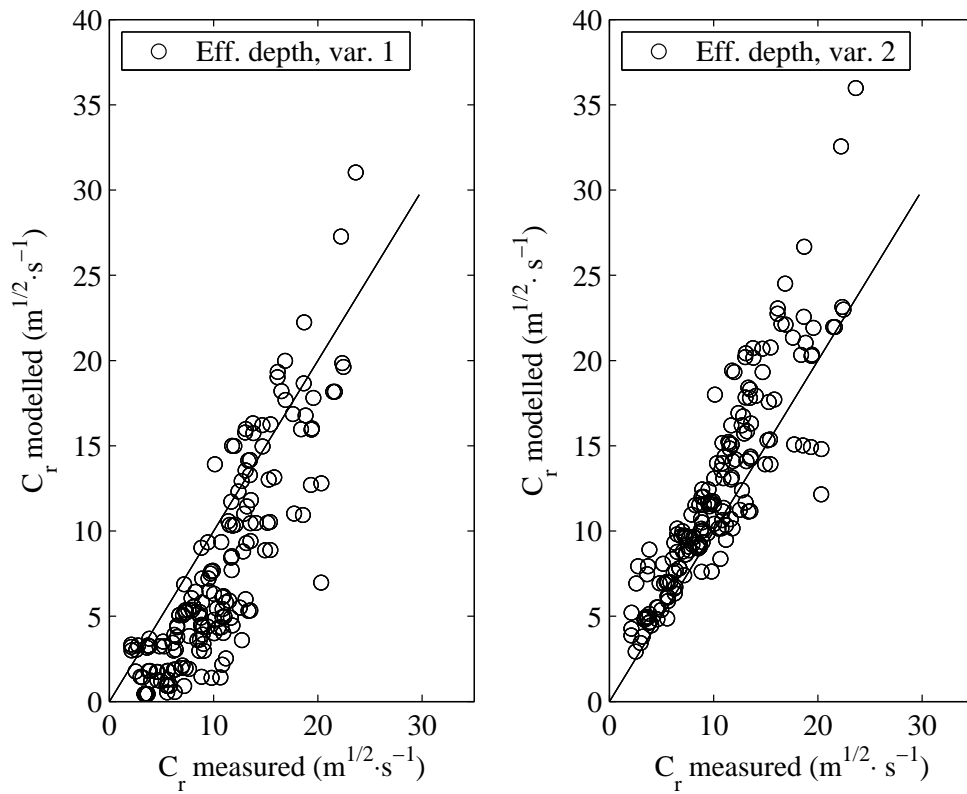
Figure 4.15: Comparison of measured with modelled data for the method of effective water depth for variant 1 (left panel) and variant 2 (right panel).
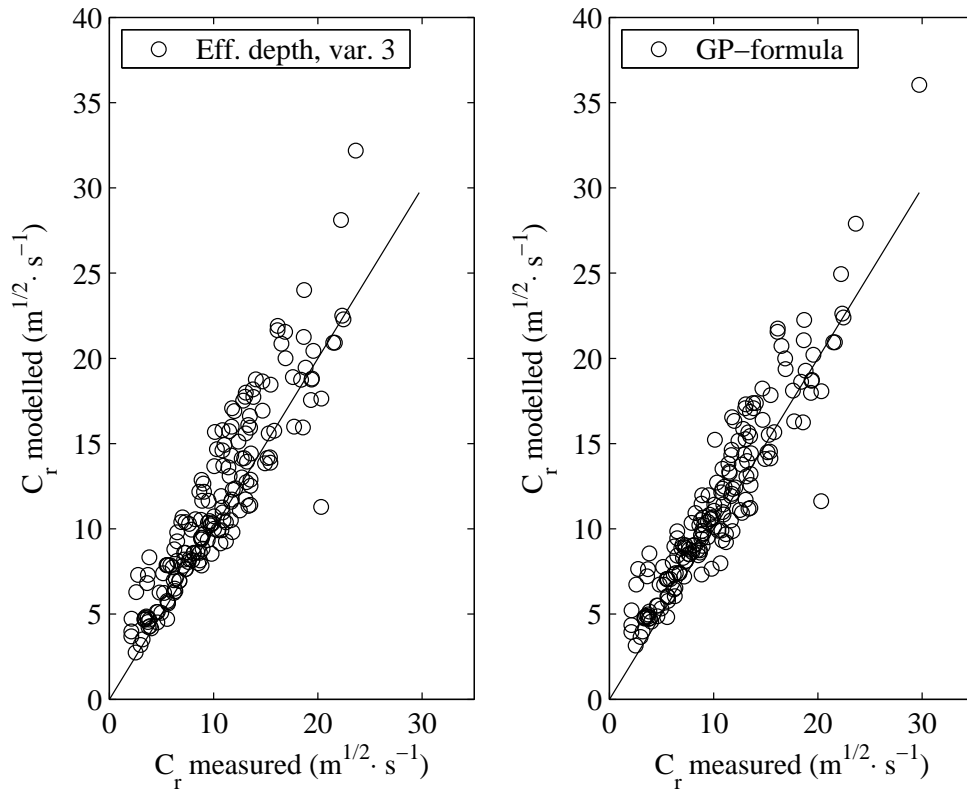
Figure 4.16: Comparison of measured with modelled data. Left panel: the method of effective water depth, variant 3, Eq. (4.76) with Eq. (4.122) and Eq. (4.119). Right panel: the GP-formula Eq. (4.155).

an improved form of the simpler formula for effective water depth. Figure 4.16, left panel, shows the comparison with the flume data for variant 3. The RMSE is 2.71 $m^{1/2} \cdot s^{-1}$.

Finally, the flume data were compared with the results of the improved form of the Genetic Programming formula, Eq. (4.155). Figure 4.16 presents the results. The RMSE equals 2.18 $m^{1/2} \cdot s^{-1}$. This very simple formula gives the best fit to the flume data. Table 4.2 presents a summary of the RMSEs of the various expressions.

Table 4.2: Root mean square errors ($m^{1/2} \cdot s^{-1}$) of the resistance formulations, including the 1-DV numerical model, for a comparison with flume data.

Expression	RMSE
1-DV model	1.86
Analytical approach	2.28
Eff. water depth, var. 1	4.28
Eff. water depth, var. 2	3.53
Eff. water depth, var. 3	2.71
GP-formula	2.18

4.7.2 Comparison with modelling data of the representative roughness

There is not sufficient experimental data to test the analytical formulae for the representative roughness for a broad range of plant properties and water depths. Yet, a comparison can be made with model data generated by the one-dimensional vertical (1-DV) model. It was shown in the previous section that this model gives a reasonably accurate simulation of the representative roughness, at least, for data from flume experiments.

First an extensive data set of input-output combinations is generated. To avoid unnatural combinations of stem diameter and density, a set of vegetation parameters that are representative of (Dutch) floodplain vegetation has been selected from Van Velzen *et al.* (2003a) and Van Velzen *et al.* (2003b). Table 4.3 presents the vegetation characteristics.

The final data set has been created based on the combination of vegetation types with different values for the Chézy bed roughness (30, 50 and 70 $m^{1/2} \cdot s^{-1}$), the depth-averaged velocity (0.1, 0.5 and 1.0 m/s) and the water depth (0.2, 0.5, 1.0, 2.0 and 5.0 m). This resulted in a data set of 810 different combinations of 439 submerged and 371 non-submerged cases. The 1-DV model was applied with 100 layers over the vertical, with a double exponential distribution of the layer thickness. For submerged vegetation the layer thickness decreases near the bed and around the top of the vegetation. For non-submerged vegetation the layer thickness decreases near the top of the vegetation and near the bed. Applying this non-uniform layer distribution increases the accuracy of the model in the

Table 4.3: Selected vegetation types for typical floodplain vegetation, from Van Velzen *et al.* (2003a).

Vegetation type	Diameter (m)	Density (m^{-2})	Height (m)	Drag coeff. (-)
Pioneer vegetation	0.003	50	0.15	1.8
Production grassland	0.003	15,000	0.06	1.8
Natural grassland	0.003	4,000	0.10	1.8
Herbaceous natural grassland	0.003	5,000	0.20	1.8
Creeping thistle vegetation	0.003	1,000	0.30	1.8
Dry herbaceous vegetation	0.005	46	0.56	1.8
Dewberry vegetation	0.005	112	0.50	1.8
Great willowherb vegetation	0.005	26	0.95	1.8
Herbaceous reed vegetation	0.005	32	2.00	1.8
Wet herbaceous vegetation	0.005	50	0.35	1.8
Sedges	0.006	20	0.30	1.8
Reed canary grass	0.002	200	1.0	1.8
Great bullrush	0.004	300	0.50	1.8
Cattail	0.0175	20	1.50	1.8
Reed	0.0046	80	2.50	1.8
Softwood shrub	0.034	3.8	6.0	1.5
Hardwood forest	0.115	0.2	10.0	1.5
Softwood forest	0.14	0.2	10.0	1.5

regions with the highest shear. All parameter combinations were evaluated with the 1-DV model, generating the representative roughness and the bed shear stress as outputs. When comparing the results of the analytical expressions with the numerical model, it must of course be realized that the numerical model is a simplification of reality, as well, hence has its limitations. Nonetheless, comparison with flume data has shown that the numerical model gives an accurate description of the vertical profiles for flow and turbulence (Uittenbogaard, 2003).

Figure 4.17 presents the results of the comparison of Chézy values derived from the numerical model with Chézy values derived from the analytical formulae. The value for the c_p coefficient in the *Analytical approach* was taken from Eq. (4.131), instead of Eq. (4.123), because this gave an improved fit. However, the results for the *Analytical approach* are disappointing. This approach strongly overestimates the Chézy values. Although the expressions for this approach are better in describing the vertical profile for velocity, it does not serve as a good resistance predictor. The results for the *Method of effective water depth, variant 3* and the *GP-formula*, applying Eq. (4.131) for the c_p-value, are
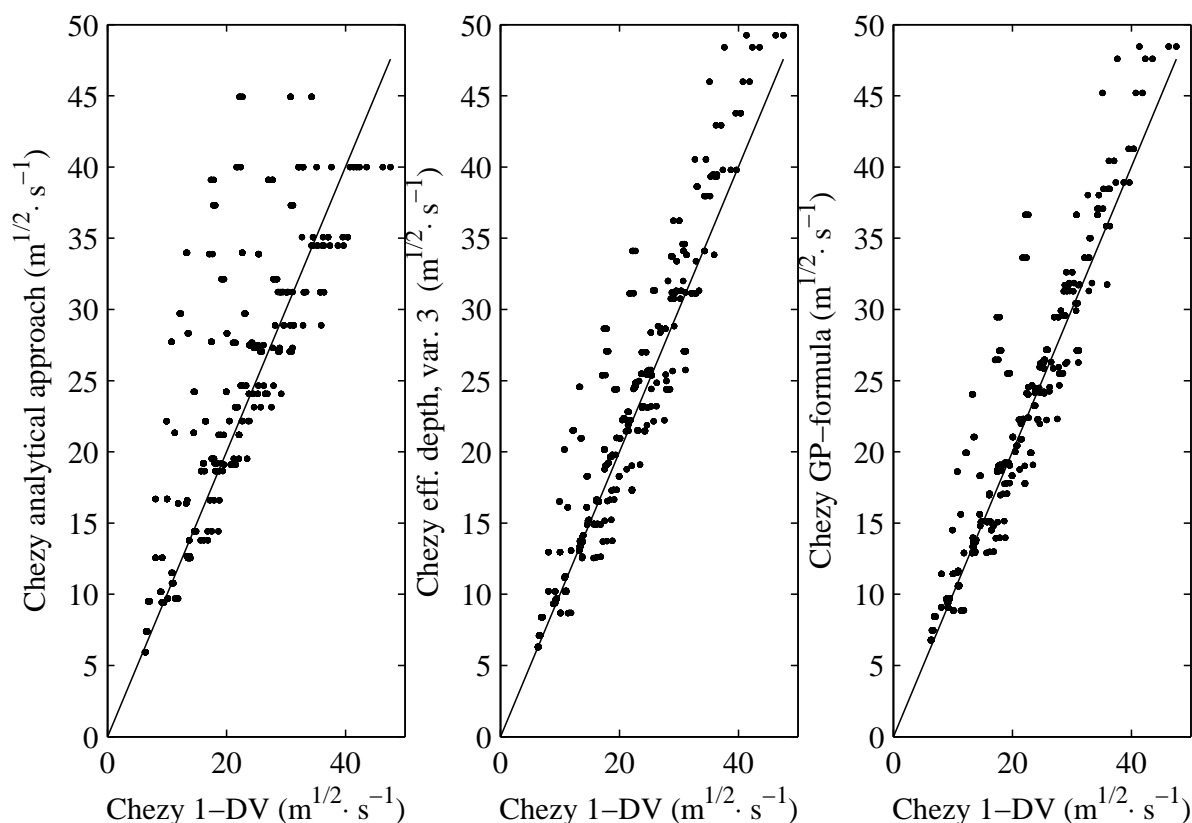
Figure 4.17: Comparison of Chézy values from the 1-DV model with Chézy values from the analytical formulae. Left panel: comparison with Chézy values from the *Analytical approach*. Middle panel: comparison with Chézy values from the *Reduction factor approach*. Right panel: comparison with Chézy values from the *GP-formula*.

very similar to each other. Both approaches differ only with respect to the zero-plane displacement of height k and the description of the roughness height z_0 in the logarithmic velocity profile. Considering the simple description of the velocity profiles through and above vegetation in both approaches, the good fit is a rather surprising result. Table 4.4 presents the RMSEs for the three approaches.

Table 4.4: Root mean square errors $(\mathrm{m}^{1/2}{\cdot}\mathrm{s}^{-1})$ of three resistance formulations, for a comparison with resistance data generated with the 1-DV numerical model.

Expression	RMSE
Analytical approach	4.82
Eff. water depth, var. 3	2.59
GP-formula	2.41

Finally, a comparison is made between the analytical expressions and the computational results for one selected type of vegetation, reed. The properties of reed are depicted in
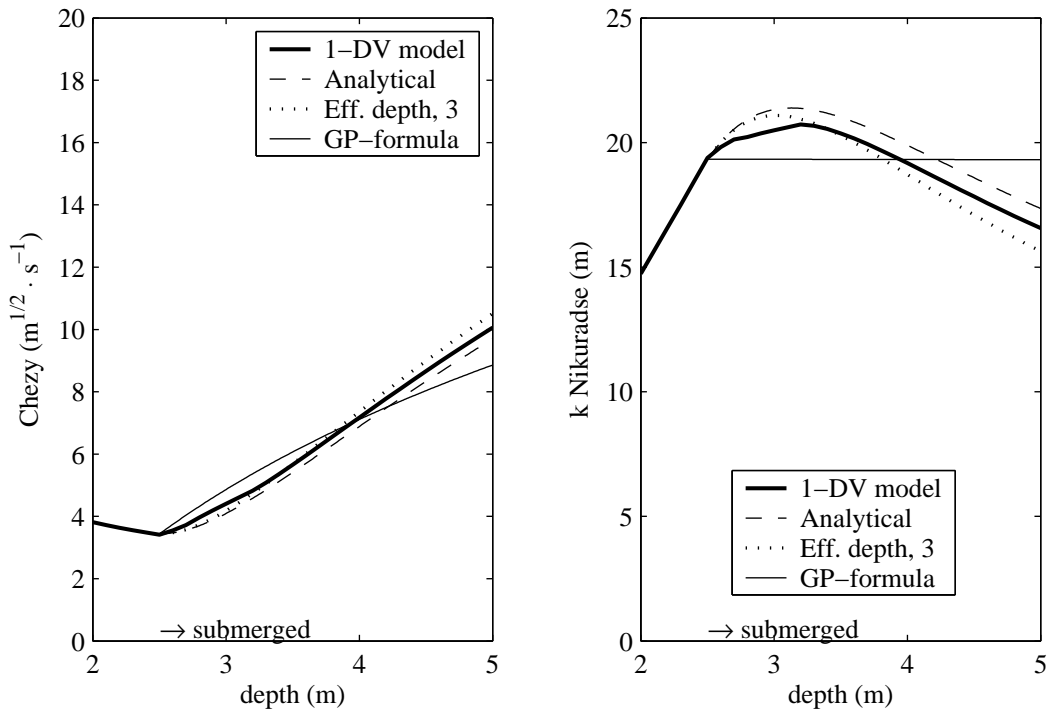
Figure 4.18: Comparison of resistance values from the 1-DV model with the analytical solutions for reed. Left panel: Chézy values. Right panel: Nikuradse values.

Fig. 4.10. The bed roughness was chosen at 50 m$^{1/2}$·s^{-1}. Figure 4.18 presents the results for the representative roughness, presented as Chézy values and as Nikuradse roughness height:

$$k_N = \frac{12h}{10^{C_r/18}} \tag{4.157}$$

First of all, for the non-submerged condition ($h \leq k$), the results of Eq. (4.70) overlap with the numerical modelling results. For the submerged condition the results for both the *Analytical approach* and the *Method of effective water depth, variant 3* fit best when Eq. (4.123) for c_p is applied. The results for these approaches fit well to the modelled profile. The results of the *GP-formula* however, do not agree well with the numerical modelling results. Expressed as a Nikuradse roughness value, the *GP-formula* gives a constant roughness height (m), which is not in line with the numerical model results. A conclusion to be drawn from this is that the *Analytical approach* and the *Method of effective water depth, variant 3* are capable of describing the resistance over depth with a high accuracy, but the value of c_p needs to be fitted. The *GP-formula*, on the other hand, does not represent the detailed relation of resistance over depth, but does well as an overall estimator of the representative roughness, see the previous section.

Figure 4.19: Comparison of modelled bed shear stress values with the 1-DV model against calculated bed shear stress values using the reduction factor approach, for submerged vegetation (left panel) and non-submerged vegetation (right panel).

4.8   Comparison of the bed shear stress expressions with data

There is very scarce experimental data found in literature to test the derived formulae for the bed shear stress. This is due to the fact that bed shear stress on a vegetated bed is very hard to measure directly in flume experiments. Researchers that deal with bed shear stress in flume studies with vegetation usually derive the bed shear stress indirectly, via measurements of the Reynolds stress profile over the vertical (e.g. Okabe *et al.*, 1997), or they calculate the bed shear stress analytically (e.g. Tollner *et al.*, 1982, Nakagawa *et al.*, 1992). One recent publication was found in which Thompson *et al.* (2004) measure the bed shear stress directly using hot-film anemometry. Therefore, the analytical formulae for bed shear stress were compared first with the set of 1-DV model data described in the previous subsections. Next, a comparison is made with the data by Thompson *et al.* (2004).

4.8.1 Comparison of the bed shear stress expressions with modelling data

Comparison with the bed shear stress calculated with the reduction factor approach

In the *Reduction factor approach*, simplifying assumptions have been made for the momentum balance and vertical flow velocity profile, which lead to relatively simple expressions for the bed shear stress. For submerged vegetation, the bed shear stress for a vegetated bed can be calculated by the multiplication of a reduction factor with the total fluid shear stress (Eq. (4.25) and Eq. (4.27)). For non-submerged vegetation, simply the common equation for bed shear stress, based on the depth-averaged flow velocity and the bed roughness can be applied (Eq. (4.37)).

Figure 4.19 presents the comparison of bed shear stress results from the 1-DV model with results from the reduction factor approach, for submerged vegetation (left panel) and non-submerged vegetation (right panel). The RMSEs are 0.49 N·m^{-2} and 1.26 N·m^{-2} respectively. The fit for submerged conditions is reasonably good, however, the plot shows multiple lines of scatter, which are associated with the bed roughness. For a smooth bed, the reduction factor approach underestimates the modelled bed shear stress compared with the numerical model results. For non-submerged conditions, the reduction factor approach gives only a limited set of predictions. To be precise, only nine different values for the bed shear stress are calculated, these are combinations of the three different bed roughness values and the three different flow velocities that were defined for this data set. For non-submerged conditions, the reduction factor approach is not dependent on the water depth.

Comparison with the bed shear stress calculated with the analytical approach

In the analytical approach, a rather complex expression for the bed shear stress was found. This expression contains one unknown coefficient for the vegetation height-averaged turbulence intensity, c_p (Eq. (4.43)). However, it was shown that that the turbulence intensity is a function of z, see Fig. 4.9. Moreover, it was shown that in order to fit the analytical expression of the vertical velocity profile inside the vegetation layer to the numerical 1-DV modelling results, a lower value for c_p near the bed must be applied, see Fig. 4.11. To calculate the bed shear stress, the value for c_p near the bed must be determined. This value, defined as c_{pbed}, is likely to differ from the fitted c_p-value for the representative roughness, since the latter is related to the whole velocity profile, whereas the former is related to the near-bed part of the velocity profile.

The c_{pbed} cannot be estimated from the 1-DV model directly. In this model, the turbulent kinetic energy, k_T, at the bed is governed by a boundary condition which assumes that the turbulent energy near the bed is produced by the wakes of the sediment particles, or bed forms, under conditions of fully turbulent flow near the bed, i.e. $Re = u_{*b} k_s / \nu > 55$

(Hinze, 1975). The Dirichlet boundary condition reads:

$$k_T\big|_{z=0} = \frac{u_{*b}^2}{\sqrt{c_\mu}} \tag{4.158}$$

where u_{*b} is the shear velocity at the bed (m/s) and c_μ is a k-ϵ turbulence model closure coefficient (0.09). Therefore:

$$\frac{\sqrt{k_T\big|_{z=0}}}{u_b} = c_{pbed} = \frac{1}{c_\mu^{\frac{1}{4}}} \frac{u_{*b}}{u_b} \tag{4.159}$$

where u_b is the near-bed velocity (m/s). Applying the logarithmic boundary layer velocity profile of Uittenbogaard *et al.* (2000) at $z = 0$:

$$\frac{u_b}{u_{*b}} = \frac{1}{\kappa} \ln\left(\frac{9z_0}{z_0}\right) \tag{4.160}$$

yields a fixed ratio of u_*/u_b of about 0.187, irrespective of the bed roughness height, z_0. Substitution of this ratio in Eq. (4.159) yields a constant value for c_{pbed} of 0.34. The 1-DV model, therefore, computes vertical profiles for the turbulence intensity that reach 0.34 at the bed. For flow through and over vegetation, however, the production of shear turbulence can be dominant near the bed, especially in the case of short vegetation. The constant value for the turbulence intensity at the bed seems a shortcoming of the 1-DV model in case of flow through and over vegetation. This can be improved by making the boundary condition dependent on the vegetation-induced turbulence as well.

Applying the constant value of 0.34 for c_{pbed} in the analytical approach does not give a good fit with the 1-DV modelling results. Therefore, a formula for c_{pbed} was investigated. Three conditions were defined a priori:

1. A formula for c_{pbed} is inversely dependent on the bed roughness, C_b;
2. A formula for c_{pbed} is dependent on the water depth, h, and inversely dependent on the plant height k;
3. The unit of c_{pbed} is dimensionless;

This has led to the following formula for c_{pbed}:

$$c_{pbed} = \frac{h}{k} \frac{g}{C_b^2} \tag{4.161}$$

Since the expression for c_{pbed} is derived from comparison with numerical modelling results, it is subject to the assumptions made in the 1-DV model. Further improvements of the 1-DV model with regard to the turbulence intensity near the bed may change this result.

Figure 4.20 presents the comparison of modelled with calculated bed shear stress data, applying Eq. (4.161). To be able to compare with Fig. 4.19, the submerged condition
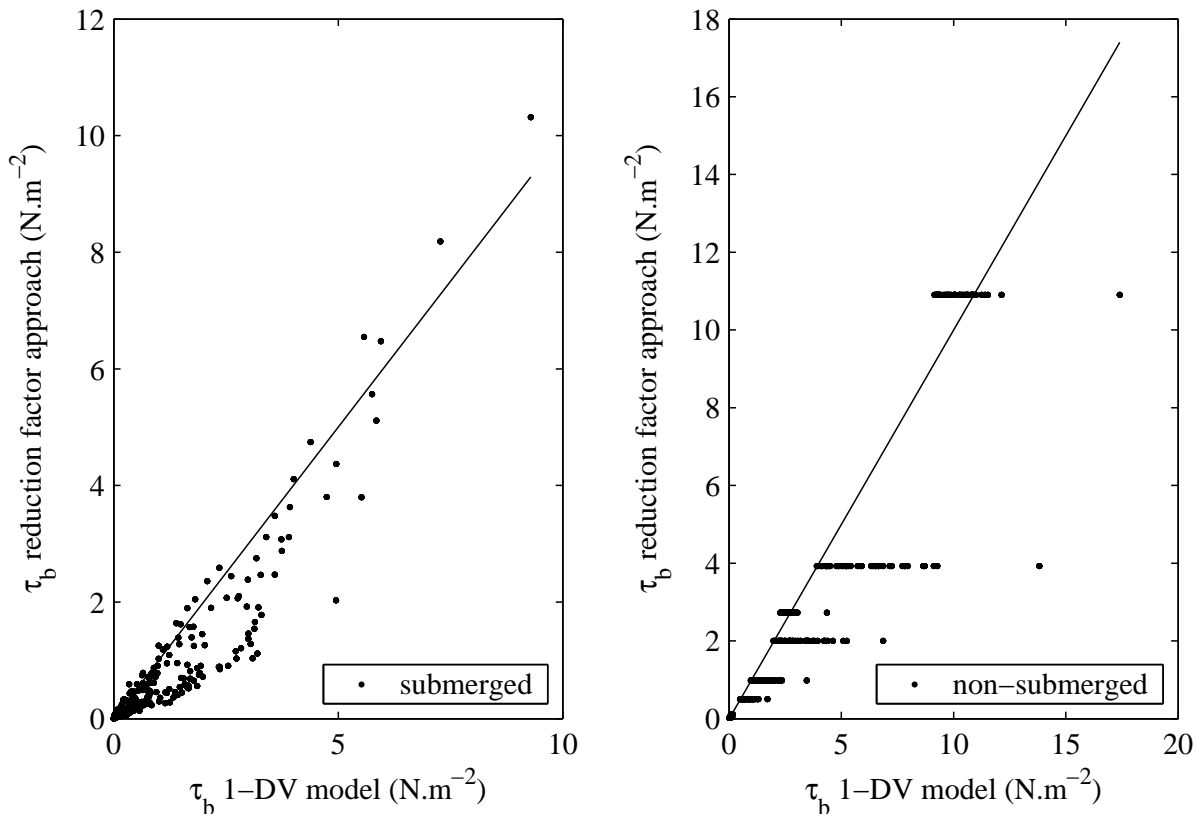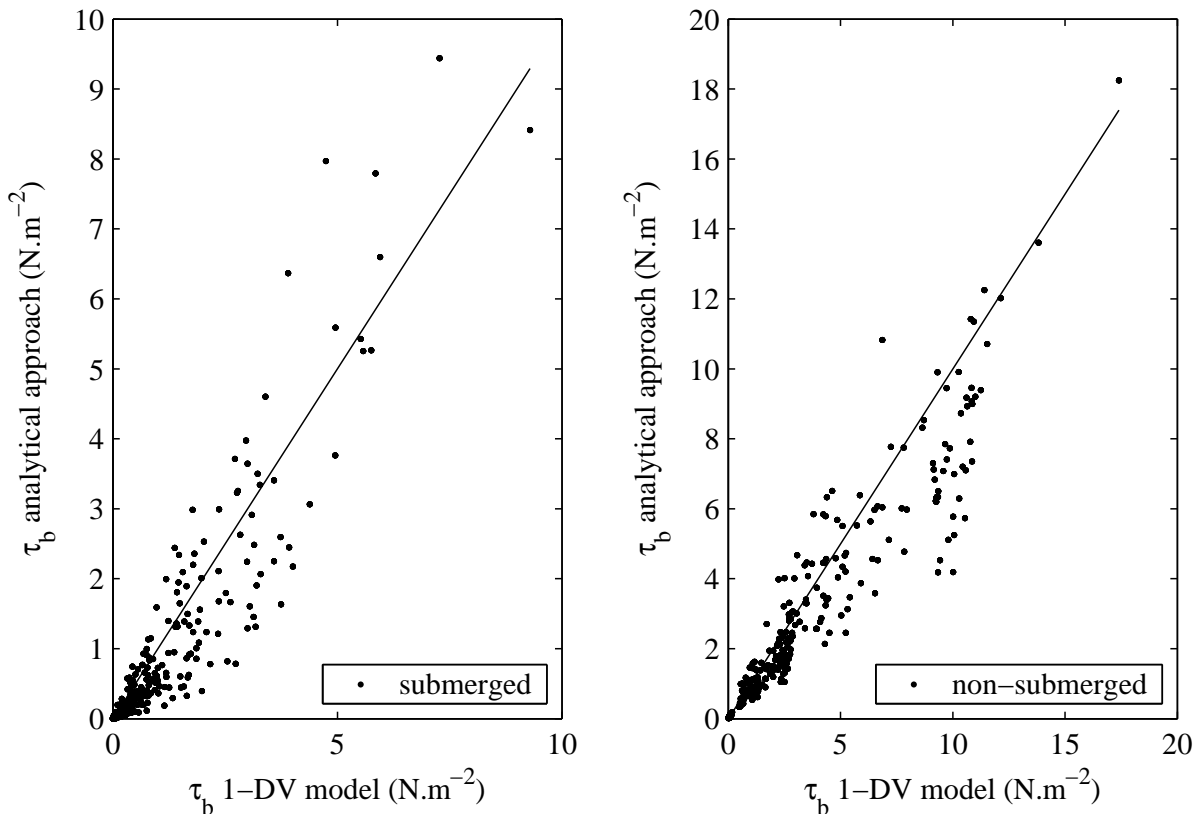
Figure 4.20: Comparison of modelled bed shear stress values with the 1-DV model with calculated bed shear stress values using the analytical approach, for submerged vegetation (left panel) and non-submerged vegetation (right panel).

(left panel) and the non-submerged condition (right panel) are presented separately. The RMSEs are 0.43 N·m^{-2} and 1.18 N·m^{-2} respectively.

Finally, a comparison is made between the analytical expressions and the computational results for reed. Reed is chosen as a rather extreme example that neatly shows the complex details of the profile of bed shear stress over depth, Fig. 4.21. The properties of reed are depicted in Fig. 4.10. The bed roughness was chosen at 50 m$^{1/2}$·s^{-1} and the depth-averaged velocity equals 0.5 m/s (at every water depth shown, so the discharge increases with increasing water depth). The results of the *Analytical approach* have been fitted with the numerical model results by applying a multiplication factor of 2 to the equation for c_{pbed}. Figure 4.21 shows that the *Analytical approach* better represents the specific relation over depth than the *Reduction factor approach*. For non-submerged conditions, the latter calculates a constant bed shear stress of 0.98 N·m^{-2}, directly following from Eq. (4.37) for a logarithmic velocity profile in open channel flow. For the submerged conditions, first and foremost, the *Reduction factor approach* underestimates the bed shear stress as computed by the 1-DV model. Secondly, for shallow submerged depths, the *Reduction factor approach* shows an incorrect increase of the bed shear stress first, which is caused
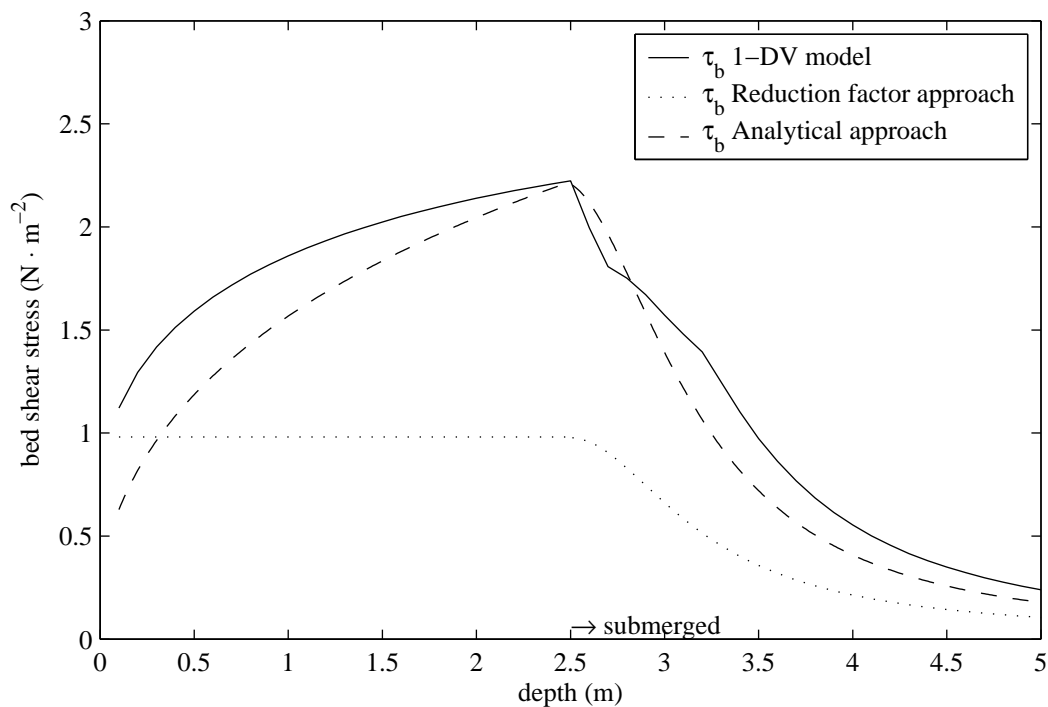
Figure 4.21: Comparison of bed shear stress values from the 1-DV model with the analytical expressions for reed, at a constant depth-averaged flow velocity of 0.5 m/s. From a depth of 2.5 m onwards, the reed is submerged.

by the miscalculation of the flow resistance in this region.

The numerical 1-DV modelling result shows a profile that can be divided into various regions over depth. At a water depth of 0.10 m, the bed roughness has a significant influence in relation to the vegetation resistance. The vertical profile of horizontal velocity (not shown here), resembles a logarithmic profile and the resulting bed shear stress, therefore, is near 1.0 N·m^{-2}. As the water depth increases, the flow profile starts deviating more and more from a logarithmic profile and becomes uniform over depth, with the exception of the near-bed region. At the bed, the eddy viscosity increases with an increasing water depth, and although the velocity gradient ($\partial u/\partial z$) decreases, the net result is an increasing bed shear stress. From 2.5 m onwards, the reed is submerged. When the water depth increases, the flows through and above the vegetation divide such, that the flow velocity inside the vegetation decreases and the flow velocity above the vegetation increases. The effect, therefore, is a decreasing bed shear stress. However, there is an additional effect of the turbulence inside the vegetation. When the reed is shallow submerged, there is not much shear turbulence generated at the top of the reed. Moreover, this does not affect the turbulence intensity near the bed. At increasing water depths, more and more shear turbulence is generated and gradually this affects the bed shear stress. In this case there is a transient region between water depths of 2.7 m and 3.2 m in which the influence of the turbulence intensity is growing. From a water depth of 3.2 m onwards, the bed shear

stress is fully affected by shear turbulence inside the vegetation, and of course decreases as a result of a decreasing flow velocity near the bed.

4.8.2 Comparison of the bed shear stress expressions with measured data

Thompson *et al.* (2004) determined the bed shear stress for non-submerged idealized vegetation. The idealized vegetation consisted of rectangular prisms with a width of 2.54 cm and a thickness of 0.95 cm, type R, trapezoidal prisms of 0.95 cm by 4.13 cm, and a thickness of 0.95 cm, with the large base oriented at the bottom, or the small base oriented at the bottom, type TL and TS, respectively, and cylinders, with diameters 0.95 cm and 2.54 cm, type SC and C, respectively. They applied three different densities of 1, 4, and 9 elements per 0.145 m^2, yielding 6.9, 27.6 and 62.1 elements m^{-2}, respectively, which are rather low densities. Two different flow rates were applied of 0.0045 m^3/s and 0.0105 m^3/s, yielding depth-averaged velocities of 0.46 to 0.78 m/s at water depths of 0.024 to 0.058 m. Thompson *et al.* (2004) measured the instantaneous bed shear stress applying hot-film anemometry on a measurement area of 0.28 × 0.28 m, and determined the time averaged and spatial averaged bed shear stress. The bed consisted of a flat aluminium sheet covered with uniform sand of 1 mm diameter glued to the surface. They measured the drag force on the vegetation elements, as well, and determined the vegetal shear stress. The total shear stress, τ_t, was determined by the sum of the bed shear stress and the vegetal shear stress. Unfortunately, they did not determine the energy gradient, which could have been a check on the total shear stress.

The measurements of the bed shear stress can be compared with the analytical expressions from the *Reduction factor approach* and the *Analytical approach*. In the *Reduction factor approach* the bed shear stress for non-submerged vegetation is calculated by the multiplication of the reduction factor f_{nonsub} with the total shear stress, Eq. (4.35):

$$\tau_{bv,nonsub} = \frac{1}{1 + \frac{C_D m D h C_b^2}{2g}} \, \tau_t \tag{4.162}$$

The idealized vegetation dimensions, mDh, were determined by Thompson *et al.* (2004). For cylinders, D is the cylinder diameter, for rectangles, D equals the width, and for trapezoids, D equals the depth-averaged submerged width. The drag coefficients, C_D, were determined for cylinders (0.80), rectangles (1.55), trapezoids type TL (1.34) and trapezoids type TS (1.65). Thompson *et al.* (2004) determined the bed roughness indirectly from measurements of flow depth and velocity for flow conditions without vegetal elements, applying:

$$\tau'_p = \rho g R i \tag{4.163}$$

and:

$$C_p = \frac{\tau'_p}{\rho u^2} \tag{4.164}$$
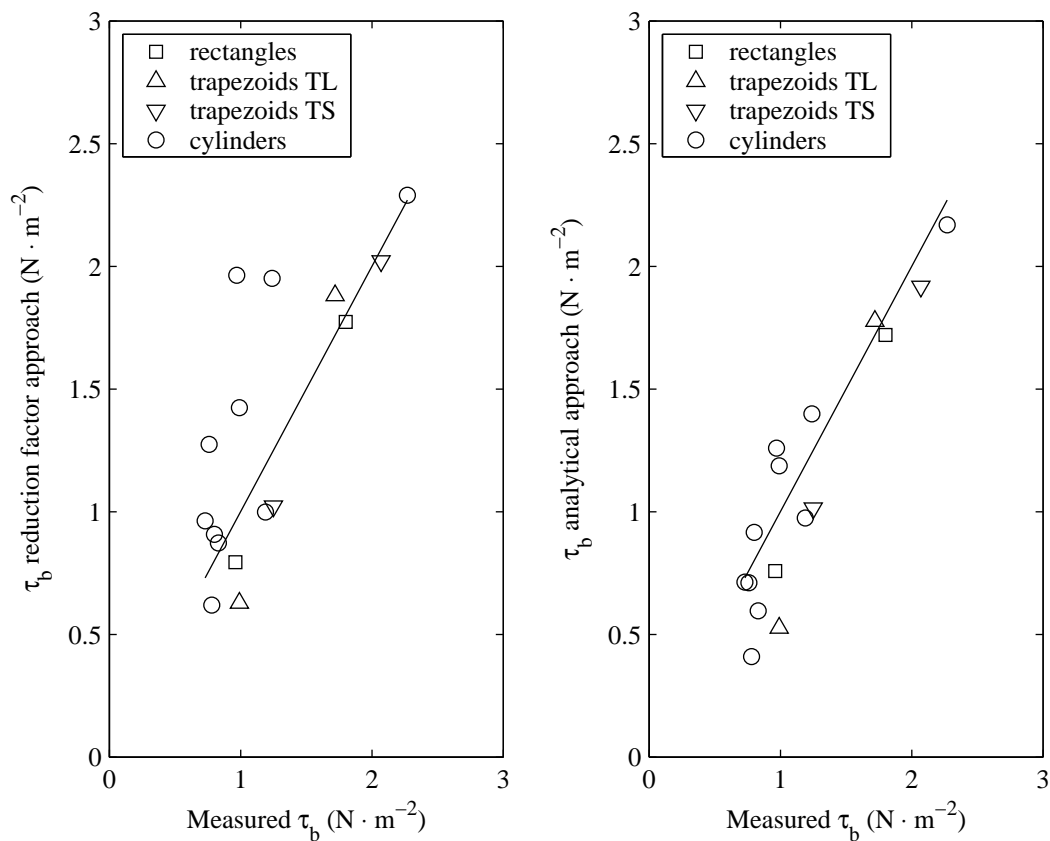
Figure 4.22: Comparison of measured bed shear stress values from Thompson *et al.* (2004) with the analytical expressions. Left panel: *Reduction factor approach*. Right panel: *Analytical approach*.

where τ_p' is the average particle shear stress (N·m^{-2}), R is the hydraulic radius (m), i is the channel slope (-), u is the average velocity (m/s) and C_p is the particle drag coefficient (-). A best-fit nonlinear equation was determined for the relation between the particle drag coefficient and the flow rate:

$$C_p = 0.0016Q^{-0.2266} \qquad (4.165)$$

yielding C_p is 0.0054 and 0.0045 for flow rates of 0.0045 m^3/s and 0.0105 m^3/s, respectively. Note that:

$$C_p = \frac{g}{C_b^2} \qquad (4.166)$$

so the Chézy roughness of the bed, C_b, becomes 42 and 47 m$^{1/2}$·s^{-1}, respectively. Figure 4.22, left panel, presents the results of the comparison of the measurements of Thompson *et al.* (2004) with the *Reduction factor approach*. The fit is reasonably well, although for a number of flume runs with cylinders the *Reduction factor approach* overestimates the bed shear stress.

The *Analytical approach* is presented in section 4.5.3. The energy gradient, i, in this

approach is determined from the measured total shear stress, by applying:

$$i = \frac{\tau_t}{\rho g R};$$
(4.167)

The bed shear stress in the *Analytical approach* depends on the coefficient for c_{pbed}, Eq. (4.161). Figure 4.22 presents the results of the comparison of the measurements of Thompson *et al.* (2004) with the *Analytical approach*. For the *Analytical approach* a reasonably good fit could be obtained by applying a multiplication factor of 0.08 to the equation for c_{pbed}. This is a significantly lower value than was found for reed, where a multiplication factor of 2 was needed to fit to the results of the 1-DV model.

In addition, as a check on the data, the representative Chézy roughness in their experiment is determined with:

$$C_r = \sqrt{\frac{\rho g u^2}{\tau_t}}$$
(4.168)

In some cases the representative Chézy roughness is higher than the Chézy bed roughness. This indicates that the total resistance of the bed and the vegetation is lower than the resistance of the bed itself. Since this is not in agreement with their findings, it suggests a measurement error in the determination of the depth-averaged flow velocity, probably due to non-uniform flow conditions. A direct application of Eq. (4.37) to determine the bed shear stress, therefore, does not fit well with the observations.

4.9   Summary and conclusions

Although this chapter deals with finding analytical expressions for the bed shear stress, some important findings with regard to the hydraulic resistance of vegetation have been made. It has been concluded that the solidity can be disregarded in simple analytical formulae for the hydraulic resistance. Although strictly speaking the solidity should be included when describing flow through a porous medium, experimental evidence points out that its effect is negligible for most practical applications.

4.9.1 Representative roughness of vegetation

Based on the method of effective water depth, an improved analytical formula for the representative roughness of vegetation has been derived, which includes the zero-plane displacement of the logarithmic velocity profile, Eq. (4.90). However, this expression is rather complex and needs an estimate for the zero-plane displacement, d. The physical basis for this displacement has been made clear and based on the analysis of the flow velocity profile inside submerged vegetation, and an estimate for the mixing length of turbulence inside the vegetation, an analytical expression for d has been found. This also

led to an improved, relatively simple, formula for the representative roughness based on the method of effective water depth:

$$C_r = \sqrt{\frac{1}{C_b^{-2} + \frac{C_D m D k}{2g}} + \frac{(h-k)^{3/2} \frac{\sqrt{g}}{\kappa} \ln\left(\frac{h-k}{e z_0}\right)}{h^{3/2}}} \tag{4.169}$$

in which:

$$z_0 = (k-d) \exp\left(-\kappa \sqrt{\frac{2L}{c_p \ell}\left(1 + \frac{L}{h-k}\right)}\right) \tag{4.170}$$

$$d = k - L\left(1 - \exp\left(-\frac{k}{L}\right)\right) \tag{4.171}$$

$$L = \sqrt{\frac{c_p \ell}{C_D \, m \, D}} \tag{4.172}$$

and as a closure coefficient:

$$c_p \ell = 0.05(h-k) \tag{4.173}$$

A comparison of the results for the representative roughness with flume data found in literature shows the appropriateness of this formula. Furthermore, the applicability for floodplain conditions, based on a comparison with 1-DV model data, proved to be good. This was not the case for the complex formula that was derived by an analytical solution of the momentum balance of flow through vegetation. Moreover, an even simpler formula was found by applying Genetic Programming, which appears to be a simple and good approximation for the representative roughness, valid for a wide range of vegetation properties and flow conditions:

$$C_r = \sqrt{\frac{1}{\frac{1}{C_b^2} + \frac{1}{2g} C_D m D k} + \frac{\sqrt{g}}{\kappa} \ln \frac{h}{k}} \tag{4.174}$$

4.9.2 The bed shear stress on a vegetated bed

Two analytical approaches for the bed shear stress on a vegetated bed have been developed, based on a description of vegetation as cylinders and underlying assumptions for the vertical profile of horizontal velocity. One yields a relatively simple expression for submerged vegetation, giving a reduction factor on the total fluid shear stress:

$$\tau_{bv} = \frac{1}{1 + \frac{C_D m D k C_b^2}{2g}} \rho g h i \tag{4.175}$$

For non-submerged vegetation the bed shear stress can be approximated by:

$$\tau_{bv,nonsub} = \frac{\rho g}{C_b^2} \overline{u}^2 \tag{4.176}$$

The other analytical expression for the bed shear stress is a relatively complex expression, based on an analytical solution of the momentum balance for flow through and over vegetation and is valid for submerged as well as non-submerged conditions:

$$\tau_b = \frac{\rho\, c_p\, \ell}{2L} \left[\frac{B - u_{s0}^2 \frac{A}{1-A} \exp\left(-\frac{k}{L}\right)}{\exp\left(\frac{k}{L}\right) - \frac{1-A}{1+A} \exp\left(-\frac{k}{L}\right)} - \frac{B - u_{s0}^2 \frac{A}{1-A} \exp\left(\frac{k}{L}\right)}{\frac{1+A}{1-A} \exp\left(\frac{k}{L}\right) - \exp\left(-\frac{k}{L}\right)} \right] \tag{4.177}$$

in which:

$$A = \frac{2L\, \kappa^2}{\ln^2(9)\, c_{pbed}\, \ell} \tag{4.178}$$

and:

$$B = \frac{2L\, g\, (h - k)\, i}{c_{pbed}\, \ell} \tag{4.179}$$

And furthermore:

$$L = \sqrt{\frac{c_{pbed}\, \ell}{C_D\, m\, D}} \tag{4.180}$$

$$\ell = c_l \left(\frac{1 - \lambda}{m}\right)^{\frac{1}{2}} \tag{4.181}$$

$$\lambda = \frac{\pi}{4} D^2 m \tag{4.182}$$

$$u_{s0} = \sqrt{\frac{2\, g\, i}{C_D\, m\, D}} \tag{4.183}$$

And as a closure coefficient:

$$c_{pbed} = \frac{h}{k} \frac{g}{C_b^2} \tag{4.184}$$

The energy gradient, i, is determined by the hydraulic resistance of the vegetation.

A comparison of the bed shear stress calculated with both analytical expressions with measurements and with results of a numerical 1-DV model, shows that the complex formulations of the analytical approach give better estimates for the bed shear stress compared to the reduction factor approach, especially for a smooth bed. The analytical approach shows the dependence on water depth for non-submerged conditions, which is not included in the reduction factor approach. In conclusion, the *Analytical approach* has a physical basis and is capable of describing the bed shear stress on a vegetated bed accurately, but needs calibration of the closure coefficient for c_{pbed}, which is a large disadvantage. Moreover, it should be realized that the closure coefficient for bulk hydraulic conditions and vegetation characteristics was found by fitting to the numerical modelling results. Especially with regard to the simulation of the bed shear stress, the 1-DV model is open to further improvement with regard to the bed boundary condition of the k-ϵ turbulence model.

Chapter 5

Experimental study

5.1 Introduction

In this chapter, the results of an experimental study on the effects of submerged vegetation on bedload transport are described. Part of it is written down in Baptist (2003). The objective of the experiment was to determine the bedload transport rate on a vegetated bed and to apply a bed shear stress estimate based on the results of Chapter 4 to test the incorporation of vegetation effects into an existing sediment transport relationship.

To date, the effects of vegetation on sediment transport are poorly understood. A lot of research efforts have been put into the effects of vegetation on the hydraulic resistance and turbulence, see section 4.1, but the effects of vegetation on suspended load and bedload sediment transport have been studied less. With regard to suspended sediment transport, studies include field and laboratory measurements as well as numerical modelling (Nakagawa *et al.*, 1992; Tsujimoto & Shimizu, 1994; Watanabe & Hoshi, 1996; Houwing *et al.*, 2001; López & García, 1998, Teeter *et al.*, 2001; Madsen *et al.*, 2001). Studies on bedload sediment transport, sometimes in combination with suspended load transport, for *non-submerged* vegetation include Tollner *et al.* (1982), Elliott (2000), Deletic (2001) and Jordanova and James (2003).

This chapter deals with the effects of *submerged* vegetation on bedload transport. Abt *et al.* (1994) tested sediment entrapment and retention potential in an experimental, meandering stream system as a function of discharge and vegetative blade length, using submerged natural vegetation (primarily Kentucky bluegrass). They distinguish between deposition enhancement and sediment retention. They observed that the sediment deposition was inversely related to blade length. This effect was attributed to the characteristics of the blades; the shorter blades were stiff, the medium-sized blades were oscillating in the flow and the longest blades flattened to the bed thus preventing sediment to deposit. The retention of sediment was largest for the longer blades, due to the same phenomenon that these armour the deposited sediments. Sediment gradation was measured as well and it was found that the fines were transported through the system and that the larger grain

sizes were transported as a bed-load and entrapped inside the vegetation, resulting in a doubling of medium grain size.

Prosser *et al.* (1995) measured flow resistance and sediment yield of an eroding natural grass bed. The grass was partly submerged and partly non-submerged. The sediment transport was solely bedload transport of soil aggregates. Sediment yield was found to be related to plant length. Partitioning of the measured total fluid shear stress into the vegetation resistance and bed resistance suggested that on a densely grassed surface over 90% of flow resistance is exerted by plant stems.

There is considerable Japanese research in the field of sediment transport and vegetation. Okabe *et al.* (1997) conducted flume experiments on the bedload rate of a movable bed with submerged artificial vegetation. They applied a 1-DV model for vegetated flow to determine the shear velocity at the bed, by fitting the observed and modelled vertical velocity profiles. The shear velocity determined the dimensionless effective stress at the bed, which was related to the dimensionless bedload rate of Ashida & Michiue. The results showed a reasonable fit of the sediment yield of the eroding bed with the theoretical transport rate.

Kitamura *et al.* (1998) conducted a flume experiment with a partly vegetated channel. They measured the bedload rate in the non-vegetated part and compared the results with a 3-D model for vegetated flow in combination with the bedload formula of Ashida & Michiue. The results showed that the sediment transport rate increases with increasing width of the vegetation zone. However, when the vegetation zone becomes very wide, the sediment transport rate decreases, due to a decreasing bed shear stress, which is affected by a three-dimensional flow structure.

Tsujimoto (1999) presents a 2D depth-averaged model that solves the horizontal distributions of shear velocity, depth-averaged velocity and kinematic eddy viscosity for an experimental channel that is partly covered by vegetation. His model introduces the drag force of the vegetation in the 2-DH momentum balance, and also introduces the additional production and dissipation of turbulence by the vegetative stems. Although not clearly stated, this model should be valid only for non-submerged vegetation conditions. The results confirm the two-dimensional patterns of sedimentation around a vegetated section.

5.2   Material and methods

Experiments have been conducted in a 35 m long, 80 cm wide, straight, horizontal open channel with concrete bottom and glass walls. The flume set-up is presented in Fig. 5.1. A longitudinal section of artificial, flexible vegetation was installed with a density of
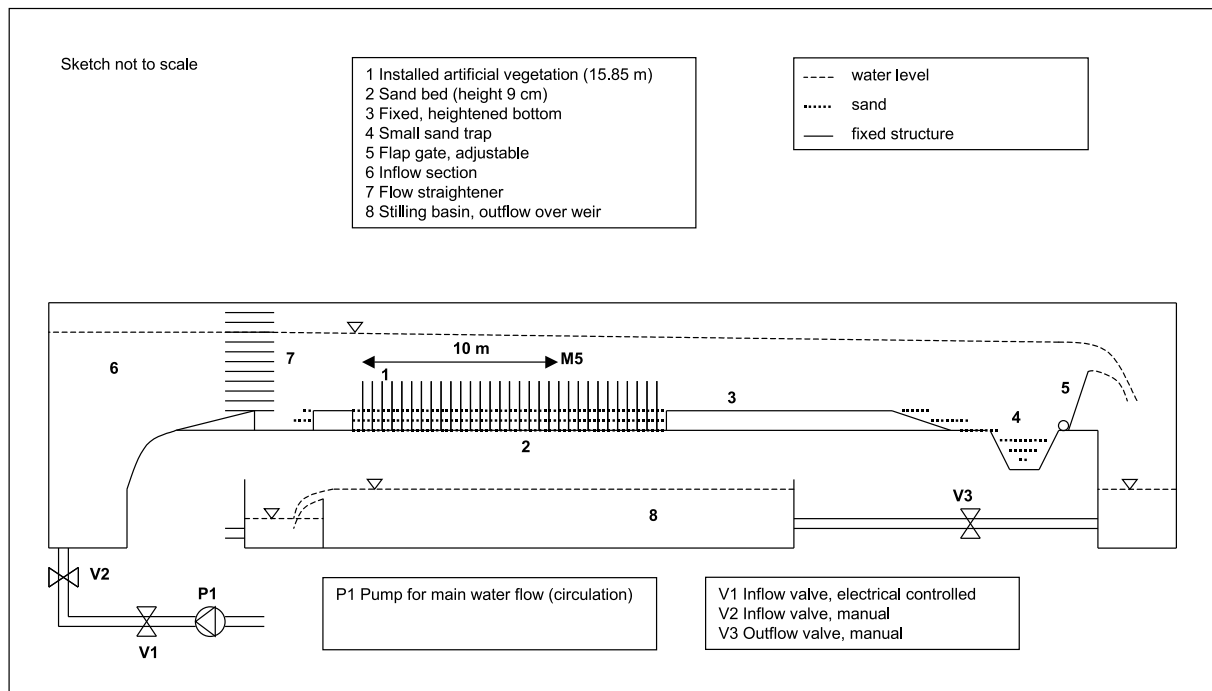
Figure 5.1: Flume set-up.

400 stems per m^2, over a length of 15.85 m. Plastic aquarium plants from Metaframe Corporation, USA, type Anacharis (*Egeria densa*) X-large were used. In total 4755 plants of 27 cm length were mounted onto 18 mm wood-cement boards in a rectangular pattern of 5 by 5 cm by sticking each plant (upside down) into 2.0 mm diameter drilled holes. The vegetation consisted of 2.0 mm thick stems with leaves attached to the stems. Each leaf was 0.5 mm thick, 15.0 mm long and 4.0 mm wide at its widest point. The leaves were placed along the stem in groups of five, evenly distributed around the stem, but in alternating groups of two over the stem height. The distance between each alternating group of five leaves was 0.5 cm, Fig. 5.2. A 9 cm thick layer of sand was distributed evenly between the submerged plants using a carriage with a perforated metal box that drove on top of the flume. The upright plant height protruding from the bed was therefore 18 cm. The quartz sand had a D$_{50}$ of 320 μm, and a D$_{90}$ of 450 μm, the sieve curve is presented in Fig. 5.3. Downstream of the plant section a fixed floor continued for some metres. This floor was raised to the elevation level of the sand bed. This structure was sloping down near the end of the flume. Upstream of the vegetated section also a raised, fixed floor with a length of 1.25 m was installed. Stainless steel mesh screens damped the inflow turbulence and achieved smooth inlet conditions.

All instruments used were developed and built by WL | Delft Hydraulics. Vertical profiles of the longitudinal (u), transverse (v) and vertical (w) velocities were measured with two two-dimensional Electromagnetic Velocity Sensors (EMSs), E30type, mounted in two different directions. Mean and turbulent velocity statistics were obtained from 600 s records
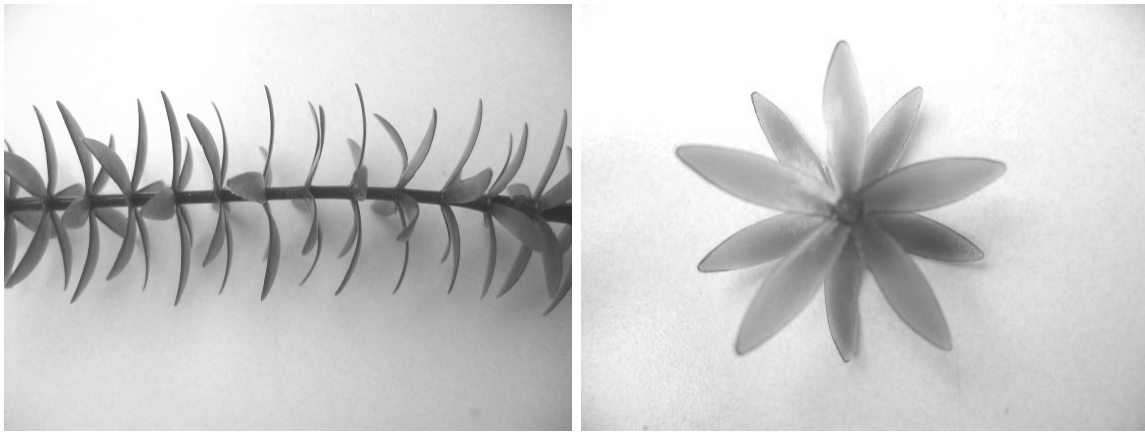
Figure 5.2: The stem and leaves of the artificial vegetation.
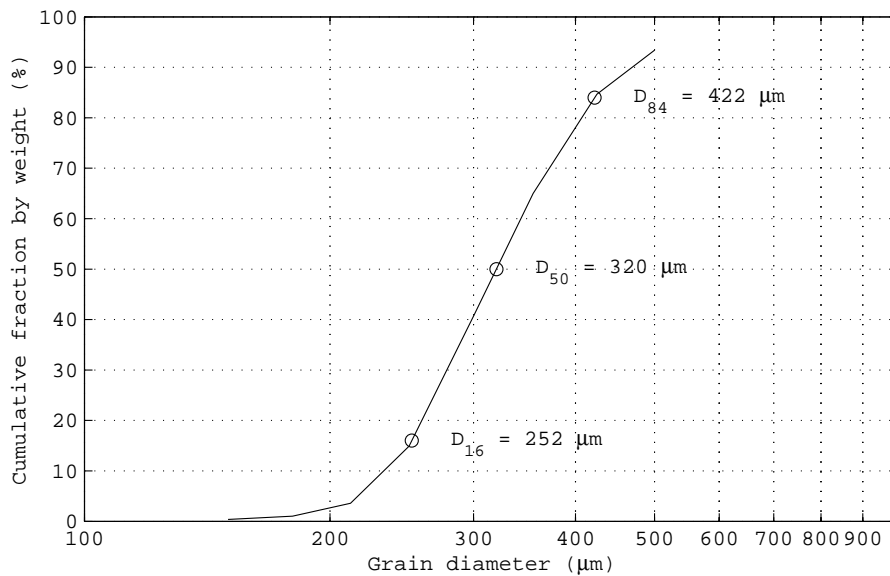
Figure 5.3: Sieve curve of the quartz sand.

sampled at 5 Hz at fixed positions along the flume. These instruments were mounted at location M5, which is at 10 m distance from the beginning of the vegetated section, in the centre of the flume, see Fig. 5.1. This location is chosen to be far enough from the beginning of the flume to have well-developed vertical profiles for velocity and Reynolds stress.

The longitudinal profile of the water level was measured with a Dynamic Liquid-level Meter. The longitudinal bed profile was measured with two electric conductivity Bed Profilers. One profile was located near the centre of the flume, at a distance of 0.375 m from the right flume wall, since in the exact centre, a row of plants is present. The other profile was located at a distance of 0.135 m from the right flume wall, which is at one sixth of the flume width. The two profilers are considered representative for the bed profile changes in the middle one third of the flume and both one third sections on each
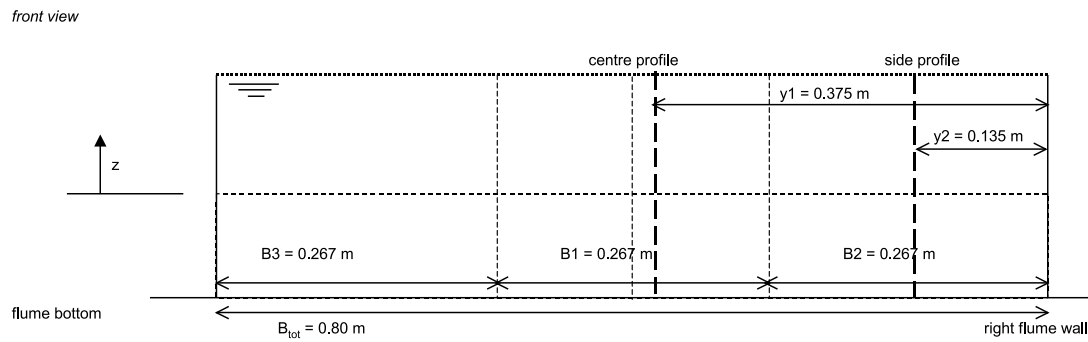
Figure 5.4: Cross section over the flume width, with the positions of the longitudinal bed profilers. y1 is the distance of the centre profile to the right flume wall, y2 is the distance of the side profile to the right flume wall. B1 is the 1/3 flume section ascribed to the centre profile. B2 and B3 are two 1/3 flume sections ascribed to the side profile.

Table 5.1: Hydraulic conditions for the test runs. Tests labelled with "R", are reference tests with similar hydraulic conditions as the first three tests, but without vegetation

Test	Flume discharge (m^3/s)	Depth-averaged velocity (m/s)	Depth at location M5 (m)
Test 1	0.081	0.38	0.265
Test 2	0.129	0.53	0.305
Test 3	0.106	0.46	0.287
Test 1R	0.085	0.41	0.260
Test 2R	0.155	0.60	0.323
Test 3R	0.113	0.45	0.315

side, assuming equivalent conditions on both sides, see Fig. 5.4. These instruments were mounted on a carriage with adjustable speed.

Mean velocities of 0.3 to 0.6 m/s at flow depths of about 30 cm were chosen to represent floodplain conditions at flood situations and to be sufficient to initiate sand particle motion. Two series of experiments were conducted. In the first series, three experiments were carried out with artificial plants mounted to the flume floor. In the second series (denoted with R) three experiments with similar flow conditions were carried out for a situation with bare sediment, as reference tests. The differences between the vegetated tests and the reference tests, with regard to their shear stress profiles and sediment transport were studied.

The hydraulic conditions for the different experiments are presented in Table 5.1. The data for Test 1 proved to be not of sufficient quality for in-depth analysis, so the emphasis in the following sections is put on Tests 2 and 3 and their reference tests, Tests 2R and 3R respectively. The experiments were set up to analyse the differences in sediment transport
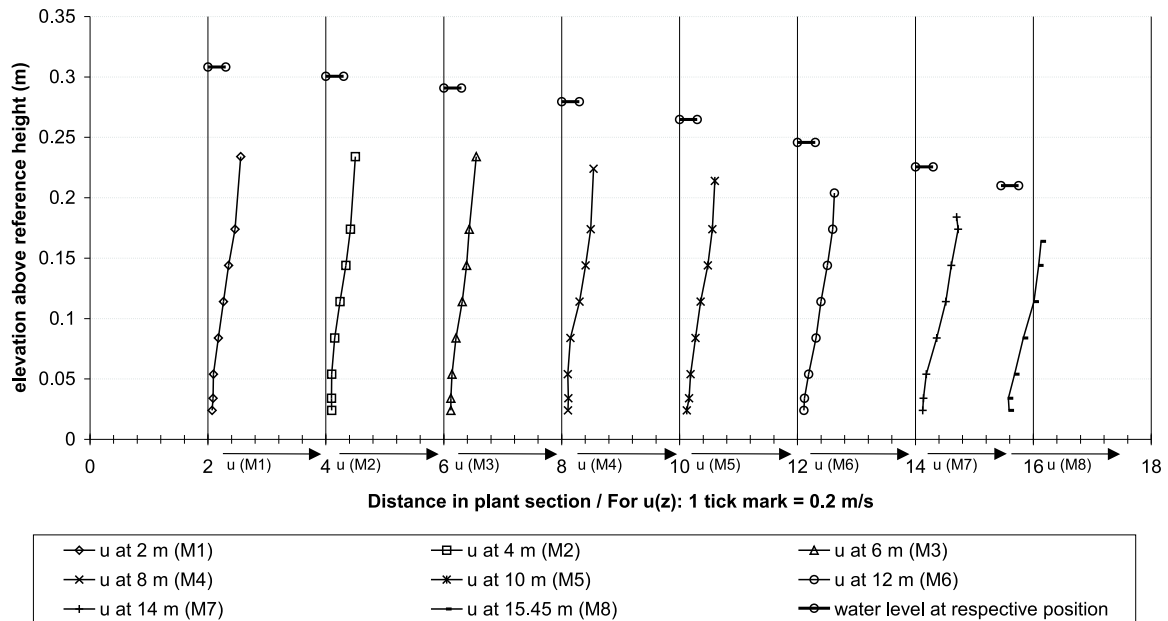
Figure 5.5: Vertical profiles of horizontal velocity along the flume length for Test 1.

for flow with a vegetated bed compared to similar flow conditions for a bare bed. However, the depth-averaged velocities for the reference tests were in general higher than for the tests with vegetation.

The duration of the series of tests with vegetation was about 30 hours; for the series without vegetation the duration was about 3 hours. No sediment was fed and flow was stopped as soon as a significant amount of sand had been eroded from the movable bed section and had been deposited in the downstream section of the flume. The amount of sediment that was transported out of the section with the movable bed was determined in two ways. The first approach was direct weighing of all sand deposited in the downstream section of the flume. In the second approach the volumetric change of the movable bed section was determined from the average of the two bed profiler measurements. The results of this flume experiment are reported in Thannbichler (2002), as well.

5.3 Flow and Reynolds stress profiles

For all experiments, Reynolds numbers ($>8 \cdot 10^5$) and Froude numbers ($\ll 1$) indicate turbulent, subcritical flow. Figure 5.5 shows vertical profiles for horizontal velocity along the flume length. Note that the flow has a non-uniform character; the hydraulic resistance of the vegetation causes a backwater curve.
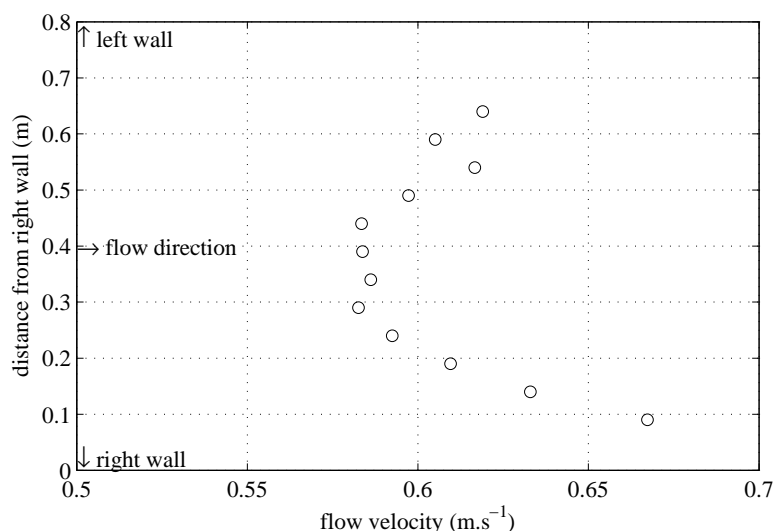
Figure 5.6: Lateral profile of horizontal flow velocities, measured at 19.1 cm above the bed, in Test 3.

Figures 5.7 and 5.8 show vertical profiles for velocity, (u), and Reynolds stress (τ_{xz}) measured at 10 m distance from the beginning of the vegetated section. Since the bed of the flume is movable, the elevations of the measuring points were corrected for the actual bed level. The observed vertical profiles for velocity show deceleration of the flow within the vegetation layer. The Reynolds stress profiles show a linear profile above the vegetation, a maximum at the top of the vegetation, and a clear deviation from the linear shear stress profile inside the vegetation. For comparison, Fig. 5.9 shows the vertical profiles for velocity and Reynolds stress measured in Test 3R, which is the reference of Test 3 for a bare bed. Note that the magnitude of the Reynolds stress differs with about one order of magnitude from the Reynolds stress for the vegetated case. Viscous stress can be neglected, especially for the vegetated cases.

During the test runs it was observed that the erosion near the side walls was higher than in the middle of the flume. A lateral profile of horizontal flow velocities confirmed that the lower side wall roughness compared to the vegetation roughness caused an uneven flow distribution over the width, even above the vegetation, Fig. 5.6.

5.4   Bed level changes and sediment transport rate

It proved difficult to flatten the bed in between the vegetation before the start of a new test run. Therefore, the initial bed profile shows bed level variations up to several centimetres. During the runs, the bed level exhibited erosion that started at the most downstream end of the plant section, where the flow velocities were highest due to the non-uniform flow conditions. The erosion gradually proceeded upstream. Large bedforms were travelling
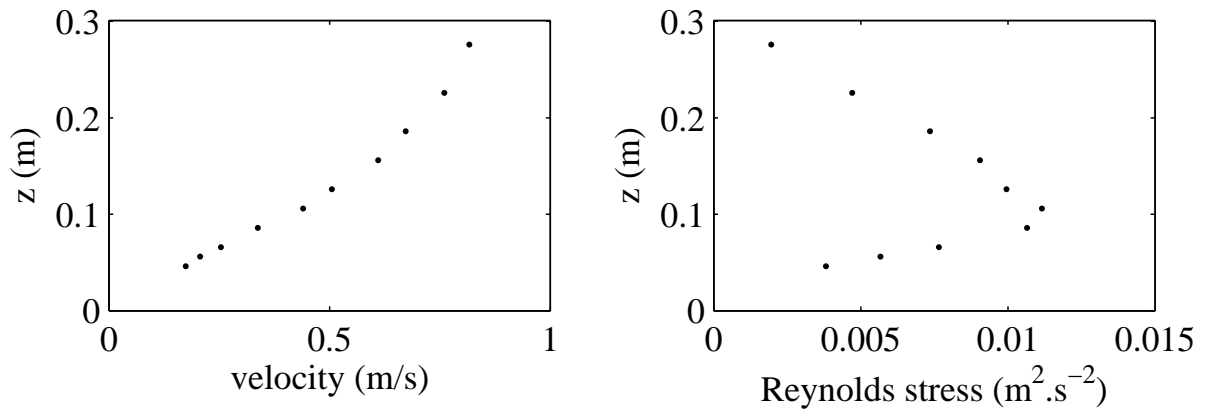
Figure 5.7: Vertical profile of horizontal velocity (left panel) and Reynolds stress (right panel) for Test 2.
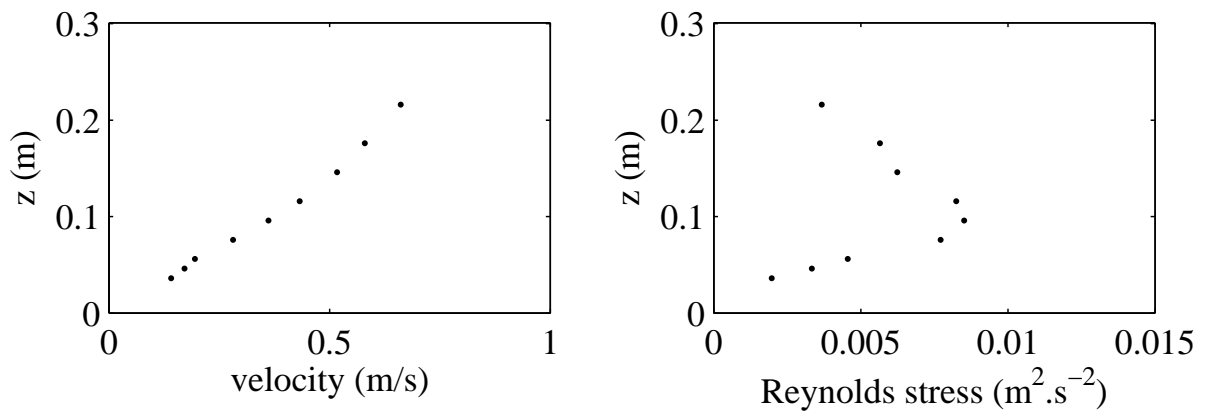
Figure 5.8: Vertical profile of horizontal velocity (left panel) and Reynolds stress (right panel) for Test 3.
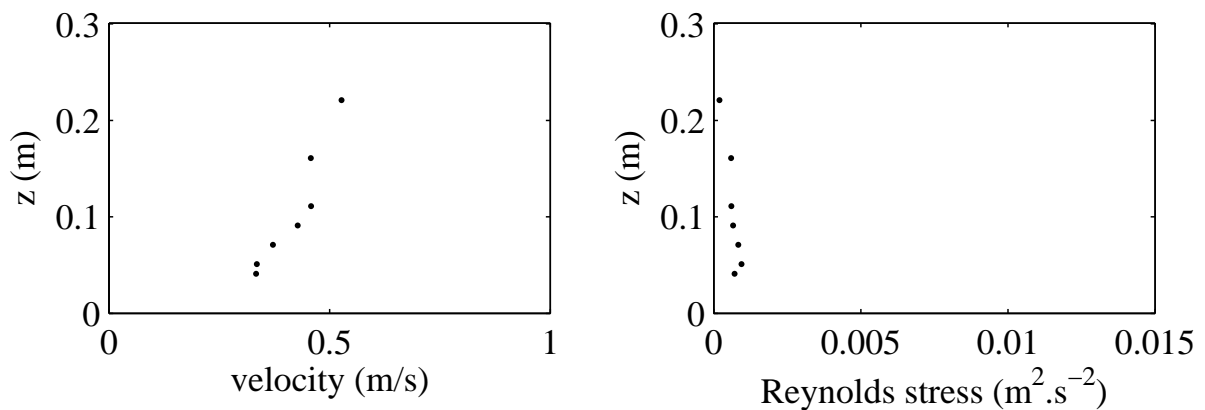
Figure 5.9: Vertical profile of horizontal velocity (left panel) and Reynolds stress (right panel) for Test 3R. Note the difference of one order of magnitude for the Reynolds stress compared with Test 3 (Fig. 5.8).

downstream. Figures 5.10 and 5.11 present the bed level profile development along the centre line of the flume showing these trends. The raw data were smoothed by applying a moving average with a two-sided window of about 0.17 m to show the large bedforms more clearly. The net erosion in Test 2 is larger than in Test 3. The high bed levels measured at about 2 m from the beginning of the plant section in Test 2 result from the formation of a local dune-like bed feature, that was formed due to local scour at the beginning of the section. This local phenomenon will not be analysed further. An example for the bed level development in the reference run Test 3R is shown in Fig. 5.12. Here, the bed starts flat and in a relatively short period, compared to the vegetated tests, bedforms developed. The bed level does not show net erosion at the end of the section, as was observed in the vegetated tests, but it shows net sedimentation in the majority of the section. The sand for this sedimentation stems from the scour at the very beginning of the section. It should be noted that there was a net transport of sand out of the section.

The sediment transport rate of the bed was obtained using two different methods for the vegetated tests (see section 5.2) and by direct weighing only for the non-vegetated tests. The resulting net transports of sand from the vegetated and non-vegetated beds are presented in Table 5.2.

Table 5.2: Transport rate for the test runs.

Test	Direct weighing (kg.h^{-1})	From bed profiles (kg.h^{-1})
Test 2	11.6	9.0
Test 3	5.9	4.7
Test 2R	44.0	–
Test 3R	10.4	–

5.5 Hydraulic roughness and blockage area

The local representative roughness of the artificial vegetation at location M5, 10 m from the beginning of the vegetated section, can be determined using Chézy's formula applied to the local water level slope, the local water depth and the local depth-averaged velocity:

$$C_r = \frac{\overline{u}}{\sqrt{ih}} \tag{5.1}$$

The local water level slope is difficult to determine, due to the non-uniform backwater curve. The slope of a linear regression through the water level measurements is, therefore, dependent on the length of the evaluated section. Table 5.3 shows the estimates for the
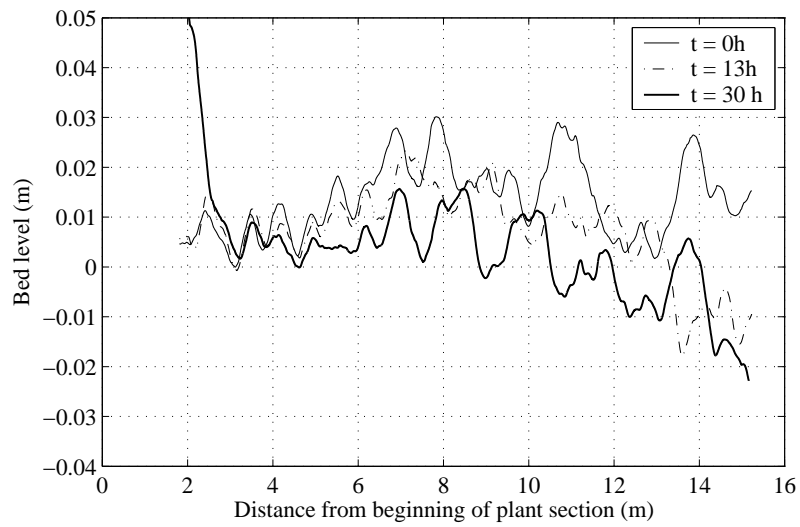
Figure 5.10: Bed levels for Test 2, at t=0 (thin line), t=13 (dash-dot line) and t=30 hours (thick line).
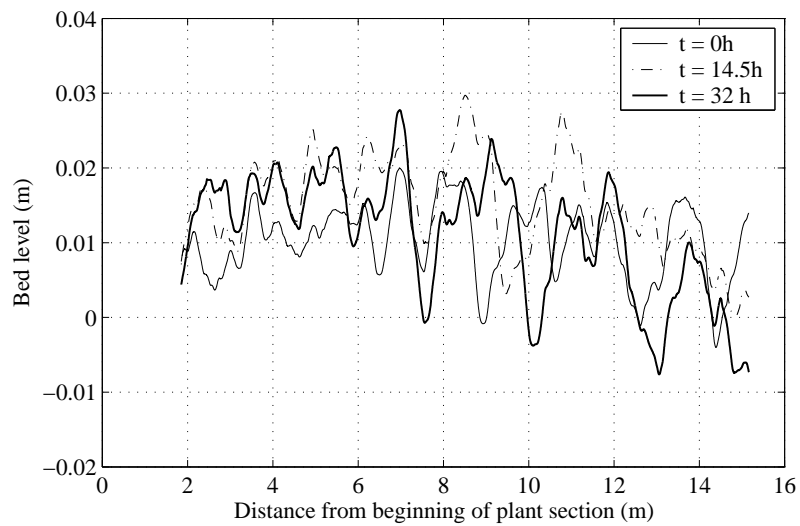
Figure 5.11: Bed levels for Test 3, at t=0 (thin line), t=14.5 (dash-dot line) and t=32 hours (thick line).
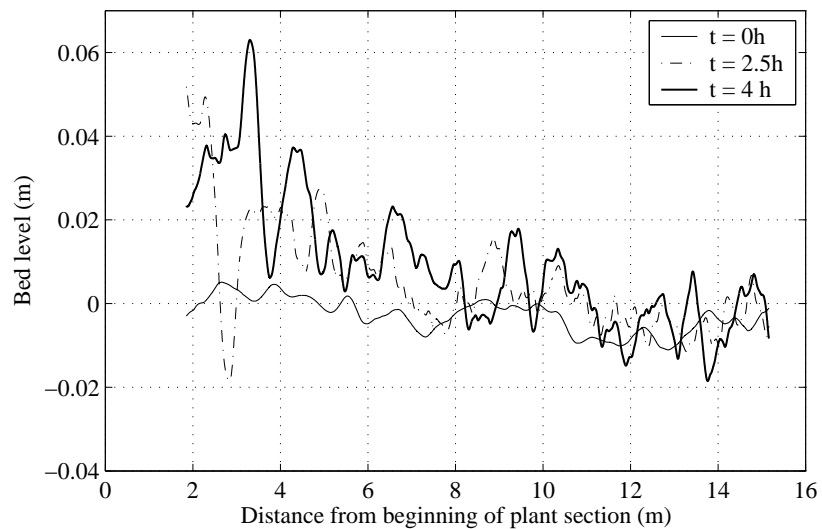
Figure 5.12: Bed levels for Test 3R, at t=0 (thin line), t=2.5 (dash-dot line) and t=4 hours (thick line).

Table 5.3: Representative Chézy values for Test 2 and 3, location M5, derived from water level slope measurements.

Test	Water level slope (-)	Representative Chézy ($\mathrm{m^{1/2} \cdot s^{-1}}$)
Test 2, 9.5 m - 10.5 m	$7.5 \cdot 10^{-3}$	11.1
Test 2, 9.0 m - 11.0 m	$7.5 \cdot 10^{-3}$	11.1
Test 3, 9.5 m - 10.5 m	$4.9 \cdot 10^{-3}$	12.3
Test 3, 9.0 m - 11.0 m	$6.1 \cdot 10^{-3}$	11.0

Table 5.4: Total shear stress, water level slope and representative Chézy values for Test 2 and 3, location M5, derived from the Reynolds stress measurements.

Test	Total shear stress ($\mathrm{N \cdot m^{-2}}$)	Energy gradient (-)	Representative Chézy ($\mathrm{m^{1/2} \cdot s^{-1}}$)
Test 2	18.40	$6.15 \cdot 10^{-3}$	12.24
Test 3	13.77	$4.89 \cdot 10^{-3}$	12.28

representative roughness based on linear regression of the water level measurements for two section lengths: between 9.5 m to 10.5 m and between 9.0 m to 11.0 m. In addition, an alternative method was applied, based on the shear stress measurements. A possible disadvantage of this method, however, is that the applied EMSs have limited capabilities of measuring smaller scale turbulence fluctuations. This may lead to an underestimation of the turbulent shear stress, leading to a possible overestimation of the Chézy roughness. The shear stress is characterized by the Reynolds stress, omitting the viscous stress:

$$\tau_{xz} = -\rho \overline{u'w'} \tag{5.2}$$

The Reynolds stress measurements at the four highest locations, shown in Figures 5.7 and 5.8, were linearly extrapolated to the bed. This yields the total shear stress:

$$\tau_t = \rho g h i \tag{5.3}$$

Together with the local water depth and depth-averaged velocity given in Table 5.1, the energy gradient, i, and the representative Chézy value for location M5 can be determined, see Table 5.4. Combining the estimates for both methods shows that the representative Chézy values for both tests are in the range of 11.0 ($\mathrm{m^{1/2} \cdot s^{-1}}$) to 12.3 ($\mathrm{m^{1/2} \cdot s^{-1}}$).

The horizontally averaged momentum balance of flow with vegetation contains an additional drag force from the vegetation, see Chapter 4:

$$\rho g i + \frac{\partial \tau_{xz}(z)}{\partial z} - \frac{1}{2} \rho C_D(z) m(z) D(z) u^2(z) = 0 \tag{5.4}$$

where τ_{xz} is the shear stress in xz-directions and i is the energy gradient (from Table 5.4). By applying Eq. (5.4) to the vertical profiles for flow and Reynolds stress, the vegetation

property for $C_D(z)m(z)D(z)$ can be derived. It is common to write the product of density and diameter as $a(z)$, the *blockage area* per volume (Nepf & Vivoni, 2000):

$$a = mD \tag{5.5}$$

The drag coefficient, C_D is the bulk drag coefficient for the vegetation. Table 5.5 presents the vertical profile for the product of the blockage area and the bulk drag coefficient for Test 2 and Test 3.

Table 5.5: Product of blockage area and bulk drag coefficient for Test 2 and Test 3.

Test 2		Test 3	
z (m)	aC_D (m^{-1})	z (m)	aC_D (m^{-1})
0.116	0.00	0.106	0.53
0.096	1.51	0.086	2.22
0.076	6.50	0.066	10.79
0.061	12.10	0.051	11.59
0.051	16.14	0.041	18.60

The results show that the product of the bulk drag coefficient and the blockage area is not constant over the height. When the blockage area for the vegetation over the height is known, a vertical profile for the bulk drag coefficient follows. Previous studies have shown that the bulk drag coefficient for flexible vegetation as well as for rigid cylinders is not constant over the height and deviates from 1.0 at the top and near the bed (Nepf & Vivoni, 2000; García *et al.*, 2004). However, due to the complex geometry of the flexible vegetation that has been applied in this experiment, the vertical profile for the blockage area is not known a priori. Moreover, assuming that the vegetation can be schematised as rigid cylinders with a density of 400 m^{-2} and a cylinder diameter of 0.002 m (the stem diameter), the bulk drag coefficient results in values up to 23, which is considered unrealistically large. Although the individual plants were placed in a density of 400 m^{-2}, the leaves contribute to the blockage of flow as well. The leaves cannot be modelled by an increased drag coefficient alone. Therefore, a constant drag coefficient of 1.0 is assumed and a profile for the blockage area is derived. It then follows that the blockage area is lowest near the top of the vegetation and increases towards the bed. Since it was observed that the vegetation in the flow was not so much bending, but in a rather constant angle with the bed, a constant blockage area over height was expected. However, the vegetation is swaying in the flow and it is hypothesised that the movements temporarily open up the vegetation near the top (see Fig. 5.13). The blockage area near the top should, therefore, be considered averaged over time. The time-averaged blockage area decreases near the top and is highest near the bed. The deflected plant height is subsequently determined by the minimum blockage area, yielding different values for Test 2 and Test 3 of 0.116 m and
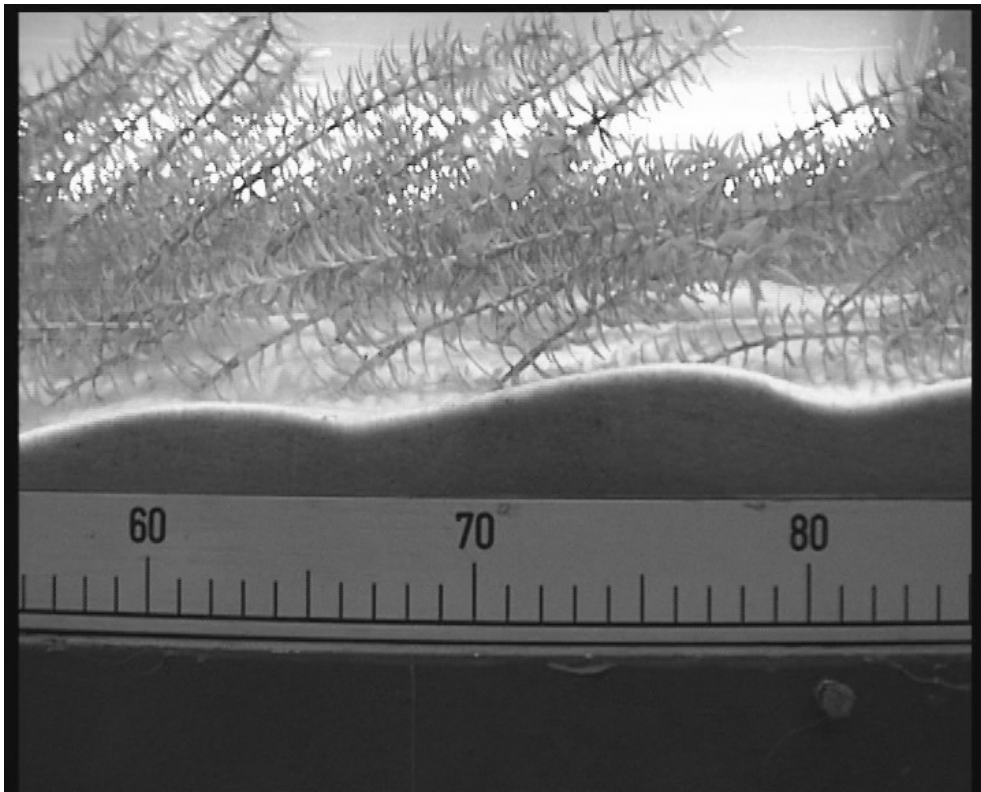
Figure 5.13: Vegetation in the flow.

0.106 m respectively. Now two unknown parameters need to be determined, the effective density, m, and the effective diameter, D. This is elaborated in the next section.

5.6 Determination of the bed shear stress

The time-averaged bed shear stress follows from the momentum balance, Eq. (5.4), integrated through to the bed, at $z = 0$. A problem, however, is that it is not exactly known how the profile of the Reynolds stress extrapolates to the bed. The extrapolation is very sensitive to the estimates of the Reynolds stress and the plant force near the bed, because it is found by subtraction of two large and almost equal numbers. Therefore, to estimate the bed shear stress, the 1-DV numerical model was applied. An important model parameter for the determination of the bed shear stress is the bed roughness, C_b. The bed roughness of a flat sand bed with a grainsize of $D_{90} = 450$ μm is calculated by:

$$C_b = 18 \log \left(\frac{12h}{3D_{90}} \right) \tag{5.6}$$

At the typical water depths of the flume experiment this yields a C_b of 62 m$^{1/2}$·s^{-1}. However, the sand bed between the vegetation was not flat, see Fig. 5.10 or 5.11. To estimate the bed roughness of the vegetated bed, the theoretical logarithmic velocity
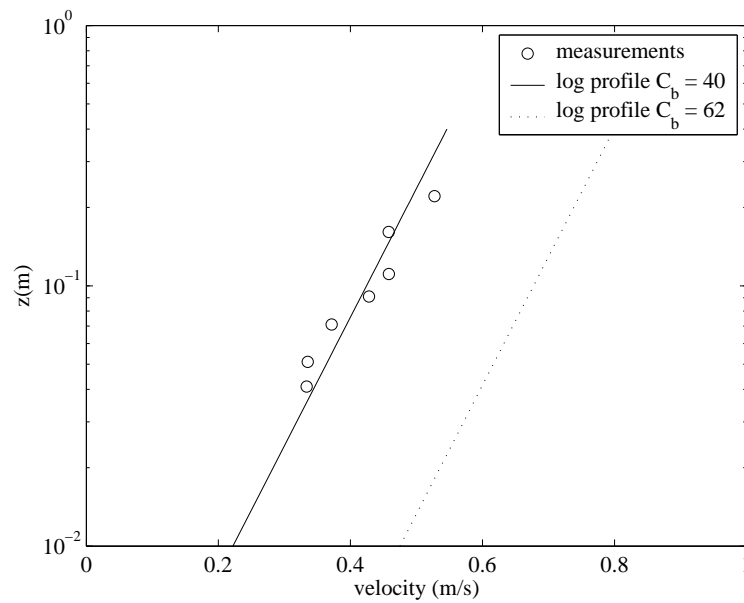
Figure 5.14: Fit of logarithmic velocity profile to Test 5 to determine the bed roughness C_b.

profile is fitted to the velocity measurements of the reference Test 3R. Since the bedforms in the bed level profile of Test 3R (Figure 5.12) have about the same dimensions as the bedforms in the vegetated tests, it is assumed that this is representative of the bed roughness. The theoretical logarithmic velocity profile is given by:

$$u(z) = \frac{u_*}{\kappa} \ln\left(\frac{z}{z_0}\right) \tag{5.7}$$

The bed shear velocity, u_*, is determined at 0.035 m/s, calculated from the linear interpolation of the Reynolds stress measurements, see Fig. 5.9. A best fit was obtained with a z_0 of $8 \cdot 10^{-4}$ m. Applying a White-Colebrook formula, this corresponds to a Chézy value of 40 m$^{1/2}$·s^{-1}. Figure 5.14 shows the fit of the logarithmic profile to the measurements, and for comparison, the logarithmic profile for a bed roughness with a Chézy value of 62 m$^{1/2}$·s^{-1}.

5.6.1 1-DV model application to determine the bed shear stress

The 1-DV model has been applied to simulate the measured profiles for shear stress and horizontal flow velocity for the experimental tests at location M5. One hundred vertical layers were defined that have a non-uniform, double exponential distribution, with the highest densities at the top of the vegetation and near the bed. Hydraulic conditions were chosen according to Table 5.1. The blockage area for a bulk drag coefficient of 1.0 presented in Table 5.5 was applied, only with one difference: it was assumed that for Test 3, the blockage area at height $z = 0.106$ m is zero, thus representing the top of the vegetation. Furthermore, the blockage area for the lowest measuring point was assumed
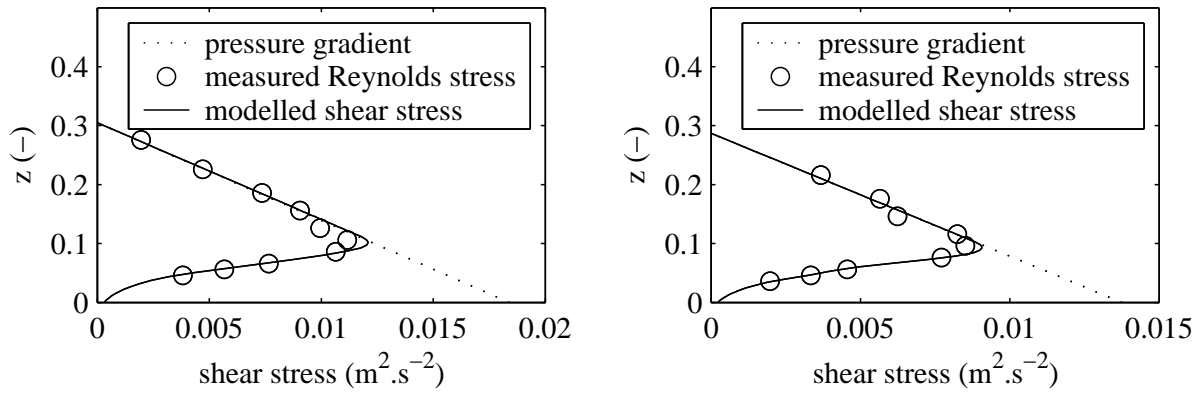
Figure 5.15: Vertical profiles for the pressure gradient, the Reynolds stress and modelled shear stress for Test 2 (left panel) and Test 3 (right panel), $D = 0.0017$ m, $C_D = 1$, applying a vertical profile for m, $c_l = 1$.
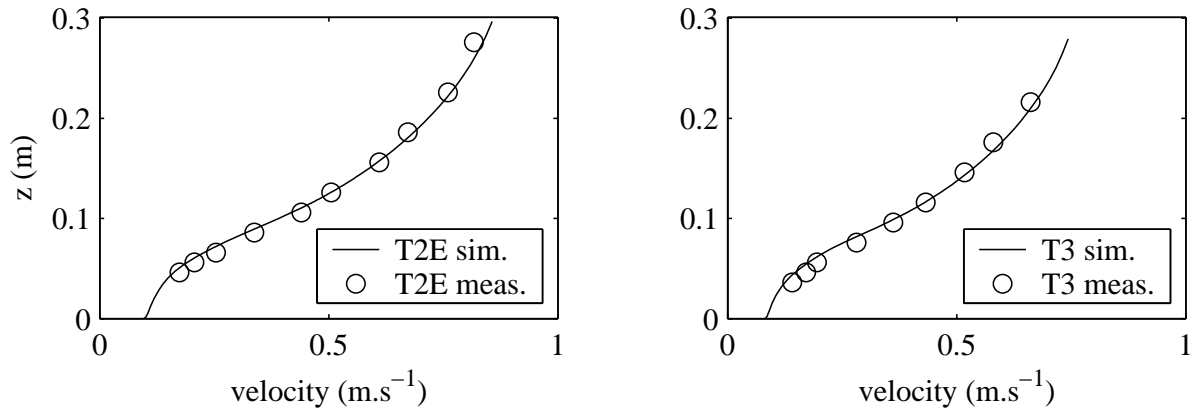
Figure 5.16: Simulated and measured vertical velocity profiles for Test 2 (left panel) and Test 3 (right panel), $D = 0.0017$ m, $C_D = 1$, applying a vertical profile for m, $c_l = 1$.

to hold through to the bed. The c_l parameter in the numerical 1-DV model was set at 1.0. The model was subsequently calibrated on the comparison of the measured and modelled shear stress profiles by assuming a constant effective stem diameter, D. The calibration thus resulted in an effective density profile over the vertical. A best fit was found for both tests for an effective stem diameter of 1.7 mm. The effective density then follows from the blockage area in Table 5.5. Figure 5.15 presents the modelled and measured shear stress profile and Fig. 5.16 presents the simulated and measured horizontal velocity profiles. The values for the resulting effective density are presented in Table 5.6 and presented graphically in Fig. 5.17.

Table 5.6 and Fig. 5.17 firstly show that the effective densities change over the vegetation height. Their vertical profile stem from the swaying and non-uniform nature of the vegetation. Secondly, the effective densities become large, even over 10,000 m^{-2} for Test 3. This can be explained by the influence of the leaves on the resistance against flow and
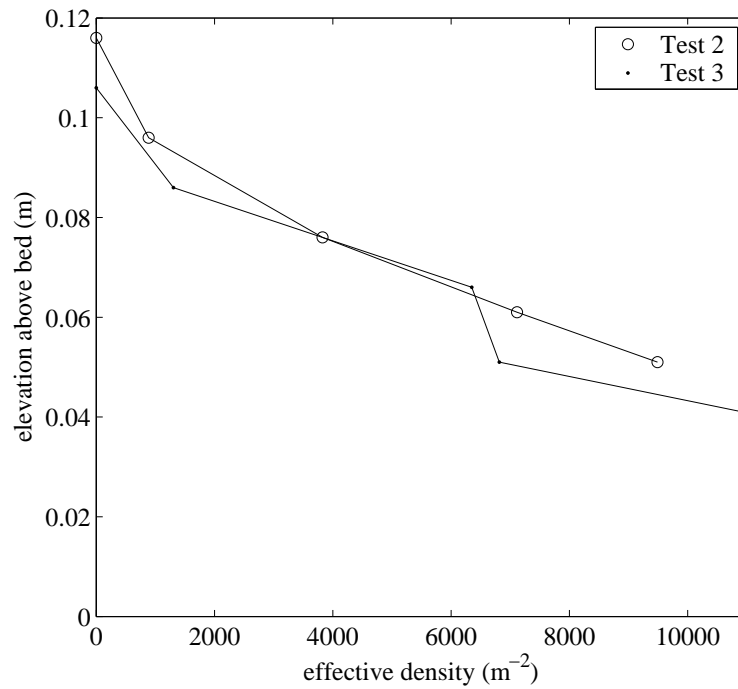
Figure 5.17: Vertical profiles of the effective density for Test 2 and Test 3.

the break-up of turbulent eddies. The rather complex geometry of the artificial vegetation cannot be described adequately by the stems of the vegetation only, which are cylinders with a stem diameter of 2 mm, placed 0.05 m apart. The presence of the leaves must be included as well, and parameter fitting yields an effective diameter of 1.7 mm, placed with a minimum distance of about 0.01 m apart.

Table 5.6: Effective density profile, $m(z)$, for Test 2 and Test 3.

Test 2		Test 3	
z (m)	m (m^{-2})	z (m)	m (m^{-2})
0.116	0	0.106	0
0.096	$0.9 \cdot 10^3$	0.086	$1.3 \cdot 10^3$
0.076	$3.8 \cdot 10^3$	0.066	$6.3 \cdot 10^3$
0.061	$7.1 \cdot 10^3$	0.051	$6.8 \cdot 10^3$
0.051	$9.5 \cdot 10^3$	0.041	$10.9 \cdot 10^3$

Another parameterization can be made by applying the 1-DV model with a constant density and diameter over depth. Then a vertical profile for the bulk drag coefficient must be applied, following from Table 5.5. As noted before, for plant properties $m = 400$ m^{-2} and $D = 0.002$ m, this yields high values for the bulk drag coefficient, up to 23, which are considered unrealistically high. However, the model fit will be presented here for Test 2 as an example. It is now important to adjust the c_l parameter as well, since this determines the characteristic length scale of the turbulent eddies that are generated
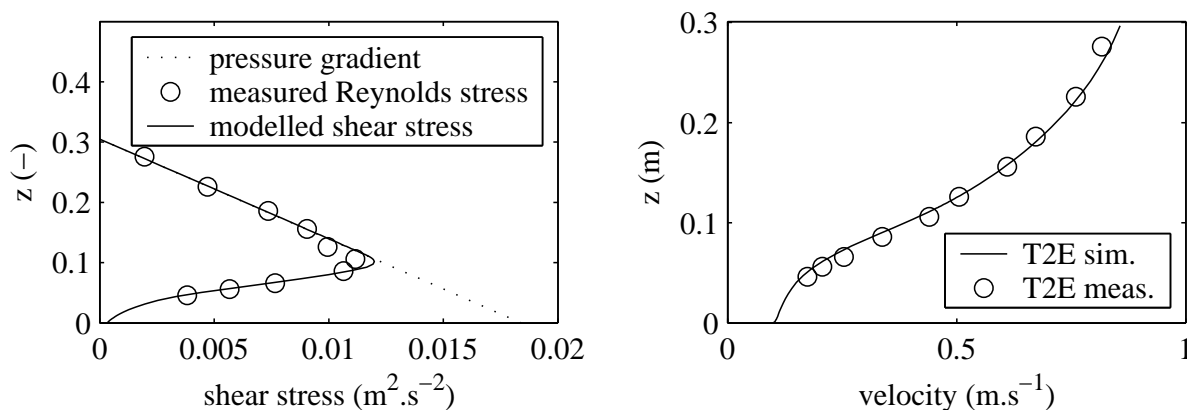
Figure 5.18: Vertical profiles for the pressure gradient, the Reynolds stress and modelled shear stress (left panel) and velocity (right panel) for Test 2, $m = 400$ m^{-2}, $D = 0.002$ m, applying a vertical profile for C_D and c_l fitted to 0.28.

by the grid distance of the plant stems. This stem distance is given by the square root of the reciprocal of the density, omitting the fraction of horizontal surface area in Eq. (4.41). As a first estimate for the stem distance, the height-averaged density for Test 2, following from Table 5.6, is calculated. This density is 6078 m^{-2} and yields a stem distance which is $(400/6078)^{0.5} = 0.26$ times smaller than the distance between cylinders placed as 400 m^{-2}. An estimate of the c_l parameter is therefore 0.26. Indeed, a best fit for the shear stress profile was obtained with a value for c_l of 0.28, which is near this estimate, see Fig. 5.18. However, it can be concluded that without a detailed description of the measurable parameters density and diameter, the exact values for the model coefficients C_D and c_l cannot be determined.

Although Figures 5.15 to 5.18 merely show the quality of the parameter fitting rather than the quality of the model, the 1-DV model simulations provide an estimate of the time-averaged bed shear stress, τ_b, for the experiments with vegetation. The bed shear stress for the non-vegetated cases was determined with the 1-DV model, as well, for equal depth-averaged velocities and flow depths as used in the experiments with vegetation, but assuming open channel flow (so these bed shear stress values do not stem from the reference tests). The results in Table 5.7 show that the reduction in bed shear stress as a result of the presence of the vegetation is about 80% compared to a situation without vegetation.

5.6.2 Determination of the bed shear stress by analytical estimators

In this section, the bed shear stress is estimated by the *Reduction factor approach* and the *Analytical approach*, described in Chapter 4.

Table 5.7: Comparison of bed shear stress values derived from the 1-DV model, with and without vegetation.

Test	Bed shear stress with vegetation ($N \cdot m^{-2}$)	Bed shear stress without vegetation ($N \cdot m^{-2}$)	Reduction in bed shear stress due to vegetation (%)
Test 2	0.32	1.42	77.6
Test 3	0.23	1.07	78.8
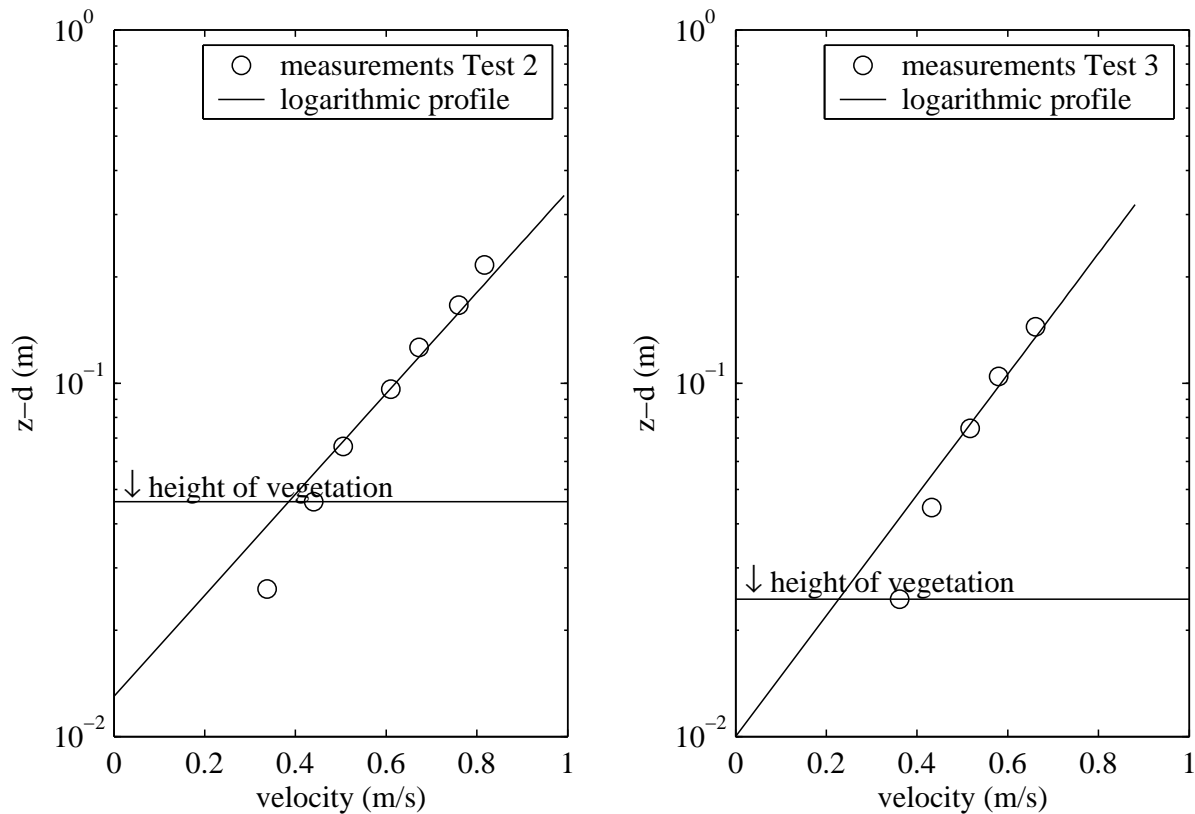
Figure 5.19: Fit of logarithmic velocity profile to the velocity measurements above the vegetation for Test 2 (left panel) and Test 3 (right panel).

Reduction factor approach

To estimate the bed shear stress with the *Reduction factor approach*, uniform plant characteristics over the vertical must be assumed, i.e. an effective uniform drag coefficient, diameter and density. For a C_D value of 1, the effective cylinder diameter has been determined at 0.0017 m (see section 5.6.1). The effective uniform density can be determined from the measured hydraulic roughness of the vegetation. In Chapter 4, it was found that two expressions for the representative roughness showed the best fit with flume data from literature, i.e., the *method of effective water depth variant 3*, and the formula found with *Genetic Programming*. The roughness formula of the *Analytical approach* will be elabo-

rated in the next section. Here, two estimates for the effective density are given, which are derived by solving Eqs. (4.76) and (4.155) for m. This yields estimates for m_{eff3}, the effective uniform density from the method of effective water depth variant 3 and m_{effGP}, the effective uniform density from the GP-formula:

$$m_{eff3} = \frac{2g\left(\left(C_r^2 - 2C_r E1 + E1^2\right)^{-1} - C_b^{-2}\right)}{C_D Dk} \tag{5.8}$$

where:

$$E1 = \frac{(h-k)^{3/2} \frac{\sqrt{g}}{\kappa} \ln\left(\frac{h-k}{e z_0}\right)}{h^{3/2}} \tag{5.9}$$

and:

$$m_{effGP} = \frac{2g\left(\left(C_r^2 - 2C_r E2 + E2^2\right)^{-1} - C_b^{-2}\right)}{C_D Dk} \tag{5.10}$$

$$E2 = \frac{\sqrt{g}}{\kappa} \ln\left(\frac{h}{k}\right) \tag{5.11}$$

Two Chézy values need to be known to estimate the effective density, i.e. the Chézy value for the bed roughness, C_b, and the representative Chézy value for the roughness of the vegetation, C_r. The first is derived from Fig. 5.14. For the latter, C_r, the range of values that was determined at 11.0 to 12.3 $\mathrm{m^{1/2} \cdot s^{-1}}$ (Tables 5.3 and 5.4) is applied. An unknown parameter is z_0, the roughness height of the top of the vegetation, which needs to be determined in Eq. (5.9). This value can be determined by a fit of the theoretical logarithmic velocity profile, Eq. (4.87), to the velocity measurements above the vegetation. For this purpose, first the zero-plane displacement, d, is determined from the measured shear stress profile, applying Eq. (4.114). The fit of the logarithmic velocity profile is presented in Fig. 5.19.

Resulting values for d, z_0 and the range of values for the effective density for Test 2 and Test 3 are presented in Table 5.8. The results firstly show that the estimate for the effective density is very sensitive to the uncertainty in the representative roughness. Secondly, the results show a relatively large difference in estimates for the effective density derived by both formulae. Thirdly, comparing the results for the effective density with those listed in Table 5.6 shows that the estimates for the effective densities of Test 2 and Test 3 are in the range of the estimated densities derived with the 1-DV numerical model. However, the results show a difference in estimates for the effective density between the tests, whereas it was expected that these should be about equal, see Fig. 5.17. This difference is mainly due to the value for z_0, which indicates that the roughness of the top of the vegetation is reduced for Test 3 compared with Test 2. It shows that the estimate for the effective density is very sensitive to this parameter as well, and can be affected by measurement errors.

Although the *GP-formula* scores best as a general roughness predictor, see section 4.7.2, it was also shown that this formula lacks to describe the detailed relationship for roughness

Table 5.8: Zero-plane displacement, d, roughness height for the top of the vegetation, z_0, representative roughness, C_r, and effective density estimates, for Test 2 and 3, location M5.

Test	d	z_0	C_r	m_{eff3}	m_{effGP}
	(m)	(m)	$(\mathrm{m}^{1/2}\cdot\mathrm{s}^{-1})$	(m^{-2})	(m^{-2})
Test 2	0.060	0.013	11.1 - 12.2	$4.5\cdot10^3$ - $2.9\cdot10^3$	$7.9\cdot10^3$ - $4.6\cdot10^3$
Test 3	0.072	0.010	11.0 - 12.3	$8.5\cdot10^3$ - $4.5\cdot10^3$	$10.6\cdot10^3$ - $5.3\cdot10^3$

Table 5.9: Reduction factor and bed shear stress estimate, for Test 2 and 3, location M5.

Test	Reduction factor for m_{eff3} (-)	Bed shear stress $(\mathrm{N}\cdot\mathrm{m}^{-2})$
Test 2	0.014 - 0.021	0.31 - 0.39
Test 3	0.008 - 0.015	0.18 - 0.27

and depth, see Fig. 4.18. Furthermore, having determined the zero-plane displacement and the roughness height for the top of the vegetation, we opt for m_{eff3} as the best estimator for the effective depth. Subsequently, the bed shear stress for location M5 can be estimated by applying Eq. (4.27) with the estimates for the effective densities m_{eff3}. The reduction factor, f, and the resulting bed shear stress values are presented in Table 5.9.

For both tests, the *Reduction factor approach* results in a range of bed shear stress values that contains the estimate derived by the 1-DV model, see Table 5.7. These results further show that the uncertainty range for the reduction factor and bed shear stress is very sensitive to the estimate for the representative roughness.

Analytical approach

To estimate the bed shear stress with the *Analytical approach*, plant characteristics have to be assumed uniform over the vertical as well. Now the effective density will be determined from the representative roughness estimates by applying the formulations in the *Analytical approach*. The effective density cannot be determined directly by solving the complicated Eq. (4.107) for m, instead, values were found by fitting. To determine the bed shear stress, the coefficient for the turbulence intensity near the bed, $c_{p,bed}$, is calculated by Eq. (4.161). The results are given in Table 5.10. These results show a range of bed shear stress estimates, which are relatively high compared with the result of the 1-DV model. Again, similar to the *Reduction factor approach*, the calculation of the bed shear stress is very sensitive to the uncertainty in the representative roughness.

Table 5.10: Effective density, calculated $c_{p,bed}$-values and calculated bed shear stress values for the *Analytical approach*, Test 2 and 3, location M5.

Test	Effective density m ($\mathrm{m^{-2}}$)	$c_{p,bed}$ calculated (-)	Bed shear stress ($\mathrm{N \cdot m^{-2}}$)
Test 2	$1.3 \cdot 10^3$ - $3.1 \cdot 10^3$	0.0161	0.34 - 0.58
Test 3	$1.7 \cdot 10^3$ - $5.4 \cdot 10^3$	0.0166	0.18 - 0.37

5.6.3 Discussion

Three different methods have been applied in this section to determine the bed shear stress from the measurements. The most reliable might be the application of the 1-DV model, since this does not require the schematisation of uniform plant characteristics over the height and the physical process descriptions are most advanced. However, without detailed measurements of the exact blockage area of the flow, the schematisation of plant characteristics needs to be fitted. The *Reduction factor approach*, as well as the *Analytical approach* are based on uniform plant characteristics over the plant height. These were estimated from the measured hydraulic resistance in combination with their respective equations to calculate the resistance. The results show that the calculation of the bed shear stress is very sensitive to the estimate of the representative roughness, therefore, it is very important to determine the representative roughness accurately. In this respect, measuring a water level slope, or applying an EMS to measure shear stresses, are both methods that have their drawbacks. As a further consequence, it proves to be important to accurately describe the vegetation geometry for complex types of vegetation to determine the bed shear stress. For natural vegetation types this gives measurement problems.

In conclusion, the experiment showed a reduction of the bed shear stress of a vegetated bed, which can be estimated reasonably well with numerical or analytical models, given an accurate description of the vegetation geometry. This reduced bed shear stress will subsequently be applied to determine the sediment transport rate in the experiment.

5.7 Analysis of the sediment transport rate with a simple 1-DH model

Since the flow in the flume is non-uniform, the flow conditions known at one location cannot be used straightforwardly to estimate the sediment transport rate along the flume. Therefore, a simple 1-DH morphodynamic model has been developed. This model simulates the backwater curve in the water level above the vegetated section, which is determined by the representative roughness of the submerged vegetation. The resulting longitudinal gradient in flow and bed shear stress, affected by the vegetated bed, are applied

in a sediment transport formula, leading to a change in bed level profile. The modelled changes in bed level profiles are subsequently compared to the measured changes, to assess the quality of modelling the reduced bed shear stress in the sediment transport formula.

In this simple 1-DH model, the bed shear stress is given by the *Reduction factor approach*, Eq. (4.27) with the values from Table 5.9. The vegetation characteristics that have been derived for location M5 are assumed to hold for the entire section. It was, however, observed that the net vegetation height was higher in the beginning of the vegetated section compared to the end of the section. These height changes were due to the increasing flow velocities over the flume length that made the vegetation bend more. On the other hand, this effect was compensated for during the test runs. The eroding bed at the end of the vegetated section enlarges the net length of the vegetation that protrudes from the bed. For the sake of simplicity, these kinds of effects were not accounted for by the simple 1-DH model.

5.7.1 Backwater curve

The backwater curve is given by the differential equation:

$$\frac{\partial h}{\partial x} = \frac{i_b - i_f}{1 - Fr^2} \tag{5.12}$$

where i_b is the bed slope:

$$i_b = \frac{\partial z_b}{\partial x} \tag{5.13}$$

i_f is the friction slope:

$$i_f = \frac{Q^2}{C_r^2 B^2 h^3} \tag{5.14}$$

and Fr is the Froude number:

$$Fr = \frac{Q^2}{g B^2 h^3} \tag{5.15}$$

where x is the longitudinal position, z_b is the bed level, Q is the flume discharge, C_r is the representative Chézy value for the vegetation roughness, B is the flume width and h is the water depth. Equation (5.14) for the friction slope, is valid for a flume of infinite width, i.e. without friction of the walls. For flume experiments, it would be better to use a hydraulic radius instead of the water depth, or to account for the differences in the roughness between the bed and the walls following Vanoni and Brooks (1957). However, since the resistance of the vegetation is much larger than the wall friction, Eq. (5.14) is considered a valid assumption. The differential equation for the backwater curve is solved by a predictor-corrector method with a given step-size in the longitudinal direction, starting from the downstream boundary condition, progressing upstream.

5.7.2 Sediment transport rate

The erosion and sedimentation rate along the flume is simulated with a sediment balance equation:

$$(1 - \epsilon_p)\frac{\partial z_b}{\partial t} + \frac{\partial s}{\partial x} = 0 \tag{5.16}$$

where ϵ_p is the porosity of the sediment, and s is the sediment transport capacity per unit width. For the sediment transport capacity the bed load transport formula of Van Rijn (1984) is applied, assuming that suspended load transport is negligible for the low bed shear stresses considered in this experiment. This assumption is verified on the basis of the visual observation of a very low concentration of suspended particles in the water. For non-uniform flow conditions, as observed in the flume experiment, the adjustment of the bed load transport to the hydraulic conditions proceeds almost instantaneously, therefore a local transport predictor is applicable:

$$\Phi_b = \begin{cases} \alpha 0.053 D_*^{-0.3} T^{2.1} & \text{for T} < 3.0 \\ \alpha 0.1 D_*^{-0.3} T^{1.5} & \text{for T} \geq 3.0 \end{cases} \tag{5.17}$$

where α is a calibration coefficient, Φ_b is the dimensionless transport parameter, D_* is the dimensionless grain diameter and T is the dimensionless bed shear parameter, respectively:

$$\Phi_b = \frac{s}{\sqrt{g \Delta D_{50}^3}} \tag{5.18}$$

$$D_* = D_{50} \left(\frac{\Delta g}{\nu^2}\right)^{1/3} \tag{5.19}$$

and

$$T = \frac{\mu \tau_b - \tau_{bcr}}{\tau_{bcr}} \tag{5.20}$$

where μ is a bed form factor, τ_b is the bed shear stress and τ_{bcr} is the time-averaged critical bed shear stress for the initiation of movement of particles, following from Shields' curve (Van Rijn, 1993). The common way is to calculate the bed shear stress by:

$$\tau_b = \rho g \frac{\overline{u}^2}{C^2} \tag{5.21}$$

and the bed form factor by:

$$\mu = \left(\frac{C}{C'}\right)^2 \tag{5.22}$$

where $\overline{u}$ is the depth-averaged velocity (m/s), C is the overall Chézy coefficient of the flow and C' is the grain-related Chézy coefficient, which is 62 $\text{m}^{1/2} \cdot \text{s}^{-1}$ in this experiment, see section 5.6. In Van Rijn's approach, the bed form factor eliminates the bed form roughness. Here, we consider a similar approach, but instead of the bed form factor, we apply the bed shear stress reduction factor for submerged vegetation, calculated by the *Reduction factor approach*, described in Chapter 4, Eq. (4.25):

$$T_{veg} = \frac{f \tau_b - \tau_{bcr}}{\tau_{bcr}} \tag{5.23}$$
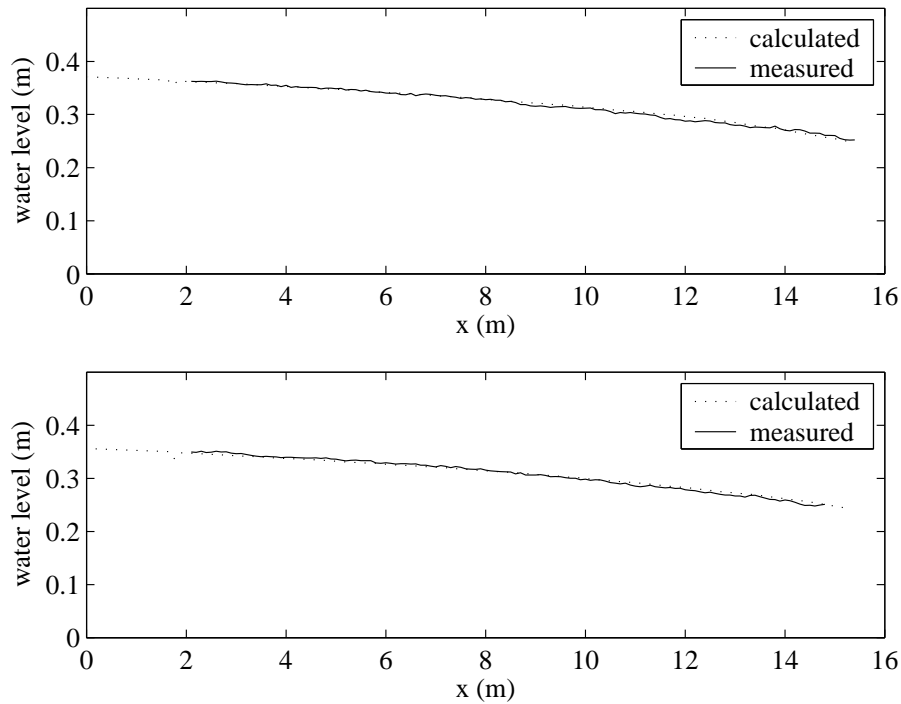
Figure 5.20: Measured and calculated water level profiles at the start of the experiment, for Test 2 (line) and Test 3 (dash-dot line).

5.7.3 Application and results of the 1-DH morphological model

The 1-DH morphological model is applied to simulate the morphological changes in the longitudinal profile of the bed. In each test, the longitudinal bed level profile was measured at two locations over the flume width, one along the centre line of the flume and one at a side line, at distance of one sixth of the flume width from the right flume wall. These data were preprocessed. First, a moving average with a two-sided window of about 0.85 m wide was applied to filter out the small bedforms. Second, the smoothed profiles were averaged over the flume width, with a weighted average of 1/3 for the centre line profile and 2/3 for the side line profile, see Figure 5.4.

The backwater curve is calculated first and compared with the initial water level profiles, measured at the start of the experiment, see Fig. 5.20. This yields an estimate for the representative roughness over the flume length. From the resulting backwater curve, the longitudinal profile for depth-averaged flow velocities follows, which is applied to calculate a longitudinal profile of bed shear stress using the *Reduction factor approach*. The effective density of the vegetation was chosen such that the bed shear stress at location M5 is in correspondence with the results of the 1-DV model at that location, see Table 5.7 and falls within the range of Table 5.9. Table 5.11 presents some important input parameters of the 1-DH morphological model.
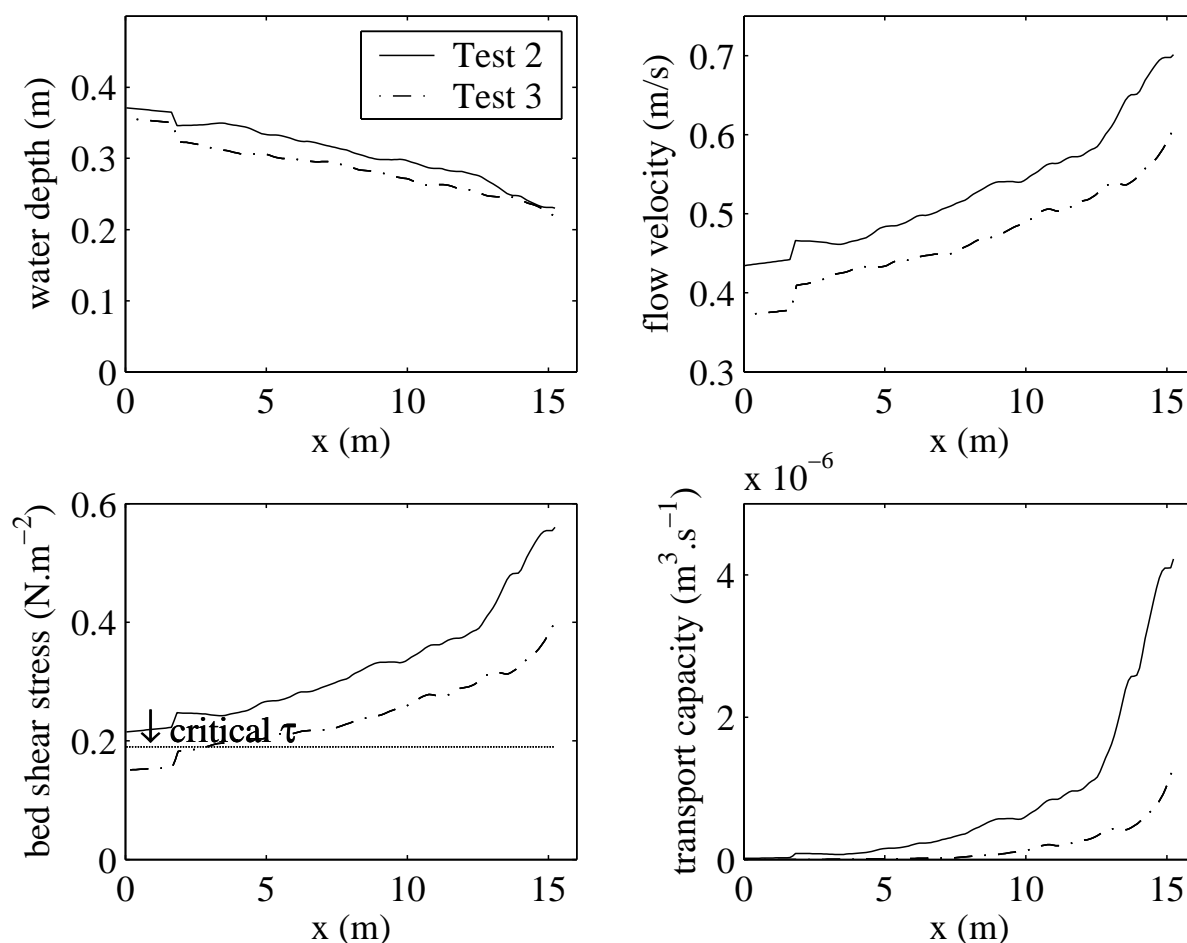
Figure 5.21: Initial profiles for the water depth, depth-averaged flow velocity, bed shear stress and the sediment transport capacity, for Test 2 (line) and Test 3 (dash-dot line).

Table 5.11: Input parameters of the 1-DH morphological model.

Test	Chézy $(m^{1/2}{\cdot}s^{-1})$	downstream water depth (m)	effective density (m^{-2})	reduction factor (-)
Test 2	11.8	0.23	$3.8{\cdot}10^3$	0.016
Test 3	11.0	0.22	$5.0{\cdot}10^3$	0.013

The resulting longitudinal gradient in flow conditions is subsequently applied in the bed load formula of Van Rijn, with the adjusted dimensionless bed shear parameter T_{veg}, Eq. (5.23). Together with the sediment balance equation this leads to a change in bed level profile. Calibration of the results is achieved via the calibration coefficient α. The porosity of the bed is assumed to be 0.4. For sand particles with a D_{50} of 320 μm, Shields' critical bed shear stress is 0.19 N·m^{-2}.

Figure 5.21 presents the initial profiles (at $t = 0$) for the water depth, depth-averaged flow velocity, bed shear stress and the sediment transport capacity. Note that in Test 3 the

Table 5.12: Measured and modelled transport rate for Test 2 and Test 3.

Test	Direct weighing (kg/h)	From bed profiles (kg/h)	Model output (kg/h)
Test 2	11.6	9.0	10.3
Test 3	5.9	4.7	5.4

first part of the section has average bed shear stress values that are beneath the critical bed shear stress.

Figures 5.22 and 5.23 present the 1-DH model results for Test 2 and Test 3. The results show that the model could be fitted reasonably well, with the exception of the dune-like bed feature present in the beginning of the section in Test 2, which is deliberately not modelled. For Test 2 a best fit was obtained using a calibration factor of $\alpha = 1$, for Test 3, $\alpha = 2$. The values for the time-averaged bed shear stress in Test 3 are near, or even under, the critical shear stress. Under these conditions, the bed load formula is less accurate, which explains a higher value for the calibration coefficient. Furthermore, based on the longitudinal profiles, it was found that the sediment transport rate in Test 3 was not equal over the flume width. The bed level in the first 6 m of the vegetated section showed net erosion of the side profile and net sedimentation of the centre profile, levelling out after 32 hours. Remarkably, both the sedimentation and the erosion took partly place in that part of the section where the time-averaged bed shear stress is below or around the critical bed shear stress according to Shields. This suggests firstly that the critical bed shear stress for the initiation of movement is exceeded by turbulence fluctuations. Secondly, sediment is redistributed in lateral direction, so that the middle part of the flume is filled up from the sides, until an even bed level is achieved. The non-uniform flow distribution observed (see Fig. 5.6) yields a secondary current and could thus be a driving force for lateral redistribution of sediment.

Table 5.12 presents the measured and modelled sediment transport rates of the bed for Test 2 and Test 3. The transport rates were determined over the entire duration of the flume experiment, for the measurements as well as for the model simulations. It must be noted that it was observed visually that the erosion was not equally distributed over the width of the flume. Especially near the sidewalls of the flume the erosion was more severe. The walls have a lower roughness compared to the vegetation and therefore the flow velocities and associated transport rates were higher along the walls (see Fig. 5.6).

The application of the simple 1-DH morphodynamic model shows that the sediment transport rate for a vegetated bed can be described reliably by a common sediment transport formula, as long as the bed shear stress reduction is accounted for.
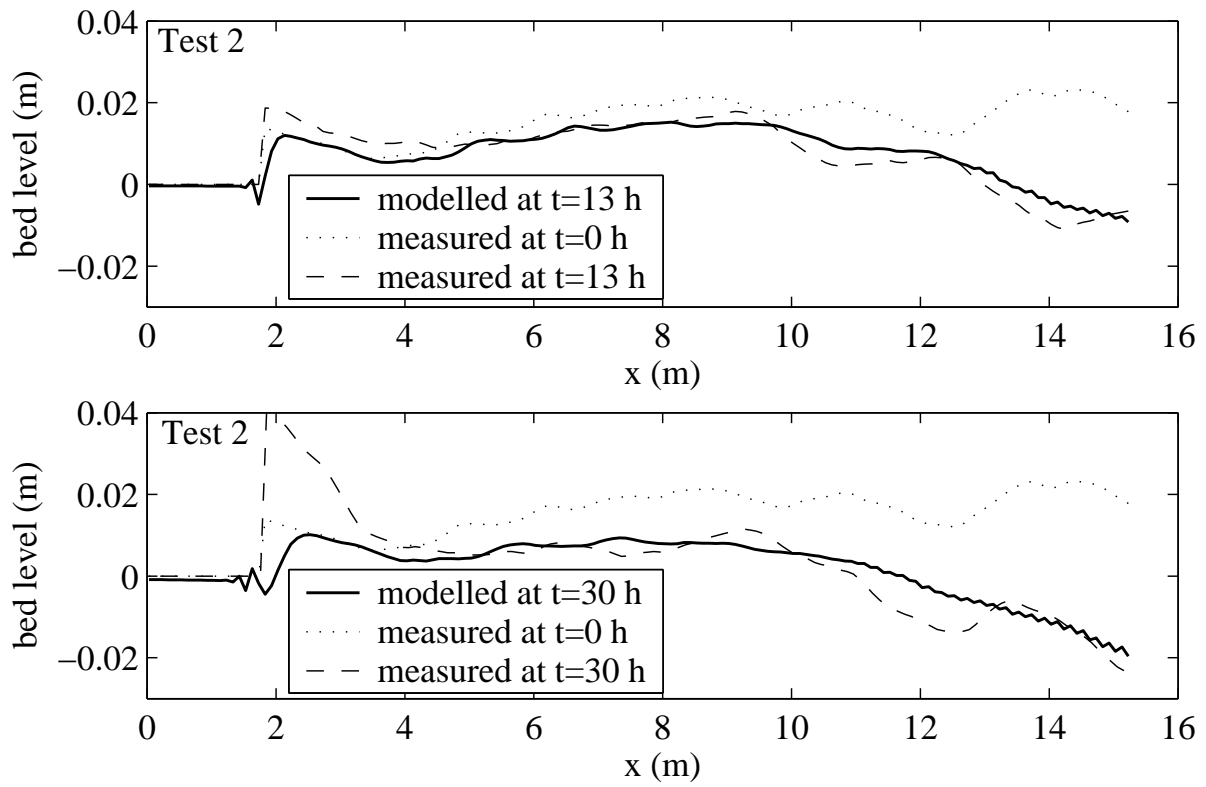
Figure 5.22: Measured bed level profiles at t=0, t=13 and t=30 h and model results for t=13 h (top panel) and t=30 h (lower panel) for Test 2, $\alpha = 1$.
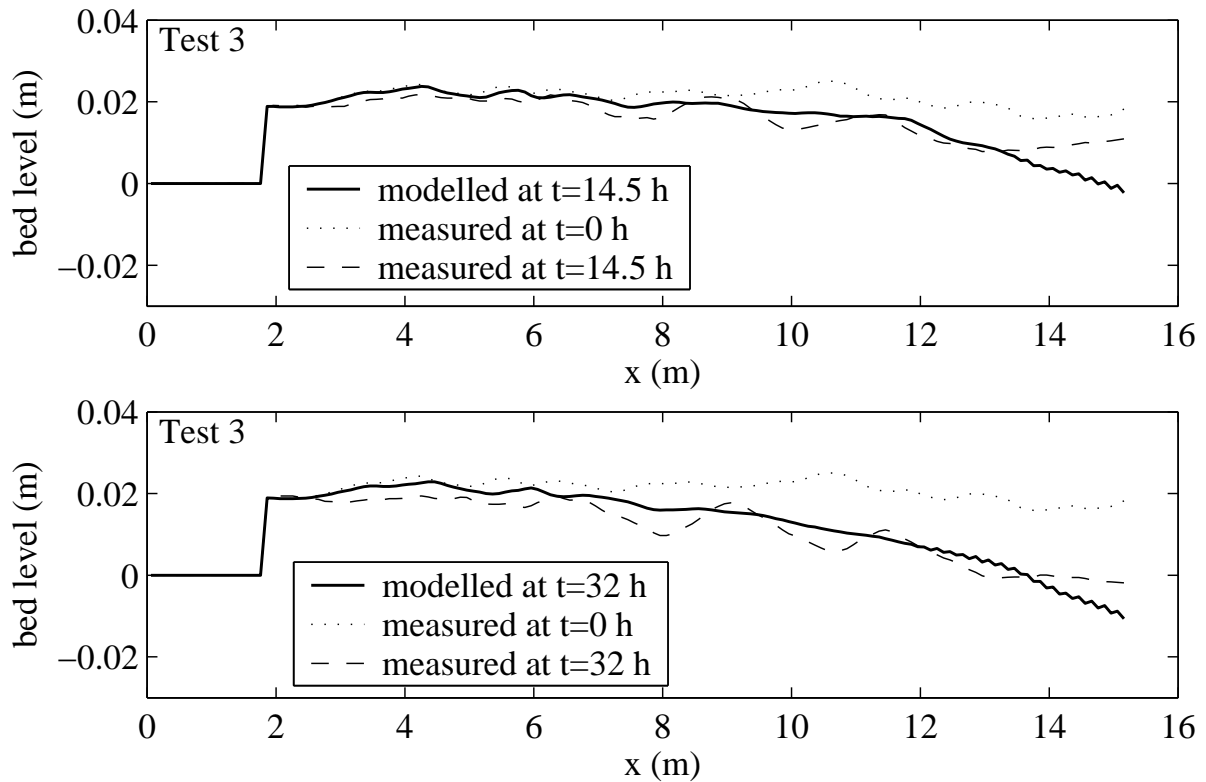
Figure 5.23: Measured bed level profiles at t=0, t=14.5 and t=32 h and model results for t=14.5 h (top panel) and t=32 h (lower panel) for Test 3, $\alpha = 2$.
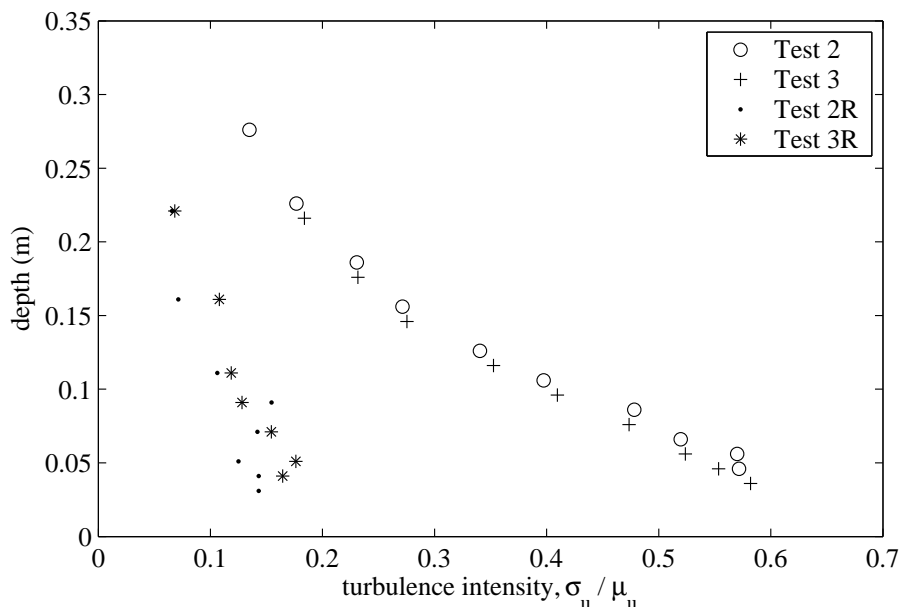
Figure 5.24: Turbulence intensity for tests with (2 and 3) and without (2R and 3R) vegetation.

5.8   Stochastic sediment pick-up

The results of the 1-DH model suggest that bed load transport can explain the observed bed level changes. However, especially for conditions leading to bed shear stresses near the critical threshold of motion, it is assumed that turbulence events are an additional mechanism for sediment transport. This section theoretically investigates the pick-up of sediment affected by vegetation. It is hypothesized that an increased turbulence intensity inside the vegetated layer is capable of picking up the sediment more effectively and thus bringing it into transport.

Figure 5.24 compares the turbulence intensity for tests with and without vegetation. The comparison shows that the turbulence levels within the vegetation, expressed as the ratio of the standard deviation of the instantaneous velocity over the mean velocity, are increased by a factor 4 compared to the cases without vegetation. Closer to the bed, the mean turbulence intensity probably decreases, however, it is hypothesized that in this experiment, turbulence events inside the vegetation can penetrate down to the bed and pick-up sediment. It should be noted that for higher types of vegetation, the turbulence intensity inside the vegetation will decrease and thus the shear turbulence generated at the top of the vegetation cannot reach down to the bed, see Fig. 4.9.

To account for the sediment pick-up by the turbulence fluctuations in the flow, a stochastic pick-up formula can be applied. Pioneering work on stochastic pick-up relations have been carried out by Einstein (1950), Paintal (1971), Grass (1970) and Yalin (1977). Further analysis and improvements have been made in later work by De Ruiter (1982), Zanke (1990), Cheng and Chiew (1998) and Kleinhans and Van Rijn (2002). Here, we will extend

the methodology of De Ruiter (1982), which in turn is based on the work of Einstein (1950). A first study to apply De Ruiter's approach to describe the effect of turbulence on the pick-up rate in the flume experiment described in this thesis was executed by Helal Ahmed (2003).

The stochastic character of flow, due to turbulence fluctuations, is represented in a probability distribution for the bed shear stress. This probability distribution is especially relevant for conditions near the initiation of motion. The critical bed shear stress for initiation of motion, τ_{cr}, is commonly derived from Shields (1936). In deterministic sediment transport models, the time-averaged bed shear stress, τ_b, is evaluated with respect to the critical bed shear stress. Only when τ_b is larger than τ_{cr}, sediment transport occurs. However, at conditions near the initiation of motion, the time-averaged bed shear stress can be smaller than τ_{cr}, but the tail of the probability density function for the bed shear stress may exceed the critical value, yielding transport after all. This is envisaged in Fig. 5.25, showing two imaginary cases of bed shear stress probability distributions. The probability density function (pdf) of case 1 has an average bed shear stress of 0.5 N·m^{-2}, and the pdf of case 2 has an average bed shear stress of 2.0 N·m^{-2}. The critical bed shear stress is in itself a stochastic parameter too, and Grass (1970) applies a minimum overlap region between the two pdf's, but here we consider a deterministic threshold value. The value for the critical bed shear stress is 0.6 N·m^{-2} in this example. In case 2, the entire pdf is well over the critical threshold, so each instantaneous bed shear stress value leads to sediment transport. In case 1, the time-averaged bed shear stress is smaller than the critical threshold, however, the right tail of the pdf exceeds the critical threshold.

Stochastic pick-up rate

Usually, the stochastic sediment pick-up rate is expressed as the average number of particles (n_p) picked up from the bed per unit time and per unit area (Paintal, 1971; Yalin, 1977):

$$n_p = \left(\frac{4\eta}{\pi D^2} \right) \frac{P_c}{T} \tag{5.24}$$

where η is a dimensionless coefficient (=0.03, De Ruiter (1982)), $4/\pi$ is a shape constant for spherical particles, D is the particle diameter, P_c is the probability of the instantaneous bed shear stress τ to exceed a critical value τ_c and T is a characteristic time scale for entrainment of a particle. The sediment pick-up rate in terms of mass per unit area and time for spherical particles is:

$$E = \frac{1}{6} \pi \rho_s D^3 n_p \tag{5.25}$$

Substitution of Eq. (5.24) in Eq. (5.25) yields:

$$E = \frac{2}{3} \eta \rho_s D \frac{P_c}{T} \tag{5.26}$$

The probability, P_c, and the time-scale, T, are discussed below.
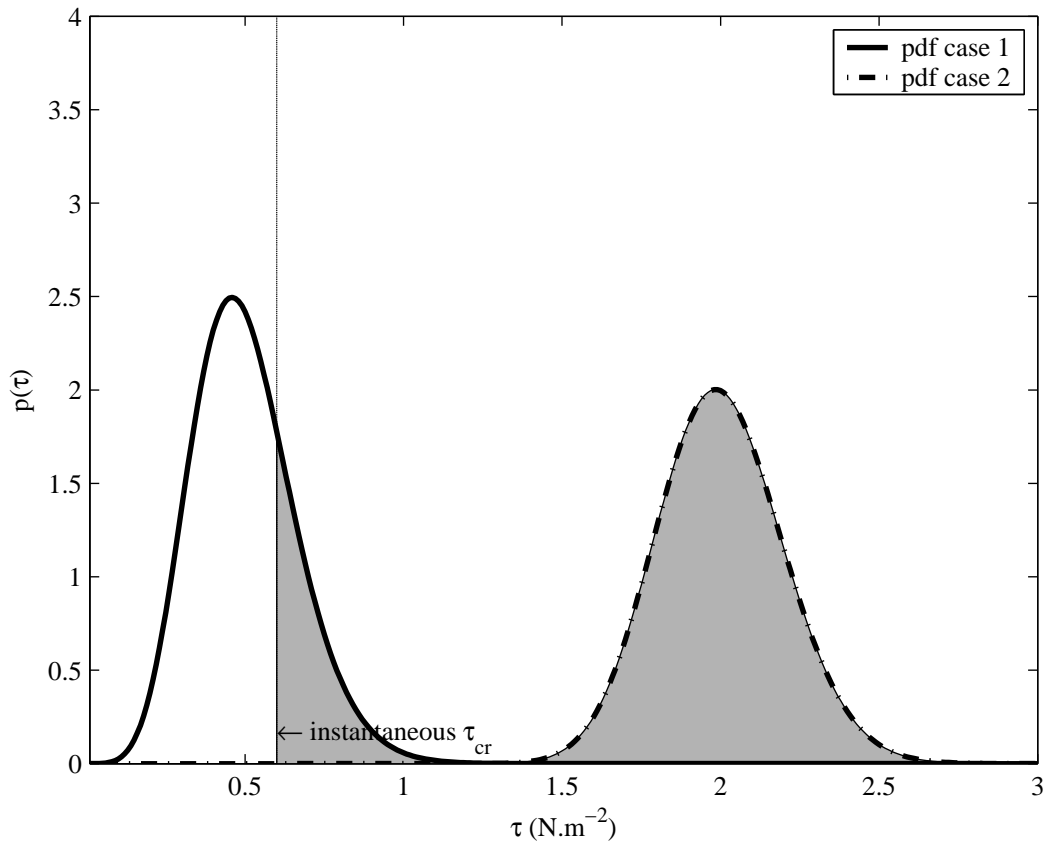
Figure 5.25: Probability density functions for two imaginary cases compared with the critical bed shear stress for initiation of motion.

Probability density function for bed shear stress

For the probability density function (pdf) of the instantaneous bed shear stress, a normal distribution is often assumed (De Ruiter, 1982; Van Rijn, 1993), although early measurements showed a clear deviation from the normal distribution (Grass, 1970). The normal distribution for bed shear stress is given by:

$$p_{norm}(\tau) = \frac{1}{\sigma_\tau \sqrt{2\pi}} \, e^{\frac{-(\tau - \tau_{avg})^2}{2\sigma_\tau^2}} \tag{5.27}$$

where τ is the instantaneous bed shear stress, τ_{avg} is the time-averaged bed shear stress and σ_τ is the standard deviation of the instantaneous bed shear stress.

Recently, Papanicolaou *et al.* (2002) have proposed to apply a noncentral χ^2-distribution for the bed shear stress. The noncentral χ^2-distribution is the distribution that results when one or more normally distributed variables with non-zero means and identical variance are squared and, when possible, summed. The underlying assumption to choose this distribution is that bed shear stress is proportional to the near-bed velocity squared, as in:

$$\tau_b = \alpha u_b{}^2 \tag{5.28}$$

where α is a scaling factor. Since the pdf of velocity resembles a normal distribution with non-zero mean in a fully random turbulent flow (Tamburrino & Sandoval, 1998), the pdf of bed shear stress is likely to resemble a noncentral χ^2-distribution with one degree of freedom. Zaman (2004) studied the instantaneous velocity fields for the horizontal velocity, u, and the vertical velocity, w, observed in the flume experiment described in this thesis, and found that there is a clear structuring of turbulence in the vegetated layer. The flow is, therefore, not random and this lead to the hypothesis that the w-component of flow has an effect on the bed shear stress in vegetated flows, but this can not be elaborated without further data.

The noncentral χ^2-distribution has originally been obtained by Fisher (1928), who gives a number of equivalent expressions for the pdf, as functions of the noncentrality parameter, s, and the number of degrees of freedom, n. The noncentrality parameter is defined by:

$$s^2 = \sum_{i=1}^{n} m_i^2 \tag{5.29}$$

where m_i are the means of n gaussian random variables. The mean and variance of the χ^2-distribution are given by:

$$\mu_\chi = n\sigma_r^2 + s^2 \tag{5.30}$$

$$\sigma_\chi^2 = 2n\sigma_r^4 + 4n\sigma_r^2 s^2 \tag{5.31}$$

where σ_r is the standard deviation of the gaussian random variables.

A relatively simple expression for a noncentral χ^2-distribution with one degree of freedom ($n=1$) is given by Proakis (1989). In a slightly modified form this becomes:

$$p_\chi(\tau) = \frac{1}{\sqrt{2\pi\alpha\tau}\,\sigma_b} e^{-(\tau/\alpha + \mu_b^2)/2\sigma_b^2} \cosh\left(\frac{\sqrt{\tau/\alpha}\,\mu_b}{\sigma_b^2}\right) \quad \text{for } \tau > 0 \tag{5.32}$$

where τ is the instantaneous bed shear stress, σ_b is the standard deviation of the near-bed velocity, μ_b is the average near-bed velocity and α is:

$$\alpha = \frac{\tau_{avg}}{\sigma_b^2 + \mu_b^2} \tag{5.33}$$

For this distribution the mean and variance then become:

$$\mu_\tau = \alpha\left(\sigma_b^2 + \mu_b^2\right) \tag{5.34}$$

$$\sigma_\tau^2 = \alpha\left(2\sigma_b^4 + 4\sigma_b^2\mu_b^2\right) \tag{5.35}$$

A notable disadvantage of the noncentral χ^2-distribution is that it is derived for u^2, whereas in fact the bed shear stress is dependent on the near-bed velocity as in:

$$\tau_b = \alpha\,|u_b|\,u_b \tag{5.36}$$

Therefore, Hofland (submitted) has derived a probability density function for $|u|\,u$:

$$p_{Hof}(\tau) = \begin{cases} \frac{1}{2\sqrt{2\pi\alpha\tau}}e^{-\frac{1}{2}(\sqrt{\tau/\alpha}-\delta)^2} & \text{for } \tau > 0 \\ \frac{1}{2\sqrt{-2\pi\alpha\tau}}e^{-\frac{1}{2}(\sqrt{-\tau/\alpha}+\delta)^2} & \text{for } \tau < 0 \end{cases} \tag{5.37}$$

where

$$\delta = \mu_b/\sigma_b \tag{5.38}$$

equal to the inverse of the (near-bed) turbulence intensity in Fig. 5.24.

Characteristic time scale for entrainment of a particle

The time scale T in the sediment pick-up rate formula is usually assumed to be proportional to D/w (Einstein, 1950), or D/u_* (Paintal, 1971; Yalin, 1977), where w is the fall velocity of a particle and u_* the shear velocity. However, De Ruiter (1982) considers the characteristic time scale equal to the time period during which a particle is moved from its initial position over a distance of half its diameter (in a uniformly accelerated motion). The time scale follows from the analysis of lift and drag forces on a particle and results in (Van Rijn, 1983):

$$T(\tau) = \left[\left(\frac{\rho_s}{\rho_s - \rho}\right)\left(\frac{\tau_c^o}{\tau - \tau_c}\right)\left(\frac{D}{g\tan\phi}\right)\right]^{0.5} \tag{5.39}$$

where ρ_s is the density of the sediment, ρ is the density of the fluid, τ_c^o is the critical instantaneous bed shear stress at a horizontal bed, τ_c is the critical instantaneous bed shear stress at an arbitrary sloped bed, and ϕ is the angle of repose of a particle. Since the flume bed was horizontal, it is assumed here that $\tau_c^o = \tau_c$. The angle of repose can be estimated from the lee slope of a natural bedform, which was determined in the flume experiment at about 40 degrees.

Stochastic sediment pick-up rate

It is assumed that the characteristic time scale T is much smaller than the average time period during which the instantaneous bed shear stresses exceed the critical shear stress in a typical turbulent bursting event (De Ruiter, 1982). Therefore, the probability of a particle being entrained from the bed per unit time, P_c/T, can be expressed as the integral over all instantaneous bed shear stress values larger than the critical bed shear stress, τ_c, divided by the time scale T. Together with Eq. (5.26) the complete expression for the pick-up rate of sediment can now be defined by:

$$E = \frac{2}{3}\eta\rho_s D \int_{\tau_c}^{\infty} \frac{p(\tau)}{T(\tau)} \, \mathrm{d}\tau \tag{5.40}$$

where $p(\tau)$ is a probability density function (pdf) for the bed shear stress. Applying the
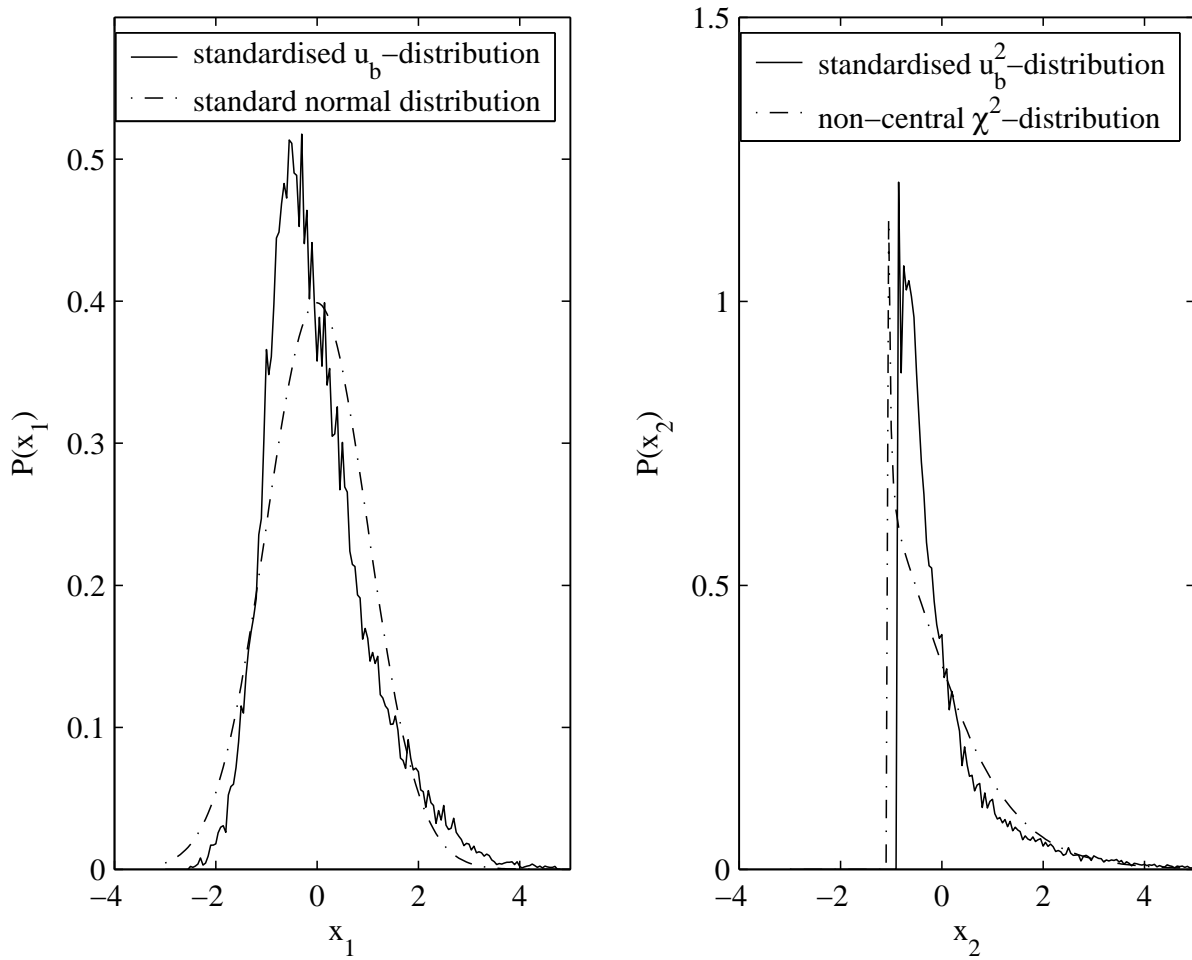
Figure 5.26: Probability density functions for the near-bed instantaneous velocity in Test 2. Left panel: Standardised instantaneous velocity compared with the standard normal distribution. Right panel: standardised squared velocity compared with the χ^2-distribution.

pdf of the noncentral χ^2-distribution, Eq. (5.32), yields for the pick-up rate:

$$E_{chi} = \frac{2}{3}\eta\rho_s D \int_{\tau_c}^{\infty} \frac{1}{T(\tau)} \frac{1}{\sqrt{2\pi\alpha\tau}\,\sigma_b} e^{-(\tau/\alpha+\mu_b^2)/2\sigma_b^2} \cosh\left(\frac{\sqrt{\tau/\alpha}\,\mu_b}{\sigma_b^2}\right) \; \mathrm{d}\tau \quad \text{for } \tau > 0 \quad (5.41)$$

Applying the pdf of the Hofland-distribution, Eq. (5.37), where the negative side ($\tau < 0$) is mirrored to the positive side, and where the pdf is normalised by dividing τ by σ^2, yields for the pick-up rate:

$$E_{Hof} = \frac{2}{3}\eta\rho_s D \int_{\tau_c}^{\infty} \frac{1}{T(\tau)} \frac{1}{2\sqrt{2\pi\alpha\tau}\sigma_b} \left(e^{-\frac{1}{2}(\sqrt{\tau/(\sigma_b\alpha)}-\delta)^2} + e^{-\frac{1}{2}(\sqrt{\tau/(\sigma_b\alpha)}+\delta)^2}\right) \; \mathrm{d}\tau \quad \text{for } \tau > 0$$
$$(5.42)$$

This expression is equivalent to the one derived from the noncentral χ^2-distribution.

Applying the pdf of a normal distribution, Eq. (5.27), yields for the pick-up rate:

$$E_{nor} = \frac{2}{3}\eta\rho_s D \int_{\tau_c}^{\infty} \frac{1}{T(\tau)} \frac{1}{\sigma_\tau\sqrt{2\pi}} e^{-(\tau-\tau_c)^2/2\sigma_\tau^2} \; \mathrm{d}\tau \quad \text{for } \tau > 0 \quad (5.43)$$
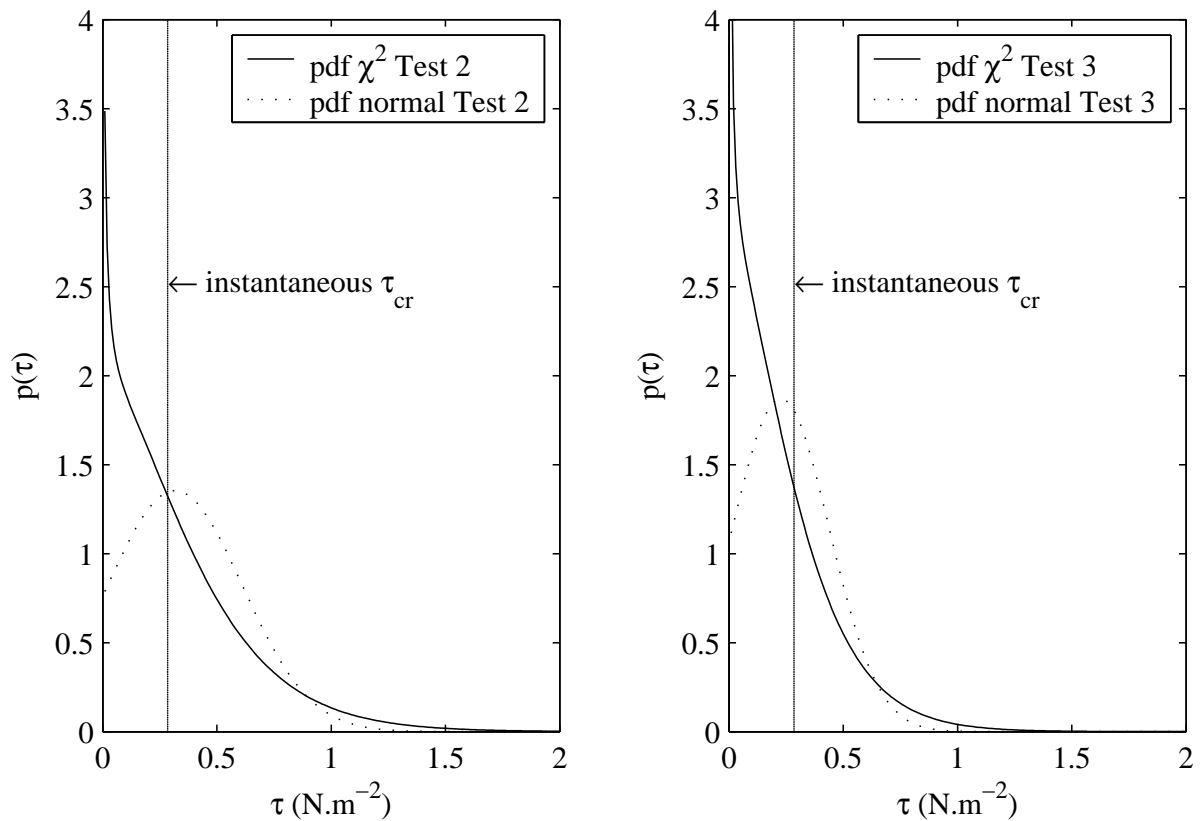
Figure 5.27: Probability density functions for Test 2 (left panel) and Test 3 (right panel).

Results

Figure 5.26 shows probability density functions of the measured instantaneous flow ve-
locity in Test 2, at location M5, closest to the bed, which is at 4.6 cm above the bed.
The left panel shows the standardised distribution of the flow velocity, $x_1 = (u_b - \mu_b)/\sigma_b$,
compared with the standard normal distribution. The right panel shows the standardised
distribution of the squared flow velocity, $x_2 = (u_b^2 - \mu_b^2)/\sigma_b^2$, compared with the non-
central χ^2-distribution. The measured flow velocity distribution does not fully resemble a
standard normal distribution. This is probably due to the non isotropic character of the
turbulence inside vegetation, as was shown by Zaman (2004) for the flume experiment
described in this thesis. Likewise, the squared velocity distribution does not fully resem-
ble the theoretical χ^2-distribution, but, for argument's sake, further analysis is applied to
the theoretical distribution. The rather odd shape of the χ^2-distribution stems from the
atypical high turbulence intensity. In open channel flow, the turbulence intensity is much
lower, yielding a χ^2-distribution with a bell-like shape, similar to the normal distribution,
however, with a longer right tail. Note, that the imaginary distributions shown in Fig.
5.25 are χ^2-distributions as well, but with a lower turbulence intensity. Consequently, for
flow through vegetation, it is important to apply the proper pdf for the bed shear stress,
which is the χ^2-distribution, instead of the commonly applied normal distribution.

Figure 5.27 shows the probability density functions for the instantaneous bed shear stress, based on the χ^2-distribution, Eq. (5.32) for Test 2 and 3 of this flume experiment. For comparison, the commonly applied normal distribution, Eq. (5.27), is shown, as well. The input values for the parameters in these equations stem from the near-bed measurements of instantaneous flow, see Table 5.13. An exception is the value for the normal standard deviation of the bed shear stress, this is taken equal to the resulting standard deviation of the χ^2-distribution.

Table 5.13: Input data for the pdf's of bed shear stress.

Parameter	Test 2	Test 3
τ_{avg}	0.317	0.227
σ_b	0.100	0.082
μ_b	0.175	0.141
σ_τ	0.295	0.213

The instantaneous critical bed shear stress depicted in Fig. 5.27 is calculated as 1.5 times the time-averaged Shields' critical bed shear stress, in accordance with measurements by Grass (1970) and Yalin and Karahan (1979). Although the instantaneous critical bed shear stress is a stochastic variable, as well, it is considered here to be not stochastic.

Analysis of the turbulence intensity measurements in the flume experiment shows that, relatively close to the bed, the turbulence intensity, σ_b/μ_b has increased from about 0.15 for a bare bed, to about 0.57 for a vegetated bed, see Fig. 5.24. This means that the sediment pick-up is increased compared with non-vegetated conditions. Finally, Table 5.14 shows the comparison of sediment pick-up rates for Test 2 and Test 3, applying the stochastic pick-up formula based on the χ^2-distribution, Eq. (5.41). A comparison is made for values for the turbulence intensity, $1/\delta$, defined as σ_b/μ_b, for bare bed conditions and for vegetated conditions.

Table 5.14: Theoretical sediment pick-up rate E in kg·m^{-2}·s^{-1}.

Test	$1/\delta$	Pick-up rate
	(-)	(kg·m^{-2}·s^{-1})
Test 2	0.57	0.703
	0.15	0.556
Test 3	0.58	0.409
	0.15	0.115

The sediment pick-up rates for Test 2 and Test 3 show 26% and 256% higher pick-up rates, respectively, for the vegetated bed compared with a bare bed. In conclusion, the increased turbulence intensity inside the vegetation leads to an enhanced pick-up rate.

This can be an additional sediment transport mechanism if two conditions are met. First, the time-averaged bed shear stress is low, i.e., near the threshold of motion, and second, the vegetation height is low, so the increased shear turbulence can reach down to the bed.

5.9   Conclusions and discussion

The effects of vegetation on sediment transport are twofold:

1.   A reduction of the time-averaged bed shear stress, due to reduced time-averaged near-bed velocities and fluid stresses;

2.   An increase of the sediment pick-rate, due to an increased near-bed turbulence intensity.

The primary effect is that of reduction of bed shear stress. Only for short vegetation and near the threshold of motion the increased pick-up rate can become an important additional transport mechanism.

From this flume experiment it is concluded that the reduced bed shear stress on a vegetated bed can be described reasonably well with a numerical 1-DV model or with the analytical expressions, given an accurate description of the vegetation geometry. Subsequently, the sediment transport rate for a vegetated bed can be described reliably by a common sediment transport formula, as long as the bed shear stress reduction is accounted for. However, swaying of flexible vegetation leads to a non-uniform profile of its geometrical properties over the height. In addition, complicated vegetation structures, such as those with leaves, lead to complicated effects on the break-up of turbulence vortices. Therefore, flexible vegetation with a complicated geometry in principle needs a more complex description of the geometry than rigid, vertically homogeneous cylinders, such as applied in the analytical expressions. This flume experiment has shown a reduction of the bed shear stress inside the vegetation by 80%. This reduction percentage cannot be applied to other cases directly, because the reduction is very much dependent on the submerged depth and the vegetation properties. Furthermore, the bed shear stress inside the submerged vegetation was not measured directly, but was derived from model simulations with a numerical 1DV-model. These values could therefore be dependent on model assumptions, boundary conditions and model schematisation.

The sediment transport rate in these experiments has been derived from measurements of erosion under non-uniform flow conditions. This is the case for the vegetated tests as well as for the reference tests. The results are therefore not comparable to formulations for equilibrium conditions with uniform flow. It was, however, found that the reduced bed shear stress in the vegetated tests can be applied reliably in a common sediment transport formula, as long as the time-averaged bed shear stress is well above the threshold

of motion. An additional mechanism found is that increased turbulence levels inside the vegetation are more effectively picking up sediment.

In the experiment described herein, the longitudinal water level profile has been obtained with a capacitance wave height meter, which proved to be a suitable instrument, especially since the water level gradient is relatively steep. The longitudinal bed level profile has been determined with bed profilers. These too give a high level of detail, and proved suitable for this type of experiment. On the other hand, a pathway needed to be cleared inside the vegetation, which may have affected local flow properties.

As a final conclusion, Coleman (1982) is cited: "The understanding of sediment transport principles is at present quite incomplete, and the development of this understanding has been far outstripped by the development of computational capability which allows for the development of many sophisticated mathematical models of situations involving sediment transport. For this reason, modelers should exercise caution that they do not produce computationally elegant models that in fact do not correctly predict sediment transport phenomena."Although this statement was written in 1982, it is still true and may be even more so, since the emphasis has been put on computational techniques rather than experimental situations in the last decades. Consequently, complicated interactions like those investigated in this study need more experimental research.

Chapter 6

Modelling bed shear stress in the Allier, France, a 3-D case study

6.1 Introduction

In the previous chapters, it was concluded that the traditional way to model the bed shear stress for vegetated regions yields erroneous results. Subsequently, two analytical expressions were derived to estimate the bed shear stress on a vegetated bed. The simulation of a flume experiment showed that the sediment transport capacity can be simulated reliably using these expressions, as long as the bed shear stress is well above the threshold of motion.

In this chapter, the analytical expressions for the bed shear stress will be applied to a real-world case study, the Allier, France. The results of a 3-D model for vegetated flow will be compared with the results of a 2-D depth-averaged (2-DH) model including the bed shear stress estimators. The objective of this case study is to demonstrate that the bed shear stress estimators in 2-DH provide similar values for the bed shear stress as the 3-D model. Applying these bed shear stress estimators in 2-DH models enables long-term morphodynamic modelling.

6.2 Study area

The study area is part of the Allier, France. The Allier is a gravel bed, rain-fed river that originates in the Massif Central and joins the Loire River in Nevers, about 400 km downstream of its origin. The study area of about 6 km² in size lies 5 km upstream of the town of Moulins, France (Figure 6.1). It is located in the meandering section of the Allier and it is part of a nature reserve in which most of the river banks are unprotected. The Allier is considered as a landscape reference for the to-be-restored Border Meuse in the Netherlands. The Allier is highly dynamic, large amounts of sand and gravel are transported during floods and its morphology changes considerably from year to year.
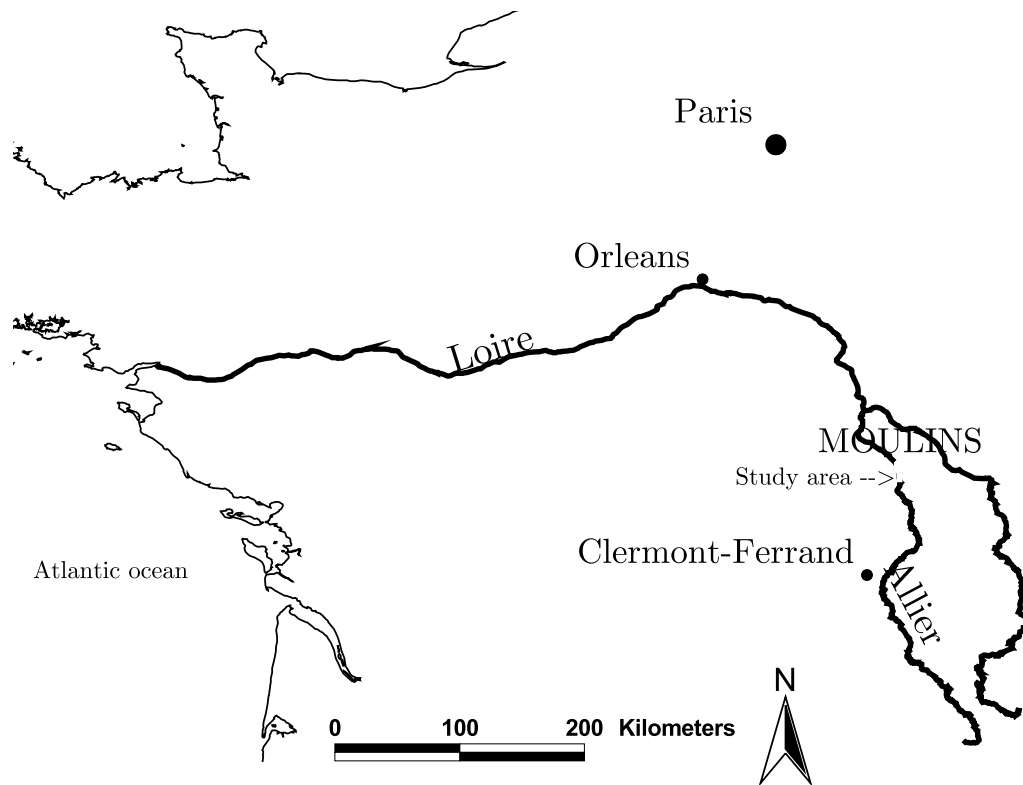
Figure 6.1: Location of the study area along the Allier.

The riparian vegetation is characterised by pioneer species on the low-lying dynamic point-bars, herbaceous vegetation and grass on the higher parts and extensive softwood floodplain forests, mainly consisting of poplars, on the older and higher floodplains. Due to the river dynamics, this river shows natural rejuvenation of vegetation such that older forests are removed by erosion and young pioneer vegetation can start growing on the point-bars. The rejuvenation also leads to the presence of large woody debris, mainly trees, into the river.

6.3   Material and methods

6.3.1 Terrain data and vegetation

Two field campaigns were carried out in 2002 and 2003 to collect data on the terrain topography and the vegetation distribution. These campaigns were organised jointly by Delft University of Technology, Faculty of Civil Engineering and Geosciences, WL | Delft Hydraulics, Utrecht University, Department of Physical Geography, Radboud University, Department of Environmental Studies and Meander Consultancy and Research, under the heading of the Netherlands Centre for River Studies.

Figure 6.2: Oblique aerial photograph of the study area. Flow is from top to bottom. Photograph by G.W. Geerling.

A Real-Time Kinematic Differential Global Positioning System (RTK-DGPS) was applied to obtain terrain coordinates in x, y and z direction with an accuracy of about 5 cm in each direction. Approximately 3000 elevation points have been collected in each field campaign in order to map the floodplain heights. The morphology of the river bed was obtained by levelling river cross-sections. Interpolation of the elevation data on a 10 x 10 m rectangular grid resulted in a Digital Elevation Model of the study area (Van den Bosch, 2003). Figure 6.2 shows an oblique aerial photograph of the study area in which the upper and lower borders of the photograph correspond to the upstream and downstream model boundaries, respectively. Figure 6.3 presents the bed topography of the study area overlaid on an aerial photograph of the surrounding area.

Vegetation structures were identified and mapped in the field to obtain a ground truth for the analysis of stereoscopic aerial photos taken in the year 2000. The vegetation in the area was classified based on the main vegetation types present, Fig. 6.4. For forests and shrubs an additional qualification was made with respect to their horizontal distribution (open or closed cover). A closed cover is defined as more than 60% cover, and an open cover is defined as between 20% and 60 % cover (Breedveld & Liefhebber, 2003). At less than 20% cover of shrubs or trees, the vegetation type is based on the dominant vegetation, usually grassland. In 2003, vegetation characteristics height, diameter and density were obtained for floodplain forest and shrub (Wijma, 2005). For floodplain forests consisting of poplar (*Populus nigra*) and willow (*Salix alba*), with an average age of approximately 10 years,

Table 6.1: Vegetation types in the Allier study area and their physical properties height, k, diameter, D, density, m and Nikuradse equivalent roughness height, k_N at 2 m water depth.

Vegetation type	k (m)	D (m)	m (m^{-2})	k_N (m)
Production forest	10	0.042	2	6.5
Closed floodplain forest	10	0.042	1.2	4.6
Open floodplain forest	10	0.042	0.4	1.8
Closed floodplain shrub	5	0.01	10.2	7.3
Open floodplain shrub	5	0.01	3.4	3.4
Herbaceous vegetation	0.50	0.005	400	2.3
Floodplain grassland	0.20	0.003	3000	1.1
Production grassland	0.10	0.003	4000	0.8
Pioneer vegetation	0.10	0.003	50	0.15

a mean stem diameter of 0.042 m and a mean density of 2 stems m^{-2} was measured inside the forest. For three forest types, the diameter of 0.042 m was applied and the density varied over 100% cover, 60 % cover and 20% cover, see Table 6.1. Floodplain shrubs, with an average age of 2 years, had a mean stem diameter of 0.01 m and a mean density of 17 m^{-2}. Estimates of vegetation properties of grassland, herbaceous vegetation and pioneer vegetation have been obtained from measurements in Dutch floodplains (Van Velzen *et al.*, 2003a; Van Velzen *et al.*, 2003b). Table 6.1 presents the vegetation types that were distinguished in the study area, and their properties height, k, diameter, D and density, m. The drag coefficient, C_D is assumed equal to 1.

The use of a traditional 2-DH model requires estimates for the bed roughness yielding the total flow resistance of vegetation and sediment. In this study, the Nikuradse equivalent roughness height was determined for each vegetation type by applying the 1-DV model described in Appendix B. The Chézy bed roughness was defined at 50 m$^{1/2}$·s^{-1} and the applied water depth was 2 m, which is the average depth for the lower floodplain parts in the study area during a typical 1:5 year flood event of around 800 m^3/s. The Nikuradse roughness heights thus obtained are presented in Table 6.1 as well.

6.3.2 Model set-up

A schematisation and hydrodynamic model of the study area that was applied and calibrated on a flood event in May 2001 (Kapinga, 2003; Van den Bosch, 2003) is used for further investigations into the bed shear stress distribution. Four different model cases have been investigated and the results for the bed shear stress have been compared:

1.   *3-D model*: a 3-D model that includes vegetation resistance as vertical cylinders, which computes the vertical profile of the shear stress;

Figure 6.3: Bed topography and model domain of the study area. Flow is from south to north. Height relative to sea level (m).

2. *2-DH model with Nikuradse*: a 2-DH model that includes vegetation resistance via the Nikuradse equivalent roughness height introduced in the White-Colebrook formula, and subsequently calculates the bed shear stress based on the equivalent Chézy values;

3. *2-DH model with Reduction factor*: a 2-DH model that calculates the vegetation resistance and subsequently the bed shear stress based on the *Reduction factor approach*;

4. *2-DH model with Analytical approach*: a 2-DH model that calculates the vegetation resistance and subsequently the bed shear stress based on the *Analytical approach*.

For all four cases, the bankfull discharge of 858 m^3/s of a flood that occurred in May 2001 is chosen as a steady discharge condition. In this study we are interested in the distribution of bed shear stress for a high water level, so that the vegetated parts of the river are flooded. This justifies the choice of a steady discharge. The model boundary conditions consist of a discharge boundary upstream and a water level boundary downstream. The
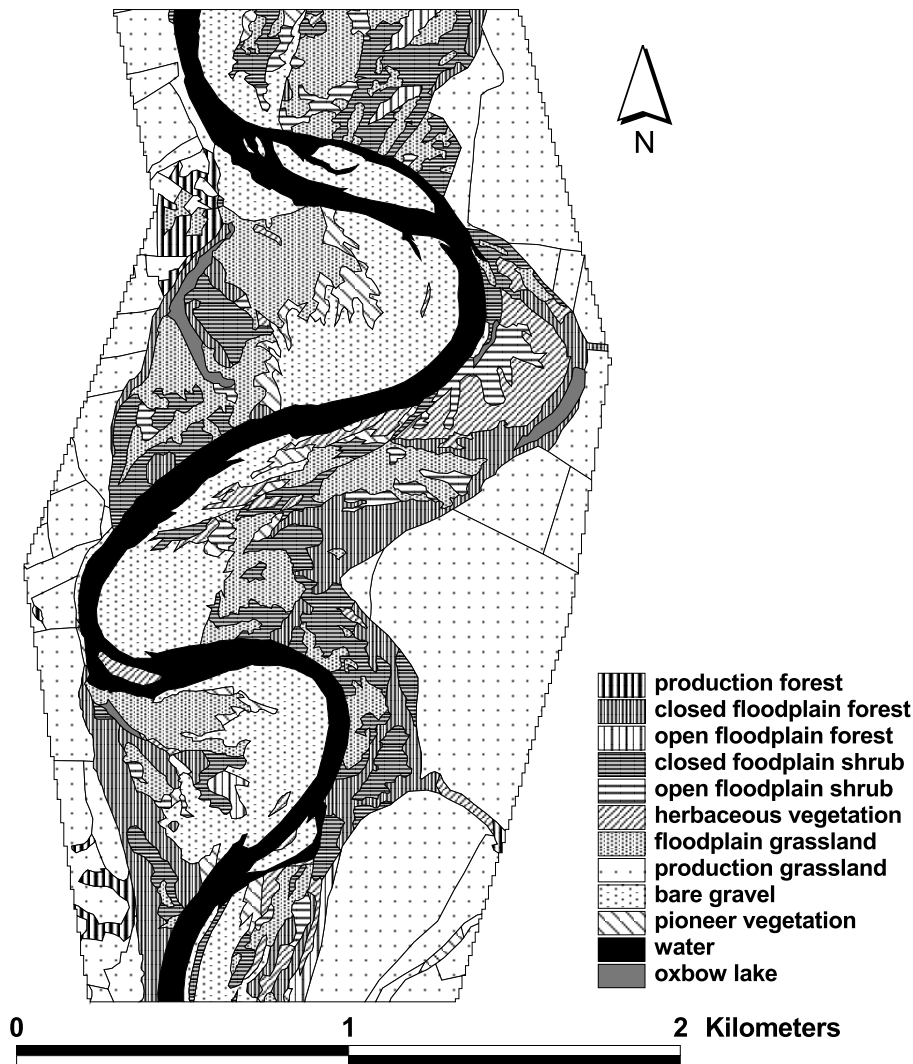
Figure 6.4: Vegetation types in the Allier study area.

model outcome for water levels were validated by comparing the simulated water levels with observed water levels during the May 2001 event. The latter were obtained in an indirect way: photographs were taken during a site visit, showing a waterline that was referred to the digital terrain data. For comparability, the 3-D model, as well as the 2-DH models, were applied with the same model boundary conditions for upstream discharge and downstream water level.

3-D model

The 3-D hydrodynamic model solves the Reynolds equations in three dimensions, under the assumptions that the vertical accelerations are small compared to the gravitational acceleration (the shallow water approximation) and the density variations are small with respect to the water density itself (Boussinesq approximation). The model is a research version of the software package Delft3D, which has been developed by WL | Delft Hy-

draulics. The difference with the standard version is the inclusion of the effect of vegetation on the flow. This is based on the same equations as defined for the 1-DV model, and is described in Appendix C.

In this application, the 3-D model is defined with 20 layers over the vertical. The thickness of each layer is unevenly distributed; the two lowest layers, near the bed, are 2.5% of the water depth to compute the bed shear stress more accurately, the top layer is 10% of the water depth and the remaining layers are 5% of the water depth. The bed resistance is represented with a constant Chézy value of 50 $\mathrm{m}^{1/2}\cdot\mathrm{s}^{-1}$. The vegetation resistance is determined by the cylinder properties of the vegetation and their corresponding drag force. In the 3-D model, the bed shear stress is computed by:

$$\tau_b = \rho u_*^2 \tag{6.1}$$

where u_* is the shear velocity (m/s). For turbulent flow over a rough bed, u_* is determined by the flow velocity in the near-bed computational layer, u_b (m/s), under the assumption of a logarithmic boundary layer (Uittenbogaard et al., 2000):

$$u_* = \frac{\kappa\, u_b}{\ln\left(\frac{\frac{1}{2}z_b + 9z_0}{z_0}\right)} \tag{6.2}$$

where z_b is the thickness of the near-bed computational layer (m) and z_0 is the roughness height of the bed (m).

2-DH models

The 2-DH models are applications of Delft3D in depth-averaged mode, and do not have special formulations for vegetation resistance. The depth-averaged mode includes secondary currents in analytical form, based on De Vriend (1981). The three 2-DH models were applied with equal settings for all model parameters, with the exception of the bed roughness description. In the Delft3D model, the bed roughness can be defined for each computational cell in a separate roughness file. A choice can be made between Manning values, Chézy values or the White-Colebrook formula. For the latter choice, bed roughness values must be given in terms of Nikuradse equivalent roughness heights, which are subsequently used in the White-Colebrook formula to calculate Chézy values. The three 2-DH model applications differ in the roughness values used and the method to compute the bed shear stress.

In the *2-DH model with Nikuradse*, the traditional approach was used in which the Chézy bed roughness is defined by Nikuradse roughness values. For the vegetated parts, the values shown in Table 6.1 were applied. For the bare, gravel parts a roughness height of 0.05 m was taken, which corresponds to Chézy values of 48 to 54 $\mathrm{m}^{1/2}\cdot\mathrm{s}^{-1}$ at water depths

of 2 to 4 metres. The bed shear stress was computed by:

$$\tau_b = \rho g \frac{\overline{u}^2}{C_b^2} \tag{6.3}$$

where ρ is the density of water (kg·m^{-3}), g is the gravitational acceleration (m·s^{-2}), $\overline{u}$ is the depth-averaged flow velocity (m/s) and C_b is the Chézy value for the bed roughness (m$^{1/2}$·s^{-1}).

In the *2-DH model with Reduction factor approach*, representative Chézy roughness values were calculated on the basis of the vegetation properties given in Table 6.1. The representative Chézy roughness for non-submerged conditions is computed with:

$$C_{r,nonsub} = \sqrt{\frac{1}{C_b^{-2} + \frac{1}{2g}C_D mDh}} \quad \text{for } h \leq k \tag{6.4}$$

where h is the water depth (m). For submerged conditions, the representative roughness is computed with alternative formula for representative roughness Eq. (4.155), which proved to be valid for bulk conditions of water depths and vegetation properties:

$$C_r = \sqrt{\frac{1}{C_b^{-2} + \frac{1}{2g}C_D mDk}} + \frac{\sqrt{g}}{\kappa} \ln \frac{h}{k} \tag{6.5}$$

An iterative procedure is required in which an initial run was made with equivalent Nikuradse roughness values, yielding initial water depths. Next, representative Chézy values for vegetation were computed at these water depths and defined for each computational cell of the numerical model. The adjusted roughness values were applied in a next run, leading to adjusted water depths. This procedure was iterated until the water depth and corresponding representative Chézy values no longer changed. The bare, gravel parts of the model area were assigned a Chézy value of 50 m$^{1/2}$·s^{-1}. Finally, the bed shear stress was computed based on the *Reduction factor approach* for the vegetated parts, Eq. (4.27):

$$\tau_{bv} = \frac{1}{1 + \frac{C_D mDk C_b^2}{2g}} \frac{\rho g}{C_r^2} \overline{u}^2 \tag{6.6}$$

For the bare and non-submerged vegetated parts, the bed shear stress in the *Reduction factor approach* is determined by Eq. (4.37):

$$\tau_{bv,nonsub} = \frac{\rho g}{C_b^2} \overline{u}^2 \tag{6.7}$$

In the *2-DH model with Analytical approach*, representative Chézy roughness values were calculated in a similar, iterative procedure, but now based on the *Analytical approach* described in section 4.5. However, the representative Chézy roughness for non-submerged

and submerged conditions is calculated in the same way as in the *2-DH model with Reduction factor approach*, to exclude differences in model outcome due to different roughness methods.

The bed shear stress was computed with the *Analytical approach* for the vegetated parts described in section 4.5.3:

$$\tau_b = \frac{\rho \, c_p \, \ell}{2L} \left[\frac{B - u_{s0}^2 \frac{A}{1-A} \exp\left(-\frac{k}{L}\right)}{\exp\left(\frac{k}{L}\right) - \frac{1-A}{1+A} \exp\left(-\frac{k}{L}\right)} - \frac{B - u_{s0}^2 \frac{A}{1-A} \exp\left(\frac{k}{L}\right)}{\frac{1+A}{1-A} \exp\left(\frac{k}{L}\right) - \exp\left(-\frac{k}{L}\right)} \right] \tag{6.8}$$

in which:

$$A = \frac{2L \, \kappa^2}{\ln^2(9) \, c_{pbed} \, \ell} \tag{6.9}$$

and:

$$B = \frac{2L \, g \, (h - k) \, i}{c_{pbed} \, \ell} \tag{6.10}$$

And furthermore:

$$L = \sqrt{\frac{c_{pbed} \, \ell}{C_D \, m \, D}} \tag{6.11}$$

$$u_{s0} = \sqrt{\frac{2 \, g \, i}{C_D \, m \, D}} \tag{6.12}$$

And as a closure coefficient:

$$c_{pbed} = \frac{h}{k} \frac{g}{C_b^2} \tag{6.13}$$

The energy gradient i (-) follows from the representative roughness C_r:

$$i = \frac{\overline{u}^2}{h C_r^2} \tag{6.14}$$

The bed shear stress on the bare parts was computed with Eq. (4.37).

6.4   Results

The results of the flow computations for the four model cases are almost equal with respect to the water depths and depth-averaged flow velocities. The results show significant differences in bed shear stress distribution, see Figs. 6.5 and 6.6. In the 2-DH model with Nikuradse, the bed shear stress increases along with the bed roughness and therefore shows very high values at locations where vegetation is flooded. In the 3-D case, the bed shear stress is considerably less in the vegetated parts. The latter is also the case for both approximations in which the bed shear stress is calculated with the *Reduction factor approach* and with the *Analytical approach*.

Evidence in favour of the 3-D approach and both approximations in 2-DH is circumstantial. A direct measuring of the bed shear stress on a vegetated bed in field situations is
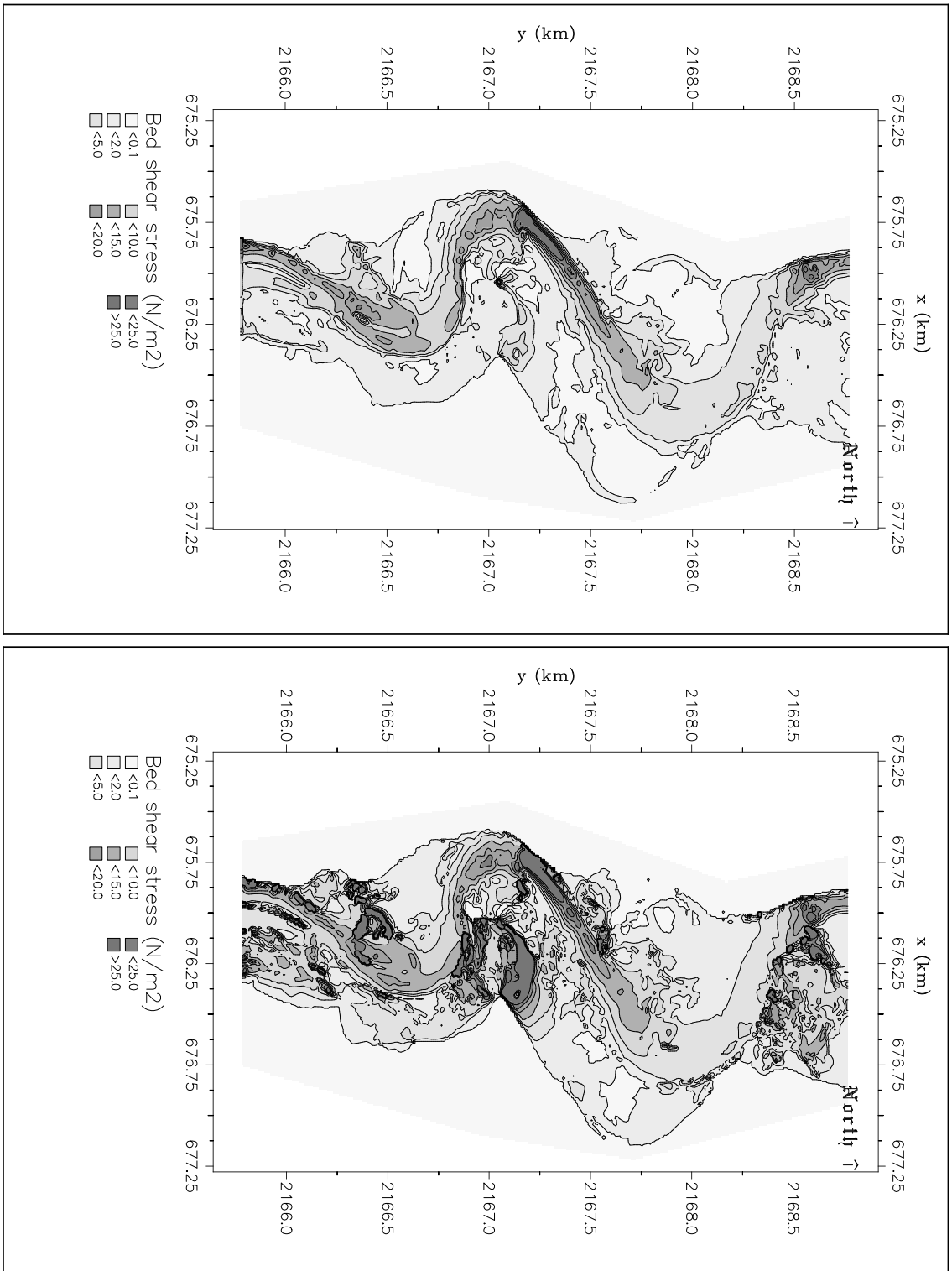
Figure 6.5: Bed shear stress distribution for two model cases. Left panel: 3-D model. Right panel: *2-DH model with Nikuradse.* Flow is from south to north. Coordinates in French system Lambert 2 étendu.
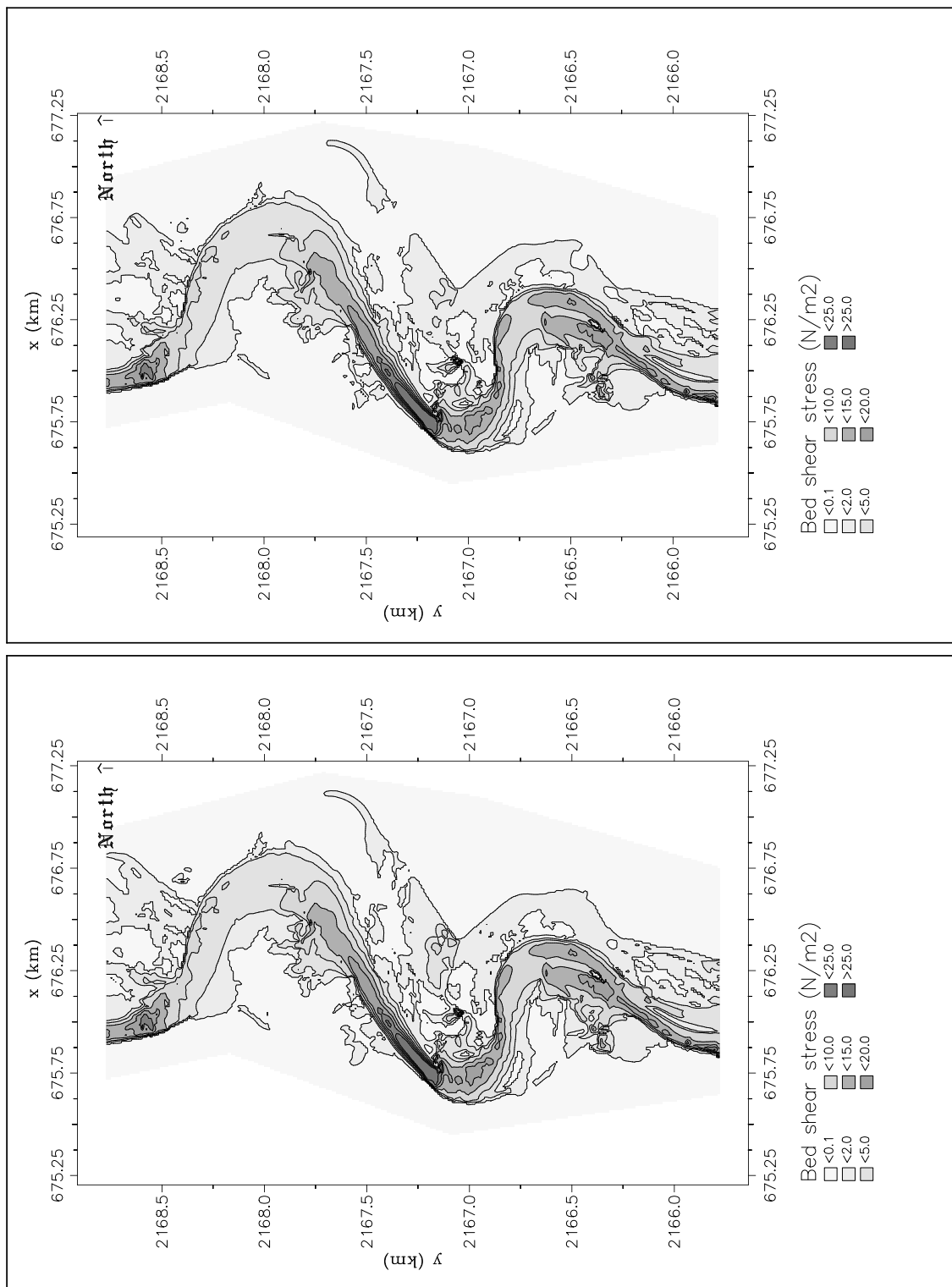
Figure 6.6: Bed shear stress distribution for two model cases. Left panel: *2-DH model with Reduction factor approach*. Right panel: *2-DH model with Analytical approach*. Flow is from south to north. Coordinates in French system Lambert 2 étendu.
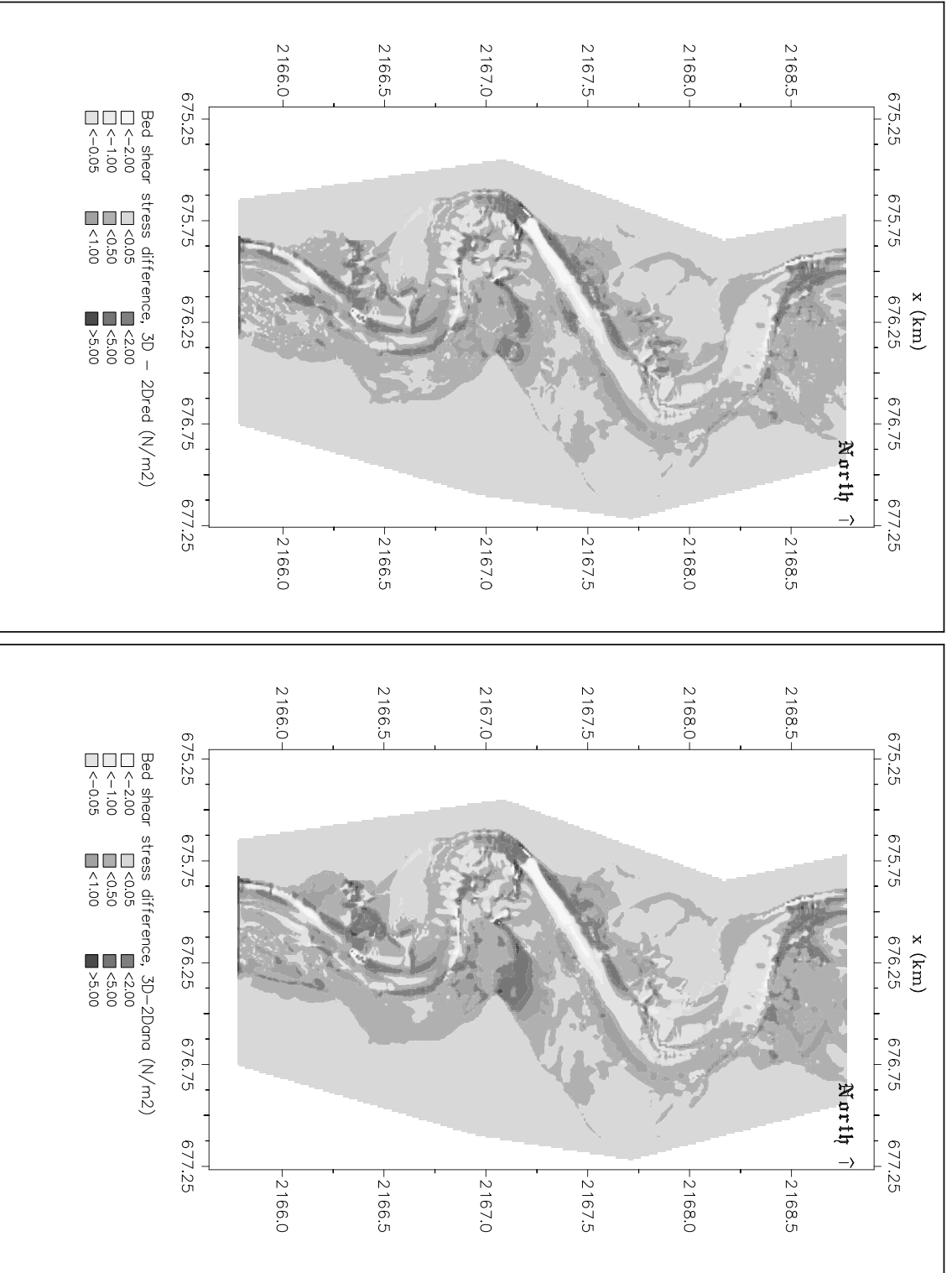
Figure 6.7: Bed shear stress model differences in the Allier study area. Left panel: Results from the *Reduction factor approach* subtracted from 3-D model results. Right panel: Results from the *Analytical approach* subtracted from 3-D model results.

not possible. For a number of locations in the study area, the modelled bed shear stress values from the *2-DH model with Nikuradse* are so high that erosion of the bed must be expected. However, examination of the terrain and vegetation in 2002 does not show any signs of erosion that should have occurred in 2001. For example the area downstream of point (676.25, 2176.0) shows bed shear stress values beyond 50 N·m^{-2} in the 2-DH model application with Nikuradse. In open channel flow with a normal bed roughness (50 m$^{1/2}$·s^{-1}) this would occur at a depth-averaged flow velocity of about 3.5 m/s, whereas the model predicts a plausible 1 m/s; the calculated high bed shear stress stems from the extreme bed roughness. Moreover, such high bed shear stress values would lead to sediment pick-up of particles of up to tens of centimetres diameter. In absence of upstream sediment supply, which is the case at this location, this would lead to severe erosion. Field observations, however, don't show any evidence of erosion. We therefore expect that the bed shear stress distribution is modelled more reliably in the 3-D approach, as well as with the approximations in 2-DH, which resemble the 3-D computational results well.

Figure 6.7 presents a comparison of the results obtained with the *Reduction factor approach* and the *Analytical approach* subtracted from the results of the 3-D model. Both analytical approaches yield similar results. In the vegetated regions, both approaches tend to *underestimate* the bed shear stress, especially for non-submerged vegetation. The magnitude of the differences between the 3-D and the 2-DH computations is generally less than 5 N·m^{-2}, however, the relative difference can be quite large, since in these regions the bed shear stress is relatively small. In some parts of the main channel, both methods *overestimate* the bed shear stress compared with the 3-D model. The magnitude of the differences in the main channel are less than 5 N·m^{-2}, as well, and are due to small differences between the depth-averaged flow velocity in the 2-DH models compared with the near-bed flow velocity in the 3-D model.

6.5   Discussion

This case-study has shown that the analytical approaches for the bed shear stress on a vegetated bed greatly improve model predictions compared with the common approach of modelling an enhanced bed roughness, although there are still significant changes compared with a full 3-D computation. The computational effort, however, is significantly less for the 2-DH computations. In this case, a fairly simple computation was made, in which a steady discharge was modelled over a simulation period of 4 hours. The 3-D computation took over 20 hours of computational time, whereas the 2-DH computations took only half an hour. In view of larger simulation periods, for example to model morphodynamic changes during a flood wave over a time period of several days, the 2-DH model approach is more feasible. As a next step of research it is foreseen to validate the model of the Allier

with measurements of morphological changes resulting from a river flood. This activity includes the modelling of bed load transport during a flood, dependent on the reduced bed shear stress on the vegetated parts, and subsequently modelling the morphodynamic changes. This should demonstrate that the reduced bed shear stress is a prerequisite in modelling the morphodynamics correctly.

Similar 3-D models for vegetation resistance as used in this case-study have been developed by others, as well. Stoesser *et al.* (2003) applied a 3-D model for vegetation resistance on the Restrhein. In their model, effects of vegetation on the turbulence closure scheme were neglected, in order to avoid calibration of the turbulence closure coefficients. Nicholas and McLelland (2004) applied a 3-D numerical model for natural river floodplains. They did not add any further source terms to the k-ϵ turbulence equations, because it was not clear that such modifications would improve the simulation results. Contrary to the 3-D models of Stoesser *et al.* (2003) and Nicholas and McLelland (2004), in our 3-D model the effects of vegetation are introduced in the k-ϵ turbulence closure scheme. Uittenbogaard (2003) has shown that this gives a good fit to laboratory measurements of mean flow, eddy viscosity, Reynolds stress and turbulence intensity. Besides the drag coefficient, the next most important calibration parameter in our 3-D model, at least with regard to turbulence, is the c_ℓ parameter that determines the characteristic eddy size inside the vegetation layer. The model coefficients of the k-ϵ equations did not need any further calibration.

6.6   Conclusions

It can be concluded that the relatively simple formulations of the *Reduction factor approach* greatly improve model predictions for the bed shear stress on a vegetated bed compared with the common bed roughness approach, the *2-DH model with Nikuradse*. Clearly, a proper 2-DH approximation method for the bed shear stress description is an important prerequisite for modelling the effects of vegetation on the bed shear stress and subsequently the transport of sediment and the changes in morphology with 2-DH models.

Chapter 7

General discussion and recommendations

This thesis addresses the biogeomorphological processes in river floodplains from various viewpoints. The major theme is to investigate and apply the modelling of sediment transport and morphodynamics affected by floodplain vegetation. It started with a 1-DH model application of a river section, applying a river management concept, "Cyclic Floodplain Rejuvenation". It then went to more detailed 2-DH morphodynamic modelling of a floodplain with secondary channels. From here on, the need for an improved analytical description of the bed shear stress on a vegetated bed led to an elaboration of the mechanics of flow through and over vegetation and resulted in different analytical expressions. Subsequently, a flume experiment on sediment transport over a vegetated bed was carried out and analysed. Finally, in a case-study of a highly dynamic, meandering river with large vegetated floodplains, the bed shear stress distribution affected by vegetation was modelled.

First and foremost, this thesis has shown that modelling the effects of vegetation on flow and sediment transport is not straightforward. Discussions and recommendations on each chapter of this thesis are given in the next sections.

7.1 Cyclic Floodplain Rejuvenation

The study on Cyclic Floodplain Rejuvenation described in this thesis was the first to quantify this management strategy. The results of this study are promising, but there are still many questions and uncertainties. In the forthcoming years, more aspects of CFR will be investigated in pilot-studies in sections of the Rhine and Meuse. In addition, a number of issues need to be addressed.

7.1.1 Monitoring

In this study, mathematical models have been applied to predict vegetation composition and morphology following hydraulic measures in the river floodplains. In view of the

current state of knowledge, the model results must be viewed as a guide of direction, not as a prediction of truth. Therefore, it is important to keep track of the natural dynamic river changes, which requires monitoring.

Two main objectives are important to the monitoring strategy. Firstly, it must provide enough information to evaluate the hydraulic effects of the developments in the river landscape. And secondly, when management actions are required, there must be enough information to decide where and how to interfere. Therefore, in addition to information regarding the hydraulic resistance of the floodplains, data are required on the types of ecotope and their ecological status, so as to be able to make sound management choices. The monitoring data should have a spatial component, but in order to see changes over time, it needs a temporal component, as well. To meet these goals, remote sensing techniques seem promising. They are applicable at various levels of scale and give quantitative landscape data, both spatial and temporal (when subsequent images are combined). At present, there is an ongoing research program investigating the applicability of remote sensing techniques for floodplain mapping of ecotopes and hydraulic resistance (Geerling *et al.*, 2001; Asselman *et al.*, 2002; Straatsma *et al.*, 2003). It is recommended to continue research on this topic and make this type of monitoring operational for Cyclic Floodplain Rejuvenation.

7.1.2 Combination of flood protection strategies

In this thesis, flood protection measures were limited to measures applied in floodplains. It was concluded that without further measures implemented in the adjacent land, it is necessary to apply Cyclic Floodplain Rejuvenation in order to warrant flood safety in the long run. Yet, there are also possibilities for nature rehabilitation in combination with flood protection in the riparian zones landwards of the embankments. These measures include the construction of flood relief channels (so-called green rivers), or the designation of detention areas. A combination of measures inside and outside of the river embankments may be the best compromise to warrant flood safety, reduce the required frequency and extent of Cyclic Floodplain Rejuvenation and create a large nature area. These synergetic advantages are worth investigating further.

7.1.3 Socio-economic assessment of Cyclic Floodplain Rejuvenation

Application of CFR measures has both social and economical implications. Firstly, large-scale river measures, such as floodplain lowering, are expensive. Secondly, they need to be repeated every 25 to 35 years in the CFR strategy. A cost-benefit analysis was not part of this study, but is necessary before this strategy will be applied at a large-scale.

The application of the CFR strategy has social implications, as well. After all, every once in a while, the river landscape needs to be rejuvenated. This means for example that

floodplain forests need to be removed and channels need to be re-excavated regularly in floodplains that are in use by recreants and residents of nearby towns. There is a concern that there will be a resistance against bulldozers in the floodplains. Future study should focus on the societal values of floodplain nature and the consequences of river management activities.

7.2   Modelling secondary channel biogeomorphology

The most important recommendation of the study on secondary channel biogeomorphology, viz. to find better formulations for the quantification of the bed shear stress on a vegetated bed in 2-DH numerical models, was already addressed in this thesis. Further recommendations concern improved hindcasting of the actual morphological changes in the Gameren floodplain. Remind that the case-study presented herein aimed at forecasting long-term morphological changes. First of all, the analytical expressions for the bed shear stress can be applied to this case-study. However, the model also needs other improvements. It is recommended to refine the grid locally, for example at the location of the bridge, to apply hydrographs of river discharge instead of steady flow conditions, and to improve the calibration of the sediment transport formula of Engelund and Hansen by the measured morphological changes. Moreover, some model problems remain to be overcome. Many of the observed morphological changes are rather small in size and dependent on local flow conditions, such as local vortices. Furthermore, the sediment of the Gameren floodplain is graded and consists of fine sands and cohesive fractions. The cohesive character of the sediment is reflected in the steep banks of the channels. In addition, the presence of old bricks forms a protection against erosion in some places. The problem of modelling morphodynamics affected by local turbulence, graded sediment, vegetation and cliff erosion needs further research. This cannot be done without data from well-documented field sites. It is therefore recommended to continue monitoring in the Gameren floodplain and build up a valuable set of field data for further validation of morphodynamic models.

7.3   Analytical expressions for the representative roughness and the bed shear stress

To derive analytical expressions for the representative roughness of vegetation and the bed shear stress on a vegetated bed, simplifying assumptions need to be made. In case of the *Reduction factor approach* this leads to a very schematic view of the complex reality. To determine the bed shear stress on a vegetated bed, this approach assumes a uniform flow profile inside the vegetation layer, disregarding penetration of shear turbulence. The

resulting expression for the bed shear stress is simple, and resembles the one found by Raupach (1992). A comparison was made with results from a numerical 1-DV model for flow over and through vegetation developed by Uittenbogaard (2003) and with measurements by Thompson *et al.* (2004). The comparison with model data shows that the *Reduction factor approach* lacks a dependency on water depth for non-submerged vegetation, see Fig. 4.21, and it tends to underestimate the bed shear stress, especially for smooth bed conditions, see Fig. 4.20. The comparison with the observed data showed a reasonable fit, see Fig. 4.22.

The *Analytical approach* yields relatively complex expressions for representative roughness and bed shear stress. Although these expressions can describe the physical processes more accurately, a disadvantage is that it is shown in this thesis that the results are highly dependent on the closure coefficient for the turbulence intensity, either inside the vegetation layer, c_p, or at the bed, c_{pbed}. An expression for c_p is needed to calculate the hydraulic resistance of vegetation. For flume conditions an expression for c_p was found that gives reasonable agreement with measurements, Eq. (4.131). However, this expression fails at a large range of water depths and vegetation characteristics. The expression given by Van Velzen *et al.* (2003a), Eq. (4.123), yields a better fit, but this is still not satisfying. Alternative, simpler expressions for the representative roughness were derived as well, which seem to give good approximations valid for floodplain conditions with a wide variety in water depths and vegetation properties, see Fig. 4.17.

An expression for c_{pbed} was found by comparing the analytical formula for the bed shear stress with the results of the 1-DV numerical model. An expression was derived that seems applicable to a large range of water depths and vegetation properties, Eq. (4.161). It was found that the bed boundary condition in the k-ϵ turbulence model is open to improvement, which may affect the expression found for c_{pbed}. A detailed analysis of 1-DV modelling results for the bed shear stress for a bed covered by reed has shown that the *Analytical approach* is capable of describing the bed shear stress relationship with increasing depth more accurately, especially for non-submerged conditions. A comparison with observations by Thompson *et al.* (2004) has shown the applicability of this approach, as well. However, the expression for c_{pbed} needed to be fitted with a factor 2 for the comparison with the model results for reed and a factor 0.08 for the comparison with observations. This is a rather wide range, limiting the general applicability of this approach.

Although the *Analytical approach* has a physical basis, solving the momentum balance for flow through and over vegetation, it's applicability is limited by the closure coefficients c_p and c_{pbed}. These coefficients stem from the assumption of a mixing length approach for the eddy viscosity inside the vegetation layer, assuming a vegetation height-averaged turbulence intensity c_p, or an estimation of this value at the bed. The application is therefore theoretically limited to relatively tall and dense vegetation. This thesis shows that

no simple, accurate expression for either c_p, or c_{pbed} was found that is applicable to a wide range of water depths and vegetation properties, without freely adjustable parameters. It is recommended to continue detailed investigations of the shear stress partitioning on vegetated beds, for example to improve numerical models. However, since the flow characteristics inside vegetation layers are highly three-dimensional, simple analytical solutions most probably fail to represent the intricate details. In this respect, the *Reduction factor approach* seems a simple, sufficiently accurate and generally applicable technique for real-world applications.

7.4 Recommendations for further experimental study

The experimental study described in this thesis is one of the first of its kind and rather limited in varying conditions. It gives more insight, but it also raises new questions. It is highly recommended to execute further experimental study on the effects of vegetation on sediment transport. Some considerations on the set-up of further experiments are given here.

In the experiment described in this thesis, flexible plastic model plants have been used. Although these may reflect real-world conditions better, they complicate the process descriptions and analysis. It is therefore recommended to take one step back and carry out experiments with rigid cylinders, because that provides a better basis of the model descriptions. As a second step, flexible cylinders can be used and more complicated vegetation geometries can be tested subsequently.

One of the largest problems in determining sediment transport on a vegetated bed is to obtain globally uniform flow and transport conditions. In order to determine the sediment transport capacity, an equilibrium bed slope should be obtained and the sediment input should equal the sediment output. This could not be achieved in the experiment described in this thesis. The experimental set-up for vegetated flow experiments usually requires the vegetation to be fixed on the floor of the flume and leave it partly buried in sediment. When the initial bed slope does not equal the equilibrium slope, the resulting bed level changes will inevitably cause a change in protruded height of the vegetation. This affects the local hydraulic resistance and turbulence intensity and consequently the local sediment transport capacity. It is recommended to apply adjustable tilting flume equipped with a recirculation loop for sediment-laden flows. Many of those exist, albeit not in the Netherlands.

Although an adjustable tilting flume can overcome the problem of tuning an equilibrium bed slope, flow experiments over a vegetated bed are inherently non-uniform. This is due to the adaptation of flow conditions from open channel flow to flow through and

over vegetation in the beginning of the vegetated section. Therefore, there is a certain adaptation length in the vegetated section in which the initial logarithmic or uniform flow profile, together with the Reynolds stress profile, adjusts to the vegetated flow conditions. An experiment with sediment input, therefore, will suffer from non-uniform flow conditions in the upstream part of the vegetated section. The experience gained in this study shows that this leads to a scour hole in the beginning of the vegetated section and subsequent deposition immediately downstream of it. A better experiment, therefore, consists of a tilted, fixed, vegetated bed section first, long enough to reach equilibrium flow, followed by a tilted, movable, vegetated bed section. This section should be equipped with a sediment feeding system that does not disturb the flow field inside the vegetation. This problem has not been solved yet. An alternative is to measure bed erosion without feeding sediment upstream.

Another problem encountered in the experiment described in this thesis is that of the relatively low resistance of the flume walls. This leads to a non-uniform flow distribution over the width of the flume, in which the flow velocities near the wall are higher. A new experimental set-up should prevent this by placing vegetation closer to the flume walls.

Flow measurements should focus on the quantification of instantaneous velocities, ideally simultaneously in three directions, inside and above the vegetation. Instead of using an EMS, a submersible Laser Doppler Anemometer (LDA) is recommended. An LDA is capable of measuring in a smaller volume, with a higher frequency and can be applied closer to the bed. Alternative techniques, such as Particle Image Velocimetry, or Acoustic Doppler Current Profilers, give problems due to the presence of vegetation. One should at least measure long enough at each location for a time-averaged turbulence quantification. Preferably, one should measure in various locations around an individual plant stem to obtain a spatially averaged turbulence description (López & García, 2001). To obtain vertical profiles for velocity, Reynolds stress or turbulence intensity, the more measurements over the water column, the better. In the case of limited capacity, optimisation is recommended by concentrating measuring points in the top of the vegetation and in the near-bed region. Furthermore, it is recommended to choose various locations along the flume to determine vertical profiles, so as to identify the non-uniform flow conditions in the upstream part of the vegetated section and to check the uniformity of the flow in the remaining part.

Measurements of the bed shear stress can be carried out by applying hot - film anemometry (Thompson et al., 2004). This technique is able to measure the bed shear stress at the required resolution level without any apparatus - related interference. It requires a fixed bed, however. Measurements are recommended that focus on determining the probability density function for the shear stress. These measurements need a long sampling period to fill the tails of the probability density function.

The bed level profilers that were used in the experiment described in this thesis need a clear pathway. This prevents random placement of the vegetation, or placement in too dense a grid or an alternating grid. Alternative methods for measuring bed level or bed forms, such as with video imagery, may fail because of the presence of vegetation. If the sidewall effects are nulled out, bedform development can be viewed from the side of the flume only.

For further flume experiments, it is recommended to determine suspended sediment concentrations. These must be determined over the vertical at various locations along the flume, since there is an adaptation length needed to obtain equilibrium sediment concentrations. An optical probe can be utilised here. These measurements may result in adapted formulations for suspended load transport, in addition to the approach for bed load transport, elaborated in this thesis.

A test programme may consist of many combinations of parameter variations for flume discharge, water depth, plant type, plant density, plant height, plant diameter, plant stiffness, and sediment size, depending on the specific research question of the flume experiment. Research focusing on finding a generally applicable bed load transport formula for vegetated flows, for example, needs relatively coarse sediments and many combinations of flows and vegetation properties. Research focusing on the trapping of silt in submerged vegetation needs fine suspended sediments, relatively low flow velocities and measuring sedimentation. As a third example, research focusing on the two transport mechanisms of a reduced bed shear stress and an increased turbulence intensity at conditions near the initiation of motion needs relatively low flows, very detailed turbulence measurements and measuring the motion of individual particles.

Furthermore, a correct description of the bed shear stress (distribution) on a vegetated bed determines only partly the sediment transport capacity. Vegetation also influences the erodibility of the bed. The root system of vegetation binds the sediment together, thus decreasing the erodibility. Another influence is that the layer of fine cohesive sediments and organic material that builds up on a vegetated bed decreases the erodibility, as well. Typically, the erodibility of grassed Dutch floodplains is affected by these effects. These effects, however, are outside the scope of this thesis. It is recommended that future work be devoted to the erodibility of vegetated beds.

Finally, partly vegetated, compound or curved channels, with or without groynes, can also be tested, widening the scope of study to other subjects.

7.5   Modelling floodplain biogeomorphology in real-world rivers

In this thesis, analytical formulae are derived for the hydraulic resistance of vegetation. In order to describe vegetation resistance, it is important to adequately describe the vegetation geometry. It is recommended to perform measurements of real vegetation geometry and ideally, to perform flume experiments with real vegetation, such as described by Järvelä (2002). In addition, it is recommended to search for simple expressions for the geometry of shrubs and trees. From these expressions the projected area over the height can be determined without describing extensively the complete structure in terms of cylinder diameters and density. Järvelä (2004) proposes an ordering scheme comparable to a drainage network. An alternative technique can be investigated based on fractal geometry (Breedveld & Coene, 2003).

When applying the vegetation cylinder methodology in field situations, a difficulty is that floodplains have inhomogeneous vegetation types with a complex structure. This shifts the modelling problem from estimating a representative bed roughness value to estimating vegetation properties for density, diameter, height and drag coefficient. Of these properties, the drag coefficient is one that cannot be measured directly in the field. In principle, the drag coefficient of a smooth cylinder is known from experimental studies and theory and is dependent on the flow Reynolds number (Schlichting, 1962). The bulk drag coefficient of multiple cylinders is dependent on the placement (even, staggered, random) and decreases with increasing density (Li & Shen, 1973; Hughes, 1997). Furthermore, the drag coefficient varies over the vertical (Nepf & Vivoni, 2000). In models of vegetation resistance, the drag coefficient is usually estimated, for example in an effort to account for the additional roughness of leaves (see Chapter 5). It must be noted that the outcome for vegetation resistance is much more sensitive to the estimate of the geometrical properties of the vegetation than to the estimate of the drag coefficient. Results of a literature review on drag coefficients for vegetated flows are presented in Table 7.1. This table shows that a wide variety of values is found in numerical model studies, or determined in flume experiments and field measurements.

In principle it is possible, though not easy, to obtain the complete vertical structure of grasses, herbaceous vegetation, bushes, floodplain forests and other vegetation types. A direct method is to measure branch diameters and lengths in the field. For heterogeneous vegetation types multiple measurements can be aggregated to obtain characteristic vegetation properties that are translated to cylinder dimensions. An indirect method is making photographs of vegetation types with a white screen on the background and subsequently determining the percentage of vegetation cover on the screen using photo analysis software (Ritzen *et al.*, 2001). Floodplain vegetation can subsequently be classified in various roughness classes, depending on vegetation type and succession stage. With these methods, vegetation properties, such as height, diameter and density, or the vertical surface

Table 7.1: Values for drag coefficients found in literature. Above: Applied drag coefficients in numerical studies. Below: Measured drag coefficients in the field or in laboratory flumes.

Applied drag coefficients.

Reference	C_D	Comments
Nakagawa *et al.* (1992)	1.2 - 1.5	Assumption for cylinders
Watanabe and Hoshi (1996)	1.2	Assumption for cylinders
Naot *et al.* (1996)	0.976 - 1.15	For high Re-numbers, based on Schlichting (1962)
López and García (1997) and		
López and García (1998) and		
López and García (2001)	1.13	Based on experiments by Dunn (1996)
Klopstra *et al.* (1997)	1.4	For cylinders, from literature survey
	2.0	For strips, from literature survey
Fischer-Antze *et al.* (2001)	1.0	Assumed unity for high Re-numbers
Helmiö (2002)	1.0	idem
Stoesser *et al.* (2003)	1.0	idem
Jordanova and James (2003)	1.03 - 1.06	Calculated for multiple stems according to
		Li and Shen (1973)
Uittenbogaard (2003)	2.0	Based on modified Ergun equation,
		Macdonald *et al.* (1979)
Nicholas and McLelland (2004)	1.0	Assumed unity for turbulent flows

Measured drag coefficients.

Reference	C_D	Comments
Li and Shen (1973)	0.4 - 1.6	For paralell, staggered and random row of cylinders
Klaassen and Van der Zwaard (1974)	1.5	Mean bulk drag coefficient for parallel arrays of
		fruit trees
Shields and Gippel (1995)	0.6	For model Large Woody Debris (LWD)
Dunn (1996)	1.13	For rigid and flexible cylinders
Nepf (1999)	1.2 - 0.2	Bulk drag coefficient for random and staggered
		arrays in increasing density
Meijer and Van Velzen (1999)	0.91 - 1.18	For steel bars
Manga and Kirchner (2000)	1.96	Field-determined apparent C_D for LWD
	1.14	For circular cylinders
Nepf and Vivoni (2000)	0.1 - 2.5	Vertical profile of C_D
Wilson and Horritt (2002)	0.05 - 1.0	For grass, depending on Re-number
Stone and Shen (2002)	1.05	Average value of their and other studies
Neary (2003)	1.0 - 1.5	Based on experiments of
		Shimizu and Tsujimoto (1994)

area can be derived. Nonetheless, additional difficulties arise in describing flexible vegetation. Chapter 5 has shown that swaying of the vegetation leads to a non-uniform profile of vegetation properties over the height. In addition, the experimental study has shown that complicated vegetation structures, such as those with leaves, lead to complicated effects on the break-up of turbulent vortices, thus to a more complex description of the vegetation. A correct description of the vegetation geometry, therefore, is one of the research challenges in the future.

On the other hand, an accurate description of vegetation resistance is of limited value in real-world studies. Numerical flow models are commonly calibrated by adjusting a roughness parameter. This roughness parameter is representative of the bulk effect of momentum losses by bed friction, vegetation friction, discrepancies in elevation data, momentum losses in the exchange of the main channel and the floodplains, the presence of obstacles in the flow, and any other momentum loss. It was shown by Werner (2004) that a precise description of vegetation resistance distribution in a floodplain land use map does not necessarily lead to better model predictions of the water level. A pragmatic solution is to treat the vegetation resistance independently from the bed resistance, and use the latter for calibrating the model to observed water levels and flow velocities. This means that we would better work with lumped parameters and learn how to live with limited accuracy in real-world studies.

Chapter 8

Conclusions

This thesis concerns the modelling of biogeomorphological interactions in river floodplains. It deals mainly with one side of these interactions, viz. the effects of floodplain vegetation on flow, sediment transport and morphology. These effects were investigated and analysed with a combination of numerical model studies in one-, two- and three-dimensions, an analytical study on the bed shear stress on a vegetated bed, a flume experimental study and a field study. The objectives of this thesis were formulated as follows (see Section 1.3):

- to develop a methodology to assess the required frequency and extent of Cyclic Floodplain Rejuvenation measures necessary with respect to the flood levels and landscape diversity, with the Waal River as an example;
- to assess the morphodynamic behaviour of secondary channels under different conditions of vegetation development;
- to improve two-dimensional numerical model instruments for modelling floodplain biogeomorphology with regard to the quantification of the bed shear stress on a vegetated bed.

The first objective was elaborated in Chapter 2, where a 1-DH model was applied to investigate the strategy "Cyclic Floodplain Rejuvenation". The second objective was elaborated in Chapter 3, where a 2-DH model was applied to study the long-term morphodynamics of secondary channels, affected by vegetation growth. These studies led to the formulation of the third objective, which was subsequently elaborated in Chapters 4, 5 and 6. In Chapter 4, two analytical expressions for the bed shear stress on a vegetated bed were derived. In Chapter 5, a flume experiment on sediment transport over a vegetated bed was carried out and analysed. In Chapter 6, a comparison was made between a 3-D approach and a 2-DH approach, using the analytical expressions for bed shear stress on a vegetated bed.

The conclusions of this thesis are addressed per chapter in the next sections.

8.1   Cyclic Floodplain Rejuvenation

- Without further measures implemented in the adjacent land (i.e. green rivers, detention areas), it is necessary to regularly reset vegetation succession and to remove deposited sediment in order to sustain safe flood levels and increase landscape diversity.

- The flood management strategy of Cyclic Floodplain Rejuvenation (CFR) is able to sustain safe flood levels in the Waal River when rejuvenation is applied every 25 to 35 years on average, each time in an area of about 15% of the total floodplain area.

- The frequency and extent of CFR measures fit to the historical reference for the Waal River and results in a diverse floodplain vegetation that largely complies with the historical reference, although vegetation types such as marshland and wet herbaceous vegetation will be present insufficiently.

- CFR is optimally applicable in river stretches where a relatively large allowable rise of more than 20 cm in water level is available before the critical flood level is reached. A large allowable rise is favourable because then the rejuvenation frequency can be limited to once per several decades and undisturbed vegetation succession to softwood forests with a closed canopy can be allowed in the floodplains.

- CFR is not an appropriate strategy in rivers sections just upstream of a hydraulic bottleneck.

8.2   Modelling secondary channel biogeomorphology

- The lifetime of river improvement measures, such as the construction of secondary channels, is determined to a large extent by the interaction between vegetation and sediment.

- Riparian vegetation increases the hydraulic resistance of the banks and therefore concentrates the flow in the channel, which leads to an increased sediment transport capacity. In aggrading channels, the inflow opening fills up and consequently vegetation can develop within the channels. The restoration of secondary channels and the subsequent natural development result in an increase of biodiversity, but at the same time a conflict may arise with flood safety.

- The common approach of modelling vegetation resistance as increased bed roughness leads to overestimation of the bed shear stress and hence to erroneous results for the sediment transport capacity and floodplain morphology.

8.3   Analytical expression for the bed shear stress on a vegetated bed

- Based on earlier approaches, two analytical expressions for the bed shear stress on a vegetated bed were derived. One is relatively simple, giving a reduction factor on the total fluid shear stress (*Reduction factor approach*), the other is a relatively complex expression, based on an analytical solution of the momentum balance for vegetated flow (*Analytical approach*).

- A comparison of the bed shear stress calculated with both analytical expressions and with a numerical 1-DV model shows that for submerged conditions the complex formulations of the *Analytical approach* give better estimates for the bed shear stress compared to the *Reduction factor approach*, especially for a smooth bed. For non-submerged conditions, the *Analytical approach* also gives a better estimate. The *Analytical approach* includes the dependence on water depth for non-submerged conditions, which is absent from the *Reduction factor approach*.

8.4   Experimental study on the sediment transport on a vegetated bed

- The effects of vegetation on sediment transport are twofold:
  1. A reduction of the bed shear stress, due to reduced near-bed velocities and fluid stresses;
  2. An increase of the sediment pick-up rate, due to an increased near-bed turbulence intensity.

  The primary effect is that of reduction of the bed shear stress. Only near the threshold of motion the increased pick-up rate for shorter vegetation becomes an important additional transport mechanism.

- In this experiment, the bed shear stress on the vegetated bed is reduced by 80% compared to a bare bed.

- The reduced bed shear stress on a vegetated bed can be described reasonably well with a numerical 1-DV model or with analytical expressions, given an accurate description of the vegetation geometry.

- The sediment transport rate for a vegetated bed can be described reliably by a common sediment transport formula, as long as the bed shear stress reduction is accounted for.

- Flexible vegetation with a complicated geometry in principle needs a more complex description of the geometry than rigid, vertically homogeneous cylinders, such as applied in the analytical expressions.

8.5 Modelling bed shear stress in a real-world river, case-study Allier River, France

- The bed shear stress distribution of a river with flooded vegetated areas can be described well in a 2-DH numerical model with the application of analytical expressions for the bed shear stress reduction, compared with a 3-D numerical model.

- The relatively simple formulations of the *Reduction factor approach* improve model predictions for bed shear stress on a vegetated bed already significantly.

- When describing vegetation resistance as drag resistance of cylinders in flow, instead of an increased bed roughness, the modelling problem is shifted from estimating a representative bed roughness to estimating vegetation properties for density, diameter, height and drag coefficient.

References

Abernethy, B., & Rutherford, I. D. (1998). Where along a river's length will vegetation most effectively stabilise stream banks? *Geomorphology*, *23*, 55-75.

Abernethy, B., & Rutherford, I. D. (2000). Does the weight of riparian trees destabilize riverbanks? *Regul. Rivers: Res. Mgmt.*, *16*, 565-576.

Abernethy, B., & Rutherford, I. D. (2001). The distribution and strength of riparian tree roots in relation to riverbank reinforcement. *Hydrol. Process.*, *15*, 63-79.

Abt, S. R., Clary, W. P., & Thornton, C. I. (1994). Sediment deposition and entrapment in vegetated streambeds. *Journal of Irrigation and Drainage Engineering*, *120*(6), 1098-1111.

Amoros, C. A. (2001). The concept of habitat diversity between and within ecosystems applied to river side-arm restoration. *Environmental Management*, *28*(6), 805-817.

Amoros, C. A., Roux, L., Reygrobellet, J. L., Bravard, J., & Pautou, G. (1987). A method for applied ecological studies of fluvial hydrosystems. *Regul. Rivers: Res. Mgmt.*, *1*, 17-36.

Asselman, N. E. M. (2001). *Sediment processes in floodplains* (Tech. Rep. No. CFR 8). WL | Delft Hydraulics.

Asselman, N. E. M., & Middelkoop, H. (1998). Temporal variability of contemporary floodplain sedimentation in the Rhine-Meuse delta, the Netherlands. *Earth Surf.Process.Landforms*, *23*, 595-609.

Asselman, N. E. M., Middelkoop, H., Ritzen, M. R., Straatsma, M. W., Van Velzen, E. H., & Jesse, P. (2002). Assessment of the hydraulic roughness of river flood plains using laser altimetry. In F. J. Dyer, M. C. Thoms, & J. M. Olley (Eds.), *The structure, function and management implications of fluvial sedimentary systems* (p. 381-388). Alice Springs: IAHS publication 276.

Asselman, N. E. M., & Van Wijngaarden, M. (2002). Development and application of a 1D floodplain sedimentation model for the River Rhine in The Netherlands. *Journal of Hydrology*, *268*, 127-142.

Babovic, V., & Abbott, M. B. (1997). The evolution of equations from hydraulic data, Part I: Theory and Part II: Application. *Journal of Hydraulic Research*, *35*(3), 397-430.

Babovic, V., & Keijzer, M. (1999). Computer supported knowledge discovery - a case study in flow resistance induced by vegetation. In *28th International IAHR Conference.* Graz.

Babovic, V., & Keijzer, M. (2000). Genetic programming as a model induction engine. *Journal of Hydroinformatics, 2*(1), 35-60.

Baptist, M. J. (2001a). *Numerical modelling of the biogeomorphological developments of secondary channels in the Waal river* (Tech. Rep. No. CFR 11). Delft University of Technology, Faculty of Civil Engineering and Geosciences, Hydraulic Engineering Section.

Baptist, M. J. (2001b). *Review on biogeomorphology in rivers: processes and scales* (Tech. Rep. No. CFR 3). Delft University of Technology, Faculty of Civil Engineering and Geosciences, Hydraulic Engineering Section.

Baptist, M. J. (2003). A flume experiment on sediment transport with flexible, submerged vegetation. In *International workshop on riparian forest vegetated channels: hydraulic, morphological and ecological aspects.* 20 - 22 February 2003, Trento, Italy.

Baptist, M. J., & Mosselman, E. (2002). Biogeomorphological modelling of secondary channels in the Waal river. In D. Bousmar & Y. Zech (Eds.), *River flow 2002 symposium* (p. 773-782). Louvain-la-Neuve, Belgium: Swets & Zeitlinger, Lisse, the Netherlands.

Baptist, M. J., Penning, W. E., Duel, H., Smits, A. J. M., Geerling, G. W., Van der Lee, G. E. M., & Van Alphen, J. S. L. (2004). Assessment of cyclic floodplain rejuvenation on flood levels and biodiversity in the Rhine River. *River Research and Applications, 20*(3), 285-297.

Bolton, S., & Shellberg, J. (2001). *Ecological issues in floodplains and riparian corridors* (Tech. Rep.). University of Washington, Centre for Streamside Studies.

Breedveld, M. J., & Liefhebber, D. (2003). *Vegetatie- en morfodynamiek van de Allier; Een studie naar de vegetatie- en morfodynamiek van de Allier als basis voor dynamisch riviermanagement in Nederland aan de hand van historische luchtfoto's* (Tech. Rep.). Katholieke Universiteit Nijmegen, Leerstoel Natuurbeheer Stroomgebieden, Afdeling Milieukunde, Faculteit der Natuurwetenschappen, Wiskunde en Informatica.

Breedveld, S., & Coene, J. (2003). *Boompjes, wiskundig gevormd* (Tech. Rep. No. 3D Computer Graphics in4006). Delft University of Technology, Faculty of Electrical Engineering, Mathematics and Computer Science.

Breugem, W. P. (2004). *The influence of wall permeability on laminar and turbulent flows; theory and simulations.* Ph.D. thesis, ISBN 90-9018924-6, Delft University of Technology.

Brooks, A. P., & Brierley, G. J. (2002). Mediated equilibrium: the influence of riparian

vegetation and wood on the long-term evolution and behaviour of a near-pristine river. *Earth Surf.Process.Landforms*, *27*, 343-367.

Brown, A. G. (1997). Biogeomorphology and diversity in multiple-channel river systems. *Global Ecology and Biogeography Letters*, *6*(Floodplain forests special issue), 179-185.

Brunke, M. (2002). Floodplains of a regulated southern alpine river (Brenno, Switzerland): ecological assessment and conservation options. *Aquatic Conserv: Mar. Freshw. Ecosyst.*, *12*, 583-599.

Buijse, A. D., Coops, H., Staras, M., Jans, L. H., Van Geest, G. J., Grift, R. E., Ibelings, B. W., Oosterberg, W., & Roozen, F. C. J. M. (2002). Restoration strategies for river floodplains along large lowland rivers in europe. *Freshwater Biology*, *47*, 889-907.

Bulle, H. (1926). *Untersuchungen über die Geschiebeableitung bei der Spaltung von Wasserlaufen*. Berlin: VDI-Verlag.

Campana, T. R. (1999). *Hydraulic resistance of submerged floodplain vegetation*. M.Sc. thesis H.E.043, IHE-Delft.

Carollo, F. G., Ferro, V., & Termini, D. (2002). Flow velocity measurements in vegetated channels. *Journal of Hydraulic Engineering*, *128*(7), 664-673.

Cheng, N.-S., & Chiew, Y.-M. (1998). Pickup probability for sediment entrainment. *Journal of Hydraulic Engineering*, *124*(2), 232-235.

Coleman, N. L. (1982). Experimental studies of sediment transport: an overview. In G. Keramidas & C. Brebbia (Eds.), *International conference on computational methods and experimental measurements* (p. 671-681). Washington D.C.: Springer-Verlag, Berlin.

Cornelissen, P., & Vulink, J. T. (2001). Effects of cattle and horses on vegetation structure. In B. Gerhen & M. Görner (Eds.), *Proceedings natur- und kulturlandschaft 4*. Höxter/Jena, Germany.

Darby, S. E. (1999). Effect of riparian vegetation on flow resistance and flood potential. *Journal of Hydraulic Engineering*, *125*(5), 443-445.

Dawson, F. H., & Charlton, F. G. (1988). *Bibliography on the hydraulic resistance of vegetated watercourses* (Tech. Rep.). Freshwater Biological Association, Occasional Publication No. 25, ISNN 0308-6739, 25 pp.

De Heij, L. (2001). *Ewijkse Plaat; Ontwikkeling van vegetatiestructuur en hydraulische ruwheid (1989-2000)* (Tech. Rep. No. Milieukunde 202). University of Nijmegen.

De Ruiter, J. C. C. (1982). The mechanism of sediment transport on bedforms. In B. Sumer & A. Muller (Eds.), *Euromech 156: Mechanics of sediment transport* (p. 137-142). Istanbul, 12-14 July 1982: A.A. Balkema, Rotterdam.

De Vriend, H. J. (1981). *Steady flow in shallow channel bends*. Ph.D. thesis, Delft University of Technology.

De Vriend, H. J. (2001). Long-term morphological prediction. In G. Seminara (Ed.), *River, estuarine and coastal morphology* (p. 163-190). Berlin: Springer Verlag.

Deletic, A. (2001). Modelling of water and sediment transport over grassed areas. *Journal of Hydrology*, *248*(1-4), 168-182.

Dijkstra, J. T. (2003). *The influence of vegetation on scroll bar development.* M.Sc thesis, Delft University of Technology, Faculty of Civil Engineering and Geosciences, Section Hydraulic Engineering.

Dister, E. (1980). *Geobotanische Untersuchungen in der Hessischen Rheinaue als Grundlage für die Naturschutzarbeit.* Ph.D. thesis.

Dittrich, A., & Koll, K. (1997). Velocity field and resistance of flow over rough surfaces with large and small relative submergence. *International Journal of Sediment Research*, *12*(3), 21-33.

Duel, H., Baptist, M. J., Geerling, G., Smits, A. J. M., & Van Alphen, J. S. L. (2002). Cyclic Floodplain Rejuvenation as a strategy for both flood protection and enhancement of the biodiversity of the river Rhine. In *Fourth international ecohydraulics symposium.* Cape-Town, South-Africa.

Duel, H., Baptist, M. J., & Penning, W. E. (Eds.). (2001). *Cyclic Floodplain Rejuvenation; a new strategy based on floodplain measures for both flood risk management and enhancement of the biodiversity of the river Rhine.* Delft: Netherlands Centre for River Studies, NCR report 14-2001.

Duel, H., & Kwakernaak, C. (1992). Rivierdynamiek in uiterwaarden; Ecologische perspectieven en consequenties voor de rivierafvoer. *Landschap*, *9*(4), 255-270.

Dunn, C. J. (1996). *Flow structure and resistance in a laboratory channel with simulated vegetation.* M.Sc thesis, University of Illinois, Urbana-Champaign.

Einstein, H. A. (1950). *The bed-load function for sediment transportation in open channel flow* (Tech. Rep. No. 1026). United States Dept. of Agriculture.

Einstein, H. A., & Banks, R. B. (1950). Fluid resistance of composite roughness. *Transactions of the Amer. Geoph. Union*, *31*(4), 603-610.

Elliott, A. H. (2000). Settling of fine sediment in a channel with emergent vegetation. *Journal of Hydraulic Engineering*, *126*(8), 570-577.

Engelund, F., & Hansen, E. (1967). *A monograph on sediment transport in alluvial streams.* Copenhagen: Teknisk Forlag.

Fathi-Maghadam, M., & Kouwen, N. (1997). Nonrigid, nonsubmerged, vegetative roughness on floodplains. *Journal of Hydraulic Engineering*, *123*(1), 51-57.

Fischer-Antze, T., Stoesser, T., Bates, P., & Olsen, N. R. B. (2001). 3D numerical modelling of open-channel flow with submerged vegetation. *Journal of Hydraulic Research*, *39*(3), 303-310.

Fisher, K. R., & Knight, D. W. (2002). Improved roughness and velocity prediction for in-

stream habitats - Development and comparison of methods. In *Fourth ecohydraulics conference.* Cape Town.

Fisher, R. A. (1928). The general sampling distribution of the multiple correlation coefficient. *Proceedings of the Royal Society of London, 121A*, 654-673.

Frissell, C., Liss, A. W. J., Warren, C. E., & Hurley, M. D. (1986). A hierarchical framework for stream habitat classification; viewing streams in a watershed context. *Environmental Management, 10*(2), 199-214.

García, M. H., López, F., Dunn, C. J., & Alonso, C. V. (2004). Flow, turbulence and resistance in a flume with simulated vegetation. In S. J. Bennett & A. Simon (Eds.), *Riparian vegetation and fluvial geomorphology* (Vol. Water Science Application 8, p. 11-27). Washington, D.C.: American Geophysical Union.

Garratt, J. (1992). *The atmospheric boundary layer.* New York, NY.: Cambridge University Press.

Geerling, G. W., Smits, A. J. M., & Kloosterman, H. (2001). *Monitoring & dynamisch rivierbeheer, RS en Ruimte voor Rivieren* (Tech. Rep. No. 4.2001). KUN, Leerstoel Natuurbeheer Riviergebieden. Rijkswaterstaat Meetkundige Dienst.

Ghisalberti, M., & Nepf, H. M. (2002). Mixing layers and coherent structures in vegetated aquatic flows. *Journal of Geophysical Research, 107*(C2), 3-1 to 3-11.

Ghisalberti, M., & Nepf, H. M. (2004). The limited growth of vegetated shear layers. *Water Resources Research, 40*(doi:10.1029/2003WR002776, 2004).

Goodwin, C. N., Hawkins, C. P., & Kershner, J. L. (1997). Riparian restoration in the Western United States: Overview and perspective. *Restoration Ecology, 5*(4S), 4-14.

Gran, K., & Paola, C. (2001). Riparian vegetation controls on braided stream dynamics. *Water Resources Research, 37*(12), 3275-3283.

Grass, A. J. (1970). Initial instability of fine bed sand. *Journal of the Hydraulics Division ASCE, 96*(HY3), 619-632.

Gregory, K. J. (1992). Vegetation and river channel process interactions. In P. Boon, P. Calow, & G. E. Petts (Eds.), *River conservation and management* (p. 255-269). John Wiley & Sons Ltd.

Gregory, K. J., & Gurnell, A. M. (1988). Vegetation and river channel form and process. In H. Viles (Ed.), *Biogeomorphology* (p. 11-42). Oxford: Basil Blackwell Ltd.

Gregory, S. V., Swanson, F. J., Mckee, W. A., & Cummins, K. W. (1991). An ecosystem perspective of riparian zones; focus on links between land and water. *BioScience, 41*(8), 540-551.

Grift, R. E. (2001). *How fish benefit from floodplain restoration along the lower River Rhine.* Ph.D. thesis, Wageningen University.

Gurnell, A. M. (1995). Vegetation along river corridors: hydrogeomorphological interactions. In A. Gurnell & G. Petts (Eds.), *Changing river channels* (p. 237-260). John Wiley & Sons, Ltd.

Gurnell, A. M. (1997). The hydrological and geomorphological significance of forested floodplains. *Global Ecology and Biogeography Letters*, *6*, 219-229.

Gurnell, A. M., & Gregory, K. J. (1995). Interactions between semi-natural vegetation and hydrogeomorphological processes. *Geomorphology*, *13*, 49-69.

Harris, N. M., Babovic, V., & Falconer, R. A. (2003). Velocity predictions in compound channels with vegetated floodplains using genetic programming. *Int. J. River Basin Management*, *1*(2), 117-123.

Hasegawa, K., Asai, S., Kanetaka, S., & Baba, H. (1999). Flow properties of a deep open experimental channel with a dense vegetation bank. *Journal of Hydroscience and Hydraulic Engineering*, *17*(2), 59-70.

Hegland, S. T., Van Leeuwen, M., & Oostermeijer, J. G. B. (2001). Population structure of *Salvia pratensis* in relation to vegetation and management of Dutch dry floodplain grasslands. *Journal of Applied Ecology*, *38*, 1277-1289.

Helal Ahmed, M. (2003). *On suspended sediment transport through sugmerged vegetation.* M.Sc. thesis H.E.449, IHE, Delft.

Helmiö, T. (2002). Unsteady 1D flow model of compound channel with vegetated floodplains. *Journal of Hydrology*, *269*(1-2), 89-99.

Hession, W. C., Pizzuto, J. E., Johnson, T. E., & Horwitz, R. J. (2003). Influence of bank vegetation on channel morphology in rural and urban watersheds. *Geology*, *31*(2), 147-150.

Hinze, J. O. (1975). *Turbulence* (2nd ed.). New York: McGraw-Hill.

Hoffmann, M. (2004). Application of a simple space-time averaged porous media model to flow in densely vegetated channels. *J. of Porous Media*, *7*(3), 183-191.

Hofland, B. (submitted). The probability density function for instantaneous drag forces and shear stresses on a bed. *Submitted to Journal of Hydraulic Engineering.*

Hong, H. T. M. (1995). *Hydraulic resistance of flexible roughness.* M.Sc thesis H.H.237, IHE Delft.

Houwing, E. J., Tanczos, I. C., Kroon, A., & De Vries, M. B. (2001). Interaction of submerged vegetation, hydrodynamics and turbidity; analysis of field and laboratory results. In *Intercoh conference 2001.*

Hughes, F. M. R. (1997). Floodplain biogeomorphology. *Progress in Physical Geography*, *21*(4), 501-529.

Hughes, F. M. R., Adams, W. M., Muller, E., Nilsson, C., Richards, K. S., Barsoum, N., Decamps, H., Foussadier, R., Girel, J., Guilloy, H., Hayes, A., Johansson, M., Lambs, L., Pautou, G., Peiry, J.-L., Perrow, M., Vautier, F., & Winfield, M. (2001). The importance of different scale processes for the restoration of floodplain woodlands. *Regul. Rivers: Res. Mgmt.*, *17*, 325-345.

Hupp, C. R. (1992). Riparian vegetation recovery patterns following stream channelization: a geomorphic perspective. *Ecology*, *73*(4), 1209-1226.

Hupp, C. R., & Osterkamp, W. R. (1996). Riparian vegetation and fluvial geomorphic processes. *Geomorphology, 14*, 277-295.

Ikeda, S., & Kanazawa, M. (1996). Three-dimensional organized vortices above flexible water plants. *Journal of Hydraulic Engineering, 122*(11), 634-640.

Ikeda, S., Yamada, T., & Toda, Y. (2001). Numerical study on turbulent flow and honami in and above flexible plant canopy. *International Journal of Heat and Fluid Flow, 22*, 252-258.

Jackson, P. S. (1981). On the displacement height in the logarithmic velocity profile. *Journal of fluid mechanics, 111*, 15-25.

Jacobs, J. M., & Wang, M.-H. (2003). Atmospheric momentum roughness applied to stage-discharge relationships in flood plains. *Journal of Hydrologic Engineering, 8*(2), 99-104.

Jagers, H. R. A. (2003). *Modelling planform changes of braided rivers.* Ph.D. thesis, University of Twente.

James, C. S., Birkhead, A. L., Jordanova, A. A., & O'Sullivan, J. J. (2004). Flow resistance of emergent vegetation. *Journal of Hydraulic Research, 42*(4), 390-398.

Jans, L. (2004). *Evaluatie nevengeulen Gamerensche Waard 1996 - 2002* (Tech. Rep. No. RIZA 2004.024 (in Dutch)). Ministerie van Verkeer en Waterstaat, Rijkswaterstaat RIZA.

Jans, L., Backx, J., Greijdanus-Klaas, M., De Jonge, J., Van der Meij, V., Oosterbaan, J., Van der Scheer, A., Schropp, M., & Van Wijngaarden, M. (2001). *Monitoring nevengeulen; integrale jaarrapportage 1999/2000* (Tech. Rep. No. RIZA 2001.062x). Rijkswaterstaat, RIZA.

Jansen, P. P., Van Bendegom, L., Van den Berg, J., De Vries, M., & Zanen, A. (Eds.). (1979). *Principles of river engineering: the non-tidal alluvial river* (1994 ed.). Delft: Delftse Uitgevers Maatschappij.

Järvelä, J. (2002). Flow resistance of flexible and stiff vegetation: a flume study with natural plants. *Journal of Hydrology, 269*(1-2), 44-54.

Järvelä, J. (2003). Influence of vegetation on flow structure in floodplains and wetlands. In A. Snchez-Arcilla & A. Bateman (Eds.), *River, coastal and estuarine morphodynamics 2003* (Vol. Vol II, p. 845-856). Barcelona, Spain: IAHR.

Järvelä, J. (2004). Determination of flow resistance caused by non-submerged woody vegetation. *Int. J. River Basin Management, 2*(1), 1-10.

Jongman, R. (1992). Vegetation, river management and land use in the Dutch Rhine floodplains. *Regul. Rivers: Res. Mgmt., 7*, 279-289.

Jordanova, A. A., & James, C. S. (2003). Experimental study of bed load transport through emergent vegetation. *Journal of Hydraulic Engineering, 129*(6), 474-478.

Kapinga, S. (2003). *Scour around large wooden debris; Determination of flow velocities during floods by studying local scour holes in the river Allier.* M.Sc thesis, Delft

University of Technology, Faculty of Civil Engineering and Geosciences, Section Hydraulic Engineering.

Karanxha, A. (2002). *Interaction between vegetation - flow - sediment transport and morphology.* M.Sc. thesis H.E.121, IHE, Delft.

Katul, G., Wiberg, P., Albertson, J., & Hornberger, G. (2002). A mixing layer theory for flow resistance in shallow streams. *Water Resources Research*, *38*(11), 1250, doi:10.1029/2001WR000817, 2002.

Kerle, F., Zöllner, F., Kappus, B., Marx, W., & Giesecke, J. (2001). *Fish habitat and vegetation modelling in floodplains with Casimir* (Tech. Rep. No. CFR 13). IWS, University of Stuttgart.

Kirkby, M. (1990). The landscape viewed through models. *Zeitschrift fur Geomorphologie*, *Suppl.-Bd. 79*, 63-81.

Kitamura, T., Jia, Y., Tsujimoto, T., & Wang, S. S. Y. (1998). Sediment transport capacity in channels with vegetation zone. In *Iche*.

Klaassen, G. J., Stolker, C., Van Velzen, E. H., & Verheij, H. (1999). *Naar een ruwheidsvoorspeller voor moerasvegetatie op basis van riet en gras* (Tech. Rep.). WL | Delft Hydraulics, RWS/RIZA.

Klaassen, G. J., & Van der Zwaard, J. J. (1974). Roughness coefficients of vegetated floodplains. *Journal of Hydraulic Research*, *12*(1), 43-63.

Kleinhans, M. G., & Van Rijn, L. C. (2002). Stochastic prediction of sediment transport in sand-gravel bed rivers. *Journal of Hydraulic Engineering*, *128*(1), 412-425.

Klijn, F. (1997). *A hierarchical approach to ecosystems and its implications for ecological land classification; with examples of ecoregions, ecodistricts and ecoseries of the netherlands.* Ph.D. thesis, University of Leiden.

Klopstra, D., Barneveld, H., Van Noortwijk, J. M., & Van Velzen, E. H. (1997). Analytical model for hydraulic roughness of submerged vegetation. In *27th International IAHR Conference* (p. 775-780). San Fransico.

Klopstra, D., Barneveld, H. J., & Van Noortwijk, J. M. (1996). *Analytisch model hydraulische ruwheid van overstroomde moerasvegetatie* (Tech. Rep. No. PR051). HKV.

Kouwen, N., & Unny, T. E. (1973). Flexible roughness in open channels. *Journal of the Hydraulics Division*, *99(HY5)*, 713-728.

Kouwen, N., Unny, T. E., & Hill, H. M. (1969). Flow retardance in vegetated channels. *Journal of the Irrigation and Drainage Division*, *95*(IR2), 329-342.

Li, R. M., & Shen, H. W. (1973). Effect of tall vegetations on flow and sediment. *Journal of the Hydraulics Division*, *99*(HY6), 1085-1103.

LNV. (2000). *Nature for people, people for nature; Policy document for nature, forest and landscape in the 21st century* (Tech. Rep.). Ministry of Agriculture, Nature Management and Fisheries.

López, F., & García, M. H. (1997). *Open-channel flow through simulated vegetation: Turbulence modelling and sediment transport* (Tech. Rep. No. Technical Report WRP-CP-10). Hydrosystems Laboratory, University of Illinois.

López, F., & García, M. H. (1998). Open-channel flow through simulated vegetation: Suspended sediment transport modelling. *Water Resources Research, 34*(9), 2341-2352.

López, F., & García, M. H. (2001). Mean flow and turbulence structure of open-channel flow through non-emergent vegetation. *Journal of Hydraulic Engineering, 127*(5), 392-402.

Macdonald, I. F., El-Sayed, M. S., Mow, K., & Dullien, F. A. L. (1979). Flow through porous media-the ergun equation revisited. *Ind. Eng. Chem. Fundam., 18*(3), 199-208.

Madsen, J. D., Chambers, P. A., James, W. F., Koch, E. W., & Westlake, D. F. (2001). The interaction between water movement, sediment dynamics and submersed macrophytes. *Hydrobiologia, 444*, 71-84.

Manga, M., & Kirchner, J. W. (2000). Stress partitioning in streams by large woody debris. *Water Resources Research, 36*(8), 2373-2379.

Marston, R. A., Girel, J., Pautou, G., Píegay, H., Bravard, J. P., & Arneson, C. (1995). Channel metamorphosis, floodplain disturbance, and vegetation development: Ain River, France. *Geomorphology, 13*, 121-131.

Mason, D. C., Cobby, D. M., Horritt, M. S., & Bates, P. D. (2003). Floodplain friction parameterization in two-dimensional river flood models using vegetation heights derived from airborne scanning laser altimetry. *Hydrol. Process., 17*, 1711-1732.

Massman, W. J. (1997). An analytical one-dimensional model of momentum transfer by vegetation of arbitrary structure. *Boundary-Layer Meteorology, 83*(3), 407-421.

McKenney, R., Jacobson, R. B., & Wertheimer, R. C. (1995). Woody vegetation and channel morphogenesis in low-gradient, gravel-bed streams in the Ozark Plateaus. *Geomorphology, 13*, 175-198.

Meijer, D. G., & Van Velzen, E. H. (1999). Prototype-scale flume experiments on hydraulic roughness of submerged vegetation. In *28th International IAHR Conference.* Graz.

Meijer, D. M. (1998a). *Modelproeven overstroomd riet* (Tech. Rep. No. PR177). HKV lijn in water.

Meijer, D. M. (1998b). *Modelproeven overstroomde vegetatie* (Tech. Rep. No. PR121.10). HKV lijn in water.

Middelkoop, H. (1997). *Embanked floodplains in the Netherlands; Geomorphological evolution over various time scales.* Ph.D. thesis, Rijksuniversiteit Utrecht.

Middelkoop, H., & Asselman, N. E. M. (1998). Spatial variability of floodplain sedimentation at the event scale in the Rhine-Meuse delta, the Netherlands. *Earth Surf.Process.Landforms, 23*, 561-573.

Mosselman, E. (2001). *Morphological development of side channels* (Tech. Rep. No. CFR 9). WL | Delft Hydraulics.

Murota, A., Fukuhara, T., & Sato, M. (1984). Turbulence structure in vegetated open channel flows. *Journal of Hydroscience and Hydraulic Engineering, 2*(1), 47-61.

Murray, A. B., & Paola, C. (2003). Modelling the effect of vegetation on channel pattern in bedload rivers. *Earth Surf. Process. Landforms, 28*(2), 131-143.

Nakagawa, H., Tsujimoto, T., & Shimizu, Y. (1992). Sediment transport in vegetated bed channel. In *5th International Symposium on River Sedimentation.* Karlsruhe.

Nakamura, F., Swanson, F. J., & Wondzell, S. M. (2000). Disturbance regimes of stream and riparian ecosystems - a disturbance-cascade perspective. *Hydrol. Process., 14,* 2849-2860.

Naot, D., Nezu, I., & Nakagawa, H. (1996). Hydrodynamic behavior of partly vegetated open channels. *Journal of Hydraulic Engineering, 122*(11), 625-633.

Neary, V. S. (2003). Numerical solution of fully developed flow with vegetative resistance. *Journal of Engineering Mechanics, 129*(5), 558-563.

Nepf, H. M. (1999). Drag, turbulence, and diffusion in flow through emergent vegetation. *Water Resources Research, 35*(2), 479-489.

Nepf, H. M., & Vivoni, E. R. (1999). Turbulence structure in depth-limited vegetated flow: Transition between emergent and submerged regimes. In *28th International IAHR Conference.* Graz.

Nepf, H. M., & Vivoni, E. R. (2000). Flow structure in depth-limited, vegetated flow. *Journal of Geophysical Research, 105*(C12), 28,547-28,557.

Nezu, I., & Naot, D. (1999). Partly vegetated open channels; new experimental evidence. In *28th international iahr conference.* Graz.

Nicholas, A. P., & McLelland, S. J. (2004). Computational fluid dynamics modelling of three-dimensional processes on natural river floodplains. *Journal of Hydraulic Research, 42*(2), 131-143.

Nikora, V., Koll, K., McEwan, I., Mclean, S., & Dittrich, A. (2004). Velocity distribution in the roughness layer of rough-bed flows. *Journal of Hydraulic Engineering, 130*(10), 1036-1042.

Nikuradse, J. (1930). Turbulente Strömung in nichtkreisförmigen Rohren. *Ing.-Arch., 1*(306).

NW4. (1999). *Fourth national policy document on water management* (Tech. Rep.). Ministry of Transport, Public Works and Water Management.

Oberez, A. (2001). *Turbulence modeling of hydraulic roughness of submerged vegetation.* M.Sc. thesis H.E.100, IHE, Delft.

Okabe, T., Yuuki, T., & Kojima, M. (1997). Bed-load rate on movable beds covered by vegetation. In *27th iahr-conference.* San-Francisco.

Paintal, A. S. (1971). A stochastic model of bed load transport. *Journal of Hydraulic Research*, *9*(4), 527:553.

Papanicolaou, A. N., Diplas, P., Evaggelopoulos, N., & Fotopoulos, S. (2002). Stochastic incipient motion criterion for spheres under various bed packing conditions. *Journal of Hydraulic Engineering*, *128*(4), 369-380.

Pautou, G., Peiry, J. L., Girel, J., Blanchard, E., Hughes, F., Richards, K., Harris, T., & El-Hames, A. (1997). Space-time units in floodplains: the example of the Drac River upstream of Grenoble (French Alps). *Global Ecology and Biogeography Letters*, *6*(Floodplain forests special issue), 311-319.

Pedroli, G. B. M., Postma, R., Kerkhofs, M. J. J., & Rademakers, J. M. G. (1996). Welke natuur hoort er bij de rivier? Naar een natuurstreefbeeld afgeleid van karakteristieke fenomenen van het rivierenlandschap. *Landschap*, *13*, 97-111.

Perry, A. E., Schofield, W. H., & Joubert, P. N. (1969). Rough wall turbulent boundary layers. *Journal of fluid mechanics*, *37*(2), 383-413.

Peters, B. (2002). *Successie van natuurlijke uiterwaardlandschappen* (Tech. Rep.). Katholieke Universiteit Nijmegen.

Petryck, S., & Bosmajian III, G. (1975). Analysis of flow through vegetation. *Journal of the Hydraulics Division*, *101*(HY7), 871 - 884.

Piégay, H. (1997). Interactions between floodplain forests and overbank flows: data from three piedmont rivers of southeastern France. *Global Ecology and Biogeography Letters*, *6*, 187-196.

Poggi, D., Porporato, A., Ridolfi, L., Albertson, J. D., & Katul, G. G. (2004). The effect of vegetation density on canopy sub-layer turbulence. *Boundary-Layer Meteorology*, *111*(3), 565-587.

Postma, R., Kerkhofs, M. J. J., Pedroli, G. B. M., & Rademakers, J. M. G. (1995). *Een stroom natuur. Natuurstreefbeelden voor Rijn en Maas* (Tech. Rep. No. 95.060 (in Dutch)). Rijkswaterstaat, RIZA.

Proakis, J. G. (1989). *Digital communications* (2nd Ed. ed.). New York: McGraw Hill.

Prosser, I. P., Dietrich, W. E., & Stevenson, J. (1995). Flow resistance and sediment transport by concentrated overland flow in a grassland valley. *Geomorphology*, *13*, 71-86.

Raat, A. (2001). Ecological rehabilitation of the Dutch part of the River Rhine with special attention to fish. *Regul. Rivers: Res. Mgmt.*, *17*, 131-144.

Rademakers, J. M. G., & Wolfert, H. P. (1994). *Het Rivier-Ecotopen-Stelsel; een indeling van ecologisch relevante ruimtelijke eenheden ten behoeve van ontwerp* (Tech. Rep. No. 'Ecologisch Herstel Rijn en Maas' 61 (in Dutch)). RIZA.

Raupach, M. R. (1992). Drag and drag partition on rough surfaces. *Boundary-Layer Meteorology*, *60*, 375-395.

Raupach, M. R. (1994). Simplified expressions for vegetation roughness length and zero-

plane displacement as functions of canopy height and area index. *Boundary-Layer Meteorology*, *71*, 211-216.

Ree, W. O., & Crow, F. R. (1977). *Friction factors for vegetated waterways of small slope* (Tech. Rep. No. ARS-S-151). Agricultural Research Service, U.S. Department of Agriculture.

Richards, K., Brasington, J., & Hughes, F. (2002). Geomorphic dynamics of floodplains: ecological implications and a potential modelling strategy. *Freshwater Biology*, *47*, 559-579.

Righetti, M., & Armanini, A. (2002). Flow resistance in open channel flows with sparsely distributed bushes. *Journal of Hydrology*, *269*(1-2), 55-64.

Ritzen, M. R., Straatsma, M. W., & Middelkoop, H. (2001). *Fototechnische bepaling van vegetatiedichtheid* (Tech. Rep.). Universiteit Utrecht, Fysische Geografie.

Rodrigues, S. (2000). *Approche des relations végétation - sédimentation dans un environnement fluviatile: cas de la Loire moyenne* (Tech. Rep.). Université F. Rabelais, Géologie des Environnements Aquatiques Continentaux.

Rodríguez Uthurburu, J. (2004). *Evaluation of physically based and evolutionary data mining approaches for modelling resistance due to vegetation in SOBEK 1D-2D.* M.Sc. thesis H.H.485, Unesco IHE, Delft.

Salo, J., Kalliola, R., Häkkinen, I., Mäkinen, Y., Niemelä, P., Puhakka, M., & Coley, P. D. (1986). River dynamics and the diversity of the Amazon lowland forest. *Nature*, *322*, 254-258.

Schielen, R. M. J., Bons, C. A., Gijsbers, P. J. A., & Knol, W. C. (Eds.). (2001). *DSS Large Rivers; Interactive flood management and landscape planning in river systems.* Delft: NCR-publication 13-2001.

Schiemer, F., Baumgärtner, C., & Tockner, K. (1999). Restoration of floodplain rivers: The 'Danube restoration project'. *Regul. Rivers: Res. Mgmt.*, *15*, 231-244.

Schlichting, H. (1962). *Boundary-layer theory* (4th ed.). New York: McGraw-Hill book company.

Schoor, M. M. (1999). *De netto sedimentatie op de Ewijkse Plaat, berekend met de krigingmethode* (Tech. Rep. No. 99.118x (in Dutch)). RIZA.

Schwartz, M. (in press). *Encyclopedia of Coastal Science.* Dordrecht: Kluwer Academic Publishers.

Shi, Z., & Hughes, M. R. (2002). Laboratory flume studies of microflow environments of aquatic plants. *Hydrol. Process.*, *16*, 3279-3289.

Shields, A. (1936). Anwendung der Aehnlichkeitsmechanik und der Turbulenzforschung auf die Geschiebebewegung. *Mitteilungen der Preuschischen Versuchsanstalt für Wasserbau and Schiffbau*, 26pp.

Shields, F. D. J., Knight, S. S., & Cooper, C. M. (2000). Cyclic perturbation of lowland river channels and ecological response. *Regul. Rivers: Res. Mgmt.*, *16*, 307-325.

Shields, F. J., & Gippel, C. (1995). Prediction of effects of woody debris removal on flow resistance. *Journal of Hydraulic Engineering, 121*(4), 341-354.

Shimizu, Y., & Tsujimoto, T. (1994). Numerical analysis of turbulent open-channel flow over vegetation layer using a k-ϵ turbulence model. *J. Hydrosci. Hydr. Eng., 11*(2), 57-67.

Silva, W., Klijn, F., & Dijkman, J. (2001). *Room for the Rhine Branches in The Netherlands; What the research has taught us* (Tech. Rep. Nos. R3294, RIZA 2001.031). WL | Delft Hydraulics & Arnhem, RIZA.

Simons, J. H. E. J., Bakker, C., Schropp, M. H. I., Jans, L. H., Kok, F. R., & Grift, R. E. (2001). Man-made secondary channels along the river Rhine (the Netherlands); results of post-project monitoring. *Regul. Rivers: Res. Mgmt., 17*(473-491).

Smits, A. J. M., Havinga, H., & Marteijn, E. C. L. (2000). New concepts in river and water management in the Rhine River basin: how to live with the unexpected? In A. Smits, P. Nienhuis, & R. Leuven (Eds.), *New approaches to river management* (p. 267-286). Leiden: Backhuys Publishers.

SOBEK. (2002). *SOBEK user manual* (Tech. Rep.). WL | Delft Hydraulics.

Sorber, A. M. (1997). *Oeversedimentatie tijdens de hoogwaters van 1993/1994 en 1995* (Tech. Rep. No. rapport 97.015 (in Dutch)). RIZA.

Specht, F.-J. (2002). *Einflusch von Gerinnebreite und Uferbewuchs auf die hydraulisch-sedimentologischen Verhältnisse naturnaher Flieschgewässer.* Ph.D. thesis, Technische Universität Braunschweig.

Stanhill, G. (1969). A simple instrument for the field measurement of turbulent diffusion flux. *Journal of Applied Meteorology, 8*, 509-513.

Starkel, L. (1990). Fluvial environment as an expression of geoecological changes. *Zeitschrift fur Geomorphologie, Suppl.-Bd., 79*, 133-152.

Steiger, J., Gurnell, A. M., & Goodson, J. M. (2003). Quantifying and characterizing contemporary riparian sedimentation. *River Research and Applications, 19*, 335-352.

Stephan, U., & Gutknecht, D. (2002). Hydraulic resistance of submerged flexible vegetation. *Journal of Hydrology, 269*(1-2), 27-43.

Stoesser, T., Wilson, C. A. M. E., Bates, P. D., & Dittrich, A. (2003). Application of a 3D numerical model to a river with vegetated floodplains. *Journal of Hydroinformatics, 5*(2), 99-112.

Stolker, C., & Verheij, H. J. (2000). *Vergelijken van berekeningsmethoden voor de ruwheid van overstroomde flexibele vegetatie* (Tech. Rep. No. Q2693). WL | Delft Hydraulics.

Stone, B. M., & Shen, H. T. (2002). Hydraulic resistance of flow in channels with cylindrical roughness. *Journal of Hydraulic Engineering, 128*(5), 500-506.

Straatsma, M. W., Middelkoop, H., Pebesma, E., & Wesseling, C. (2003). Mapping of vegetation characteristics using lidar and spectral remote sensing. In N. Douben

& A. Van Os (Eds.), *Ncr days 2003; Dealing with floods within constraints. ncr Publication 24-2004* (p. 48-50).

Struiksma, N. (1999). Mathematical modelling of bedload transport over non-erodible layers. In *IAHR Symp. River, Coastal and Estuarine Morphodynamics,* (Vol. 1, p. 89-98). Genova, Italy, 6-10 Sept. 1999: IAHR.

Struiksma, N., Olesen, K. W., Flokstra, C., & De Vriend, H. J. (1985). Bed deformation in curved alluvial channels. *Journal of Hydraulic Research, 23*(1), 57-79.

Takagi, K., Miyata, A., Harazono, Y., Ota, N., Komine, M., & Yoshimoto, M. (2003). An alternative approach to determining zero-plane displacement, and its application to a lotus paddy field. *Agricultural and forest meteorology, 115*(3-4), 173-181.

Tamburrino, A., & Sandoval, F. (1998). Probability density functions of free-surface velocities and velocity gradients. *Mechanica Research Communications, 25*(6), 605-612.

Tanczos, I. C., & De Vries, M. B. (1999). *Interactie van submerse vegetatie en fysische processen* (Tech. Rep. No. Z2473/Z2540). WL | Delft Hydraulics.

Taylor, R. P., Coleman, H. W., & Hodge, B. K. (1985). Prediction of turbulent rough-wall skin friction using a discrete element approach. *Journal of Fluids Engineering, 107,* 251-257.

Teeter, A. M., Johnson, B. H., Berger, C., Stelling, G., Scheffner, N. W., Garcia, M. H., & Parchure, T. M. (2001). Hydrodynamic and sediment transport modelling with emphasis on shallow-water, vegetated areas (lakes reservoirs, estuaries and lagoons). *Hydrobiologia, 444,* 1-23.

Thannbichler, C. (2002). *A flume experiment on sediment transport with flexible, submerged vgetation.* M.Sc thesis, Delft University of Technology, Faculty of Civil Engineering and Geosciences, Hydraulic Engineering Section.

Thom, A. S. (1971). Momentum absorption by vegetation. *Q.J.R. Meteorol. Soc., 97,* 414-428.

Thompson, A. M., Wilson, B. N., & Hansen, B. J. (2004). Shear stress partitioning for idealized vegetated surfaces. *Transactions of the ASAE, 47*(3), 701-709.

Thorne, C. R. (1990). Effects of vegetation on riverbank erosion and stability. In J. Thornes (Ed.), *Vegetation and erosion; processes and environments* (p. 125-144). John Wiley & Sons.

Thorne, C. R., Hey, R. D., & Newson, M. D. (1997). *Applied fluvial geomorphology for river engineering and management.* Chisester: John Wiley & Sons.

Tockner, K., Malard, F., & Ward, J. V. (2000). An extension of the flood pulse concept. *Hydrol. Process., 14,* 2861-2883.

Tollner, E. W., Barfield, B. J., & Hayes, J. C. (1982). Sedimentology of erect vegetal filters. *Journal of the Hydraulics Division, 108*(HY12), 1518-1531.

Tooth, S., & Nanson, G. C. (1999). Anabranching rivers on the Northern Plains of arid central Australia. *Geomorphology*, *29*, 211-233.

Trimble, S. W., & Mendel, A. (1995). The cow as a geomorphic agent; A critical review. *Geomorphology*, *13*, 233-253.

Tsujimoto, T. (1999). Fluvial processes in streams with vegetation. *Journal of Hydraulic Research*, *37*(6), 789-803.

Tsujimoto, T., & Kitamura, T. (1990). *Velocity profile of flow in vegetated-bed channels* (Tech. Rep. No. KHL progressive report 1). Hydraulic Laboratory, Kanazawa University.

Tsujimoto, T., Kitamura, T., & Okada, T. (1991). *Turbulent structure of flow over rigid vegetation-covered bed in open channels* (Tech. Rep. Nos. KHL-Commun., Hydraulics Lab., Vol. 2, pp. 1-14). Kanazawa University.

Tsujimoto, T., Okada, T., & Kontani, K. (1993). *Turbulent structure of open-channel flow over flexible vegetation* (Tech. Rep. No. KHL progressive report 4). Hydraulic Laboratory, Kanazawa University.

Tsujimoto, T., & Shimizu, Y. (1994). Flow and suspended sediment in a compound channel with vegetation. In *1st int. symp. habitat hydraulics* (p. 347-370). Trondheim, Norway.

Uittenbogaard, R. (2003). Modelling turbulence in vegetated aquatic flows. In *International workshop on riparian forest vegetated channels: hydraulic, morphological and ecological aspects.* 20-22 February 2003, Trento, Italy.

Uittenbogaard, R., Bosboom, J., & Van Kessel, T. (2000). *Numerical simulation of wave-current driven sand transport* (Tech. Rep. No. Z2899.10). WL | Delft Hydraulics.

USACE. (2000). *Upper Mississippi river system habitat needs assessment* (Tech. Rep.). U.S. Army Corps of Engineers.

Van Alphen, J. S. L. (2002). How to eliminate a hydraulic bottleneck; Nijmegen, the first example in the Netherlands. In *Flood defence 2002* (p. 651-658). Beijing, China: Science Press, New York.

Van den Bosch, L. V. (2003). *Influence of vegetation on flow and morphology in the River Allier, France.* M.Sc thesis, Delft University of Technology, Faculty of Civil Engineering and Geosciences, Section Hydraulic Engineering.

Van der Lee, G. E. M., Baptist, M. J., Ververs, M., & Geerling, G. (2001a). *Application of the cyclic floodplain rejuvenation strategy to the Waal river* (Tech. Rep. No. CFR 15). WL | Delft Hydraulics, Delft University of Technology, University Nijmegen.

Van der Lee, G. E. M., Duel, H., Penning, W. E., & Peters, B. (2001b). *Modelling of vegetation succession in floodplains* (Tech. Rep. No. CFR 7). WL | Delft Hydraulics, University of Nijmegen.

Van Rijn, L. C. (1983). *Siltation in dredged trenches; Entrainment of fine sediment parti-*

cles: sediment pick-up functions (Tech. Rep. No. M 1531 part IV). Delft Hydraulics Laboratory.

Van Rijn, L. C. (1984). Sediment Transport, Part I: Bed Load Transport. *Journal of Hydraulic Engineering, 110*(10), 1431-1456.

Van Rijn, L. C. (1993). *Principles of sediment transport in rivers, estuaries and coastal seas.* Amsterdam: Aqua Publications.

Van Splunder, I. (1998). *Floodplain forest recovery; softwood forest development in relation to hydrology, riverbank morphology and management.* Ph.D. thesis, University of Nijmegen.

Van Stokkom, H. T. C., & Smits, A. J. M. (2002). Flood defense in The Netherlands: A new era, a new approach. In *Flood defence 2002* (p. 34-47). Beijing, China: Science Press, New York.

Van Velzen, E. H., Jesse, P., Cornelissen, P., & Coops, H. (2003a). *Stromingsweerstand vegetatie in uiterwaarden; Deel 1 Handboek versie 1-2003* (Tech. Rep. No. 2003.028). Rijkswaterstaat, RIZA.

Van Velzen, E. H., Jesse, P., Cornelissen, P., & Coops, H. (2003b). *Stromingsweerstand vegetatie in uiterwaarden; Deel 2 Achtergronddocument versie 1-2003* (Tech. Rep. No. 2003.029). Rijkswaterstaat, RIZA.

Vanoni, V. A., & Brooks, N. H. (1957). *Laboratory studies on the roughness and suspended load of alluvial streams* (Tech. Rep. No. E-68). Sedimentation Laboratory, California Institute of Technology, Pasadena, California.

Vera, F. M. (2000). *Grazing ecology and forest history* (Tech. Rep.). Strategic Policies Division, Ministry of Agriculture.

Verheij, H. (2000). *Uniformering k-waarden rivierecotopen* (Tech. Rep.). WL | Delft Hydraulics.

Vernon-Harcourt, L. F. (1896). *Rivers and Canals, Vol.1 Rivers.* Oxford: the Clarendon Press.

Verwey, A. (2001). Latest developments in floodplain modelling - 1D/2D integration. Keynote Address B. In *Sixth conference on hydraulics in civil engineering* (p. 13-24). Hobart, Tasmania, Australia: The Institution of Engineers, Australia.

Viles, H. A. (1988). *Biogeomorphology.* Oxford: Basil Blackwell Ltd.

Visser, P. J. (2000). *Bodemontwikkeling Rijnsysteem; Een verkenning van omvang, oorzaken, toekomstige ontwikkelingen* (Tech. Rep.). Technische Universiteit Delft, Faculteit Civiele Techniek en Geowetenschappen, Sectie Waterbouwkunde.

Ward, J. V., & Tockner, K. (2001). Biodiversity: towards a unifying theme for river ecology. *Freshwater Biology, 46*, 807-819.

Ward, J. V., Tockner, K., & Schiemer, F. (1999). Biodiversity of floodplain river ecosystems: ecotones and connectivity. *Regul. Rivers: Res. Mgmt., 15*, 125-139.

Watanabe, Y., & Hoshi, K. (1996). Influence of vegetation on flow velocity and suspended

load. In *International workshop on interactive issues of flood and environment in cold regions* (p. 63-70). 3-6 October 1996, Trento, Italy.

Werner, M. G. F. (2004). *Spatial flood extent modelling; a performance-based comparison.* Phd, Delft University of Technology.

Widdows, J., Brinsley, M. D., Salkeld, P. N., & Lucas, C. H. (2000). Influence of biota on spatial and temporal variation in sediment erodability and material flux on a tidal flat (Westerschelde, the Netherlands). *Marine Ecology Progress Series, 194*, 23-37.

Wijma, E. (2005). *Hydraulic roughness of riverine softwood forests, of the Allier (France) and the Lower Volga (Russian Federation).* M.Sc thesis, Utrecht University, Department of Physical Geography.

Wilson, C. A. M. E., & Horritt, M. S. (2002). Measuring the flow resistance of submerged grass. *Hydrol. Process., 16*(13), 2589-2598.

Wilson, C. A. M. E., Stoesser, T., Bates, P. D., & Batemann Pinzen, A. (2003). Open channel flow through different forms of submerged flexible vegetation. *Journal of Hydraulic Engineering, 129*(11), 847-853.

Wilson, N. R., & Shaw, R. H. (1977). A higher order closure model for canopy flow. *Journal of Applied Meteorology, 16*(11), 1197-1205.

Wolfert, H. P. (2001). *Geomorphological change and river rehabilitation; case studies on lowland fluvial systems in the Netherlands* (Ph.D. thesis). Alterra Scientific Contributions 6.

Wu, F.-C., Shen, H. S., & Chou, Y. J. (1999). Variation of roughness coefficients for unsubmerged and submerged vegetation. *Journal of Hydraulic Engineering, 125*(9), 934-942.

Yalin, M. S. (1977). *Mechanics of sediment transport* (Vol. 2nd Edition). Oxford, Great-Britain: Pergamon Press.

Yalin, M. S., & Karahan, E. (1979). Inception of sediment transport. *Journal of the Hydraulics Division ASCE, 105*(HY11), 1433-1443.

Zaman, S. (2004). *Modelling sediment transport rate within submerged vegetated channel; a data driven approach.* M.Sc thesis, UNESCO-IHE.

Zanke, U. (1990). Der Beginn der Sedimentbewegung als Warscheinlichkeitsproblem. *Wasser und Boden, 42*, 40-43.

Appendix A

Flume experimental data from literature

Table A.1: Flume experimental data on the resistance of submerged, rigid or flexible, artificial or natural vegetation.

Author(s)	Test	D	m	k	C_D	h	$\overline{u}$	C_r
Tsujimoto and Kitamura (1990)	A11	0.0015	2500	0.0459	1.46	0.0950	0.133	13.59
	A12	0.0015	2500	0.0459	1.46	0.0749	0.117	13.54
	A31	0.0015	2500	0.0459	1.46	0.0936	0.196	11.69
	A32	0.0015	2500	0.0459	1.46	0.0735	0.179	12.08
	A36	0.0015	2500	0.0459	1.46	0.0500	0.108	8.83
	A37	0.0015	2500	0.0459	1.46	0.0568	0.124	9.46
	A71	0.0015	2500	0.0459	1.46	0.0895	0.331	13.20
	A72	0.0015	2500	0.0459	1.46	0.0727	0.267	11.83
Murota *et al.* (1984)	A1	0.00024	4000	0.058	2.75	0.116	0.127	11.77
	A3	0.00024	4000	0.052	2.75	0.106	0.191	13.09
	A6	0.00024	4000	0.052	2.75	0.103	0.229	13.03
	A7	0.00024	4000	0.06	2.75	0.1095	0.099	13.33
	A14	0.00024	4000	0.0545	2.75	0.1015	0.167	12.00
	A20	0.00024	4000	0.0528	2.75	0.1058	0.173	13.82
	A21	0.00024	4000	0.0475	2.75	0.0915	0.258	13.78
	A22	0.00024	4000	0.0575	2.75	0.0965	0.085	10.12
Tsujimoto *et al.* (1993)	BZ1	0.00062	10000	0.065	2	0.10	0.078	7.07
	BZ2	0.00062	10000	0.065	2	0.14	0.092	8.26
	BZ3	0.00062	10000	0.065	2	0.16	0.086	9.51
	BZ4	0.00062	10000	0.065	2	0.11	0.132	7.29
	BZ5	0.00062	10000	0.065	2	0.13	0.161	7.89
	BZ6	0.00062	10000	0.065	2	0.16	0.164	8.91
	BZ7	0.00062	10000	0.064	2	0.10	0.192	8.54
	BZ8	0.00062	10000	0.064	2	0.12	0.245	8.89
	BZ9	0.00062	10000	0.064	2	0.15	0.273	20.32
	BZ10	0.00062	10000	0.063	2	0.10	0.275	8.70
	BZ11	0.00062	10000	0.062	2	0.13	0.333	9.62
	BZ12	0.00062	10000	0.061	2	0.11	0.385	11.19
Meijer (1998a)	R2	0.0057	254	1.64	1.805	1.99	0.142	2.99

table continues on next page

Author(s)	Test	D	m	k	C_D	h	$\overline{u}$	C_r
	R3	0.0057	254	1.65	1.805	2.25	0.201	4.02
	R4	0.0057	254	1.65	1.805	2.48	0.258	4.97
	R5	0.0057	254	1.55	1.805	1.75	0.152	2.52
	R6	0.0057	254	1.58	1.805	1.99	0.196	3.19
	R7	0.0057	254	1.58	1.805	2.23	0.279	4.60
	R8	0.0057	254	1.58	1.805	2.50	0.393	5.63
Meijer (1998b)	1	0.008	256	1.50	0.99	1.98	0.175	3.76
	2	0.008	256	1.50	0.98	1.99	0.233	3.89
	3	0.008	256	1.50	0.99	2.19	0.212	4.65
	4	0.008	256	1.50	0.99	2.19	0.238	4.55
	5	0.008	256	1.50	0.99	2.35	0.242	5.56
	6	0.008	256	1.50	0.98	2.33	0.337	5.62
	7	0.008	256	1.50	1	2.50	0.255	6.33
	8	0.008	256	1.50	0.99	2.47	0.368	6.19
	9	0.008	64	1.50	0.97	2.01	0.309	6.70
	10	0.008	64	1.50	0.97	2.01	0.419	6.73
	11	0.008	64	1.50	0.97	2.20	0.347	7.36
	12	0.008	64	1.50	0.96	2.19	0.468	7.29
	13	0.008	64	1.50	0.97	2.35	0.372	7.97
	14	0.008	64	1.50	0.96	2.31	0.499	7.59
	15	0.008	64	1.50	0.97	2.48	0.391	8.10
	16	0.008	64	1.50	0.96	2.46	0.535	8.08
	17	0.008	256	0.90	0.99	1.51	0.248	6.17
	18	0.008	256	0.90	0.97	1.52	0.355	6.38
	19	0.008	256	0.90	0.99	1.81	0.331	8.46
	20	0.008	256	0.90	0.97	1.80	0.473	8.69
	21	0.008	256	0.90	0.98	2.09	0.403	10.46
	22	0.008	256	0.90	0.97	2.09	0.577	10.75
	23	0.008	256	0.90	0.98	2.48	0.500	13.53
	24	0.008	256	0.90	0.97	2.46	0.808	13.35
	25	0.008	64	0.90	0.97	1.51	0.386	9.78
	26	0.008	64	0.90	0.97	1.52	0.544	9.92
	27	0.008	64	0.90	0.97	1.81	0.461	11.76
	28	0.008	64	0.90	0.97	1.78	0.661	11.68
	29	0.008	64	0.90	0.97	2.10	0.537	13.54
	30	0.008	64	0.90	0.97	2.06	0.764	13.14
	31	0.008	64	0.90	0.96	2.47	0.645	15.40
	32	0.008	64	0.90	0.97	2.47	0.902	15.18
	33	0.008	256	0.45	0.98	1.02	0.283	10.04
	34	0.008	256	0.45	0.97	0.99	0.441	10.95
	35	0.008	256	0.45	0.98	1.51	0.461	15.45
	36	0.008	256	0.45	0.97	1.50	0.680	14.94

table continues on next page

Author(s)	Test	D	m	k	C_D	h	$\overline{u}$	C_r
	37	0.008	256	0.45	0.98	1.98	0.630	18.58
	38	0.008	256	0.45	0.97	1.99	0.942	17.72
	39	0.008	256	0.45	0.97	2.46	0.802	19.33
	40	0.008	256	0.45	0.97	2.49	0.861	20.33
	41	0.008	64	0.45	0.97	1.02	0.438	15.83
	42	0.008	64	0.45	0.97	1.00	0.661	15.29
	43	0.008	64	0.45	0.96	1.50	0.624	19.44
	44	0.008	64	0.45	0.97	1.50	1.061	19.40
	45	0.008	64	0.45	0.97	2.00	0.955	21.47
	46	0.008	64	0.45	0.97	2.00	1.219	21.63
	47	0.008	64	0.45	0.97	2.48	0.883	22.35
	48	0.008	64	0.45	0.97	2.41	1.242	22.45
Kouwen *et al.* (1969)	1	0.005	5000	0.100	3	0.1506	0.030	3.41
	2	0.005	5000	0.100	3	0.2527	0.110	6.91
	3	0.005	5000	0.085	3	0.3819	0.367	10.85
	4	0.005	5000	0.100	3	0.1519	0.098	3.55
	7	0.005	5000	0.100	3	0.1509	0.143	3.68
	8	0.005	5000	0.050	3	0.2422	0.560	11.74
	9	0.005	5000	0.100	3	0.3503	0.205	10.93
	10	0.005	5000	0.100	3	0.2500	0.268	7.65
	11	0.005	5000	0.100	3	0.4000	0.156	11.05
	12	0.005	5000	0.100	3	0.3000	0.106	8.64
	13	0.005	5000	0.100	3	0.1496	0.071	3.37
	14	0.005	5000	0.100	3	0.2002	0.055	5.48
	15	0.005	5000	0.095	3	0.3000	0.271	9.03
	16	0.005	5000	0.100	3	0.2001	0.079	5.60
	17	0.005	5000	0.060	3	0.1990	0.395	8.85
	18	0.005	5000	0.100	3	0.3498	0.133	10.06
	19	0.005	5000	0.075	3	0.2998	0.400	10.33
	20	0.005	5000	0.100	3	0.3000	0.158	9.09
	21	0.005	5000	0.100	3	0.2000	0.135	5.53
	22	0.005	5000	0.100	3	0.2000	0.185	5.84
	24	0.005	5000	0.060	3	0.3486	0.536	12.83
	25	0.005	5000	0.090	3	0.3986	0.229	11.49
	26	0.005	5000	0.100	3	0.2527	0.082	7.31
	27	0.005	5000	0.090	3	0.3508	0.352	10.86
	28	0.005	5000	0.100	3	0.2594	0.196	7.03
	29	0.005	5000	0.055	3	0.3830	0.609	14.05
	30	0.005	5000	0.100	3	0.1491	0.041	3.39
López and García (2001)	1	0.0064	170	0.12	1.13	0.335	0.587	16.91
	2	0.0064	170	0.12	1.13	0.229	0.422	14.71
	3	0.0064	170	0.12	1.13	0.164	0.308	12.69

table continues on next page

Author(s)	Test	D	m	k	C_D	h	$\overline{u}$	C_r
	4	0.0064	170	0.12	1.13	0.276	0.709	15.47
	5	0.0064	170	0.12	1.13	0.203	0.531	13.51
	6	0.0064	42	0.12	1.13	0.267	0.733	23.63
	7	0.0064	42	0.12	1.13	0.183	0.570	22.23
	8	0.0064	384	0.12	1.13	0.391	0.506	13.48
	9	0.0064	384	0.12	1.13	0.214	0.298	10.73
	10	0.0064	384	0.12	1.13	0.265	0.746	11.43
	11	0.0064	97	0.12	1.13	0.311	0.625	18.69
	12	0.0064	97	0.12	1.13	0.233	0.854	16.86
López and García (1997)	13	0.0064	170	0.14	1.13	0.368	0.535	14.69
	14	0.0064	170	0.11	1.13	0.232	0.853	17.61
	15	0.0064	170	0.14	1.13	0.257	0.398	13.07
	16	0.0064	42	0.07	1.13	0.23	0.855	29.72
	17	0.0064	388	0.17	1.13	0.279	0.307	9.69
	18	0.0064	388	0.12	1.13	0.284	0.693	12.93
Järvelä (2003)	R4-1	0.0028	12000	0.205	1	0.306	0.119	5.55
	R4-2	0.0028	12000	0.155	1	0.3084	0.295	8.85
	R4-3	0.0028	12000	0.23	1	0.4065	0.090	6.28
	R4-4	0.0028	12000	0.19	1	0.4041	0.225	9.82
	R4-5	0.0028	12000	0.16	1	0.407	0.319	11.19
	R4-6	0.0028	12000	0.245	1	0.5044	0.072	7.18
	R4-7	0.0028	12000	0.22	1	0.495	0.184	10.65
	R4-8	0.0028	12000	0.26	1	0.7065	0.129	10.83
	R4-9	0.0028	12000	0.215	1	0.7037	0.185	12.71
	S3-1	0.003	512	0.295	1	0.4003	0.091	7.18
	S3-2	0.003	512	0.2	1	0.3961	0.230	11.53
	S3-3	0.003	512	0.17	1	0.3942	0.330	12.38
Ikeda and Kanazawa (1996)	1	0.00024	20000	0.04	1	0.148	0.503	19.57
	2	0.00024	20000	0.042	1	0.142	0.444	18.83
	3	0.00024	20000	0.045	1	0.146	0.349	18.39
	4	0.00024	20000	0.042	1	0.19	0.493	16.14
	5	0.00024	20000	0.04	1	0.165	0.606	18.64
	6	0.00024	20000	0.042	1	0.171	0.360	16.50
	7	0.00024	20000	0.04	1	0.18	0.444	16.15
Ree and Crow (1977)	k4	0.005	1464	0.2032	1	0.242	0.070	3.71
	k5	0.005	1464	0.2032	1	0.247	0.068	3.83
	k6	0.005	1464	0.2032	1	0.302	0.054	4.82
	k7	0.005	1464	0.2032	1	0.302	0.109	5.25
	k8	0.005	1464	0.2032	1	0.345	0.106	5.15
	k9	0.005	1464	0.2032	1	0.375	0.086	6.51
	k10	0.005	1464	0.2032	1	0.428	0.174	6.51
	k11	0.005	1464	0.2032	1	0.379	0.161	7.67

table continues on next page

Author(s)	Test	D	m	k	C_D	h	$\overline{u}$	C_r
	k12	0.005	1464	0.2032	1	0.438	0.133	8.78
	k13	0.005	1464	0.2032	1	0.431	0.268	9.44
	k14	0.005	1464	0.2032	1	0.465	0.246	10.05
	k15	0.005	1464	0.2032	1	0.521	0.208	10.88
	k16	0.005	1464	0.2032	1	0.528	0.412	12.53
	k17	0.005	1464	0.2032	1	0.570	0.376	13.08
	L2	0.005	1076	0.3048	1	0.324	0.055	2.11
	L3	0.005	1076	0.3048	1	0.342	0.052	2.12
	L4	0.005	1076	0.3048	1	0.382	0.046	2.14
	L6	0.005	1076	0.3048	1	0.463	0.058	2.59
	L7	0.005	1076	0.3048	1	0.520	0.049	2.75
	L8	0.005	1076	0.3048	1	0.493	0.101	3.63
	L9	0.005	1076	0.3048	1	0.520	0.094	3.70
	L10	0.005	1076	0.3048	1	0.585	0.081	3.84
	L11	0.005	1076	0.3048	1	0.547	0.187	6.07
	L12	0.005	1076	0.3048	1	0.617	0.154	6.24
	L13	0.005	1076	0.3048	1	0.690	0.131	6.51
	L14	0.005	1076	0.3048	1	0.619	0.298	8.94
	L15	0.005	1076	0.3048	1	0.680	0.262	9.00
	L16	0.005	1076	0.3048	1	0.751	0.227	8.78
	L17	0.005	1076	0.3048	1	0.692	0.427	11.81
	L18	0.005	1076	0.3048	1	0.749	0.377	11.65

D is diameter(m), m is density (m^{-2}), k is (deflected) vegetation height (m), h is water depth (m), $\overline{u}$ is the depth-averaged flow (m/s), C_r is the representative roughness, derived from equilibrium slope (m$^{0.5}$.s^{-1}). C_D is assumed 1 for Järvelä (2003), Ikeda and Kanazawa (1996) and Ree and Crow (1977). D is assumed 0.005 m for Ree and Crow (1977).

Appendix B

1-DV turbulence model for vegetated aquatic flows

The 1-DV turbulence model for vegetated aquatic flows been developed by Dr. R. Uittenbogaard of WL | Delft Hydraulics as an extension of an existing 1-DV model, which can be applied for thermocline formation, sediment transport and simulation of orbital surface-wave motions (Uittenbogaard *et al.*, 2000). This appendix describes the basic equations of the momentum balance and the k-ϵ turbulence model, which have been adjusted to model vegetated aquatic flows. These descriptions are based on Uittenbogaard (2003).

Momentum equation

The 1-DV model assumes uniform flow in horizontal direction. It solves the momentum equation for the pore velocity, $u(z)$ (m/s). The momentum equation reads:

$$\rho_0 \frac{\partial u(z)}{\partial t} + \frac{\partial p}{\partial x} = \frac{\rho_0}{1 - \lambda(z)} \frac{\partial}{\partial z} \left((1 - \lambda(z))(\nu + \nu_T(z)) \frac{\partial u(z)}{\partial z} \right) - \frac{F(z)}{1 - \lambda(z)} \tag{B.1}$$

where ρ_0 is the fluid density, $\partial p / \partial x$ is the horizontal pressure gradient (kg.m^{-2}.s^{-2}), ν is the kinematic viscosity of water (m^2.s^{-1}), ν_T is the eddy viscosity (m^2.s^{-1}), F is the drag force of the vegetation per unit volume (N.m^{-3}), and λ is the solidity (-), the fraction horizontal surface taken by the vegetation:

$$\lambda(z) = \frac{\pi}{4} D(z)^2 m(z) \tag{B.2}$$

where D is the stem diameter (m) and m is the stem density (m^{-2}).

The vegetation drag force imposed on the mean flow is given by:

$$F(z) = \frac{1}{2} \rho_0 C_D(z) D(z) m(z) u(z) |u(z)| \tag{B.3}$$

where C_D is the drag coefficient (-).

The pressure gradient $\partial p / \partial x$ is constant along the water depth, according the hydrostatic pressure assumption, and is either provided as input to the model, or numerically adjusted

to satisfy a given depth-averaged bulk velocity, U (m/s). The bulk velocity is defined by the volume flux of water divided by a channel's wetted cross-section and relates to the pore velocity by:

$$U = \frac{1}{h} \int_0^h (1 - \lambda) u(z) \mathrm{d}z \tag{B.4}$$

The continuity equation is given by:

$$\frac{\partial u}{\partial x} = 0 \tag{B.5}$$

k-ε turbulence model equations

The k-ϵ turbulence model provides a closure for the eddy viscosity, relating it to the turbulent kinetic energy, k_T (m^2.s^{-2}) and its dissipation rate, ϵ (m^2.s^{-3}):

$$\nu_T = c_\mu \frac{k_T^2}{\epsilon} \tag{B.6}$$

where c_μ is a constant (0.09).

The equation for the turbulent kinetic energy reads:

$$\frac{\partial k_T}{\partial t} = \frac{1}{1 - \lambda} \frac{\partial}{\partial z} \left((1 - \lambda) \left(\nu + \nu_T/\sigma_k \right) \frac{\partial k_T}{\partial z} \right) + T + P_k - B_k - \epsilon \tag{B.7}$$

The first term in the RHS represents the vertical diffusion of turbulent kinetic energy by its own mixing action, corrected for the available horizontal surface, λ. A closure coefficient $\sigma_k = 1.0$ was used in this equation.

The second term, T, is the additional turbulence source generated by the vegetation. Considering fully turbulent flow, all the work done by the fluid against the plants drag force is converted into turbulent kinetic energy, so the expression for T (Watt/m^3) is:

$$T(z) = F(z) u(z) \tag{B.8}$$

For transient or laminar flow, part or all of this power would be transferred into heat by work against viscous forces, and correction terms depending on Reynolds number would be needed.

The third term in the RHS, P_k, is the turbulence production in shear flows:

$$P_k = \nu_T \left(\frac{\partial u}{\partial z} \right)^2 \tag{B.9}$$

The fourth term, B_k is the buoyancy term, and represents the conversion of turbulent kinetic energy into gravitational energy, according to:

$$B_k = -\frac{\nu_T}{\sigma_k} \frac{g}{\rho_0} \frac{\partial \rho}{\partial z} \tag{B.10}$$

The fifth and last term, ϵ, is the dissipation rate of the turbulent kinetic energy through its work against viscous stresses. This is modelled by the ϵ-equation:

$$\frac{\partial \varepsilon}{\partial t} = \frac{1}{1-\lambda}\frac{\partial}{\partial z}\left((1-\lambda)\left(\nu + \nu_T/\sigma_\varepsilon\right)\frac{\partial \epsilon}{\partial z}\right) + c_{2\varepsilon}\frac{T}{\tau_{eff}} + P_\epsilon - B_\epsilon - \epsilon_\epsilon \tag{B.11}$$

The first term in the RHS represents the vertical diffusion of ϵ by the turbulent eddies. For the closure coefficient, $\sigma_\epsilon = 1.3$ is applied.

The last three terms in the RHS, P_ϵ, B_ϵ and ϵ_ϵ, correspond to the production, buoyancy and dissipation of ϵ, respectively, and are related to the production, buoyancy and dissipation of k_T by the expressions:

$$P_\epsilon = c_{1\epsilon}\frac{\epsilon}{k_T}P_k \tag{B.12}$$

$$B_\epsilon = c_{1\epsilon}\left(1 - c_{3\epsilon}\right)\frac{\epsilon}{k_T}B_k \tag{B.13}$$

$$\epsilon_\epsilon = c_{2\epsilon}\frac{\epsilon^2}{k_T} \tag{B.14}$$

where $c_{1\epsilon} = 1.44$, $c_{2\epsilon} = 1.92$ and $c_{3\epsilon} = 0$ or 1 (depending on stratification), are closure coefficients.

The important part is in the second term on the RHS, which corresponds to the dissipation rate of turbulence produced by vegetation. This dissipation rate depends on the effective turbulence dissipation time scale, τ_{eff}, and is affected by the closure coefficient $c_{2\epsilon} = 1.92$. Uittenbogaard (2003) relates the dissipation time scale to the different length scales that control turbulence inside vegetation. First of all, at sufficient distance from the bed as well as from the top of the vegetation, the length scale of internally generated wake turbulence is smaller than the available fluid space inside the vegetation, and therefore the relevant time scale of this small scale turbulence corresponds to the intrinsic turbulence time scale:

$$\tau_{\text{int}} = \frac{k}{\varepsilon} \tag{B.15}$$

This time scale is adopted as effective time scale by Shimizu and Tsujimoto (1994) and López and García (2001). However, it is here where the k-ϵ model of Uittenbogaard (2003) differs from that of previous authors. Shimizu and Tsujimoto (1994) and López and García (2001) did not include the penetration of shear turbulence from above the vegetation into the top layer of the vegetation. Above the vegetation a shear layer is formed by the vertical exchange of horizontal momentum with the retarded flow inside the vegetation. The large eddies that are advected from above the vegetation have to be squeezed into smaller-scale eddies of the length scale of the available space inside the vegetation. In this way, the relevant time scale for the dissipation is determined by the geometrical properties of vegetation, according to:

$$\tau_{geom} = \left(\frac{\ell^2}{c_\mu^2 T}\right)^{\frac{1}{3}} \tag{B.16}$$

where ℓ is the available length scale for eddies inside the vegetation:

$$\ell(z) = c_\ell \left(\frac{1 - \lambda(z)}{m(z)} \right)^{\frac{1}{2}} \tag{B.17}$$

in which c_ℓ is a coefficient that affects the geometrical length scale. For cylinders, $c_\ell = 1$.

The 1-DV model computes both times scales τ_{int} and τ_{geom} over the vertical and evaluates the effective time scale by a MAX-operator:

$$\tau_{eff}^{-1} = \max\left(\tau_{int}^{-1}, \tau_{geom}^{-1} \right) \tag{B.18}$$

Appendix C

3-D turbulence model for vegetated aquatic flows

The 3-D turbulence model for vegetated aquatic flows is essentially an implementation of the 1-DV model into the shallow-water equations. The present implementation in the three-dimensional model is, therefore, focused on the dominant role of the vertical derivatives of horizontal velocities. Furthermore, the present equations neglect most of the changes in fluxes due to changes in the porosity (1-λ) of the vegetation. For most terms these changes are considered negligible, except for the vertical changes in porosity particularly at the transition from clear fluid to the top of the (submerged) vegetation. Therefore, only in the description of vertical momentum exchange and vertical diffusion of turbulent energy and turbulence dissipation, the porosity is included (Uittenbogaard & Kernkamp, pers. comm.). In a later version, the full Volume-Averaged Navier-Stokes equations for porous flow will be implemented following Breugem (2004).

In the implementation in the three-dimensional model, the horizontal momentum equations, without Coriolis force, without density-driven stratification, for a hydrostatic pressure assumption and written in Cartesian coordinates, become:

$$\frac{Du}{Dt} + g\frac{\partial \varsigma}{\partial x} = \frac{1}{1-\lambda}\frac{\partial}{\partial z}\left((1-\lambda)\,\upsilon_V\frac{\partial u}{\partial z}\right) + \frac{\partial R_{xx}}{\partial x} + \frac{\partial R_{xy}}{\partial y} - \frac{F_u}{1-\lambda} \tag{C.1}$$

$$\frac{Dv}{Dt} + g\frac{\partial \varsigma}{\partial y} = \frac{1}{1-\lambda}\frac{\partial}{\partial z}\left((1-\lambda)\,\upsilon_V\frac{\partial v}{\partial z}\right) + \frac{\partial R_{xy}}{\partial x} + \frac{\partial R_{yy}}{\partial y} - \frac{F_v}{1-\lambda} \tag{C.2}$$

in which the material derivative reads:

$$\frac{D}{Dt} = \frac{\partial}{\partial t} + u\frac{\partial}{\partial x} + v\frac{\partial}{\partial y} + w\frac{\partial}{\partial z} \tag{C.3}$$

where u, v and w are the flow velocity components in x, y and z direction, respectively (m/s), ζ is the water level (m), λ is the solidity (-), and the normal stress components (divided by fluid density):

$$R_{xx} = 2\,(\nu + \nu_{\mathrm{V}} + \nu_{\mathrm{H}})\,\frac{\partial u}{\partial x} \quad ; \quad R_{yy} = 2\,(\nu + \nu_{\mathrm{V}} + \nu_{\mathrm{H}})\,\frac{\partial v}{\partial y} \tag{C.4}$$

and the shear stress component (divided by fluid density):

$$R_{xy} = (\nu + \nu_{\mathrm{V}} + \nu_{\mathrm{H}}) \left(\frac{\partial u}{\partial y} + \frac{\partial v}{\partial x} \right) \tag{C.5}$$

where ν is the molecular viscosity ($\mathrm{m^2.s^{-1}}$), ν_{V} is the eddy-viscosity of 3D-turbulence, and ν_{H} is the eddy-viscosity of 2D-turbulence (horizontal eddy motions).

The vegetation's drag force per unit horizontal area, F ($\mathrm{N/m^2}$):

$$F_u = \tfrac{1}{2} C_D m D u \sqrt{u^2 + v^2} \tag{C.6}$$

$$F_v = \tfrac{1}{2} C_D m D v \sqrt{u^2 + v^2} \tag{C.7}$$

The depth-averaged continuity equation is given by:

$$\frac{\partial \zeta}{\partial t} + \frac{\partial (hu)}{\partial x} + \frac{\partial (hv)}{\partial y} = 0 \tag{C.8}$$

where h is the local water depth (m).

The transport equations for the production and dissipation of turbulent kinetic energy become, respectively:

$$\frac{Dk_T}{Dt} = \frac{1}{1-\lambda} \frac{\partial}{\partial z} \left((1-\lambda) \left(v + \frac{v_T}{\sigma_k} \right) \frac{\partial k_T}{\partial z} \right) + T + P_k - B_k - \varepsilon \tag{C.9}$$

and:

$$\frac{D\varepsilon}{Dt} = \frac{1}{1-\lambda} \frac{\partial}{\partial z} \left((1-\lambda) \left(v + \frac{v_T}{\sigma_\varepsilon} \right) \frac{\partial \varepsilon}{\partial z} \right) + P_\varepsilon - B_\varepsilon - \varepsilon_\varepsilon + c_{2\varepsilon} \frac{T}{\tau_{eff}} \tag{C.10}$$

where:

$$T = F \sqrt{u^2 + v^2} \tag{C.11}$$

$$P_k = v_V \left[\left(\frac{\partial u}{\partial z} \right)^2 + \left(\frac{\partial v}{\partial z} \right)^2 \right] \tag{C.12}$$

ν_T is the turbulent eddy viscosity given by Eq. (B.6). The terms B_k, P_ε, B_ε, ε_ε are given by Eqs. (B.10, B.12, B.13, B.14) respectively, and the last term on the RHS of the dissipation transport equation equals that for the 1-DV model.

Acknowledgements

I have always wondered why it is common practice in PhD theses to acknowledge your partner last. I think they deserve the first place, at least, my wife does. So Roos, thank you very much for your support, your love, your kindness, your patience, and your encouragements.

Ranking second then, but I will stop ranking hereafter, comes Huib de Vriend, my promotor. I acknowledge you for being critical and supportive simultaneously. I don't know how you manage your time, but you somehow always find time to meticulously work through manuscripts. I thank you for sharing your insights and knowledge, and I have enjoyed camping with you on the banks of the Allier River, waiting for the flooding of our tents (which luckily did not happen).

I thank Erik Mosselman for supervising me and giving me to-the-point and accurate comments.

I thank Harm Duel for giving me the opportunity to start doing a PhD study in the first place. You made me move from the marine division of WL | Delft Hydraulics to the freshwater division to join your group, which was quite a move back then. You have been very supportive, trusting me with challenging projects at WL and now I have finished my PhD study I have left your fine group. I feel I have to apologize for that.

I thank Toine Smits for his stimulating enthusiasm for Cyclic Floodplain Rejuvenation and his never-lasting energy to set-up meetings and workshops.

I thank Rob Uittenbogaard for explaining his knowledge and insights in modelling turbulence. I owe you more than a red rose and a Grand Cru wine.

I thank Gerrit Klaassen for sharing his wisdom, his guidance with the flume experiment and the stream of IHE-students he provided.

For the study on Cyclic Floodplain Rejuvenation I thank my fine colleagues of WL | Delft Hydraulics who worked with me. Thank you Marcel Ververs, Nathalie Asselman, Karin Stone, Ellis Penning and Guda van der Lee. In addition I thank Franz Kerle of the University of Stuttgart and I thank Gertjan Geerling of Radboud University and Bart Peters, not only for their valuable contribution to the CFR study, but also for the good

time during the field visits in the Netherlands (Gameren, Ewijk, Millingerwaard) and Germany (visiting the Restrhine, camping in the wild along the Rhine).

For the experimental study I thank Christof Thannbichler for his magnificent work in carrying out and analysing the flume experiment. I made him drill 4755 holes of 2 mm diameter in wooden boards and subsequently stick 4755 plastic plants (upside down) in the holes. Sorry, but thanks a lot, Christof. And I thank the support staff of the Laboratory of fluid mechanics for their help.

For the Allier study I thank many people that did a lot of work and made a really fun time. Lara van den Bosch, Sander Kapinga and Jasper Dijkstra carried out field measurements in the Allier river in 2002. They collected thousands of GPS-positions. Emilie van Bemmel en Mathijs van den Broek did this in the hot summer of 2003 (and you both deserved that price). Jelle de Jong did this largely on his own in 2004. Although, these students from Delft University of Technology were helped by students from Utrecht University, so I also thank Eisse Wijma, Maarten Bakker and Sander van Rooij (2003), and Véronique Maronier, Roel Rink, André Chaigneau, Marije Hoevers, Dirkjan Douma and Deon Slagter (2004). And a very special word of thanks goes to Sander Vos, who has spent his holidays doing field measurements in the Allier for three years in a row now. In this respect I also thank Meander Consultancy and Advice for their co-operation. And then of course I thank Janrik van den Berg, Antoine Wilbers, Jurgen de Kramer and Hans Middelkoop of Utrecht University. It is extremely educational to walk in a natural river system with you.

Many thanks go the IHE-students that worked on related topics, Arnel Oberez, Andi Karanxha, Achmed Helal, Javier Rodríguez Uthurburu and Sajia Zaman. Working with them provided me a lot of insight in the complex topic of modelling biogeomorphology.

I thank my roommates for the stimulating discussions, the semi-useless chatting and for their help. Fred Havinga has been very patient in teaching me the ins and outs of Delft3D-MOR. And I specifically mention Sebastiaan, it was very helpful to have a magical mathematician in the room (and I apologize for the reference I made to your name).

I thank my fellow PhD students. The atmosphere at the sections of Hydraulic Engineering and Environmental Fluid Mechanics is really great. Thank you all!

I thank Mark Voorendt, Chantal van Woggelum, Adeeba Ramdjan and Gisela van der Wubben. Your support to the staff and students of the Hydraulic Engineering section is of incredible value.

I thank all my (former) colleagues and friends at WL | Delft Hydraulics. I mention some of you specifically: Stefan Aarninkhof, Vladan Babovic, Gerben Boot, Jos Dijkman, Frank Hoozemans, Bert Jagers, Herman Kernkamp, Frans Klijn, Maarten Keijzer, Rob Klomp, Mark van Koningsveld, Guda van der Lee, Arthur Mynett, Ursula van der Pol, Simone

Curriculum Vitae

Martin Josephus Baptist was born on 7 April 1972 in Voorburg, the Netherlands. Shortly hereafter he moved first to Goes (1973) and then to Middelburg (1976). Here he finished primary and secondary education. Martin started Environmental Studies at Wageningen Agricultural University in 1991 and graduated, cum laude, in September 1996. On the 1st of September 1996 he became an employee of WL | Delft Hydraulics, working on ecological studies mainly. At WL | Delft Hydraulics his interest and experience in studying the interaction of ecology with hydraulics and morphology grew. In 2000 he was offered a part-time Ph.D. study on this topic, he therefore became an employee of Delft University of Technology, Faculty of Civil Engineering and Geosciences, Hydraulic Engineering Section, for 60%, and remained working for WL for 40%, commencing on 15 July 2000. As of November 2004 he started a new assignment as a full-time lecturer and researcher of Delft University of Technology, Faculty of Civil Engineering, Water Resources Section.